

Uncertainty Quantification of Biodegradation Models using Surrogate Models

Dissertation
Zur Erlangung des akademischen Grades eines
Doktor der Ingenieurwissenschaften (Dr.-Ing.)
Christian-Albrechts-Universität zu Kiel

vorgelegt von
TAMADUR ADNAN ALBARAGHTHEH

Kiel
2024

CHRISTIAN-ALBRECHTS-UNIVERSITY KIEL

DOCTORAL THESIS

Uncertainty Quantification of Biodegradation Models using Surrogate Models

Author:

Tamadur Adnan Suleiman Albaraghteh

from

As-Salt - Hashemite Kingdom of Jordan

Submitted April/2024

*A thesis submitted in fulfillment of the requirements
for the degree of Doctor of Engineering (Dr.Ing.)*

at the

Christian-Albrechts-University of Kiel, Faculty of Engineering
(At Institute of Metallic Materials, Helmholtz-Zentrum Hereon)

Supervisor:
Prof. Dr. Regine Willumeit-Römer

Examiners:

Prof. Dr. Regine Willumeit-Römer
Prof. Dr. Stephan Wulfinghoff
Date of oral examination:
26th of November, 2024

Declaration of Authorship

I, Tamadur Adnan Albaraghteh, hereby confirm that my thesis entitled "Uncertainty quantification of degradation models of biodegradable implants using surrogate models" is the result of my own work. I did not receive any help or support from commercial consultants. All sources and/or materials applied here are listed and specified in the thesis. Furthermore, I confirm that this thesis has not yet been submitted as part of another examination process neither in identical nor in similar form and has been prepared subject to the Rules of Good Scientific Practice of the German Research Foundation. Furthermore, I declare that no academic degree has been revoked from me in the past.

Hiermit erkläre ich, Tamadur Adnan Albaraghteh, an Eides statt, die Dissertation "Uncertainty quantification of degradation models of biodegradable implants using surrogate models" eigenständig, d.h. insbesondere selbständig und ohne Hilfe eines kommerziellen Promotionsberaters, angefertigt und keine anderen als die von mir angegebenen Quellen und Hilfsmittel verwendet zu haben. Ich erkläre außerdem, dass die Dissertation weder in gleicher noch in ähnlicher Form bereits in einem anderen Prüfungsverfahren vorgelegen hat und unter Einhaltung der Regeln guter wissenschaftlicher Praxis der Deutschen Forschungsgemeinschaft entstanden ist. Des Weiteren erkläre ich, dass mir bislang kein akademischer Grad entzogen wurde.

Signed:

Date:

I constantly sought knowledge and truth, and it became my belief that for gaining access to the effulgence and closeness to God, there is no better way than that of searching for truth and knowledge.

Ibn Al-Haytham, Alhazen, The Optics

To Adnan and Saeda 'Haliemah'

إلى عدنانا وحليمة

Acknowledgements

It has been a very long journey, not easy and not simple. The journey of a curious little girl who enjoyed learning and discovering! I enjoyed collecting all the pieces of a challenging life puzzle. You have achieved one of your goals! The achievement of this milestone would have been impossible without the support, encouragement, and help of several amazing players.

I would like to express my sincere gratitude and appreciation to my supervisors Prof. Dr. Regine Willumeit-Römer and Dr. Berit Zeller-Plumhoff, who provided the platform, technical knowledge and support. Without the opportunity and expertise they provided, this endeavor would not have been possible.

I want to extend my sincere appreciation to The Helmholtz Incubator, for their generous financial support throughout this research, which is a part of *Uncertainty Quantification - From Data to Reliable Knowledge* project. It is also important for me to acknowledge the role of the members of the UQ team who have made this project a live and interesting endeavor.

My sincere appreciation goes to the members of my examination committee: Prof. Dr. Mikhail Zheludkevich (Chair), Prof. Dr. Regine Willumeit-Römer (Supervisor/Reviewer/Examiner), Prof. Dr.-Ing. Stephan Wulfinghoff (Reviewer/Examiner), and Prof. Dr. Sebastian Krumscheid (Examiner).

To the Imaging and Data Science team, who made this journey funny and worth living regardless of a worldwide pandemic. I would like to acknowledge the help and support of Dr. Zeller-Plumhoff during all the ups and downs of this project. I want to express my gratitude to Dr. Stefan Bruns for the insightful discussion, valuable input, and special book suggestions. I appreciate your time thoroughly reading my thesis and engaging with its content as well as for providing me with the opportunity for further international collaboration. I thank Dr. Florian Wieland for his help, the insightful discussion and for proofreading my German abstract.

In addition, I would like to express my sincere gratitude to Dr. Daniel Höche, Dr. Christian Feiler, and the entire team of the Interface Modelling Department at the Institute of Surface Science for giving me the opportunity to be part of their team over the past year.

To Suha, Taqi Eldin and their lovely angels, Sarah, Rayan, Hannah, Buthaina and Lujain thank you for always being here for me. To Giovana, Basma, Nourhan, Eric, Celso, Sana, Samah, Ehab, Osama, Mohammed, Diana, Hasmik, Andrea, and Sven thank you for being the escape from all the stress and for making Germany a good home for the past few years.

To my parents, Tariq, Wejdan, Sulieman, Neamat, Salam, Fahmi, Heba, Amr, Adnan, AbdullAl-lah, Lemar, Lubna, Tamara, Qais, Sarah, Elias and Ayser, thank you for always believing in me and for your unconditional support and love.

Tamadur Albaraghteh
Hamburg, 2024

Contents

I	Fundamentals	1
1	Introduction and motivation	3
1.1	Introduction	3
1.2	Thesis structure	6
2	Theoretical Background	9
2.1	The challenge in modelling the degradation of biodegradable implants	9
2.2	Uncertainty quantification	11
2.2.1	Variability, uncertainty and error	12
2.2.2	Uncertainty characterization	13
2.2.3	Forward and backward uncertainty quantification	15
2.2.4	Non-intrusive and intrusive uncertainty quantification	17
2.3	Quantifying uncertainty in complex biodegradation models	19
2.4	The presentation of uncertainty	22
2.4.1	Error metrics	23
2.4.2	Sensitivity analysis	24
2.4.3	Uncertainty propagation	26
2.5	Challenges and limitation of UQ	26
2.6	Surrogate models	28
2.6.1	Classification of surrogate models	29
2.6.2	Challenges and limitations of surrogate models	31
2.6.3	Assessment of surrogate models	32
	bibliography	33
II	Publications	51
3	<i>In silico</i> studies of Magnesium-based implants: a review of the current stage and challenges	53
4	Computational modelling of magnesium degradation in simulated body fluid under physiological conditions	85
5	Utilizing computational modelling to bridge the gap between <i>in Vivo</i> and <i>in Vitro</i> degradation rates for Mg-xGd implants	101
6	Best practices in developing a UQ-workflow for modelling the biodegradation of Mg-based implants	113

III Summary and Outlook	135
7 Summary and Outlook	137
7.1 Summary	137
7.2 Outlook	140
IV Other publications	143
8 Publications, their content and own contribution	145
List of figures	149

Abstract

Magnesium (Mg) and its alloys are being investigated increasingly as temporary bone implant materials due to their non-toxicity, biocompatibility, and biodegradability properties. The most challenging aspect of Mg-based implants involves adapting the degradation rate to the human body, which requires extensive *in vitro* and *in vivo* testing. Reliable computational models can aid by simulating the degradation and predict its rates. In the initial phase of the study, a comprehensive and in-depth review of the developed degradation models up to date, revealed the fact that developing reliable degradation models is challenging. This is due to the complexity and multi-scale nature of the biodegradation process. Moreover, reliable models must consider multiple aspects of implant composition and alloying elements, as well as the surrounding environment. Furthermore, biodegradation models are inevitably characterized by uncertainty associated with different aspects of them, *i.e.* uncertain validation data, parameters, hypothesis and concept as well as simulator limitations. Therefore, it is critical to quantify the uncertainties within these models. Uncertainty quantification (UQ) provides several methods to quantify different sources of uncertainty within computational models. Overall, UQ methods are computationally expensive and require a substantial number of model iterations. Thus, surrogate modelling has gained significant interest in recent years, as these models can substitute expensive models within the UQ analysis.

Kriging surrogate models are constructed to calibrate and estimate the model parameters of a generalized degradation model. This model simulates both the degradation of pure Mg in simulated body fluid (SBF) and the precipitate formation on the implant surface. The quantified degradation model could predict the behaviour of Mg implants of different shapes with the same level of uncertainty as the experiments. Moreover, the novel approach of surrogate modelling is implemented to bridge the gap between *in vitro* and *in vivo* degradation behaviour. In this study, Kriging models are constructed to calibrate and estimate the model parameters of actual geometry screw of Mg-xGd (Mg-5 wt.% Gd and Mg-10 wt.% Gd) implants in complex cell culture medium. Then the parametric space of the model is expanded to include different scenarios. The Kriging models are recalibrated using *in vivo* volume loss data of the same implants. A correlation between the *in vitro* and *in vivo* degradation of Mg²⁺-ions can be drawn using the diffusivity of Mg ions.

At the final phase of this study, a workflow to implement UQ and select the most efficient surrogate model for complex degradation models is presented. A unique set of issues related to UQ implementation is addressed, including design of computer experiments, selecting the suitable surrogate model based on the available information of the biodegradation system.

Overall, the current cumulative dissertation presents a clear workflow to quantify uncertainty within different types of biodegradation models. The published work and proposed workflow can serve as a foundation for assessing the influence of uncertainty on the reliability and robustness of the computational models of biodegradation while optimizing the ratio of accuracy and computational cost.

Zusammenfassung

Magnesium (Mg) und seine Legierungen werden aufgrund ihrer Nicht-Toxizität, Biokompatibilität und biologischen Abbaubarkeit zunehmend als Materialien für temporäre Knochenimplantate untersucht. Die größte Herausforderung bei Implantaten auf Mg-Basis ist die Anpassung der Abbaugeschwindigkeit an den menschlichen Körper, was umfangreiche *in-vitro*- und *in-vivo*-Tests erfordert. Zuverlässige Computermodelle können helfen, den Abbau zu simulieren und seine Geschwindigkeit vorherzusagen. Eine umfassende und eingehende Überprüfung der bisher entwickelten Degradationsmodelle, hat jedoch gezeigt, dass die Entwicklung zuverlässiger Degradationsmodelle eine Herausforderung darstellt. Darüber hinaus sind Degradationsmodelle zwangsläufig durch Unsicherheiten gekennzeichnet, die mit verschiedenen Aspekten verbunden sind, z.B. unsicheren experimentellen Daten, Modellparameter, Modellhypothese und -konzept, sowie Einschränkungen in der Simulationssoftware. Daher ist es von entscheidender Bedeutung, die Unsicherheiten innerhalb dieser Modelle zu quantifizieren. Die Quantifizierung der Unsicherheit (Uncertainty Quantification, UQ) bietet mehrere Methoden zur Quantifizierung verschiedener Unsicherheitsquellen in mathematischen und Computermodellen. Insgesamt sind UQ-Methoden rechenintensiv und erfordern eine erhebliche Anzahl von Modelliterationen. Die Surrogatmodellierung hat deswegen in den letzten Jahren stark an Interesse gewonnen, da diese Modelle mit begrenzten Daten aus komplexen Modellen trainiert werden können.

Kriging-Surrogatmodelle werden konstruiert, um die Modellparameter eines verallgemeinerten Degradationsmodells zu kalibrieren. Dieses Modell simuliert sowohl den Abbau von reinem Mg in simulierter Körperflüssigkeit als auch die Bildung von Salzen auf der Implantatoberfläche. Das kalibrierte Degradationsmodell konnte das Verhalten von Mg-Implantaten verschiedener Geometrien mit dem gleichen Unsicherheitsgrad wie die Experimente bestimmen.

Der neuartige Ansatz der Surrogatmodellierung wird umgesetzt, um die Lücke zwischen dem Abbauverhalten der Implantate in *in-vitro*- und *in-vivo*-Experimenten zu schließen. In dieser Studie werden Kriging-Modelle konstruiert, um die Modellparameter für den Abbau einer Schraube aus Mg-xGd (Mg-5 Gew.% Gd und Mg-10 Gew.% Gd) in komplexem Zellkulturmedium zu kalibrieren. Anschließend wird der parametrische Raum der Modellparameter erweitert, um verschiedene Szenarien einzubeziehen. Die Kriging-Modelle werden anhand von *in vivo*-Volumenverlustdaten der gleichen Implantate rekaliert. Eine Korrelation zwischen dem *in vitro*- und dem *in vivo*-Abbau von Mg²⁺-Ionen kann anhand der Diffusivität von Mg²⁺-Ionen gezogen werden.

In der letzten Phase dieser Studie wird ein Arbeitsablauf zur Implementierung von UQ und zur Auswahl des effizientesten Surrogatmodells für komplexe Abbaumodelle vorgestellt. Es wird eine Reihe von Fragen im Zusammenhang mit der UQ-Implementierung behandelt, einschließlich der Planung von Computerexperimenten und der Auswahl eines geeigneten Ersatzmodells auf der Grundlage der verfügbaren Informationen über das biologische Abbausystem. Insgesamt stellt die vorliegende kumulative Dissertation einen klaren Arbeitsablauf zur Quantifizierung der Unsicherheit in verschiedenen Arten von Computermodellen des biologischen Abbaus vor. Der vorgeschlagene Arbeitsablauf kann als Grundlage für die Bewertung des Einflusses von Unsicherheiten auf die Zuverlässigkeit und Robustheit der Computermodelle des biologischen Abbaus dienen, während gleichzeitig das Verhältnis von Genauigkeit und Rechenkosten optimiert wird.

Part I

Fundamentals

Introduction and motivation

1.1 Introduction

Magnesium (Mg) is one of the essential elements within the human body and one of the most abundant elements in the earth's crust. The unique ability of Mg and its alloys to degrade under physiological conditions has paved the way for an innovative class of metallic biomaterials. Due to their non-toxicity, biocompatibility, and biodegradability properties, they are great candidates for fabricating implants, thus making them for some applications an ideal replacement for non-degradable bone implants made of titanium-based alloys, cobalt-based alloys and stainless steel as temporary implant materials [1–4]. The rising importance of biodegradable Mg-based implants for orthopedic applications stems from their anti-inflammatory [5,6], antibacterial [7–9] and osteoinductive properties [10–12], which offer promising therapeutic outcomes for patients. Overall, the development of biodegradable Mg-based implants holds promise for the future of orthopedic medicine, offering patients safer and more effective treatment options with fewer long-term complications [13–17].

Developing biodegradable implants that match bone healing degradation kinetics is a significant challenge. It requires careful consideration of the implant degradation rate, ensuring that it adapts to the body's healing process without leaving behind harmful residues [2, 18–25]. In principle, the ideal biodegradable implant should gradually degrade as the bone heals, allowing for optimal regeneration of bone and tissue. Achieving this balance requires a substantial amount of both *in vitro* and *in vivo* experimentation to investigate the rates of degradation and the ability of the body to handle the degradation products [13, 18, 19]. The biological environment is complex and testing conditions can vary widely, leading to a significant gap between *in vitro* and *in vivo* studies [26–30]. To narrow this gap, it is necessary to conduct extensive analyses and tests. However, since over 115 million animals are sacrificed annually for biological research and industry, it is imperative that alternate effective methods be developed to facilitate the development of biodegradable implants [31–33]. Therefore, methods to enhance the *in vitro* testing to provide more accurate predictions for *in vivo* testing, such as 3D-cell printing techniques for biological systems [34] and organ-on-a-chip technologies [35], are rapidly gaining recognition as safer and more ethical alternatives to animal testing. However, further development and modification are needed to improve the performance of these techniques [36]. Another alternative is to utilize the different approaches of computational modelling (also known as *in silico* methods) to construct reliable mathematical and numerical models, which can simulate the various aspects of the degradation. Hence, reliable computational frameworks are a promising alternative to provide valuable insights into the degradation behaviour of different Mg-based implants under physiological conditions [13, 18, 19, 37–39]. Nevertheless, the ability

of degradation models to bridge the gap between experimental studies still needs to be tested.

Developing a mathematical model of the degradation of biodegradable implants is a multi-scale challenge that requires a comprehensive understanding of the complex nature of biodegradation, the various factors affecting it, and their interactions [19]. Extensive research in the *in silico* field has led to the development of various micro- and macro-scale computational models for modeling different aspects of degradation, e.g. the impact of degradation process on the implant's morphological and mechanical properties [13, 19]. Degradation models can be classified based on the basic principles of derivation including physical, phenomenological, analytical and data-driven models. Alternatively, they can be classified based on the type of degradation they simulate, such as uniform, stress and pitting degradation models [19, 37–39].

Degradation models for biodegradable implants are, in fact, influenced by uncertainty. These uncertainties arise from various sources, primarily originating from the lack of knowledge regarding the underlying physics of biodegradation, which impacts the computational model assumptions and hypotheses [40]. Other sources of uncertainty include the variability of model parameters, the lack of predictive power, and the uncontrolled randomness in experimental observations [19, 41, 42]. These Uncertainties affect critical aspects such as the reliability of input parameters, initial and boundary conditions, as well as experimental or validation data [40, 43, 44]. To reduce the complexity of the degradation model and control associated uncertainties, various techniques and assumptions can be employed. A common approach is to assume that parameters have constant values obtained from experimental testing. This technique was utilized in the computational model derived in [45], where a constant porosity value based on experimental measurements of the degradation layer was used. Another technique for simplifying assumptions involves drawing analogies with similar systems. An example of this approach can be seen in the model presented by [46], where the surface of a Mg biodegradable implant is assumed to remain smooth by neglecting pitting and cracking, similar to scenarios observed in metal degradation under low loads. However, one of the main shortcomings of degradation models is the simplification of the composition of degradation layers [19, 47–49].

In several models, magnesium hydroxide ($\text{Mg}(\text{OH})_2$) has been assumed as the primary degradation product. This assumption implies that degradation experiments should only consider pH as the main controller for degradation and ignore the effect of the ionic composition of the implant and degradation media, flow rate, temperature, and other environmental conditions [19, 37–39]. In addition to that, this assumption neglects the fact that $\text{Mg}(\text{OH})_2$ forms a stable layer in an alkaline environment ($\text{pH} > 10$), which is not the typical environment for biodegradable implants to be implanted [4]. It is crucial to address the uncertainties associated with degradation models as neglecting them may lead to inconsistencies between model predictions and actual observations. This oversight could result in poor decisions about experiment design decisions and inaccurate parameter choices. Computational models developed without considering these uncertainties will have limitations and may fail to capture the variability of the degradation process [19, 47–49]. To address these challenges, it is essential to identify, characterize, and quantify the various sources and types of uncertainty to develop robust computational models for simulating the degradation of biodegradable implants. Integrating Uncertainty Quantification (UQ) methods within the computational framework would facilitate overcoming these challenges and limitations.

The motivation to integrate the UQ methods within the computational framework to simulate biodegradation is supported by the fact that most degradation models are deterministic, meaning that input parameters, such as reaction rates, porosity, and diffusion rates, are assigned a single set of values. Therefore, degradation models will have a single response

without considering the uncertainty associated with these parameters. The difference between classical deterministic and UQ methods to evaluating a mathematical model is illustrated in Figure 1.1. A deterministic model has a fixed value for each input parameter corresponding to a single output. While UQ methods consider the entire distribution of the input parameters, which also contains the different types of uncertainty associated with them, resulting in the model output becoming a range of possible values, represented as a grey shade [50].

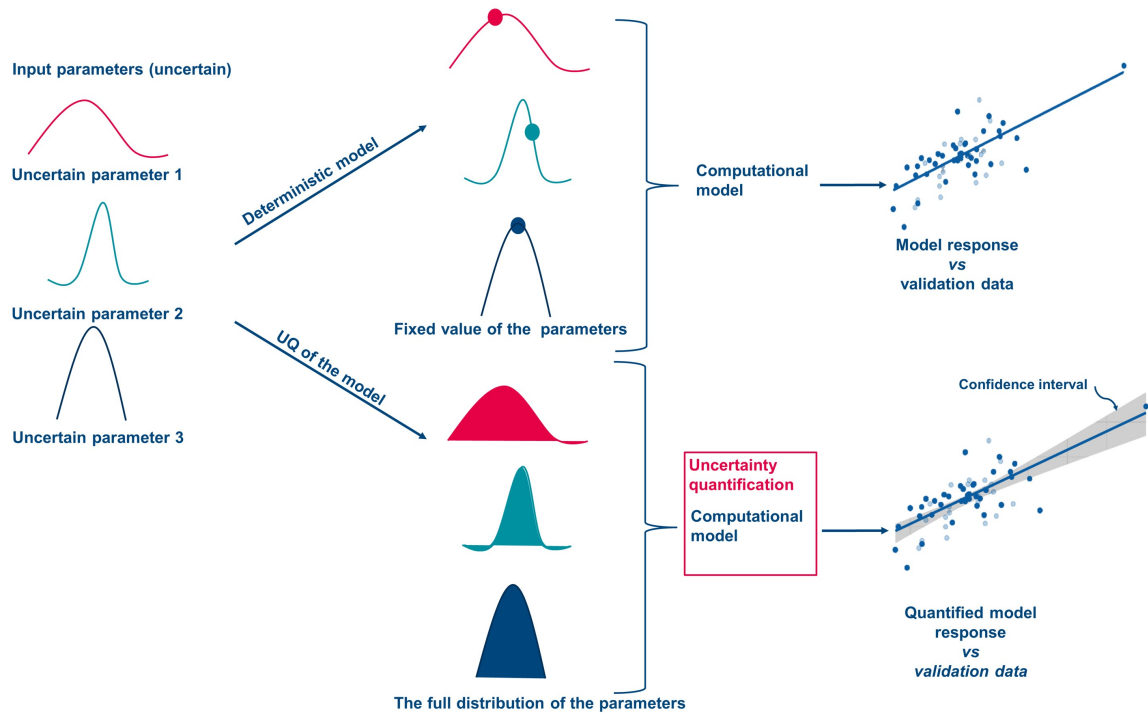


Figure 1.1: Schematic diagram of traditional deterministic model vs. applying UQ methods to model predictions (inspired by [51]).

UQ characterises and quantifies the difference between model predictions and experimental observations by identifying the various sources of uncertainty associated with the degradation. The UQ of deterministic models is illustrated in the schematic diagram in Figure 1.1. UQ provides insight into the impact of these uncertainties on model predictions. This is done by considering the full distribution of input parameters and including the probabilistic nature of these parameters, which enables the consideration of different types of uncertainty associated with these parameters, which enables the generation of different testing scenarios [43, 47, 52]. As a result of considering the probabilistic nature of the degradation model, it is possible to compile a parameter-response map that covers all possible observations of the model and their associated uncertainty, thus giving a realistic mathematical presentation of the real system [53–55]. Moreover, UQ takes into account the uncertainty of the model itself by providing robust and straightforward methods to generate random coefficients and parameters used in solving the deterministic degradation models, which are derived in the form of algebraic, ordinary (ODEs) or partial differential equations (PDEs). By using UQ methods, original model realizations are collected, and ensemble statistics are evaluated for each realization [54–56].

Classical UQ mostly relies on easy-to-implement Monte Carlo simulations (MCS). MCS do not impose limitations on the statistical properties of the input parameters, and do not change the deterministic solvers of the original model. Moreover, MCS are ideal for accelerating com-

putational model solutions using parallel computing. The main bottleneck in UQ analysis using MCS is that it is time-consuming and computationally expensive. This significant issue arises from the necessity of repeatedly evaluating complex and multi-scale degradation models [19, 53, 56, 57].

Surrogate models provide a practical alternative to classic UQ analysis. A further advantage of surrogate models is that they allow assessments of the effect of uncertainty on the reliability and robustness of the computational framework, while maintaining an efficient accuracy-to-computational cost ratio [58–61]. The complex and multi-scale degradation models are treated as a black-box that is approximated with an easy-to-evaluate explicit surrogate model [59, 60]. Generally, surrogate models are an important component that is incorporated into the UQ field [59, 60]. The importance of surrogate models relies on their ability to capture the behaviour of more complex computational models, particularly when data is limited, by mapping the input-response variables. This allows for efficient UQ analysis using surrogate models instead of the original, more computationally expensive models [45, 57, 59, 60]. The reliability of a surrogate model is directly impacted by the nature of the physical system being modelled and its computational representation. This, in turn, determines the most suitable surrogate modelling techniques. In general, a variety of surrogate models are available in the literature and their construction has different levels of complexity and data requirements and intimately depends on the nature and complexity of the original system. For example, polynomial surrogate models, e.g. polynomial chaos expansion, are suitable for high-dimensional problems, while Kriging, which is an interpolation method, exhibits excellent performance for low-to-medium-dimensional problems [62]. Moreover, the availability and accuracy of the calibration/validation data, whether linear or non-linear, will also play a significant role in the choice of the appropriate type of surrogate model [57, 59, 60, 63].

1.2 Thesis structure

This thesis is motivated by the challenges of modelling the complex and multi-scale degradation system of biodegradable Mg-based implants. The main aim of this thesis is to quantify the different types of uncertainty associated with degradation models by developing an efficient computational workflow to perform a variety of UQ analyses, *i.g.* model calibration, uncertainty propagation and sensitivity analysis. However, the complexity and computational cost of the quantification process are directly related to system complexity. This work utilizes multiple surrogate models to quantify the uncertainty associated with different degradation models. In order to achieve a thorough treatment of UQ, several steps must be considered

- Characterise the relationship between different parameters that affect degradation model predictions. This includes a critical review and screening of the available degradation models both *in vitro* and *in vivo*;
- Develop a workflow for constructing efficient surrogate models for different scenarios and types of degradation;
- Develop suitable surrogate models and optimize their parameters based on the degradation model;
- Identify areas where surrogate models can improve computational studies of degradation systems.

To emphasize the research objectives, the thesis was structured as follows:

Chapter 2 includes a detailed discussion of the basic concepts of uncertainty, error and uncertainty quantification, together with a brief overview of the different aspects of UQ methods and techniques, as some of these techniques will be used in subsequent studies. **Chapter 3** highlights the importance of continued research and development in the field of *in silico* testing of Mg-based implants. It presents a comprehensive discussion of the various approaches developed to model the degradation of biodegradable Mg-based implants *in vitro* and *in vivo*. This chapter begins by diving into the complex factors that influence the degradation behaviour of Mg-based implants. Furthermore, it addresses the challenges and opportunities associated with integrating these factors into different modeling approaches. Specifically, a comprehensive and critical discussion of the published models and their performance in capturing the complexity of the biodegradation is presented. Additionally, different approaches to optimize and quantify the different sources of errors and uncertainties within the proposed models have been reviewed and discussed.

Motivated by this review, **Chapter 4** introduces a novel computational model that simulates the degradation of pure Mg under physiological conditions. The model captures the degradation behaviour of pure Mg and the formation of different precipitates on the implant surface. Kriging surrogate models are constructed based on the degradation model. The use of Kriging surrogate models enhances the calibration process of the key model parameters by considering the probabilistic nature of these models. Furthermore, they enable sensitivity analysis, which provides insightful knowledge about the dynamics of the degradation, by identifying the most influential parameters in degradation. Furthermore, especially in precipitate formation, sensitivity analysis yields more information about the competing reaction between calcium precipitation and phosphate ions for hydroxyapatite formation. Finally, the performance of the calibrated degradation model against in-house experimental data shows that both degradation and precipitate formation models are in good agreement with experimental data.

In **Chapter 5** discusses the possibility to bridge the gap between *in vitro* and *in vivo* degradation studies of biodegradable Mg-based implants using computational models. Kriging surrogate models are constructed using a three-dimensional peridynamic model of degradation, developed in [64]. The constructed models are calibrated to volume loss datasets from *in vitro* and *in vivo* degradation of Mg-xGd screws in a complex cell culture medium. Based on the similarity of the diffusion process of Mg^{2+} -ions in both systems, Kriging models can map the degradation between *in vitro* and *in vivo* using the diffusion rates of Mg^{2+} -ions in both degradation systems as key parameters. Moreover, based on this calibration, time-independent ratios between the diffusion rates of Mg^{2+} -ions are established. These ratios can be utilized to infer *in vivo* degradation behaviour based on *in vitro* experiments.

A comprehensive analysis of the effectiveness of the proposed UQ workflow, is presented in **Chapter 6**. Different types of surrogate models are tested for degradation models, including Kriging, polynomial chaos expansion, and polynomial chaos Kriging. Surrogate modelling techniques are selected based on the complexity of the degradation model, available training/validation data, and computational resources. The proposed UQ workflow has been investigated using three different degradation models, in order to reflect the influence of the degradation model's complexity. In this study, the uncertainties associated with different models are presented in terms of global sensitivity analysis and uncertainty propagation.

Finally, **Chapter 7** summarises the thesis findings. Moreover, it presents a comprehensive and detailed outlook, offering insights into the potential applications of the computational models and uncertainty quantification workflows developed in this work.

Overall, this cumulative thesis is based upon work that has been published or submitted for publication:

- **Chapter 3** [19] Albaraghtheh, T., Willumeit-Römer, R., Zeller-Plumhoff, B. (2022). In silico studies of magnesium-based implants: A review of the current stage and challenges. *Journal of Magnesium and Alloys*. 10 (11), 2968-2996.
- **Chapter 4** [45] Zeller-Plumhoff, B.*, Albaraghtheh, T.*, Höche, D., Willumeit-Römer, R. (2022). Computational modelling of magnesium degradation in simulated body fluid under physiological conditions. *Journal of magnesium and alloys*. 10(4):965-78.
- **Chapter 5** [65] Albaraghtheh, T., Hermann, A., Shojaei, A., Willumeit-Römer, R., Cyron, C.J., Zeller-Plumhoff, B. (2023). Utilizing computational modelling to bridge the gap between *in vivo* and *in vitro* degradation rates for Mg-xGd implant. *Corrosion and Materials Degradation*, 4(2), 274–283 (**Invited**).
- **Chapter 6** Albaraghtheh, T., Willumeit-Römer, R., Zeller-Plumhoff, B. (2024). Best practices in developing a UQ-workflow for modelling the biodegradation of Mg-based implants. *Advanced Science*, **under review**.

In addition, **Chapter 8** summarizes my collaborative involvement in published research, which was not included in this thesis. Short articles covering the research topic of this thesis have been written and published as part of the UQ-dictionary, which is a part of HGF Incubator - Uncertainty Quantification project. These articles can be accessed at <https://dictionary.helmholtz-uq.de>.

Theoretical Background

Adapting the degradation rates of biodegradable Mg-based implants to the human body is one of the most challenging steps, which requires extensive *in vitro* and *in vivo* testing. Computational methods are a promising alternative to predicting degradation rates and accelerating material optimization. Mathematical models developed to simulate multi-scale complex degradation systems are characterised by uncertainty. In spite of how sophisticated biodegradation models are, they still exhibit deviations in their ability to accurately predict degradation. To quantify the uncertainty associated with biodegradation models, it is crucial to identify and classify the uncertainty inherent in the biodegradation system. The next section introduces the main pillars of UQ; the difference between uncertainty and errors, types of uncertainty within computational systems and how to classify them. Furthermore, an overview of surrogate models and the design of numerical experiments tailored specifically to studying the degradation of biodegradable Mg-based implants is discussed. Finally, methods of presenting uncertainty and how they propagate within computational systems are discussed.

2.1 The challenge in modelling the degradation of biodegradable implants

Several mathematical models have been proposed to simulate different aspects of the biodegradation process, with the ultimate goal of accurately simulating the degradation behaviour in *in vitro* and *in vivo* experiments. However, modelling the degradation of biodegradable implants poses significant challenges and uncertainty due to the complex, multi-scale nature of the biodegradation process, as illustrated in Figure 2.1. According to the schematic diagram, different types of reactions and changes occur at different stages and times during the biodegradation process [66].

One of the significant challenges in modelling the biodegradation process is the limited knowledge and understanding of the various factors that influence degradation. Under physiological conditions several factors affect and contribute to the complexity of biodegradation, which can be summarised as: medium composition, pH, temperature, CO₂ and O₂ concentrations, and medium flow rate, as well as alloying elements and materials processing methods [19, 23, 67]. These factors play a considerable role in controlling the nature of degradation by affecting both degradation rates and products [23, 68, 69]. A summary of the effect of these factors is presented in **Chapter 3**, moreover, a comprehensive discussion can be found in Gonzalez et al., [23]. Added to this, a study by Zeller-Plumhoff *et al.*, [70] explored the ionic interactions of individual ionic components of simulated body fluids (SBF) and predicted the degradation rate of pure Mg. Here a non-linear relationship was reported between degradation rate and the pre-

precipitation of calcium salts. A comparative study presented by Walker *et al.*, [69] compared the degradation rate of pure Mg and five Mg-based alloys; namely: AZ31, Mg-0.8Ca, Mg-1Zn, Mg-1Mn, Mg-1.34Ca-3Zn, in three *in vitro* media; Earle's Balanced Salt Solution (EBSS), minimum essential medium (MEM) and MEM with 40 g/L Bovine Serum Albumin (BSA) buffered with $\text{CO}_2/\text{HCO}_3^-$. In this study, degradation rates within EBSS matched *in vivo* rates. In addition, all tested implants displayed increased degradation rates when BSA was added.

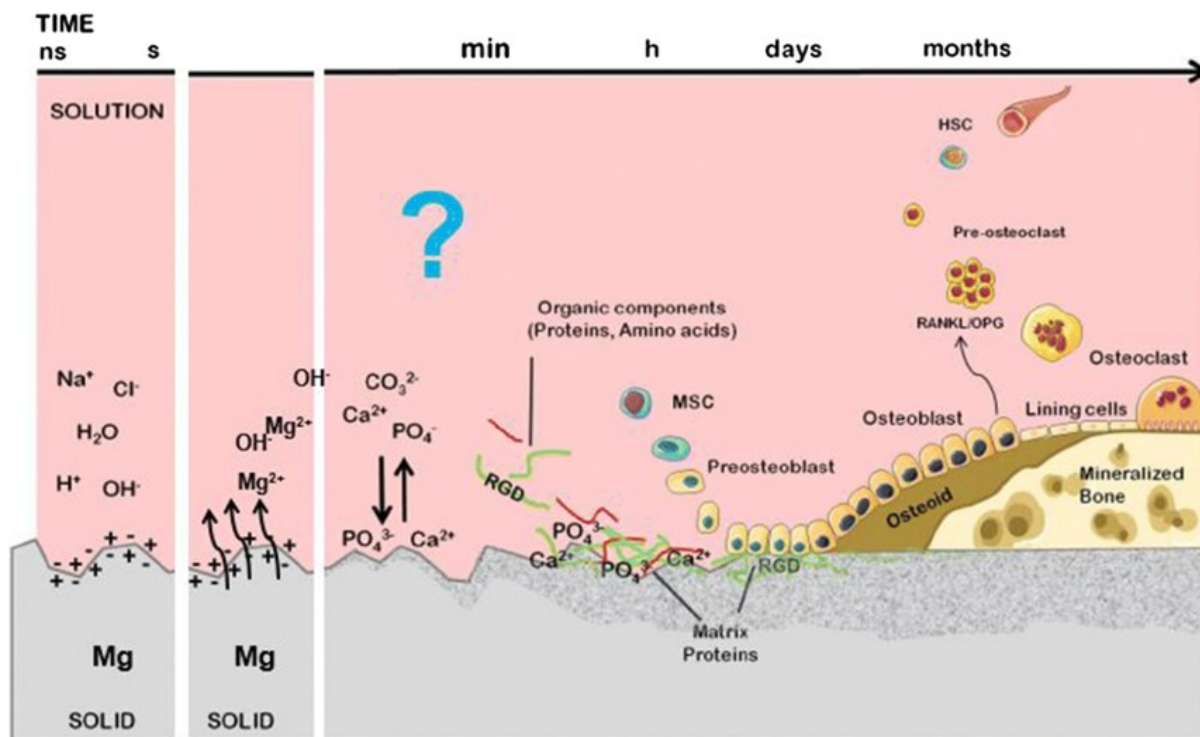


Figure 2.1: Schematic description of the complexity of the biodegradation process. Adapted from [66] under CC BY 4.0 license.

The specific mechanisms and interactions of degradation under different conditions need to be fully comprehended, in order to develop a reliable computational model that accurately predicts degradation behaviour [13, 19, 38, 39, 71]. Additionally, the gap between *in vitro* and *in vivo* degradation behaviour adds another challenge to biodegradation models. For example, a recent study by Martinez *et al.*, [72] investigated the *in vitro* and *in vivo* degradation behaviour of Mg-0.45Zn-0.45Ca (ZX00) screws. In this study, the ZX00 screws were immersed for 28 days in α -MEM for *in vitro* testing, while human-size screws were implemented in the diaphysis of sheep (*Ovis aries*) over 24 weeks. The degradation layer was found to have the same elemental composition, but the elemental distribution and thickness of the layers varied between the *in vitro* and *in vivo* tests. As a result of this variation, it is evident that degradation mechanisms are highly dependent on the surrounding environment under physiological conditions. Martinez *et al.*, findings agree with a review by Sanchez *et al.*, [73], which presented a detailed comparison of several published studies to examine whether it is possible to correlate the *in vitro* and *in vivo* degradation behaviour of Mg and Mg-based alloys. However, this study concluded that a clear correlation could not be established.

Another challenge reported is due to the limited adequate experimental data to validate and calibrate the biodegradation models, especially for newly developed implants or specific degradation conditions, can affect the reliability of the model and its predictions [13, 19]. Bajger *et al.*, [42] reported the lack of experimental data for the reaction rate constants, as well as the absence of diffusion coefficients values in the literature. Similar issues of lack of experimental

data were reported by Sanz-Herrera *et al.*, [74], which resulted in only obtaining qualitative results from the model, which investigated the role of multiple chemical components involved in the *in vitro* degradation of Mg-based implants. In a recent study by Barzegari *et al.*, [75], Bayesian optimization was implemented to overcome this problem. However, Bayesian optimization increases the computational cost of the model and only considers a limited number of parameters based on the assumption of the most effective parameters. Furthermore, dealing with non-linear and time-dependent degradation equations can introduce instability issues in the numerical methods used to solve these equations [76, 77]. The instability arises from the dependency of these equations on the mesh, which can be controlled using a convergence study, as in the case presented by Boland *et al.*, [78] for calibrating a pitting corrosion model of WE43 implants. Moreover, the computational models of degradation can be computationally demanding due to the different length scales considered in the modelling, e.g., macroscopic, microscopic and considering interactions at multiple levels, *i.e.* cellular, tissue, bone, implant [19, 79–84]. Due to this, most biodegradation models are run on high-performance-computing (HPC) clusters. For example, a biodegradation model developed by Zeller-Plumhoff and Albaraghteh *et al.*, [45] required twenty-eight minutes for a single run using 80-core 2.40 GHz Gold 6148 processor Maxwell cluster, while a biodegradation model developed by Hermann *et al.*, [64] required around three hours for single run using 24-core 2.1 GHz Intel Xeon Scalable Platinum 8160 processor.

Overcoming the mentioned challenges involves continuous improvement and validation of biodegradation models through rigorous experimental data collection and comparison. The development of a reliable computational framework for degradation that handles the various challenges mentioned above may also play a significant role in accelerating the optimization of biodegradable implants. In this case, biodegradation models should be able to process an arbitrary number of biodegradation scenarios to create a comprehensive map of the prediction space. Moreover, computational models can provide valuable insights into possible responses and anticipate challenges, resulting in developing flexible computational frameworks that effectively adapted to the changes in biodegradation behaviour under various test conditions [85, 86]. Considering different biodegradation scenarios increases the uncertainty associated with the computational framework, which must be addressed and quantified. This thesis employs UQ in order to quantify the uncertainty associated with different biodegradation models for biodegradable magnesium implants. Nevertheless, implementing UQ for a complex system, such as biodegradation models, presents a challenge due to the computational load associated with various UQ methodologies. In order to overcome this challenge, different surrogate models are tested and utilised.

2.2 Uncertainty quantification

Uncertainty quantification is a multidisciplinary field that encompasses applied mathematics, statistics and engineering. UQ is not a single-step process; it can broadly be defined as a framework, which employs computational models, observational data and theoretical analysis to identify, analyze and mitigate uncertainty associated with mathematical models, simulations and data-driven predictions [87–90]. Importantly, UQ is implemented to analyse and quantify uncertainty in different computational models, as well as to identify uncertainty sources [55, 91, 92]. In addition, identifying the influence of uncertainty facilitates a reliable understanding of physical phenomena, accurate prediction of quantities of interest (QoI) and identification of the most influential uncertainty sources that play a crucial role in model responses. Within computational frameworks, UQ includes several tasks, for example, characterization of uncertainty, uncertainty calibration, sensitivity analysis, uncertainty propagation and inverse analysis [49, 89–91]. Within scientific computing, UQ is closely combined with the concepts of

verification and validation.

As part of model-based predictive analysis and design, verification involves the connection between mathematical and computational models. The goal is to eliminate implementation errors and ensure numerical methods are used correctly. The correct implementation of numerical simulations is checked by comparing the simulation output with previously validated simulations, analytical or exact solutions of the model [89, 90]. While validation aims to check the reliability of the simulation for predicting physical system behaviour under different conditions. Validation Ensures the accuracy of a numerical simulation representing the physical system, which involves comparing the results of the simulation with experimental data or with known physical or mathematical models of the physical phenomenon [89, 90].

2.2.1 Variability, uncertainty and error

Uncertainty and error are fundamental concepts in scientific measurements and estimations. UQ considers inherent variability within a physical system. A quantity is considered variable when it changes between the same parts, over time, or between places. Notable examples of variability include manufacturing tolerances, fluctuations in working conditions and material scatter [89], as well as, the variation in degradation rate, volume loss and pH for the same time point and same implants under *in vitro* or *in vivo* conditions. Uncertainty encapsulates the degree of ignorance related to the exact behaviour, mechanism or response within any phase of a computational system. More precisely, uncertainty is an attribute of lack of knowledge and it signifies a limitation in possessing a comprehensive understanding of the computational model's actual response, encompassing its inputs, hypotheses, and assumptions [93]. Uncertainty can be visualized as a confidence interval of the model output, representing the range of possible true output values with a certain level of confidence, e.g. 90%, 95% and 99%. This interval resembles a cloud of potential model response scenarios, capturing the inherent variability and unpredictability of the computational model [47, 94]. Error, in contrast, is a deterministic value that is defined as deviations from the exact/standard measurement value. In general, error can be considered an attribute of a measurement or an estimate [89, 93]. Errors can arise from various sources, such as measurement inaccuracies, modelling assumptions, or data inconsistencies [95, 96]. To understand the difference and connection between variability, uncertainty and error terms, let us consider an experiment to measure the gravitational acceleration (g) as an example. The exact or standard value for g is 9.81 ms^{-2} , when measuring the acceleration using a pendulum in the lab we can get values of 9.91, 9.84, 9.72, and 9.65 ms^{-2} . The variation in the measurement is variability, which is a result of error. The deviation in g value from the standard value of 9.81 ms^{-2} is the error, while uncertainty is the range between 9.65 and 9.91 ms^{-2} .

Within computational frameworks, the categorisation of errors includes systematic errors, also known as deterministic or statistical bias, which can emerge as calibration errors and are quantifiable through validation against experimental data. They can also be quantified by calculating the average difference between model observations and measurements obtained through a standard or reference method. Another error category is random errors, indeterminate and uncontrollable in nature, often arising from variations among different observations in the system. These errors are inherent and cannot be eliminated. Moreover, the deviation from experimental observations or validation data in the model's predictions is known as modelling errors arising from incorrect assumptions, inaccurate measurements and failed modelling techniques [56, 93, 95]. On the other hand uncertainties are categorized based on their nature, level of knowledge or sources [47, 93, 94]. The term uncertainty is used throughout the current thesis to refer to the various types of uncertainty from different sources that are associated with the

biodegradation models, unless a different specification is given.

2.2.2 Uncertainty characterization

A comprehensive comprehension of the types, nature and sources of uncertainty within computational models is paramount to effectively address the diverse uncertainty associated with various aspects of computational models, including inputs, responses and assumptions. Although identifying and categorizing uncertainty can be challenging, especially within model-based systems, they can generally be classified into two main categories: aleatory and epistemic [97].

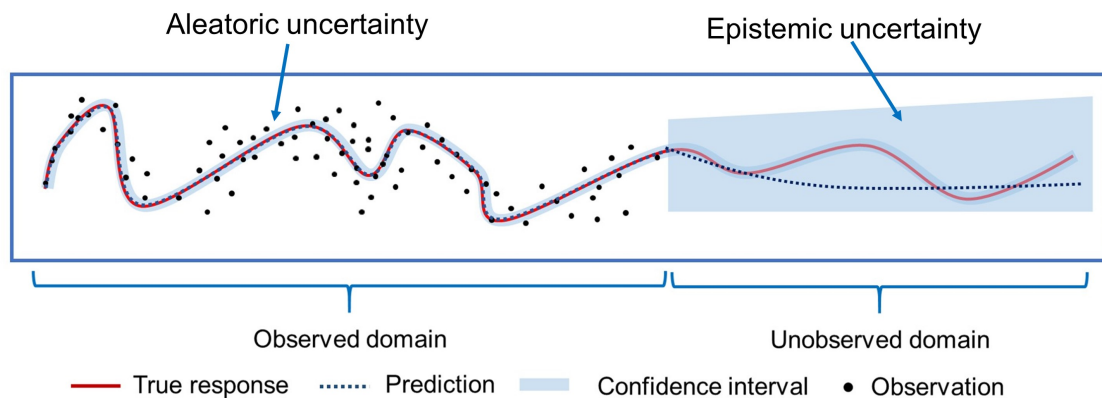


Figure 2.2: Schematic diagram of epistemic and aleatory uncertainties within the modelling domain.

Epistemic uncertainty arises from a lack of knowledge or an incomplete understanding of the nature of the system. As a result, models exhibit non-deterministic behaviour, particularly within the unobserved domain of the physical system in which the observations of the system are not available or measured, as illustrated in the schematic diagram in Figure 2.2. Epistemic uncertainty can be viewed as reducible uncertainty. It can be reduced by conducting additional experiments, deepening knowledge, consulting experts in the field, utilizing advanced models and employing accurate approximations [88, 98, 99]. Aleatory uncertainty, on the other hand, is characterised as irreducible. The nature of this uncertainty is illustrated in the schematic diagram in Figure 2.2. It encompasses inherent randomness, natural variability and stochastic uncertainty. Aleatory uncertainty is mathematically presented through probability or frequency distributions within the observed domain of the physical system. Moreover, aleatory uncertainty increases as observation data uncertainty increase [48, 49, 98–100].

To understand the difference between aleatory and epistemic uncertainty let us again consider the simplified experiment to measure gravitational acceleration. Epistemic uncertainty arises from uncertainty in the physical parameters of the experiment such as unknowing the precise length of the pendulum due to manufacturing tolerances or measurement errors. Consequently, measuring the distance traveled by the pendulum may be difficult due to a lack of knowledge. In addition, the variability in the material properties of the pendulum bob may introduce errors to the mass measurement of the pendulum, as well as the limitation in the time measurement. Another important source of epistemic uncertainty arises from neglecting the drag force of the system when considering the standard value for g of 9.8 ms^{-2} , where in reality the air resistance could be measured and incorporated to reduce the uncertainty. Meanwhile, for the same experiment, the aleatoric uncertainty arises from the inherent randomness in the

initial conditions and external disturbances, such as variations in the initial release angle or velocity of the pendulum with each run of the experiment. The imparted random disturbances in the motion of the pendulum are due to the presence of air currents or vibrations in the environment. Moreover, aleatoric uncertainty is a result of undetectable variations in the detection of the motion or time of release. Overall, even if we managed to eliminate the epistemic uncertainty by exactly setting and knowing the physical parameters a variation and variability in the measured values of the gravitational acceleration across repeated trials of the experiment would be repeated due to the aleatoric uncertainty.

Distinguishing between epistemic and aleatory uncertainties directly during system data and parameter analysis is not straightforward. This challenge creates a third category known as mixed uncertainty [88, 99, 101]. Classifying uncertainties into aleatoric, epistemic or mixed uncertainty depends on the perspective from which the system is observed [102, 103]. There is, however, a wide variation between researchers when it comes to identifying and classifying different types of uncertainty. Based on the literature, it is evident that there are contrasting perspectives, for example, Enserink *et al.*, [101] characterise uncertainty based on knowledge as only epistemic and aleatory. In contrast, Der Kiureghian and Ditlevsen [103] argue that this classification is not general but context-driven, where the classification depends on the purpose and application of the computational model under consideration. This alternative viewpoint suggests further characterisation or the adoption of different terminologies, particularly for uncertainty associated with computational frameworks guided by the target QoI. Another classification presented by Kirchner *et al.*, [98] and Walker *et al.*, [99] indicates that broadening the characterisation of uncertainty can involve defining and manifesting them at different levels within the model itself. Characterising uncertainties based on their level indicates that uncertainties are defined as a broad spectrum ranging between known and unknown, encompassing systematic or random statistical uncertainties. The spectrum of knowledge starts with deterministic knowledge and goes to total ignorance. Deterministic knowledge represents uncertainties that can be expressed using statistical methods, including probability theory, bounds, means and standard deviation. This type of uncertainty is associated with any part of the model where the deviation from the reference values can be statistically characterised [98, 99]. Conversely, total ignorance refers to uncertainty directly linked to a lack of knowledge about the system, which arises from poorly understood phenomena or complex interactions among multiple variables. A clear indication of recognized ignorance is the absence of understanding regarding the model's functional relationships and mechanisms. This level of uncertainty can be divided into two sub-levels: reducible and irreducible ignorance. Reducible ignorance entails diminishing uncertainty through enhancing knowledge through an exploratory approach, including additional experiments and studies [98, 99, 102]. In contrast, irreducible ignorance represents indeterminate uncertainty that cannot be reduced. Overall, the total ignorance level is unlimited; in fact, this level cannot be quantified, and it is characterised by high uncertainty [98, 99, 101]. In addition, there is a system-based classification of uncertainty, where uncertainty is categorized in accordance with its location within a complex computational framework. This approach of classifying uncertainty based on its location is followed to highlight the importance of the uncertain locations within the complex computational frameworks, as can be seen in the work by Ricciardi *et al.*, [104], Qian *et al.*, [105] and Posch and Pilz [106].

Based on the discussion above, accurately characterising and managing uncertainty is a critical component of any reliable computational framework and it depends on the perspective of the physical system under consideration. Once the uncertainties have been identified and characterised, it is necessary to quantify them using UQ methods. These methods can be implemented forward or backward (inverse). Moreover, based on the modification levels of the mathematical model equations or source codes, UQ methods can be seen as intrusive and

non-intrusive methods [90, 107].

2.2.3 Forward and backward uncertainty quantification

Forward UQ and Backward (or Inverse) UQ are the main two approaches to dealing with uncertainty in computational frameworks. Figure 2.3 illustrate the information flow of the UQ analysis for both forward and backward UQ analysis.

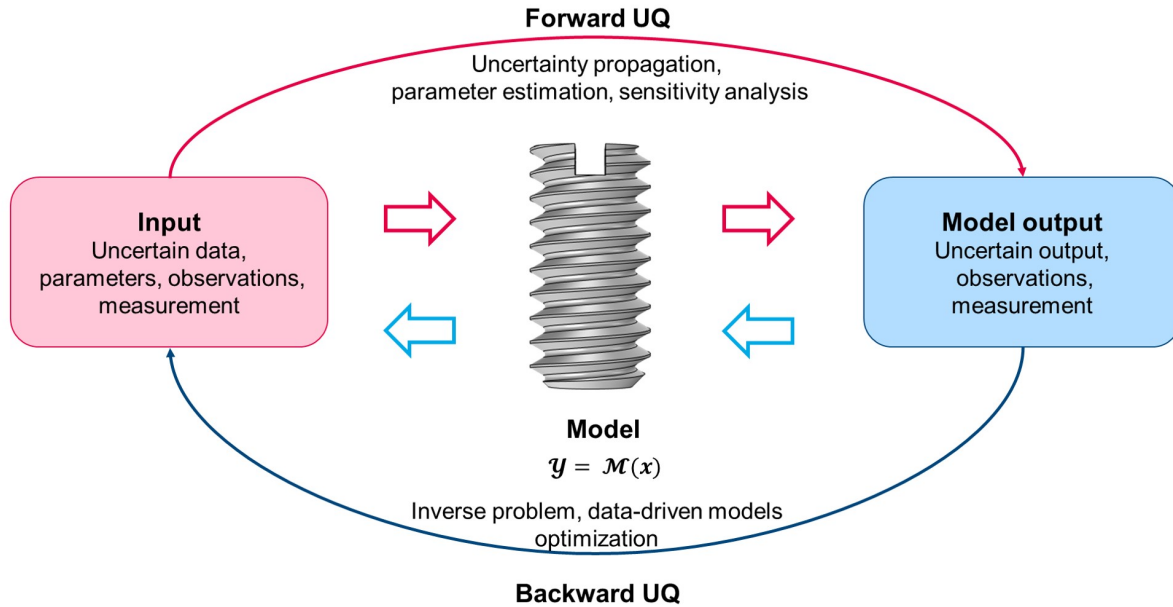


Figure 2.3: Forward and backward uncertainty quantification.

Forward UQ, Figure 2.3 green lines, refers to the flow of uncertainty information from the input to the output through the computational models and how it is propagated within the computational framework [90, 108, 109]. The main aim of Forward UQ is to quantify the range of possible model predictions while considering uncertainty in its inputs [108]. This is typically done through methods like Monte Carlo simulation, Latin Hypercube Sampling (LHS) and Polynomial Chaos Expansion. Moreover, further optimization is performed to find the optimal input parameters that minimize the discrepancy between the model and the observed data. This involves developing quantitative measures of the discrepancy using error metrics, goodness-of-fit, statistical analysis, calibration, sensitivity analysis as well as model validation [91, 108–110].

Forward UQ can be formulated mathematically by representing the uncertain input parameters μ as random variables with known probability distributions, $\mu \sim p(\mu)$. Then the input uncertainty is propagated through the computational framework (\mathcal{G}) to obtain the probability distribution of the output (QoI), $y_{QoI} = \mathcal{G}(\mu)$. At the end of the analysis, it is possible to compute the statistical properties of the output, such as mean, variance, and sensitivity indices. For this the mathematical presentation of the joint probability density function of the input parameters $p(\mu)$ and the probability density function of the output $p(y)$ is given by

$$p(y) = \int p(\mu) \delta(y - \mathcal{G}(\mu)) d\mu. \quad (2.1)$$

On the contrary, in *backward UQ* the uncertainty information flows backwards from the output to the input through the computational models (Figure 2.3, in blue). Backward UQ methods aim

to match model predictions with observed or experimental measurement data. In this case, the probability distribution of the input parameters is gathered during the simulation process. By adjusting and optimizing the combination and ranges of input parameters, Backward UQ methods quantify the agreement between a computational model's output and measured data. As for forward UQ, this involves optimization or Bayesian inference methods to find the best-fit parameters that minimize the discrepancy between the model and the observed data [90, 108, 109]. For example, the Bayesian inference method establishes a prior distribution, which reflects the assumption of what distribution best describes the model's parameters, and subsequently uses observed data to update this distribution, which is known as the posterior distribution. The posterior distribution is used to quantify the uncertainty associated with parameters and predictions [111, 112]. Mathematically this can be presented by the random input parameters μ but unlike forward UQ here μ have unknown probability distributions. Assuming that y_{data} is the observed (experimental) data with a normal error, then the likelihood function, which models how likely the observed data is given the parameter μ is defined as Likelihood $p_{like}(y_{data} | \mu)$ and given by

$$p_{like}(\mu | y_{data}) = \mathbb{N}(y_{QoI}(\mu), \sigma_{observed}^2) \quad , \quad (2.2)$$

where y_{QoI} is the output (solution) of the model, with parameter μ and $\sigma_{observed}^2$ is the standard deviation of the observed data. To update the uncertainty in μ the posterior distribution is required, computing it using Bayes' theorem resulted in

$$p_{like}(\mu | y_{data}) \propto p_{like}(y_{data} | \mu) p(\mu) \quad , \quad (2.3)$$

where $p_{like}(\mu | y_{data})$ is the posterior probability density function of the input parameters given the observed data y_{data} , $p_{like}(y_{data} | \mu)$ is the likelihood function, and $p(\mu)$ is the prior probability density function of the input parameters. Based on the posterior distribution in equation 2.3 it is possible to perform statistical analysis to estimate the most likely value for μ based on the observed data y_{data} .

A simplified formulation of forward and backward UQ can be presented by applying the concepts to the simplified experiment of measuring the gravitational acceleration. If the following computational model for measuring g is assume

$$g = \mathcal{G}(L, m, t) \quad , \quad (2.4)$$

where L is the distance traveled by pendulum in meters, m is the mass of the pendulum bob in kilograms and t represents the time in seconds. Here, L , m and t are uncertain input parameters. In terms of forward UQ methods, this system can be expressed mathematically as follows

$$L, m, t \sim p(L, m, t), \quad (2.5)$$

$$g = \mathcal{G}(L, m, t), \quad (2.6)$$

$$p(g) = \int p(L, m, t) \delta(g - \mathcal{G}(L, m, t)) dL dm dt, \quad (2.7)$$

where $p(L, m, t)$ is the joint probability density function of the input parameters and $p(g)$ is the probability density function of g . While for backward UQ, we need to infer the probability distributions of the uncertain input parameters given measured data of g . The prior distributions of input parameters are

$$L \sim p(L), \quad (2.8)$$

$$m \sim p(m), \quad (2.9)$$

$$t \sim p(t). \quad (2.10)$$

If the prior distributions in equations 2.8-2.10 are assumed to have a Gaussian distribution with a mean of μ and variance of σ^2 , the prior distributions are denoted as

$$L \sim \mathcal{N}(\mu_L, \sigma_L^2), \quad (2.11)$$

$$m \sim \mathcal{N}(\mu_m, \sigma_m^2), \quad (2.12)$$

$$t \sim \mathcal{N}(\mu_t, \sigma_t^2), \quad (2.13)$$

here, the joint prior distribution is given by

$$p(L, m, t) = p(L) p(m) p(t). \quad (2.14)$$

Assuming the measurement of g is also following a Gaussian distribution, then the likelihood function $p_{\text{like}}(g_{\text{observed}}|L, m, t)$, which represents the probability of observed g (g_{observed}) given the input parameters is given by

$$p_{\text{like}}(g_{\text{observed}}|L, m, t) = \mathcal{N}(g; \mathcal{G}(L, m, t), \sigma_g^2), \quad (2.15)$$

where σ_g^2 is the variance and $\mathcal{G}(L, m, t)$ is the forward model for g . The posterior distribution for this system using Bayes' theorem, given the input parameters and observed data g is given as

$$p(L, m, t | g_{\text{observed}}) \propto p(g_{\text{observed}} | L, m, t) p(L, m, t) \quad , \quad (2.16)$$

by substituting the likelihood expressions equation 2.15 into equation 2.16 we get

$$p(L, m, t | g_{\text{observed}}) \propto \mathcal{N}(g; \mathcal{G}(L, m, t), \sigma_g^2) \mathcal{N}(L; \mu_L, \sigma_L^2) \mathcal{N}(m; \mu_m, \sigma_m^2) \mathcal{N}(t; \mu_t, \sigma_t^2). \quad (2.17)$$

Based on equation 2.17 the uncertainty in the inputs can be updated by computing various statistics, *i.e.* the posterior mean, variance and confidence interval.

For addressing uncertainty in computational frameworks, both forward and inverse UQ methods are essential, providing insights into the range of possible inputs and improving accuracy and reliability. However, backward UQ methods are more complex than forward UQ and therefore require higher computational power. This is also reflected in the simplified example of pure Mg degradation. It is the forward UQ methods and analysis that will be the focus of the current thesis.

2.2.4 Non-intrusive and intrusive uncertainty quantification

Two distinct approaches are used to address uncertainties in the computational framework: *intrusive* and *non-intrusive* UQ methods. Figure 2.4 presents a schematic diagram illustrating the distinction between implementation of UQ using intrusive (red lines) and non-intrusive (light blue lines) methods. Defining a forward UQ problem (dark blue lines, Figure 2.4), starts by defining the QoI, discretization the mathematical model to build the numerical model, then identifying the sources of uncertainty within the system. The intrusive UQ methods (red lines) involve modifying the mathematical equations of models or the source codes of numerical models to incorporate uncertainty-related parameters directly, also referred to as stochastic parameters [113–115].

Consider a simplified case of pure Mg degradation under physiological conditions, the degradation can be assumed to be governed by the diffusion of Mg^{2+} ions from the implant surface within the degradation medium. In this case the uncertain parameter is the diffusivity of Mg^{2+} ions, and the governing equation is

$$\frac{\partial c_{\text{Mg}}}{\partial t} = -\nabla \cdot (D_{\text{Mg}} \nabla c_{\text{Mg}}) \quad , \quad (2.18)$$

where c_{Mg} and D_{Mg} are the Mg concentration and the diffusion rate constant, respectively. If D_{Mg} is assumed to follow a Gaussian distribution with a mean of μ and a standard deviation of σ , i.e., $D_{Mg} \sim \mathcal{N}(\mu, \sigma^2)$. Under intrusive UQ, this model will be modified by incorporating uncertainty directly into the model by considering D_{Mg} as a stochastic process. The modified model equation 2.18 is given by

$$\frac{\partial c_{Mg}}{\partial t} = -\nabla \cdot (D(t)\nabla c_{Mg}) \quad , \quad (2.19)$$

where $D(t)$ is a stochastic process modeling D_{Mg} 's temporal evolution. A simplified modification can be done using the Ornstein-Uhlenbeck process, which is a stochastic process that uses a random number generator to describe the mean-reverting behaviour and incorporating it directly into the mathematical or numerical models [116, 117], and $D(t)$ is given as

$$\frac{dD}{dt} = -\alpha(D - \mu) + \sigma\zeta(t) \quad , \quad (2.20)$$

where α and ζ are decay rates and white noise processes, respectively. Intrusive UQ converted the biodegradation model presented in equation 2.18 to account only for the stochastic nature of $D(t)$.

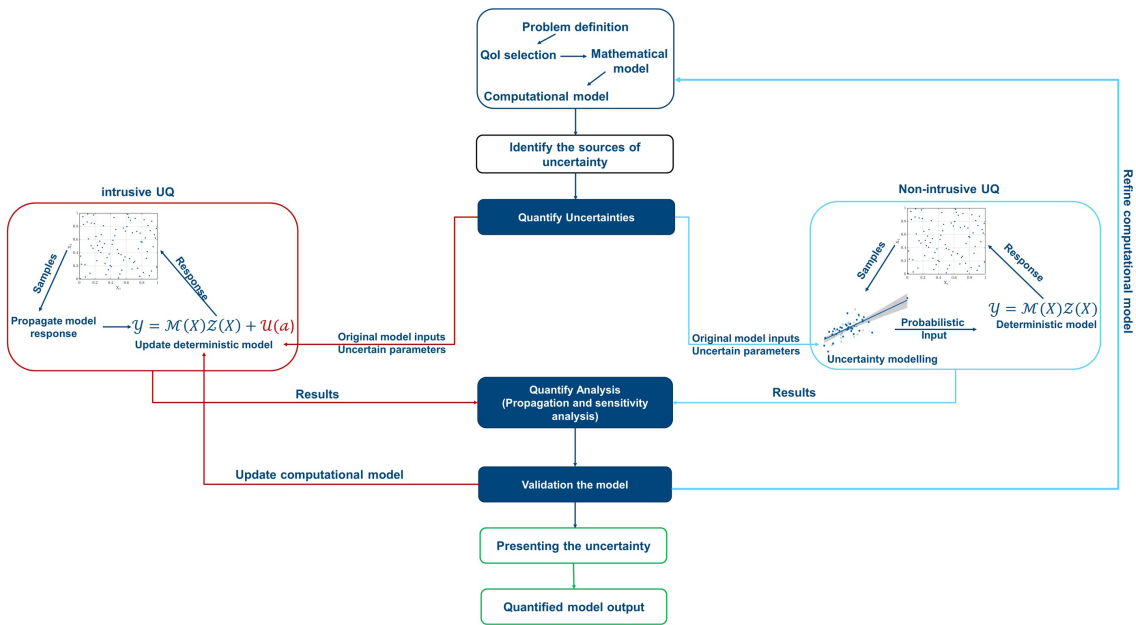


Figure 2.4: Forward intrusive (red lines) and non-intrusive (blue line) quantification analysis.

The intrusive modification allows for UQ analysis at various simulation stages, and entails the embedding of uncertainty propagation within the computational framework [114], as illustrated in Figure 2.4. However, intrusive methods can significantly increase complexity when dealing with intricate model equations or extensive source codes [107, 114]. Several methods have been developed and adapted for this analysis, largely focusing on the spectral expansion of stochastic variables, as detailed in Le Maître *et al.*, [113]. One popular example of this approach is the stochastic Galerkin method. Due to its intrusive nature, this approach necessitates modifying and developing stochastic models based on the fundamental principles of the study system. When the number of uncertain quantities increases, the size of the stochastic system also grows, as it requires code modification to evaluate model functions [113, 114]. The extensive discussion of these complex modifications and developments is beyond the scope of this thesis. A more detailed discussion can be found in [114, 118].

In general, longer computational times and increased CPU (cores per CPU) usage are often required, especially for large nonlinear or complex partial differential equation (PDE)-based models [90, 115], which is one of the significant drawbacks of intrusive methods. Moreover, these methods are limited by source code availability. For instance, adapting these methods to quantify uncertainties becomes unfeasible if the source codes are commercial or not accessible to end users, such as COMSOL, Fluent, OpenFOAM codes. Non-intrusive UQ methods have been developed to overcome intrusive methods' limitations. These methods treat computational models as *black-box models*, which refer to models in which computational models are perceived as inputs and outputs by an analyst [119].

Non-intrusive UQ methods, illustrated in Figure 2.4 (light blue lines), eliminate the need to reformulate equations or modify the model's source codes for quantifying associated uncertainties. Instead, they rely on sampling techniques, which sample the model's input space and evaluate its responses without altering its internal structure. Furthermore, these methods provide a more flexible and adaptable method for reconstructing the statistical properties of uncertainty through the use of multiple iterative deterministic simulations [49, 90, 107, 114]. In addition, these methods separate computational model evaluation and UQ analysis, as illustrated in Figure 2.4, which simplifies the implementation of these methods and reduces computational time, CPU and memory usage [114].

Throughout the current thesis, non-intrusive forward UQ methods are implemented. Non-intrusive forward UQ methods and tools effectively handle high-dimensional problems and reduce the computational burden associated with intrusive methods [43, 49, 114]. Most importantly, non-intrusive forward UQ methods are more efficient when dealing with highly sensitive models because they provide a non-invasive analysis without interfering with the original model's functionality or behaviour. Therefore, non-intrusive UQ methods are effective in quantifying uncertainty associated with biodegradation models.

2.3 Quantifying uncertainty in complex biodegradation models

As mentioned before, uncertainty is categorised as aleatory and epistemic. However, for a complex computational framework, as is the case for modelling the degradation of biodegradable implants, it is more convenient to deal with uncertainty based on the specific locations, namely input, model and output uncertainty. Considering the complexity of degradation models, this systematic classification would facilitate the quantification and description of forward uncertainty.

Input uncertainty is one of the most influential factors in computational models. It is primarily associated with the observed data that describe the physical system [88, 99]. When deviations from the physical system are observed and linked to the model's parameters, it is referred to as parameter uncertainty. Parameter uncertainty represents the inherent variability in parameters or the lack of knowledge about the true values of the model's key parameters [104–106]. Model input includes uncertain parameters, boundary and initial conditions and experimental measurements of physical properties (physical constants), e.g. density, molar mass, mass and heat capacity. Additionally, some model parameters are assumed to have constant values, which can be based on previous studies, empirical equations of state, and constitutive models, or are not directly measured, such as geometry, reaction rates, and transport properties [88, 100, 120]. However, it is crucial to acknowledge the deterministic nature of constant and exact parameters within the model input, as these parameters have negligible uncertainty, which is known or minimal uncertainty, examples of exact parameters include universal con-

stants such as the ideal gas constant R , π and e [59, 88]. Biodegradation models can consider input and parameter uncertainty in terms of implant material properties, such as density, porosity, the geometry of the implants as well as the boundary and initial conditions. For example, Jia *et al.*, [79] investigated the influence of geometrical factors on the degradation of AZ91D magnesium alloy in contact with mild steel. According to the Boundary Element Method (BEM) model, the distribution of current density in this study was similar to that observed experimentally. There was, however, a significant difference between experimental and field degradation rates. This deviation was the result of simplifying the geometry. For the same model, better agreement was achieved in a study by Lacroix *et al.*, [121], in which a realistic geometry was integrated and normal and radial components of the current distribution were calculated. Moreover, reliable literature values for parameters would not have a significant impact on the accuracy of the model. This can be seen in the biodegradation model derived in Zeller-Plumhoff and Albaraghteh *et al.*, [45], where only eight key parameters of the model were optimized, but several model parameters were taken from literature, such as molecular weights, density and diffusion coefficient. Moreover, this model considered the constant porosity of the degradation layer and its value was adopted from previous experimental studies for the same degradation systems. A similar approach was followed by Barzegari *et al.*, [75], where only three model parameters were optimized, while the rest of the parameter values were obtained from the literature.

Model uncertainty represents the second primary source of uncertainty. In the scope of this thesis, model uncertainty is categorized into mathematical model uncertainty and discrete (numerical) model uncertainty. The conceptualization, hypotheses, simplifications, and numerical approximations applied to mathematically represent the physical system introduce uncertainty into the computational models [47, 88, 122, 123]. Additionally, model uncertainty encompasses the uncertainties of variables and precisely defined parameters as evaluated by the model equations [59, 88]. Typical examples of this uncertainty associated with biodegradation models include assumptions of a homogeneous degradation layer, uniform degradation and simplifications related to the composition of the degradation media or degradation layer. As an example, phenomenological and physical biodegradation models of AZ31 Mg-based stents derived by Grogan *et al.*, [124, 125] have reported high uncertainty regarding an analytical formula when fitted to experimental data. The deviation in the predictions is a result of the derived mathematical models. While the physical model predicted a greater mass loss on the outside of the hinge and a smaller mass loss on the inside of the hinge, the phenomenological model observed non-local mass transfer [19]. Discrete model uncertainties, which are associated with discrete or numerical models are primarily induced by model structure and computational resources. Due to this, in some UQ terminologies, this uncertainty is referred to as model technical uncertainty [126–128]. In forward UQ, model technical uncertainty contributes to discrete model uncertainty and uncertainty propagation through the computational framework [126–128]. The numerical treatment, the accuracy (resolution) of the discretization method, and the numerical parameters contribute to the model's technical uncertainty. Moreover, the discrete model uncertainty is propagated by imposing mathematical formulations, numerical schemes for the solutions and discretization over time and space of the mathematical model [47, 88, 122]. Furthermore, the limitations of computing resources contribute to both model uncertainty by restricting the number of calculations, sufficient model evaluations and the computational capacity needed for further analyses; *i.e.* sensitivity analysis, Bayesian and bootstrap methods for parameter estimation, and model reliability analysis [97, 127, 129]. Within biodegradation models, discrete model uncertainty can be induced by the type of numerical schemes used to solve the mathematical equations or the implementation method of the model using different programming languages or commercial software (e.g. COMSOL).

An additional location for uncertainty is the output uncertainty, which is the cumulative uncertainty associated with all other locations within the computational framework, reflecting the propagated uncertainties in the model's predictions. In some cases, when the true values of the QoI are known, this is referred to as prediction error. However, this scenario is not always applicable since computational models often explore a broader prediction range than known or experimentally reported scenarios. For example, Albaraghteh *et al.*, [65] extended the biodegradation model up to 100-days for both *in vitro* and *in vivo* tests, however, the experimental data is only available for 56-days and 85-days for *in vitro* and *in vivo*, respectively. In such cases, output uncertainty is described as an interval in a specific range rather than a specific numerical value. This interpretation needs to be chosen carefully to avoid introducing more uncertainty to the output of the computational framework. More details are presented in **Chapter 5** of this thesis. However, output uncertainty can be reduced through additional calibration and optimization tasks, as well as quantifying the uncertainties associated with other parts of the computational framework [97, 99]. A typical example of output uncertainty within biodegradation models is the deviation between the prediction of the biodegradation models and the experimentally reported degradation behaviour of the implant, and the prediction error within QoI, i.e. degradation rates, volume loss, or mean degradation depth, based on the predicted values of the QoI and the observed experimental values for the same quantity under similar conditions. For example, the biodegradation model of commercially-pure Mg presented in Barzegari *et al.*, [75] was able to simulate the pH change in NaCl and SBF solutions with an error of 5%, while the degradation rate was predicted by the biodegradation model derived in Zeller-Plumhoff and Albaraghteh *et al.*, [45] of pure Mg in SBF with an error of 7% with respect to experimental data. Similar percentage of error was reported by Deshpande [82] for the biodegradation model investigating the micro-galvanic degradation and the effect of different metallic phases present.

In addition to uncertainty associated with the mathematical framework, uncertainty is inevitable in the experimental data used to calibrate and validate computational models. This type of uncertainty is known as measurement uncertainty and it is caused by measurement system errors and noise [130, 131]. It should be taken into account in the analysis of the outputs of the computational framework. For example, in biodegradation models, measurement uncertainty, in terms of standard deviation, is higher in *in vivo* testing compared to *in vitro*, which is due to the complexity of the system and limited data points available [26, 132]. It is important to note that this deviation affects the validation of biodegradable models as well. Biodegradation models of *in vivo* testing presented by Montoya *et al.*, [133], Gartzke *et al.*, [134] and Sanz-Herrera *et al.*, [74] only reported qualitative measurements.

Building upon the preceding discussion, it becomes possible to quantify the uncertainty inherent in the computational framework by identifying its sources. Uncertainty is quantified through various UQ tools and methods, which will be discussed in detail in this thesis's upcoming section 2.4. However, the mathematical complexity of presenting the degradation system of biodegradable implants is a challenge. Assumptions and simplifications are necessary in order to construct discrete biodegradation models. These assumptions and simplifications contribute to additional uncertainty within the computational framework. To address this challenge, biodegradation models must consider various testing scenarios [19, 85]. These scenarios are developed by combining different assumptions and ranges of the main factors and key parameters that have been identified as influential on the degradation process. Each scenario includes a range of potential model responses [99]. This approach is referred to as scenario modelling and it is a qualitative quantification that aims to bridge the gap between deterministic knowledge and total ignorance, as discussed in the previous section 2.2.2. Scenario modelling enables the testing of scenarios that have not been tested yet in the experiments. Walker *et al.*, [99]

define scenario as "a scenario is a plausible description of how the system and/or its driving forces may develop in the future". This definition indicates that a scenario is directly linked to a set of assumptions describing key relationships and driving forces. However, scenarios are not intended to predict the future, but rather provide a spectrum of potential model outcomes. In biodegradation models, scenario modelling is implemented to create a correlation between biodegradation behaviour under *in vitro* and *in vivo* testing. In this case, different scenarios can be developed to create a set of assumptions describing key relationships between the different parameters that control the biodegradation, *i.e.* the variation in pH, concentration profiles of ions, or porosity or composition of the degradation layer. Moreover, scenarios related to parameter uncertainty will help in providing best-guess estimations based on the correlation between parameters and expert knowledge. These scenarios are accepted only if they define credible parameter ranges or incorporate conditional probabilistic features, as it is the case in creating a parametric space for the key biodegradation model parameters [135]. Moreover, scenarios related to model uncertainty can reveal various interactions and correlations within computational and numerical models. This can aid in the quantification of these uncertainties. Unlike quantitative quantification of uncertainty, scenario uncertainty, being qualitative in nature, cannot be presented with probabilities; instead, it can be presented as discrete possibilities [98, 99, 102]. Integrating UQ with various possible testing scenarios of the model yields a deeper understanding of uncertainties associated with the computational model's response. This, in turn, aids in developing robust computational frameworks that can withstand a range of potential responses [55, 56, 88, 89].

2.4 The presentation of uncertainty

Communicating the results of UQ analyses transparently and coherently within UQ is crucial to effectively presenting uncertainty. A variety of strategies can be used to address the issue of uncertainty, ranging from more straightforward approaches such as probability distributions, confidence intervals, and error metrics, which represent uncertainty as a deviation between the model predictions and the reference values (experiment or reference dataset), to more complex approaches, which involve combining predictions from multiple models to achieve enhanced accuracy in prediction and representation of uncertainty [52, 136–138]. UQ employs a variety of techniques, methods, and tools to assess the accuracy and reliability of computational models and simulation predictions.

Even though there are studies that have adapted these techniques to biodegradable implants, these studies have never been devoted to quantifying the uncertainty associated with computational models. The Bayesian inference method, for example, is one of the most commonly used techniques at UQ. Barzegari *et al.*, [75] employed Bayesian inference to minimize the number of optimization iterations to calibrate the key model parameters of the biodegradation model of Mg in both NaCl and SBF solutions. The calibration process required a cumulative of 120 optimization iterations with a computational cost of 276 hours of simulation execution time using 170 computing nodes for each simulation. Another frequently employed method is the Monte Carlo method (MC). MC methods are statistical sampling methods that involve running the computational model multiple times with varying input data sets to cover the assumed range of input parameters. The different data sets are generated from an assumed probability distribution of QoI through a large number of random samples. These data sets are then used to estimate a function's expected value or simulate a system. The resulting outputs enable the quantification of uncertainty in statistical measures such as mean and variance [43, 49, 139]. Chang *et al.*, [140] presented a three-dimensional model for semi-autonomous computational pitting corrosion based on MC method. Here, the degradation probability for each micro element was assessed at each time step and MC was used to identify elements with different

material characteristics from the surrounding conditions. The computational results obtained in this study were validated using micro-computed Tomography (micro-CT). Ensemble modelling can be utilized to measure uncertainty. These methods employ multiple supervised learning algorithms to enhance the model's predictive performance. This involves training the model with randomly resampled data from the original data sets. The prediction variability is subsequently estimated based on the resulting model [141–143]. This method was applied by Zeller-Plumhoff *et al.*, [70] to predict the degradation rate of pure Mg in SBF. In this study, random forests were compared with decision trees. The algorithm was evaluated 50 times using 21-fold cross-validation, divided into training and evaluation sets. Experimental experimental measured (*i.e.* initial and controlled pH, ion concentrations, precipitation rate, fluid volume to sample area ratio, weight percentage of precipitated elements) were tested to assess their influence on the degradation rate and derived mechanisms. The goodness of the regression was evaluated using mean squared error and mean absolute error.

In the context of the present thesis, three primary methods are employed to present uncertainty associated with biodegradation models. These methods include the Error metrics, which are used to assess the quality of the calibration process of different models. Errors can be seen as a mathematical representation of uncertainty [96]. Another significant tool at UQ is sensitivity analysis. These methods assess uncertainty by measuring the sensitivity of the model's output to variations in input parameters. Moreover, sensitivity analysis identifies parameters that substantially influence model predictions and identifies their interactions [60, 104, 128, 144]. Finally, uncertainty propagation, which is a tool that depends on the other UQ methods in use. Propagation analysis involves running the complex model several times for varying values of unknown parameters. By quantifying the propagation of input uncertainty through the mathematical or computational model, it is possible to quantify the propagation of uncertainties in the model's outputs and predictions [145, 146].

2.4.1 Error metrics

In general errors present uncertainty as the discrepancy between model predictions and actual values. The actual values, or in other terminology, the reference data set, could consist of experimental data, observations from optimized models or case studies [147]. The most commonly used error metrics are: *coefficient of determination* (R^2). R^2 measure the statistical proportion of the variance in the dependent variable that can be explained by the independent variable, mathematically it is calculated as

$$R^2 = 1 - \frac{\sum_{i=1}^N (y_i - \widehat{y}_i)^2}{\sum_{i=1}^N (y_i - \bar{y}_i)^2} \quad , \quad (2.21)$$

where y_i , \widehat{y}_i , \bar{y}_i are the observation (actual), the predicted (estimated) and the actual mean, respectively. N is the number of test samples. Overall, R^2 values range between 0 and 1. As the R^2 value approaches one it indicates a better fit and lower uncertainty associated with the model predictions [148, 149]. *The mean absolute error* (MAE), which presents uncertainty as an average measure of the absolute differences between predicted and actual values. MAE is suitable for assessing the overall accuracy of a system because it calculates the average errors without considering their direction [95, 150], mathematically MAE is calculated as

$$MAE = \frac{\sum_{j=1}^N |y_t - \widehat{y}_j|}{N} \quad , \quad (2.22)$$

The mean square error (MSE), which measures the average squared deviation between the estimated values and the actual values. This error can be seen as a risk function corresponding

to the expected value of the squared error loss and it is given by

$$MSE = \frac{1}{N} \sum_{i=1}^N (y_i - \widehat{y}_i)^2, \quad (2.23)$$

where y_i and \widehat{y}_i are the observation value and the predicted value, respectively. N is the number of test samples. Furthermore, a large MSE indicates that the data set is dispersed widely around its mean value. Moreover, since the errors are squared before they are averaged, MSE results in a relatively high weight for large errors. Due to this, it is better to use either the *root mean square error (RMSE)*, which is mathematically measured as the square root of MSE or *normalized root mean square error (NRMSE)*, which is given as [95, 150]

$$NRMSE_i = \frac{\sqrt{\frac{\sum_{j=1}^N (y_j - \widehat{y}_j)^2}{N}}}{y_{max} - y_{min}} \quad (2.24)$$

with y_{max} and y_{min} the maximum and minimum experimental values. Overall, MSE is preferred over MAE . In comparison to a non-differentiable function such as MAE , MSE is a differentiable function, which facilitates the application of mathematical operations. A model's fit to experimental data can be evaluated using $RMSE$, which is more straightforward to interpret than MSE since the $RMSE$ is measured in the same units as the response variable, whereas the MSE is expressed in squared units of the response variable [151, 152]. Moreover, within biodegradation models employing error metrics provides an adequate quantification of the deviations within the system and assesses the accuracy and reliability of the calibration process of the biodegradation models with respect to experimental or reference data.

2.4.2 Sensitivity analysis

Sensitivity analysis identifies and ranks uncertain model parameters significantly impacting its predictions, which help in simplifying the model by fixing unimportant input variables to their nominal values without affecting the reliability of the model [60, 104, 144]. Moreover, sensitivity analysis determines the variation in the uncertainty associated with QoI based on the variation in the uncertainty associated with each input parameter [153, 154]. In the literature, various sensitivity analysis methods are discussed. These methods are classified into three categories: sample-based methods, linearisation, and global methods.

Sample-based methods, which use post-processing after MC sampling. These methods are relatively simple and express the system's sensitivity as a correlation between input parameters and model output [60, 155]. The linearisation methods assume that the model is linear or can be linearised around a center value. Despite the fact that these models are simple and do not require a large number of model evaluations, they are ineffective at identifying non-linear behaviour and interactions between input variables at a higher level [60, 155]. The global methods, also known as global sensitivity analysis (GSA). GSA are desirable methods that measure sensitivity across the whole input space. Moreover, they can deal with nonlinear responses, and they can measure the effect of interactions in non-additive systems [60, 155]. In the last few years, attention has been drawn to Sobol decomposition and variance-based sensitivity indices, or simply known as Sobol indices [60, 153, 156–158]. To estimate the Sobol indices MC or Quasi MC (QMC) techniques are implemented, which is computationally expensive for complex models [158–160]. In this dissertation, however, the computational cost challenge motivated the development of more efficient methods. The mathematical presentation of Sobol decomposition and variance-based global sensitivity indices is explained in a review by Chang *et al.*, [60] and can be summarised as follows: assuming a computational model $y = g(\mathbf{x})$ with

n-dimensional input variable $\mathbf{x} = (x_1, x_2, \dots, x_n)$. According to Sobol sensitivity analysis, the total variance of model output y is attributable to each input variable, taking into account their interactions. To simplify the mathematical presentation in this thesis, the computational model is assumed as a square-integrable function, which can be decomposed into 2^n orthogonal functional terms of increasing dimensions as [60, 161, 162]

$$g(\mathbf{x}) = g_0 + \sum_{i=1}^n g_i(x_i) + \sum_{1 \leq i < j \leq n} g_{ij}(x_i, x_j) + \dots + g_u(x_1, \dots, x_n) \quad , \quad (2.25)$$

where $u \in [1, \dots, n]$ and

$$\begin{aligned} g_0 &= \int g(\mathbf{x}) \prod_{k=1}^n f_{X_k}(x_k) dx_k \quad , \\ g_i(x_i) &= \int g(\mathbf{x}) \prod_{k=1, k \neq i}^n f_{X_k}(x_k) dx_k - g_0 \quad , \\ &\vdots \\ g_u(x_1, \dots, x_n) &= g(\mathbf{x}) - g_0 - \sum_{i=1}^n g_i(x_i) - \sum_{1 \leq i < j \leq n} g_{ij}(x_i, x_j) - \\ &\quad \dots - \sum_{i=1}^n g_{\sim i}(\mathbf{x}_{\sim i}) \end{aligned} \quad (2.26)$$

here $f_{X_k}(x_k)$ is the probability density function of x_k and $\mathbf{x}_{\sim i} = (x_1, \dots, x_{i-1}, x_{i+1}, \dots, x_n)$. The decomposition of the total variance of $g(\mathbf{x})$, takes into account the orthogonality of the component functions in equation 2.25,

$$V = \sum_{i=1}^n V_i + \sum_{1 \leq i < j \leq n} V_{ij} + \dots + V_u \quad , \quad (2.27)$$

where V , V_i are the total variance of $g(\mathbf{x})$ and the partial variance contribution of x_i , respectively. And V_u is the interactive variance contribution of parameters x_u , which quantifies the interactions among x_u [60]. Results for Sobol decomposition are expressed by two sensitivity indices: the Sobol' first order sensitivity indices S_i , given by equation. 2.28b, which indicates the importance of each parameter considered individually by measuring the individual variance contribution of x_i to the total variance (equation 2.27). While the total sensitivity indices S_{T_i} is determined by the equation. 2.28c, which accounts for the importance of individual parameters and interactions between parameter pairs [161]. Moreover, S_{T_i} is defined as the sum of all partial sensitivity indices S_u (equation. 2.28a) involving variable i .

$$S_u = \frac{V_u}{V} \quad , \quad (2.28a)$$

$$S_i = \frac{V_i}{Var(V)} \quad , \quad (2.28b)$$

$$S_{T_i} = S_i + \sum_{j \geq 1} S_{ij} + \dots + S_u = 1 - S_{\sim i} \quad , \quad (2.28c)$$

where $S_{\sim i}$ is the sum of all partial sensitivity indices S_u except S_i . Sobol' indices are computed using MC-based methods [161, 163]. Where the model is evaluated $N(d+2)$ times, where d is the number of parameters and N is a numerical variable of the order of hundreds or thousands of runs. For complex models the computational cost increases drastically due to the dependency of Sobol indices over computationally expensive MC methods [60, 139, 161].

2.4.3 Uncertainty propagation

In the forward UQ, uncertainty propagation aims to quantify how the input uncertainty propagates through the computational framework, ultimately affecting the uncertainty of the output QoI [164–167]. Quantification workflows contribute to uncertainty propagation by identifying uncertainties and their sources within the computational framework as well as testing several uncertainty scenarios associated with the computational framework [98, 167, 168]. Moreover, performing sensitivity analysis, which involves exploring different scenarios of uncertain input and observing the variation in the output associated with the tested scenario, helps in simplifying the tracking of uncertainty propagation and optimizing efforts to mitigate their impact [139, 169]. For simple computational models possessing analytical forms, uncertainty propagation can be executed by calculating the statistical quantities of the QoI; *i.e.* mean, variance and covariance matrices. Methods such as Taylor series expansion can be used to perform the statistical calculations. However, for complex computational frameworks, uncertainty propagation is expressed in terms of probability of failure and probability density functions (PDF), which need special numerical methods *i.e.* polynomial chaos expansion (PCE) and or Monte Carlo methods [164, 168, 170].

Uncertainty propagation in complex systems is important to efficiently identify uncertainty arises from intricate relationships between key parameters, including nonlinear transformations, feedback loops and complicated data flow [169, 171]. Most uncertainty propagation methods, such as MC simulations, PCE, LHS and sensitivity analysis, are sample-based. With an increasing complexity and dimensionality of the model, performing the uncertainty propagation analysis becomes increasingly challenging due to the need to generate a large number of random samples based on the PDF of uncertain inputs [164–166]. For example, to test various scenarios of a computational model, MC simulations generate a large number of samples based on the PDF of input parameters to identify potential outcomes [98, 172]. Despite the high computational cost of MC simulations, they are particularly valuable in the case of correlated input parameters, which require dealing with complex probability distributions. Due to the flexibility of MC methods, they are suitable for handling high dimensional problems as well as nonstandard distributions, particularly in the case of joint probability distributions of correlated parameters [163, 173]. In contrast, LHS requires a smaller number of random samples for each uncertain input parameter. The reason for this can be explained by the fact that LHS distributes samples more evenly across the probability distributions, making it computationally more efficient than MC [139, 174, 175]. Various methods can be used to visualise the propagation of uncertainty, including error metrics, sensitivity plots (bar, scattered or linear plots), histograms, kernel density estimates, PDF plots or cumulative distribution functions. To compare the spread of predictions for different scenarios, box plots may also be used [56, 90]. Uncertainty propagation has also been shown to be an important concept in the design of scientific instruments, the analysis and post-processing of experimental data, in order to determine the reliability of test results [145, 146, 168, 176]. This approach is not directly applicable to experiments related to biodegradation due to the high cost and time required. However, it ensures that a certain level of accuracy is achieved by eliminating impossible scenarios from the calculations. Moreover, during the design of an experiment it is possible to utilize uncertainty propagation to ensure a minimum number of measurements and samples [145, 168].

2.5 Challenges and limitation of UQ

Constructing UQ problems typically involves modelling complex systems with several correlated uncertain parameters. UQ analysis is directly impacted by the quality and quantity of the data and information available in these models. Therefore, a number of challenges and limitations

remain in order for UQ to achieve its full potential.

In general, two significant challenges emerge when dealing with complex computational models such as biodegradation models. The first challenge is the high computational costs, as, in general, UQ analyses require significant computational resources. These costs are primarily due to the significant amount of simulation time, memory usage and processing power required to run the UQ analysis on complex models as well as the limitations of the computational resources available for these analyses [49, 56]. Computational cost is directly proportional to the number of uncertain parameters and computational model complexity. The complexity of the computational model increases as the number of uncertain parameters increases. Therefore, computational costs can become prohibitively expensive even in the current state-of-the-art super-computing infrastructure [59, 177, 178]. Additionally, the efficiency and accuracy of UQ analysis are impacted by computational limitations, which restrict comprehensive uncertainty exploration. This is because UQ analysis includes running multi-scale and complex simulations or numerical optimization, contributing to a substantial computation burden. Consequently, this limitation results in approximation and computational errors that affect model prediction accuracy. Moreover, this challenge can restrict the scale of the models that can be analyzed and the level of detail that can be included in the UQ analysis [59, 172, 177, 178].

The second challenge encountered is the curse of dimensionality, which refers to the exponential increase in computational complexity as the number of parameters or dimensions grows [56, 167]. More precisely, the curse of dimensionality refers to the exponential increase in the amount of data required to cover the space of possible outcomes of the model as the number of uncertain key variables (dimensions) increases [179]. In general, physical phenomena can be described through highly nonlinear computational models. Overall, these models can be characterized by multiple key inputs and multiple outputs, in which complex interactions can be observed. This means the number of key parameters greatly impacts the number of model runs [179, 180]. Therefore, it is imperative to minimize the number of key parameters by excluding parameters that do not significantly affect model predictions. This will reduce the curse of dimensionality [181]. However, it is critical to keep in mind that the lack of reliable data in this case can lead to overfitting, where the models are fitted to noise rather than the actual data. In contrast, underfitting may result from too simplified models, which miss significant data patterns [179, 180].

It is difficult to identify uncertainty sources within complex systems under these challenges, which affect the implementation of UQ methods and hence the quantification process. In conclusion, it is essential to overcome these challenges to fully utilize and effectively apply UQ techniques in biodegradation systems. Consequently, a trade-off must be made between the complexity of the model, the quality and quantity of the data obtained, and the availability of computational resources. Up-to-date, several studies have been conducted on developing more efficient algorithms and techniques for model analysis, simplified modelling and efficient dealing with high-dimensional data [181, 182]. Furthermore, within the UQ field, attention is driven by exploring new methods for data acquisition and analysis to improve input data accuracy and reliability as well as to improve UQ methods efficiency and make them more scalable for larger models [56, 167, 179, 182]. The current thesis utilizes the surrogate modelling approach to reduce the complexity and computational load of biodegradation models, allowing UQ analysis to be performed.

2.6 Surrogate models

Surrogate models, also known as *metamodels*, are a series of easy-to-evaluate functions that approximate complex and computationally expensive models while maintaining high prediction accuracy [58, 65, 107]. The concept of surrogate modelling represents a widely adopted non-intrusive strategy intended to tackle the computational complexities inherent in classical UQ analysis, which arises from common general-purpose methods requiring repeated iterative model assessments under UQ analysis and scenarios [59, 107]. Through the utilization of a limited dataset containing input values and their corresponding responses, surrogate models are capable of mapping the behaviour of the original computational model, treated as a black-box [58, 65, 107, 180]. Replacing computationally expensive and complex models with a surrogate model allows UQ analysis at a reasonable time and computational cost [65, 183]. Furthermore, the use of a black-box model eliminates the mathematical complexity of complex behaviours and interactions among sub-models, rather it focuses on capturing the QoI behaviour modelled by the original model [58, 65, 119, 183].

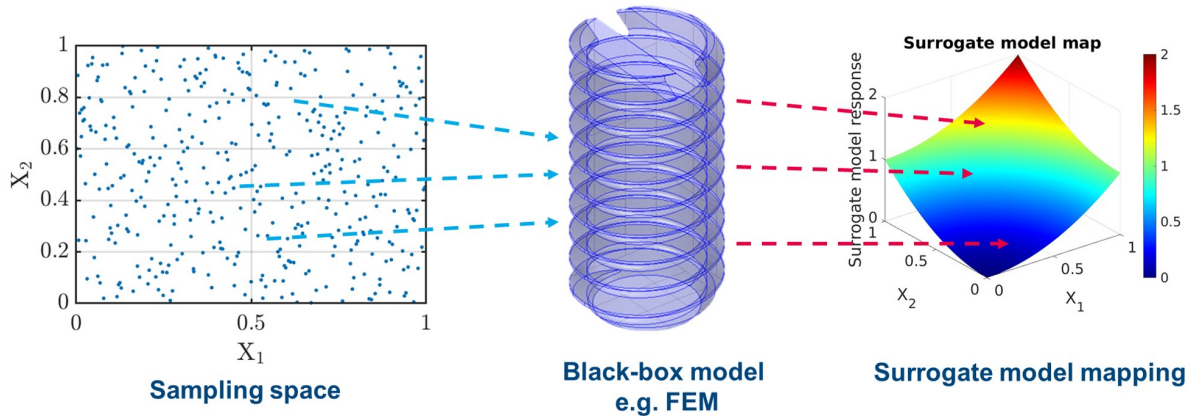


Figure 2.5: Schematic diagram of the construction of a surrogate model for a system characterised by two input parameters.

The construction of surrogate models is summarised in Albaraghteh *et al.*, [65] as “The training data for the surrogate model consist of a set of input parameters and their corresponding responses, which are collected by sampling the input distribution in the parametric space of the input parameters. The sampled parameter combinations are evaluated using an expensive computational model, and the resulting observations are exploited to build the surrogate model on the whole domain of the input distribution”. A visual summary of constructing a surrogate model for a FEM system characterised by two input parameters, denoted as X_1 and X_2 , is presented in Figure 2.5. It is imperative to clarify that surrogate models are non-physical functional approximations that do not preserve any specific mechanisms of the original systems [183, 184]. Nevertheless, surrogate models are trained to identify critical parameters and their associated physical phenomena while understanding the input-output relationships. This approach enhances predictive accuracy and reliability, distinguishing itself from purely data-driven models, ultimately enhancing the robustness of the constructed surrogate model [185–187].

From an abstract mathematical point of view, the core objective in constructing a surrogate model is to learn and map the response of a computationally expensive black-box model to variations in its uncertain input parameters, while minimizing the cost per model evaluation [187]. The general equation describing a surrogate model is [59]

$$y = \mathcal{M}(\mathbf{x}) \quad , \quad (2.29)$$

where \mathcal{M} is the surrogate shape function that maps the black-box model for the input parameters $f(\mathbf{x})$, which is presented as a vector $\mathcal{M}(\mathbf{x}) \in \mathcal{D}_x \subset \mathbb{R}^M$, to a vector of QoI, which is denoted by y . The key idea of implementing this approach is to calibrate the surrogate model based on the assumptions related to y using a limited number of model runs of the black-box model \mathcal{M} for selected values of the input parameters $\mathbf{x} = (x_1, x_2, \dots, x_n)$, this is known as *experiment design*. Intuitively, the runs should cover the parametric space of the input parameters \mathcal{D}_x [59, 188].

2.6.1 Classification of surrogate models

Surrogate models are presented and used in the literature in different forms. These models can be classified based on their types, the data required to construct them or training strategies. Further classification is done based on the specific applications of these models. Recently, hybrid surrogate models evolved, in which two or more surrogate models are combined to form a new surrogate model [56, 180, 189, 190]. Figure 2.6 summarize the most common classification of surrogate models.

Surrogate models can be classified based on their type, which is identified based on the approximation methods used to approximate the surrogate shape function \mathcal{M} . Polynomial surrogates use polynomial functions to approximate the relation between the input-output of a model. Examples of these models include PCE and Response Surface Methodology (RSM). Gaussian Regression (GPR) models, for example Kriging, employ Gaussian processes to capture the underlying trends and correlations within the training data. Support Vector Regression (SVR) surrogate models approximate the input-output relation by utilizing support vector machines, while Radial Basis Function (BF) surrogate models interpolate the input-output relation by implementing radial basis functions. Furthermore, a family of surrogate models based on artificial neural networks (ANN) is developed, in which ANN are implemented to approximate the input-output relation [59, 119, 180, 188, 189].

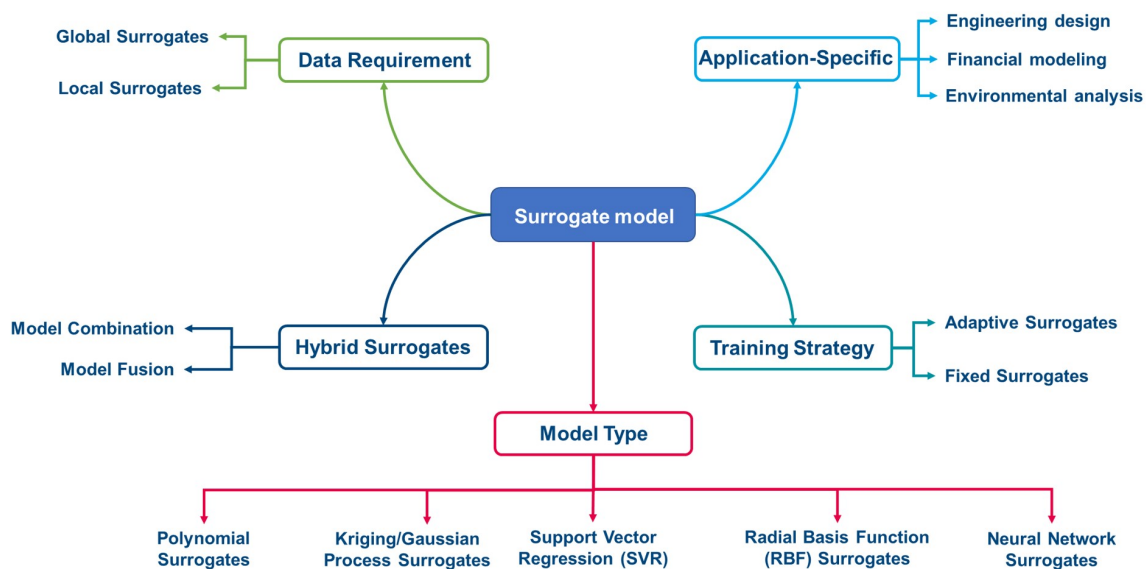


Figure 2.6: Classification of surrogate models.

It is also possible to categorise surrogate models according to their specific field of application in engineering design, financial modelling, and environmental analysis. Surrogate models can also be classified into global and local models based on the cover of data sets in the parametric space. Global surrogate models are constructed using a representative data set that covers the entire parametric space. A well-sampled parametric space is required to create

such a data set. On the other hand, if the input-output relationship exhibits non-linearity or non-uniformity across the parametric space, it is better to construct a local surrogate model, in which the model focuses on specific regions of the parametric space and only requires data sets related to these regions [176, 191]. The type of dataset used in the training strategies to build the surrogate model also differentiates the type of model. Fixed sets of training data without incorporating an adaptive learning strategy, resulting in fixed surrogate models that are limited to certain ranges. Using one-shot sampling techniques holds the advantage of promptly establishing a sample size, yet it produces a solitary fixed dataset. Nonetheless, a notable drawback inherent in one-shot sampling lies in the potential for under- or over-sampling [60].

By contrast, iteratively constructing the surrogate model by implementing certain criteria to select new data points results in adaptive surrogate models that are generally characterised by improved accuracy and performance [192, 193]. Moreover, adaptive surrogate model to handle complex and non-uniform parametric spaces by focusing on the most important regions within the parametric space [169, 194]. Added to that, adaptive surrogate models are more flexible to incorporate new data and update the model as needed, which leads to an efficient use of computational resources compared to repeatedly running the full complex original model [192–194]. It is worth mentioning that adaptive sampling techniques do not require direct modification of the surrogate model but address the imbalance in necessary sampling effort across the surrogate model sampling domain. However, if the collected samples are closely clustered, the inherent randomness of the sampling process may shift toward determinism, possibly leading to the construction of inaccurate surrogate models. Adaptive sampling incorporates different active learning algorithms to bridge the gaps within the sampling domain, ensuring the assembly of high-quality and representative datasets. Moreover, adaptive sampling techniques incorporate predefined stopping criteria, such as error metrics (R^2 , MAE , MSE), wherein the addition of new sample points no longer enhances model performance, indicating the sufficiency of the sample size [61, 126].

Another category of surrogate models is hybrid surrogate models, which have evolved to enhance the predictive capabilities of existing surrogate models and adapt to more intricate systems. The two main approaches to hybrid surrogate models are combination and fusion [119, 188, 189]. The combination approach involves combining multiple surrogate models to enhance the properties and prediction of the surrogate model. For example, the Polynomial chaos Kriging model (PCK), which is a combination of Kriging and PCE [57, 188]. While the hybrid surrogate model constructed under the model fusion approach is fused with alternative techniques based on other physical models or expert knowledge to leverage the accuracy and reliability of the new surrogate model [119, 180, 189].

The most commonly used types of surrogate models within the field of material science are Polynomial and Kriging surrogates, due to their computational efficiency, robustness and stability, and their ability to adapt and reflect the multiphysics, complexity non-linear nature [195]. Moreover, these models are more efficient in parameter estimation problems where direct values of these models are not available. For example, within the field of metal corrosion, a recent study conducted by Wang *et al.*, [196] focused on the multi-physics modelling of tribocorrosion in aluminium alloys. In this study, Kriging surrogate models were employed to solve the parameter estimation problem. UQ analysis using Kriging models provided confidence intervals for each evaluation of the FE model, which enhanced the model's predictions. Moreover, a comparative study of the Kriging model with a neural network (NN) surrogate model was performed. For the comparative study, Kriging models demonstrated excellent computational efficiency and predictability. Similar results were concluded by a study by Tak *et al.*, [197] constructed a model to evaluate and optimise corrosion rates within a crude unit situated in an actual re-

finery plant. This study estimated and optimized a model with six key parameters using the Kriging model. Moreover, Tak *et al.*, compared Kriging models with two well-known forecasting models, multiple linear regression and an artificial neural network. In both cases, Kriging models were able to accurately estimate and optimize key parameters. This study's outcomes underscore the versatility and effectiveness of Kriging algorithms, particularly the consideration of real-world refinery plant scenarios. In the literature, PCE models can be appropriately used in the propagation analysis of random input parameters in the field of engineering structures. For example, YiFei *et al.*, [198] implemented PCE combined with a hybrid K-means clustering optimizer to identify the structure damage of materials. In this study, the PCE model was used as a cost-effective substitute for an FEM model simulating the expensive structural of a small-scale laboratory dam. Implementing PCE improved the optimization strategy's efficiency and reduced the associated computational cost. Zhang and Qiu [199] proposed an efficient and accurate uncertainty analysis method for structural fatigue life prediction and fatigue reliability analysis, in which PCE was adopted to deal with independent normal random variables. This method was tested over several numerical examples of corroded metals and cracks.

The current thesis investigates the application of advanced surrogate modeling techniques to address UQ challenges in various biodegradation models. As a means of efficiently approximating biodegradation models in parameter estimation problems, Kriging surrogate models are implemented and evaluated in the subsequent chapters. Specifically, Kriging surrogate models are implemented and evaluated across the subsequent chapters as a means of efficiently approximating biodegradation models in parameter estimation problems. Furthermore, the current thesis draws upon established literature in the UQ field [200–204], which recommends the utilization of PCE models to extend the scope of the research toward UQ analysis, sensitivity analysis and uncertainty propagation within the material science domain. Thus, the current thesis presents a comprehensive workflow for addressing UQ problems in biodegradation models. The comprehensive UQ workflow developed within **Chapter 6** integrates different algorithms, UQ analysis, and comprehensive comparisons to determine the most effective computational experimental design (DOE) and the efficacy of surrogate models is compared across three distinct biodegradation models.

2.6.2 Challenges and limitations of surrogate models

The efficient utilization of surrogate models for UQ faces several challenges, starting with the accuracy of the surrogate models. These models should not introduce more uncertainty into the system. However, due to their simplifications and assumptions, a certain level of uncertainty is inherently introduced to the analysis; due to this, a trade-off between accuracy and computational efficiency needs to be considered [56, 180]. Implementing surrogate models for a particular problem involves considering specific types of data or assumptions related to the study system. Not all surrogate models apply to different problems. In some cases, applying surrogate models to different problem domains may require significant modifications or even developing a novel surrogate model [205]. Furthermore, selecting the appropriate surrogate model requires careful consideration of the problem characteristics and available data. Additionally, a representative set of training data is needed to enable the constructed surrogate model to capture complex model's behavior accurately. However, obtaining such data can be expensive and time-consuming. In other cases, this data may be unavailable, limited, or biased. This leads to poor surrogate model performance and limited generalisability [59, 188, 206]. A surrogate model's output can be challenging to interpret, particularly when complex relationships and interactions between parameters and corresponding model responses exist. Furthermore, surrogate models are sensitive to input space changes, which may raise questions about the robustness of these models, especially in unfamiliar regions of the input space [59, 180]. In order

to verify the accuracy and reliability of surrogate models, it is imperative to consider their pure mathematical nature and their non-direct relation to the physical laws or governing equations of the system under consideration [207]. Therefore, it is essential to establish suitable validation procedures and metrics to assess the performance of surrogate models [59, 126, 208].

2.6.3 Assessment of surrogate models

Assessing the accuracy of surrogate models is crucial to evaluating their ability to capture the original model's behaviour. Estimating the performance of surrogate models is essential due to the numerical approximation nature of these models before utilizing them for further estimation, prediction, and analysis. Moreover, knowledge of the local and global accuracy of the surrogate models is essential in selecting the most efficient surrogate model to approximate the original computational model. Furthermore, this knowledge can be used for fine-tuning, *i.e.*, using adaptive sampling or active learning techniques to refine and improve surrogate models. A further benefit is the reduction of uncertainty associated with surrogate models through the assessment of accuracy and quantification of error [59, 126, 208]. The choice of assessment methods depends on the nature of the physical problem, the type of surrogate model, and its outputs.

The assessment can be conducted through comparative analysis, in which the predictions of the surrogate models are compared with the original model's predictions. This comparison indicates the ability of surrogate models to capture the underlying relationships and connections [209, 210]. Furthermore, it is possible to evaluate the performance of surrogate models by testing them against domain knowledge or outlier detection. In this context, surrogate models are subjected to testing against the developer's domain expertise, which must extend beyond the scope of the original model's domain [180, 209]. Additionally, supported by domain knowledge, the performance of the surrogate models will be tested against outliers or extreme values. This testing aids in detecting the generalization of the model [180, 183, 211]. To illustrate, in the present thesis, these test approaches were employed by re-calibrating Kriging surrogate models, which were constructed based on a biodegradation model calibrated using *in vitro* data, to the *in vivo* domain and validating these models using in-house *in vivo* experimental data [65]. In specific scenarios, interval validation can be used, involving computing the confidence intervals for individual predictions, which are subsequently compared to actual values within these intervals. However, for complex computational models, this method may introduce more uncertainty into the analysis due to data limitation [212]. Another validation approach is based on test-set evaluation. Several validation methods align with this approach. Holdout Validation, for instance, involves dividing the original data set into a training set used to build the surrogate model and a test set used for performance evaluation. Then, the predictions of the surrogate model for the test sets are compared to the original model or experimental data [147]. Cross-Validation (CV) is another method within this approach. CV involves dividing the dataset into multiple folds, and the surrogate model is trained on a subset of the folds. The training process is iterated across all folds to generate performance metrics. CV is used for regression tasks to analyze the distribution of prediction errors across different CV folds. It is considered one of the most reliable techniques, particularly when dealing with complex and multi-scale computational frameworks, as is the case for biodegradation models [147, 207, 212]. One of the most common error metrics used to estimate the performance of surrogate models using this method is the Leave-one-out error (ε_{LOO}), which is given by [45]

$$\varepsilon_{LOO} = \frac{1}{N_K} \left[\frac{\sum_{i=1}^{N_K} (\mathcal{M}(x_i) - \mathcal{M}_{(-i)}(x_i))^2}{Var[\mathcal{M}(\mathcal{X})]} \right], \quad (2.30)$$

where N is the number of data points considered during constructing the surrogate model, $\mathcal{M}(x_i) - \mathcal{M}_{(-i)}(x_i)$ is the difference in prediction between the original and surrogate model observations for all training sets except x_i , and $\mathcal{M}(\mathcal{X})$ is the corresponding surrogate model response of the initial experimental design.

Moreover, error metrics can be employed to evaluate the accuracy of surrogate models. Here, different errors (MAE, MSE, NRMSE), as described in section 2.4.1 of this thesis, are computed between the surrogate model predictions and either the original model predictions or experimental validation data. RMSE provides a measure of global error over the entire design domain, indicating the accuracy of the actual surrogate model [207, 213]. However, for interpolating surrogate models, RMSE requires additional error analysis to be evaluated at test points. In this case, both MAE and relative absolute error (RAE) only indicate local deviation in the performance of the surrogate model [207]. “Nevertheless, a comprehensive comparison of different error measures for assessing the performance of surrogate models, considering the data used in their construction, was conducted by Goel and Stander [147]. This study concluded that the Prediction Sum of Squares (PRESS) error (Equation 2.31), which is derived based on the LOO-cross-validation error (Equation 2.30), provided a better assessment of surrogate model performance compared to other methods. These conclusions align with findings from other studies, for example Mehmani *et al.*, and Queipo *et al.*, [207, 213]

$$PRESS = \frac{1}{N} \sum_{i=1}^N (\widehat{y}_i - \widehat{y}_i^{(-i)})^2, \quad (2.31)$$

where \widehat{y}_i is the prediction of the surrogate model, which is constructed using all samples at the i^{th} training point, and $\widehat{y}_i^{(-i)}$ and the surrogate constructed using all sample points except the i^{th} point.

Finally, the performance of surrogate models can be inspected using visual presentation of the predictions. In this case, scatter plots, residual plots and Q-Q plots are used to visually assess the agreement between surrogate model predictions and the original model or experimental data. Several studies, for example, see Mehmani *et al.*, [207], Goel and Stander [147] and [212], investigated the different assessment methods and concluded that combining various assessment methods provides a more comprehensive view of surrogate model performance and accuracy.

In the context of this thesis, cross-validation is considered the primary assessment method, and ε_{LOO} is used to identify the best surrogate model. Furthermore, several error metrics are also used and implemented based on the degradation model type, available data, and the study objectives. Notably, an important application of surrogate model performance assessment is model refinement, in which several strategies and methods have been developed to improve the accuracy and robustness of surrogate models. This is detailed in **Chapter 6** of this thesis.

Bibliography

- [1] M. Lysaght and T. J. Webster, *Biomaterials for artificial organs*. Elsevier (2010).
- [2] H. Li, Y. Zheng, and L. Qin, "Progress of biodegradable metals." *Progress in Natural Science: Materials International* **24** (2014), no. 5 414–422.
- [3] Y. F. Zheng, X. N. Gu, and F. Witte, "Biodegradable metals." *Materials Science and Engineering R: Reports* **77** (2014) 1–34.
- [4] M. Esmaily, J. E. Svensson, S. Fajardo, N. Birbilis, G. S. Frankel, S. Virtanen, R. Arrabal, S. Thomas, and L. G. Johansson, "Fundamentals and advances in magnesium alloy corrosion." *Progress in Materials Science* **89** (2017) 92–193.
- [5] Q. Peng, K. Li, Z. Han, E. Wang, Z. Xu, R. Liu, and Y. Tian, "Degradable magnesium-based implant materials with anti-inflammatory activity." *Journal of Biomedical Materials Research Part A* **101** (2013), no. 7 1898–1906.
- [6] A. Mazur, J. A. Maier, E. Rock, E. Gueux, W. Nowacki, and Y. Rayssiguier, "Magnesium and the inflammatory response: potential physiopathological implications." *Archives of biochemistry and biophysics* **458** (2007), no. 1 48–56.
- [7] D. A. Robinson, R. W. Griffith, D. Shechtman, R. B. Evans, and M. G. Conzemijs, "In vitro antibacterial properties of magnesium metal against escherichia coli, pseudomonas aeruginosa and staphylococcus aureus." *Acta biomaterialia* **6** (2010), no. 5 1869–1877.
- [8] L. Ren, X. Lin, L. Tan, and K. Yang, "Effect of surface coating on antibacterial behavior of magnesium based metals." *Materials Letters* **65** (2011), no. 23-24 3509–3511.
- [9] M. Li, L. Ren, L. Li, P. He, G. Lan, Y. Zhang, and K. Yang, "Cytotoxic effect on osteosarcoma mg-63 cells by degradation of magnesium." *Journal of Materials Science & Technology* **30** (2014), no. 9 888–893.
- [10] G. Uppal, A. Thakur, A. Chauhan, and S. Bala, "Magnesium based implants for functional bone tissue regeneration – a review." *Journal of Magnesium and Alloys* **10** (2, 2022) 356–386.
- [11] W. Zhao, J. Wang, J. Weiyang, B. Qiao, Y. Wang, Y. Li, and D. Jiang, "A novel biodegradable mg-1zn-0.5sn alloy: Mechanical properties, corrosion behavior, biocompatibility, and antibacterial activity." *Journal of Magnesium and Alloys* **8** (6, 2020) 374–386.
- [12] F. Xing, S. Li, D. Yin, J. Xie, P. M. Rommens, Z. Xiang, M. Liu, and U. Ritz, "Recent progress in mg-based alloys as a novel bioabsorbable biomaterials for orthopedic applications." *Journal of Magnesium and Alloys* **10** (6, 2022) 1428–1456.

- [13] Y. Yang, C. He, E. Dianyu, W. Yang, F. Qi, D. Xie, L. Shen, S. Peng, and C. Shuai, "Mg bone implant: Features, developments and perspectives." *Materials & Design* **185** (2020) 108259.
- [14] M. Geetha, A. K. Singh, R. Asokamani, and A. K. Gogia, "Ti based biomaterials, the ultimate choice for orthopaedic implants – A review." *Progress in Materials Science* **54** (2009), no. 3 397–425.
- [15] J. Chen, L. Tan, X. Yu, I. Etim, M. Ibrahim, and K. Yang, "Mechanical properties of magnesium alloys for medical application: A review." *Journal of the mechanical behavior of biomedical materials* **87** (2018) 68–79.
- [16] J. Gallo, S. B. Goodman, Y. T. Konttinen, and M. Raska, "Particle disease: Biologic mechanisms of periprosthetic osteolysis in total hip arthroplasty." *Innate Immunity* **19** (2013), no. 2 213–224.
- [17] C. A. St. Pierre, M. Chan, Y. Iwakura, D. C. Ayers, E. A. Kurt-Jones, and R. W. Finberg, "Periprosthetic osteolysis: Characterizing the innate immune response to titanium wear-particles." *Journal of Orthopaedic Research* **28** (2010), no. 11 1418–1424.
- [18] M. Esmaily, J. E. Svensson, S. Fajardo, N. Birbilis, G. S. Frankel, S. Virtanen, R. Arrabal, S. Thomas, and L. G. Johansson, "Fundamentals and advances in magnesium alloy corrosion." *Progress in Materials Science* **89** (2017) 92–193.
- [19] T. Albaraghteh, R. Willumeit-Römer, and B. Zeller-Plumhoff, "In silico studies of magnesium-based implants: A review of the current stage and challenges." *Journal of Magnesium and Alloys* (11, 2022).
- [20] G. Williams, N. Birbilis, and H. N. McMurray, "Controlling factors in localised corrosion morphologies observed for magnesium immersed in chloride containing electrolyte." *Faraday Discussions* **180** (2015), no. 0 313–330.
- [21] D. Bairagi and S. Mandal, "A comprehensive review on biocompatible Mg-based alloys as temporary orthopaedic implants: Current status, challenges, and future prospects." *Journal of Magnesium and Alloys* **10** (3, 2022) 627–669.
- [22] H. Hermawan, *Biodegradable Metals: State of the Art*. Springer, Berlin, Heidelberg, Berlin, Heidelberg (2012).
- [23] J. Gonzalez, R. Q. Hou, E. P. S. Nidadavolu, R. Willumeit-Römer, and F. Feyerabend, "Magnesium degradation under physiological conditions – Best practice." *Bioactive Materials* **3** (2018), no. 2 174–185.
- [24] N. A. Agha, F. Feyerabend, B. Mihailova, S. Heidrich, U. Bismayer, and R. Willumeit-Römer, "Magnesium degradation influenced by buffering salts in concentrations typical of in vitro and in vivo models." *Materials Science and Engineering: C* **58** (2016) 817–825.
- [25] M. Kieke, F. Feyerabend, J. Lemaitre, P. Behrens, and R. Willumeit-Römer, "Degradation rates and products of pure magnesium exposed to different aqueous media under physiological conditions." (2016).
- [26] R. Willumeit-Römer, S. Bruns, H. Helmholz, D. Krüger, B. Wiese, S. Galli, J. Moosmann, and B. Zeller-Plumhoff, "The Comparability of In Vitro and In Vivo Experiments for Degradable Mg Implants." (Cham), pp. 9–16, Springer International Publishing, 2022.

- [27] A. M. Negrescu, M.-G. Necula, M. Costache, and A. Cimpean, "In vitro and in vivo biological performance of Mg-based bone implants." *Reviews in Biological and Biomedical Sciences* **3** (7, 2020) 11–41.
- [28] S. Amukarimi and M. Mozafari, "Biodegradable magnesium-based biomaterials: An overview of challenges and opportunities." (2021).
- [29] A. H. M. Sanchez, B. J. C. Luthringer, F. Feyerabend, and R. Willumeit, "Mg and Mg alloys: How comparable are in vitro and in vivo corrosion rates? A review." *Acta biomaterialia* **13** (2015) 16–31.
- [30] Diana KRÜGER, *Ex vivo and In vitro Investigation Of Biodegradable Magnesium-Gadolinium Implants*, Ph.D. thesis, Hereon, Hamburg (2022).
- [31] Public Health Service, "Policy on Humane Care and Use of Laboratory Animals." tech. rep., US Department of Health and Human Services, Washington, DC, 2015.
- [32] L. Rogozea, D. E. Diaconescu, E. A. Dinu, O. BADEA, D. POPA, O. ANDREESCU, and F. G. LEAȘU, "Biomedical research ethics." *Rom J Morphol Embryol* **55** (2014), no. 2 Suppl 719–722.
- [33] V. Nagendrababu, P. Murray, A. Kishen, M. Nekoofar, J. de Figueiredo, and P. Dummer, "Animal testing: a re-evaluation of what it means to endodontology." (2019).
- [34] V. Carvalho, I. Gonçalves, T. Lage, R. O. Rodrigues, G. Minas, S. F. Teixeira, A. S. Moita, T. Hori, H. Kaji, and R. A. Lima, "3d printing techniques and their applications to organ-on-a-chip platforms: A systematic review." *Sensors* **21** (2021), no. 9 3304.
- [35] J. Yan, Z. Li, J. Guo, S. Liu, and J. Guo, "Organ-on-a-chip: A new tool for in vitro research." *Biosensors and Bioelectronics* **216** (2022) 114626.
- [36] H.-J. Huang, Y.-H. Lee, Y.-H. Hsu, C.-T. Liao, Y.-F. Lin, and H.-W. Chiu, "Current Strategies in Assessment of Nanotoxicity: Alternatives to In Vivo Animal Testing." *International Journal of Molecular Sciences* **22** (4, 2021) 4216.
- [37] E. L. Boland, R. Shine, N. Kelly, C. A. Sweeney, and P. E. McHugh, "A Review of Material Degradation Modelling for the Analysis and Design of Bioabsorbable Stents." *Annals of Biomedical Engineering* **44** (2016), no. 2 341–356.
- [38] M. Abdallah, A. Joplin, M. Elahinia, and H. Ibrahim, "Corrosion Modeling of Magnesium and Its Alloys for Biomedical Applications: Review." *Corrosion and Materials Degradation* **1** (2020) 219–248.
- [39] Z. Zhang, X. Lu, and Y. Yan, "A novel pathway for the preparation of Mg metal from magnesite." *Journal of Magnesium and Alloys* (2021).
- [40] J. Bijak and J. Hilton, "Uncertainty Quantification, Model Calibration and Sensitivity BT - Towards Bayesian Model-Based Demography: Agency, Complexity and Uncertainty in Migration Studies." pp. 71–92. Springer International Publishing, Cham, 2022.
- [41] V. Nemani, L. Biggio, X. Huan, Z. Hu, O. Fink, A. Tran, Y. Wang, X. Zhang, and C. Hu, "Uncertainty quantification in machine learning for engineering design and health prognostics: A tutorial." *Mechanical Systems and Signal Processing* **205** (2023) 110796.
- [42] P. Bajger, J. M. A. Ashbourn, V. Manhas, Y. Guyot, K. Lietaert, and L. Geris, "Mathematical modelling of the degradation behaviour of biodegradable metals." *Biomechanics and Modeling in Mechanobiology* **16** (2017), no. 1 227–238.

- [43] R. C. Smith, *Uncertainty quantification: theory, implementation, and applications*, vol. 12. Siam (2013).
- [44] A. Senthilnathan, I. Javaheri, H. Zhao, V. Sundararaghavan, M. DeGraef, and P. Acar, "Uncertainty quantification of metallic microstructures using principal image moments." *Computational Materials Science* **215** (12, 2022) 111775.
- [45] B. Zeller-Plumhoff, T. AlBaraghteh, D. Höche, and R. Willumeit-Römer, "Computational modelling of magnesium degradation in simulated body fluid under physiological conditions." *Journal of Magnesium and Alloys* **10** (4, 2022) 965–978.
- [46] S. K. Ahmed, J. P. Ward, and Y. Liu, "Numerical Modelling of Effects of Biphasic Layers of Corrosion Products to the Degradation of Magnesium Metal In Vitro." *Materials* **11** (2018), no. 1.
- [47] V. Böhm, F. Lanusse, and U. Seljak, "Uncertainty Quantification with Generative Models."
- [48] Y. Wang and D. L. McDowell, *Uncertainty Quantification in Multiscale Materials Modeling*. Elsevier (2020).
- [49] B. Sudret, *Uncertainty quantification in the simulation of complex systems* (2018).
- [50] S. Tennøe, G. Halnes, and G. T. Einevoll, "Uncertainty: A Python Toolbox for Uncertainty Quantification and Sensitivity Analysis in Computational Neuroscience." *Frontiers in Neuroinformatics* **12** (8, 2018).
- [51] S. K. Khare, V. Blanes-Vidal, E. S. Nadimi, and U. R. Acharya, "Emotion recognition and artificial intelligence: A systematic review (2014–2023) and research recommendations." *Information Fusion* (2023) 102019.
- [52] J. A. Schaefer, V. J. Romero, S. R. Schafer, B. Leyde, and C. L. Denham, "Approaches for Quantifying Uncertainties in Computational Modeling for Aerospace Applications." in *AIAA Scitech 2020 Forum*, (Reston, Virginia), American Institute of Aeronautics and Astronautics, 1, 2020.
- [53] M. Abdar, F. Pourpanah, S. Hussain, D. Rezazadegan, L. Liu, M. Ghavamzadeh, P. Fieguth, X. Cao, A. Khosravi, U. R. Acharya, V. Makarenkov, and S. Nahavandi, "A review of uncertainty quantification in deep learning: Techniques, applications and challenges." *Information Fusion* **76** (9, 2021) 243–297.
- [54] R. C. Smith, *Uncertainty quantification: theory, implementation, and applications*, vol. 12. Siam (2013).
- [55] B. Sudret, *Uncertainty quantification in the simulation of complex systems* (2018).
- [56] R. Ghanem, D. Higdon, and H. Owhadi, *Handbook of uncertainty quantification*, vol. 6. Springer (2017).
- [57] M. P. Rumpfkeil, D. Bryson, and P. Beran, "Multi-Fidelity Sparse Polynomial Chaos and Kriging Surrogate Models Applied to Analytical Benchmark Problems." *Algorithms* **15** (3, 2022) 101.
- [58] Bárkányi, T. Chován, S. Németh, and J. Abonyi, "Modelling for digital twins—potential role of surrogate models." *Processes* **9** (2021), no. 3 476.
- [59] B. Sudret, S. Marelli, and J. Wiart, *Surrogate models for uncertainty quantification: An overview* (3, 2017).

- [60] K. Cheng, Z. Lu, C. Ling, and S. Zhou, "Surrogate-assisted global sensitivity analysis: an overview." *Structural and Multidisciplinary Optimization* **61** (2020), no. 3 1187–1213.
- [61] S. S. Jin and H. J. Jung, "Sequential surrogate modeling for efficient finite element model updating." *Computers & Structures* **168** (5, 2016) 30–45.
- [62] G. Aversano, G. D'Alessio, A. Coussement, F. Contino, and A. Parente, "Combination of polynomial chaos and Kriging for reduced-order model of reacting flow applications." *Results in Engineering* **10** (6, 2021) 100223.
- [63] A. Bhosekar and M. Ierapetritou, "Advances in surrogate based modeling, feasibility analysis, and optimization: A review." *Computers & Chemical Engineering* **108** (2018) 250–267.
- [64] A. Hermann, A. Shojaei, D. Steglich, D. Höche, B. Zeller-Plumhoff, and C. J. Cyron, "Combining peridynamic and finite element simulations to capture the corrosion of degradable bone implants and to predict their residual strength." *International Journal of Mechanical Sciences* **220** (2022) 107143.
- [65] T. Al Baraghteh, A. Hermann, A. Shojaei, R. Willumeit-Römer, C. J. Cyron, and B. Zeller-Plumhoff, "Utilizing Computational Modelling to Bridge the Gap between In Vivo and In Vitro Degradation Rates for Mg-xGd Implants." *Corrosion and Materials Degradation* **4** (3, 2023) 274–283.
- [66] R. Willumeit-Römer, "The interface between degradable mg and tissue." *Jom* **71** (2019), no. 4 1447–1455.
- [67] N. T. Kirkland, M. P. Staiger, D. Nisbet, C. H. J. Davies, and N. Birbilis, "Performance-driven design of Biocompatible Mg alloys." *JOM* **63** (2011), no. 6 28–34.
- [68] A. Yamamoto and S. Hiromoto, "Effect of inorganic salts, amino acids and proteins on the degradation of pure magnesium in vitro." *Materials Science and Engineering: C* **29** (2009), no. 5 1559–1568.
- [69] J. Walker, S. Shadanbaz, N. T. Kirkland, E. Stace, T. Woodfield, M. P. Staiger, and G. J. Dias, "Magnesium alloys: predicting in vivo corrosion with in vitro immersion testing." *Journal of Biomedical Materials Research Part B: Applied Biomaterials* **100** (2012), no. 4 1134–1141.
- [70] B. Zeller-Plumhoff, M. Gile, M. Priebe, H. Slominska, B. Boll, B. Wiese, T. Würger, R. Willumeit-Römer, and R. H. Meißner, "Exploring key ionic interactions for magnesium degradation in simulated body fluid – A data-driven approach." *Corrosion Science* **182** (2021) 109272.
- [71] E. L. Boland, R. Shine, N. Kelly, C. A. Sweeney, and P. E. McHugh, "A Review of Material Degradation Modelling for the Analysis and Design of Bioabsorbable Stents." *Annals of Biomedical Engineering* **44** (2016), no. 2 341–356.
- [72] D. C. Martinez, A. Dobkowska, R. Marek, H. Ćwieka, J. Jaroszewicz, T. Płociński, Č. Donik, H. Helmholz, B. Luthringer-Feyerabend, B. Zeller-Plumhoff, et al., "In vitro and in vivo degradation behavior of mg-0.45 zn-0.45 ca (zx00) screws for orthopedic applications." *Bioactive Materials* **28** (2023) 132–154.
- [73] A. H. M. Sanchez, B. J. C. Luthringer, F. Feyerabend, and R. Willumeit, "Mg and Mg alloys: How comparable are in vitro and in vivo corrosion rates? A review." *Acta Biomaterialia* **13** (9, 2015) 16–31.

- [74] J. A. Sanz-Herrera, E. Reina-Romo, and A. R. Boccaccini, "In silico design of magnesium implants: Macroscopic modeling." *Journal of the mechanical behavior of biomedical materials* **79** (2018) 181–188.
- [75] M. Barzegari, D. Mei, S. V. Lamaka, and L. Geris, "Computational modeling of degradation process of biodegradable magnesium biomaterials." *Corrosion Science* **190** (2021) 109674.
- [76] T. Lekszycki and F. Dell'Isola, "A mixture model with evolving mass densities for describing synthesis and resorption phenomena in bones reconstructed with bio-resorbable materials." *ZAMM-Journal of Applied Mathematics and Mechanics/Zeitschrift für Angewandte Mathematik und Mechanik* **92** (2012), no. 6 426–444.
- [77] D. Gottlieb and E. Tadmor, "The cfl condition for spectral approximations to hyperbolic initial-boundary value problems." *Mathematics of Computation* **56** (1991), no. 194 565–588.
- [78] E. L. Boland, R. N. Shirazi, J. A. Grogan, and P. E. McHugh, "Mechanical and corrosion testing of magnesium we43 specimens for pitting corrosion model calibration." *Advanced Engineering Materials* **20** (2018), no. 10 1800656.
- [79] J. ia, G. Song, and A. Atrens, "Experimental Measurement and Computer Simulation of Galvanic Corrosion of Magnesium Coupled to Steel." *Advanced Engineering Materials* **9** (2007), no. 1-2 65–74.
- [80] L. Lacroix, C. Blanc, N. Pébère, B. Tribollet, and V. Vivier, "Localized approach to galvanic coupling in an aluminum–magnesium system." *Journal of the Electrochemical Society* **156** (2009), no. 8 C259.
- [81] K. B. Deshpande, "Experimental investigation of galvanic corrosion: Comparison between SVET and immersion techniques." *Corrosion Science* **52** (2010), no. 9 2819–2826.
- [82] K. B. Deshpande, "Numerical modeling of micro-galvanic corrosion." *Electrochimica Acta* **56** (2011), no. 4 1737–1745.
- [83] K. B. Deshpande, "Validated numerical modelling of galvanic corrosion for couples: Magnesium alloy (AE44)–mild steel and AE44–aluminium alloy (AA6063) in brine solution." *Corrosion Science* **52** (2010), no. 10 3514–3522.
- [84] M. Baniassadi, M. Baghani, and Y. Remond, "Numerical modeling of degraded microstructures." in *Applied Micromechanics of Complex Microstructures*, pp. 253–297. Elsevier, 2023.
- [85] W. Thuiller, M. Guéguen, J. Renaud, D. N. Karger, and N. E. Zimmermann, "Uncertainty in ensembles of global biodiversity scenarios." *Nature Communications* **10** (3, 2019) 1446.
- [86] J. A. F. Diniz-Filho, L. Mauricio Bini, T. Fernando Rangel, R. D. Loyola, C. Hof, D. Nogués-Bravo, and M. B. Araújo, "Partitioning and mapping uncertainties in ensembles of forecasts of species turnover under climate change." *Ecography* **32** (12, 2009) 897–906.
- [87] H. N. Najm, B. J. Deusschere, Y. M. Marzouk, S. Widmer, and O. P. Le Maître, "Uncertainty quantification in chemical systems." *International Journal for Numerical Methods in Engineering* **80** (2009), no. 6-7 789–814.

- [88] C. J. Roy and W. L. Oberkampf, "A comprehensive framework for verification, validation, and uncertainty quantification in scientific computing." *Computer Methods in Applied Mechanics and Engineering* **200** (2011), no. 25 2131–2144.
- [89] W. L. Oberkampf, S. M. DeLand, B. M. Rutherford, K. V. Diegert, and K. F. Alvin, "Error and uncertainty in modeling and simulation." *Reliability Engineering & System Safety* **75** (3, 2002) 333–357.
- [90] R. G. McClarren, *Uncertainty Quantification and Predictive Computational Science*, vol. 1. Springer International Publishing, Cham (2018).
- [91] H. N. Najm, "Uncertainty Quantification and Polynomial Chaos Techniques in Computational Fluid Dynamics." *Annual Review of Fluid Mechanics* **41** (1, 2009) 35–52.
- [92] T. J. Sullivan, *Introduction to uncertainty quantification*, vol. 63. Springer (2015).
- [93] T. von Clarmann, S. Compennolle, and F. Hase, "Truth and uncertainty. A critical discussion of the error concept versus the uncertainty concept." *Atmospheric Measurement Techniques* **15** (3, 2022) 1145–1157.
- [94] K. Posch, J. Steinbrener, and J. Pilz, "Variational Inference to Measure Model Uncertainty in Deep Neural Networks."
- [95] J. Taylor, *An introduction to error analysis : the study of uncertainties in physical measurements*. University Science Books, California (1997).
- [96] W. Oberkampf, J. Helton, and K. Sentz, "Mathematical representation of uncertainty." in *19th AIAA Applied Aerodynamics Conference*, (Reston, Virginia), American Institute of Aeronautics and Astronautics, 6, 2001.
- [97] J. Zhang, J. Yin, and R. Wang, "Basic Framework and Main Methods of Uncertainty Quantification." *Mathematical Problems in Engineering* **2020** (2020) 6068203.
- [98] M. Kirchner, H. Mitter, U. A. Schneider, M. Sommer, K. Falkner, and E. Schmid, "Uncertainty concepts for integrated modeling - Review and application for identifying uncertainties and uncertainty propagation pathways." *Environmental Modelling & Software* **135** (1, 2021) 104905.
- [99] W. Walker, P. Harremoës, J. Rotmans, J. van der Sluijs, M. van Asselt, P. Janssen, and M. Kreyer von Krauss, "Defining Uncertainty: A Conceptual Basis for Uncertainty Management in Model-Based Decision Support." *Integrated Assessment* **4** (3, 2003) 5–17.
- [100] D. E. Ricciardi, O. A. Chkrebti, and S. R. Niezgod, "Uncertainty Quantification for Parameter Estimation and Response Prediction." *Integrating Materials and Manufacturing Innovation* **8** (2019), no. 3 273–293.
- [101] B. Enserink, J. H. Kwakkel, and S. Veenman, "Coping with uncertainty in climate policy making: (Mis)understanding scenario studies." *Futures* **53** (9, 2013) 1–12.
- [102] H. Agarwal, J. E. Renaud, E. L. Preston, and D. Padmanabhan, "Uncertainty quantification using evidence theory in multidisciplinary design optimization." *Reliability Engineering & System Safety* **85** (7, 2004) 281–294.
- [103] A. D. Kiureghian and O. Ditlevsen, "Aleatory or epistemic? Does it matter?." *Structural Safety* **31** (3, 2009) 105–112.

- [104] D. E. Ricciardi, O. A. Chkrebti, and S. R. Niezgoda, "Uncertainty Quantification for Parameter Estimation and Response Prediction." *Integrating Materials and Manufacturing Innovation* **8** (2019), no. 3 273–293.
- [105] Y. Qian, H. Wan, B. Yang, J.-C. Golaz, B. Harrop, Z. Hou, V. E. Larson, L. R. Leung, G. Lin, W. Lin, P.-L. Ma, H.-Y. Ma, P. Rasch, B. Singh, H. Wang, S. Xie, and K. Zhang, "Parametric Sensitivity and Uncertainty Quantification in the Version 1 of E3SM Atmosphere Model Based on Short Perturbed Parameter Ensemble Simulations."
- [106] K. Posch and J. Pilz, "Correlated Parameters to Accurately Measure Uncertainty in Deep Neural Networks." *IEEE Transactions on Neural Networks and Learning Systems* **32** (3, 2021) 1037–1051.
- [107] D. Ye, A. Nikishova, L. Veen, P. Zun, and A. G. Hoekstra, "Non-intrusive and semi-intrusive uncertainty quantification of a multiscale in-stent restenosis model." *Reliability Engineering & System Safety* **214** (10, 2021) 107734.
- [108] Wayne Isaac Tan Uy, *Forward and backward uncertainty quantification: methods, analysis, and applications*, Ph.D. thesis, Cornell University (2019).
- [109] S. Bilicz, M. Lambert, and S. Gyimóthy, "Kriging-based generation of optimal databases as forward and inverse surrogate models." *Inverse Problems* **26** (2010), no. 7 74012.
- [110] H. Zhao, Z. Gao, F. Xu, Y. Zhang, and J. Huang, "An efficient adaptive forward–backward selection method for sparse polynomial chaos expansion." *Computer Methods in Applied Mechanics and Engineering* **355** (10, 2019) 456–491.
- [111] Y. Gal and Z. Ghahramani, "Bayesian Convolutional Neural Networks with Bernoulli Approximate Variational Inference."
- [112] L. Bartsoen, M. G. Faes, M. S. Andersen, R. Wirix-Speetjens, D. Moens, I. Jonkers, and J. V. Sloten, "Bayesian parameter estimation of ligament properties based on tibio-femoral kinematics during squatting." *Mechanical Systems and Signal Processing* **182** (1, 2023) 109525.
- [113] O. P. Le Maître, O. M. Knio, H. N. Najm, and R. G. Ghanem, "A Stochastic Projection Method for Fluid Flow." *Journal of Computational Physics* **173** (11, 2001) 481–511.
- [114] J. Son and Y. Du, "Comparison of intrusive and nonintrusive polynomial chaos expansion-based approaches for high dimensional parametric uncertainty quantification and propagation." *Computers & Chemical Engineering* **134** (3, 2020) 106685.
- [115] O. M. Knio and O. P. Le Maître, "Uncertainty propagation in CFD using polynomial chaos decomposition." *Fluid Dynamics Research* **38** (9, 2006) 616–640.
- [116] O. Pablo and V. Enrique, "Valuing exchange options under an ornstein-uhlenbeck covariance model." *arXiv preprint arXiv:1711.10013* (2017).
- [117] P. Trajanovski, P. Jolakoski, L. Kocarev, and T. Sandev, "Ornstein–uhlenbeck process on three-dimensional comb under stochastic resetting." *Mathematics* **11** (2023), no. 16 3576.
- [118] B. Turnquist and M. Owkes, "multiUQ: An intrusive uncertainty quantification tool for gas-liquid multiphase flows." *Journal of Computational Physics* **399** (12, 2019) 108951.
- [119] K. McBride and K. Sundmacher, "Overview of Surrogate Modeling in Chemical Process Engineering." *Chemie Ingenieur Technik* **91** (3, 2019) 228–239.

- [120] M. Renardy, T.-M. Yi, D. Xiu, and C.-S. Chou, "Parameter uncertainty quantification using surrogate models applied to a spatial model of yeast mating polarization." *PLOS Computational Biology* **14** (2018), no. 5 e1006181.
- [121] L. Lacroix, C. Blanc, N. Pébère, B. Tribollet, and V. Vivier, "Localized Approach to Galvanic Coupling in an Aluminum-Magnesium System." *Journal of The Electrochemical Society* **156** (2009), no. 8 C259.
- [122] Q. Wang, Y. Feng, D. Wu, C. Yang, Y. Yu, G. Li, M. Beer, and W. Gao, "Polyphase uncertainty analysis through virtual modelling technique." *Mechanical Systems and Signal Processing* **162** (1, 2022) 108013.
- [123] G. Ninos, V. Bartzis, N. Merlemis, and I. E. Sarris, "Uncertainty quantification implementations in human hemodynamic flows." *Computer Methods and Programs in Biomedicine* **203** (5, 2021).
- [124] J. A. Grogan, B. J. O'Brien, S. B. Leen, and P. E. McHugh, "A corrosion model for bioabsorbable metallic stents." *Acta biomaterialia* **7** (2011), no. 9 3523–3533.
- [125] J. A. Grogan, S. B. Leen, and P. E. McHugh, "A physical corrosion model for bioabsorbable metal stents." *Acta biomaterialia* **10** (2014), no. 5 2313–2322.
- [126] R. Alizadeh, J. K. Allen, and F. Mistree, "Managing computational complexity using surrogate models: a critical review." *Research in Engineering Design* **31** (7, 2020) 275–298.
- [127] E. Acar, G. Bayrak, Y. Jung, I. Lee, P. Ramu, and S. S. Ravichandran, "Modeling, analysis, and optimization under uncertainties: a review." (2021).
- [128] M. Thapa and S. Missoum, "Uncertainty quantification and global sensitivity analysis of composite wind turbine blades." *Reliability Engineering & System Safety* **222** (6, 2022) 108354.
- [129] X. Wang, Y. Jin, S. Schmitt, and M. Olhofer, "Recent Advances in Bayesian Optimization; Recent Advances in Bayesian Optimization."
- [130] K. Hanson and F. Hemez, "Uncertainty Quantification of Simulation Codes Based on Experimental Data." *Proc AIAA Aerospace Sciences* **41** (2003).
- [131] C. Cleeton, A. H. Farmahini, and L. Sarkisov, "Performance-based ranking of porous materials for PSA carbon capture under the uncertainty of experimental data." *Chemical Engineering Journal* **437** (6, 2022) 135395.
- [132] D. Krüger, S. Galli, B. Zeller-Plumhoff, D. F. Wieland, N. Peruzzi, B. Wiese, P. Heuser, J. Moosmann, A. Wennerberg, and R. Willumeit-Römer, "High-resolution ex vivo analysis of the degradation and osseointegration of Mg-xGd implant screws in 3D." *Bioactive Materials* **13** (7, 2022) 37–52.
- [133] R. Montoya, C. Iglesias, M. L. Escudero, and M. C. García-Alonso, "Modeling in vivo corrosion of AZ31 as temporary biodegradable implants. Experimental validation in rats." *Materials Science and Engineering: C* **41** (2014) 127–133.
- [134] A.-K. Gartzke, S. Julmi, C. Klose, A.-C. Waselau, A. Meyer-Lindenberg, H. J. Maier, S. Besdo, and P. Wriggers, "A simulation model for the degradation of magnesium-based bone implants." *Journal of the mechanical behavior of biomedical materials* **101** (2020) 103411.

- [135] M. D. Rounsevell, A. Arneth, C. Brown, W. W. Cheung, O. Gimenez, I. Holman, P. Leadley, C. Luján, S. Mahevas, I. Maréchaux, R. Péliissier, P. H. Verburg, G. Vieilledent, B. A. Wintle, and Y.-J. Shin, "Identifying uncertainties in scenarios and models of socio-ecological systems in support of decision-making." *One Earth* **4** (7, 2021) 967–985.
- [136] N. Mangado, G. Piella, J. Noailly, J. Pons-Prats, and M. G. Ballester, "Analysis of uncertainty and variability in finite element computational models for biomedical engineering: characterization and propagation." *Frontiers in bioengineering and biotechnology* **4** (2016) 85.
- [137] S. Lallechere, C. F. M. Carobbi, and L. R. Arnaut, "Review of Uncertainty Quantification of Measurement and Computational Modeling in EMC Part II: Computational Uncertainty." *IEEE Transactions on Electromagnetic Compatibility* **61** (12, 2019) 1699–1706.
- [138] T. Trucano, "Prediction and Uncertainty in Computational Modeling of Complex Phenomena: A Whitepaper." tech. rep., Sandia National Laboratories (SNL), Albuquerque, NM, and Livermore, CA, 1, 1999.
- [139] J. Zhang and M. Carlo, "Modern Monte Carlo methods for efficient uncertainty quantification and propagation: A survey Statistical and Graphical Methods of Data Analysis & Sampling."
- [140] C.-J. Chang, C.-H. Chang, and T.-K. Hung, "A computational pitting corrosion model of magnesium alloys." *Frontiers in Bioengineering and Biotechnology* **10** (2022) 887444.
- [141] Abdulhamit Subasi, *Practical Machine Learning for Data Analysis Using Python*. Elsevier (2020).
- [142] V. Kotu and B. Deshpande, "Data Science Process." in *Data Science*, pp. 19–37. Elsevier, 2019.
- [143] S. M. Cabaneros and B. Hughes, "Methods used for handling and quantifying model uncertainty of artificial neural network models for air pollution forecasting." *Environmental Modelling & Software* **158** (12, 2022) 105529.
- [144] J. Salomon, J. Göing, S. Lück, M. Broggi, J. Friedrichs, and M. Beer, "Sensitivity Analysis of an Aircraft Engine Model Under Consideration of Dependent Variables." (6, 2021).
- [145] J. Lei and W. Schilling, "Parameter Uncertainty Propagation Analysis for Urban Rainfall Runoff Modelling." *Water Science and Technology* **29** (1, 1994) 145–154.
- [146] J. Xu, Y. Zhang, and C. Dang, "A novel hybrid cubature formula with Pearson system for efficient moment-based uncertainty propagation analysis." *Mechanical Systems and Signal Processing* **140** (6, 2020) 106661.
- [147] T. Goel and N. Stander, "Comparing three error criteria for selecting radial basis function network topology." *Computer Methods in Applied Mechanics and Engineering* **198** (5, 2009) 2137–2150.
- [148] A. Carriquiry, "Measurement Error Models." *International Encyclopedia of the Social & Behavioral Sciences* (2001) 9435–9442.
- [149] W. L. Oberkampf, S. M. DeLand, B. M. Rutherford, K. V. Diegert, and K. F. Alvin, "Error and uncertainty in modeling and simulation." *Reliability Engineering & System Safety* **75** (3, 2002) 333–357.

- [150] S. G. Rabinovich, *Evaluating Measurement Accuracy*. Springer International Publishing, Cham (2017).
- [151] R. J. Hyndman and A. B. Koehler, "Another look at measures of forecast accuracy." *International journal of forecasting* **22** (2006), no. 4 679–688.
- [152] J. S. Armstrong and F. Collopy, "Error measures for generalizing about forecasting methods: Empirical comparisons." *International journal of forecasting* **8** (1992), no. 1 69–80.
- [153] A. Saltelli, K. Aleksankina, W. Becker, P. Fennell, F. Ferretti, N. Holst, S. Li, and Q. Wu, "Why so many published sensitivity analyses are false: A systematic review of sensitivity analysis practices." *Environmental Modelling & Software* **114** (2019) 29–39.
- [154] A. Saltelli, "Sensitivity analysis for importance assessment.." *Risk analysis : an official publication of the Society for Risk Analysis* **22** (6, 2002) 579–590.
- [155] C. Pichery, "Sensitivity Analysis." *Encyclopedia of Toxicology: Third Edition* (9, 2014) 236–237.
- [156] M. Renardy, T.-M. Yi, D. Xiu, and C.-S. Chou, "Parameter uncertainty quantification using surrogate models applied to a spatial model of yeast mating polarization." *PLOS Computational Biology* **14** (2018), no. 5 e1006181.
- [157] M. Gelleszun, P. Kreye, and G. Meon, "Representative parameter estimation for hydrological models using a lexicographic calibration strategy." *Journal of Hydrology* **553** (2017) 722–734.
- [158] A. Puy, W. Becker, S. Lo Piano, and A. Saltelli, "A COMPREHENSIVE COMPARISON OF TOTAL-ORDER ESTIMATORS FOR GLOBAL SENSITIVITY ANALYSIS." *International Journal for Uncertainty Quantification* **12** (2022), no. 2 1–18.
- [159] S. Kucherenko, D. Albrecht, and A. Saltelli, "Exploring multi-dimensional spaces: a Comparison of Latin Hypercube and Quasi Monte Carlo Sampling Techniques."
- [160] A. Saltelli, P. Annoni, I. Azzini, F. Campolongo, M. Ratto, and S. Tarantola, "Variance based sensitivity analysis of model output. Design and estimator for the total sensitivity index." *Computer Physics Communications* **181** (2, 2010) 259–270.
- [161] I. Azzini, T. A. Mara, and R. Rosati, "Comparison of two sets of Monte Carlo estimators of Sobol' indices." *Environmental Modelling & Software* **144** (10, 2021) 105167.
- [162] X. Y. Zhang, M. N. Trame, L. J. Lesko, and S. Schmidt, "Sobol sensitivity analysis: A tool to guide the development and evaluation of systems pharmacology models." *CPT: Pharmacometrics and Systems Pharmacology* **4** (2, 2015) 69–79.
- [163] A. Barbu and S.-C. Zhu, *Monte Carlo Methods*, vol. 35. Springer (2020).
- [164] Y. Shuxing, F. Xiong, and F. Wang, "Polynomial Chaos Expansion for Probabilistic Uncertainty Propagation." 7, 2017.
- [165] L. Meyn, *An uncertainty propagation methodology that simplifies uncertainty analyses* (2000).
- [166] X. Yin, S. Lee, W. Chen, W. K. Liu, and M. F. Horstemeyer, "Efficient Random Field Uncertainty Propagation in Design Using Multiscale Analysis." *Journal of Mechanical Design* **131** (2, 2009).

- [167] C. Lataniotis, S. Marelli, and B. Sudret, "EXTENDING CLASSICAL SURROGATE MODELING TO HIGH DIMENSIONS THROUGH SUPERVISED DIMENSIONALITY REDUCTION: A DATA-DRIVEN APPROACH." *International Journal for Uncertainty Quantification* **10** (2020), no. 1 55–82.
- [168] A. Tabandeh, N. Sharma, and P. Gardoni, "Uncertainty propagation in risk and resilience analysis of hierarchical systems." *Reliability Engineering & System Safety* **219** (3, 2022) 108208.
- [169] C. Wang, X. Qiang, M. Xu, and T. Wu, "Recent Advances in Surrogate Modeling Methods for Uncertainty Quantification and Propagation." *Symmetry* **14** (6, 2022) 1219.
- [170] M. Askarian, R. Zarghami, F. Jalali, and N. Mostoufi, "Uncertainty propagation in condensate stabilization column." *Computer Aided Chemical Engineering* **31** (2012) 115–119.
- [171] S. Mohammadi and S. Cremaschi, "Efficiency of Uncertainty Propagation Methods for Estimating Output Moments." *Computer Aided Chemical Engineering* **47** (1, 2019) 487–492.
- [172] Y. Liu, L. Li, S. Zhao, and S. Song, "A global surrogate model technique based on principal component analysis and Kriging for uncertainty propagation of dynamic systems." *Reliability Engineering & System Safety* **207** (9, 2021) 107365.
- [173] D. P. Kroese, T. Brereton, T. Taimre, and Z. I. Botev, "Why the Monte Carlo method is so important today." *WIREs Computational Statistics* **6** (2014), no. 6 386–392.
- [174] S. Bae, C. Park, and N. Kim, "Estimating Effect of Additional Sample on Uncertainty Reduction in Reliability Analysis Using Gaussian Process." *Journal of Mechanical Design* **142** (4, 2020) 1–27.
- [175] C. Fedon, E. Y. Cervantes, L. Salamon, and B. Erasmus, "Application of deterministic sampling methods for uncertainty quantification in manufacturing tolerances in neutron physics." *Nuclear Engineering and Design* **373** (3, 2021) 111023.
- [176] Y. Liu, L. Li, S. Zhao, and S. Song, "A global surrogate model technique based on principal component analysis and Kriging for uncertainty propagation of dynamic systems." *Reliability Engineering & System Safety* **207** (3, 2021) 107365.
- [177] X. Wu, C. Wang, and T. Kozłowski, *Kriging-based Surrogate Models for Uncertainty Quantification and Sensitivity Analysis* (2017).
- [178] R. Yondo, E. Andrés, and E. Valero, "A review on design of experiments and surrogate models in aircraft real-time and many-query aerodynamic analyses." *Progress in Aerospace Sciences* **96** (1, 2018) 23–61.
- [179] D. A. I. J. F. D. A. S. P. A. J. Keane, "Front Matter Colour Plates Sampling Plans Constructing a Surrogate Exploring and Exploiting a Surrogate Visualization Constraints Infill Criteria with Noisy Data Exploiting Gradient Information Multi-Fidelity Analysis Multiple Design Objectives Appendix: ." *Engineering Design via Surrogate Modelling* (2008) i–xviii.
- [180] A. I. J. Forrester, A. Sóbester, and A. J. Keane, *Engineering Design via Surrogate Modelling*. Wiley (7, 2008).
- [181] H. Gupta and S. Razavi, "Challenges and Future Outlook of Sensitivity Analysis." in *Sensitivity Analysis in Earth Observation Modelling*, pp. 397–415. Elsevier, 2017.

- [182] M. Abdar, F. Pourpanah, S. Hussain, D. Rezazadegan, L. Liu, M. Ghavamzadeh, P. Fieguth, X. Cao, A. Khosravi, U. R. Acharya, V. Makarenkov, and S. Nahavandi, "A review of uncertainty quantification in deep learning: Techniques, applications and challenges." *Information Fusion* **76** (12, 2021) 243–297.
- [183] B. Sudret, S. Marelli, and J. Wiart, *Surrogate Models for Uncertainty Quantification: An Overview* (2017).
- [184] G. Makrygiorgos, G. M. Maggioni, and A. Mesbah, "Surrogate modeling for fast uncertainty quantification: Application to 2D population balance models." *Computers & Chemical Engineering* **138** (7, 2020) 106814.
- [185] A. Al Kajbaf and M. Bensi, "Application of surrogate models in estimation of storm surge: A comparative assessment." *Applied Soft Computing* **91** (6, 2020) 106184.
- [186] T. Würth, C. Krauß, C. Zimmerling, and L. Kärger, "Physics-informed neural networks for data-free surrogate modelling and engineering optimization – An example from composite manufacturing." *Materials & Design* **231** (7, 2023) 112034.
- [187] C. K. J. Hou and K. Behdinan, "Dimensionality reduction in surrogate modeling: A review of combined methods." *Data Science and Engineering* **7** (2022), no. 4 402–427.
- [188] N. Tsokanas, R. Pastorino, and B. Stojadinović, "A Comparison of Surrogate Modeling Techniques for Global Sensitivity Analysis in Hybrid Simulation." *Machine Learning and Knowledge Extraction* **4** (12, 2021) 1–21.
- [189] C. K. J. Hou and K. Behdinan, "Dimensionality Reduction in Surrogate Modeling: A Review of Combined Methods." *Data Science and Engineering* **7** (12, 2022) 402–427.
- [190] M. Böttcher, F. Leichsenring, A. Fuchs, W. Graf, and M. Kaliske, "Efficient Utilization of Surrogate Models for Uncertainty Quantification." *PAMM* **20** (1, 2021).
- [191] Y. Liu, L. Li, and S. Zhao, "A global surrogate model for high-dimensional structural systems based on partial least squares and Kriging." *Mechanical Systems and Signal Processing* **164** (9, 2022) 108246.
- [192] F. Boukouvala, F. J. Muzzio, and M. G. Ierapetritou, "Feasibility analysis of black-box processes using an adaptive sampling kriging based method." in *Computer Aided Chemical Engineering* (E. N. Pistikopoulos, M. C. Georgiadis, and A. C. Kokossis, eds.), vol. 29, pp. 432–436. Elsevier, 2011.
- [193] J. N. Fuhg, A. Fau, and U. Nackenhorst, "State-of-the-Art and Comparative Review of Adaptive Sampling Methods for Kriging."
- [194] C. Kamath, "Intelligent sampling for surrogate modeling, hyperparameter optimization, and data analysis." *Machine Learning with Applications* **9** (2022) 100373.
- [195] J. P. Kleijnen and E. Mehdad, "Multivariate versus univariate Kriging metamodels for multi-response simulation models." *European Journal of Operational Research* **236** (7, 2014) 573–582.
- [196] K. Wang, Y. Wang, X. Yue, and W. Cai, "Multiphysics modeling and uncertainty quantification of tribocorrosion in aluminum alloys." *Corrosion Science* **178** (2021) 109095.
- [197] K. Tak, J. Kim, H. Kwon, J. H. Cho, and I. Moon, "Kriging models for forecasting crude unit overhead corrosion." *Korean Journal of Chemical Engineering* **33** (2016), no. 7 1999–2006.

- [198] L. YiFei, H.-L. Minh, S. Khatir, T. Sang-To, T. Cuong-Le, C. MaoSen, and M. Abdel Wahab, "Structure damage identification in dams using sparse polynomial chaos expansion combined with hybrid K-means clustering optimizer and genetic algorithm." *Engineering Structures* **283** (5, 2023) 115891.
- [199] Z. Zhang and Z. Qiu, "Fatigue reliability analysis for structures with hybrid uncertainties combining quadratic response surface and polynomial chaos expansion." *International Journal of Fatigue* **144** (3, 2021) 106071.
- [200] B. Sudret, *Sparse polynomial chaos expansions for uncertainty quantification and sensitivity analysis* (2019).
- [201] B. Sudret, *Sparse polynomial chaos expansions for uncertainty quantification and sensitivity analysis* (2019).
- [202] N. Lüthen, S. Marelli, and B. Sudret, "Sparse Polynomial Chaos Expansions: Literature Survey and Benchmark." *SIAM/ASA Journal on Uncertainty Quantification* **9** (1, 2021) 593–649.
- [203] T. A. Mara and W. E. Becker, "Polynomial chaos expansion for sensitivity analysis of model output with dependent inputs." *Reliability Engineering & System Safety* **214** (2021) 107795.
- [204] P. S. Palar, T. Tsuchiya, and G. T. Parks, "Multi-fidelity non-intrusive polynomial chaos based on regression." *Computer Methods in Applied Mechanics and Engineering* **305** (6, 2016) 579–606.
- [205] P. Kersaudy, B. Sudret, N. Varsier, O. Picon, and J. Wiart, "A new surrogate modeling technique combining Kriging and polynomial chaos expansions – Application to uncertainty analysis in computational dosimetry." *Journal of Computational Physics* **286** (9, 2015) 103–117.
- [206] S. S. Garud, I. A. Karimi, and M. Kraft, "Smart Sampling Algorithm for Surrogate Model Development." *Computers & Chemical Engineering* **96** (1, 2017) 103–114.
- [207] A. Mehmani, S. Chowdhury, and A. Messac, "Predictive quantification of surrogate model fidelity based on modal variations with sample density." *Structural and Multidisciplinary Optimization* **52** (8, 2015) 353–373.
- [208] Y. Xu, A. Renteria, and P. Wang, "Adaptive surrogate models with partially observed information." *Reliability Engineering & System Safety* **225** (9, 2022) 108566.
- [209] F. A. Viana, C. Gogu, and T. Goel, "Surrogate modeling: tricks that endured the test of time and some recent developments." *Structural and Multidisciplinary Optimization* **64** (2021), no. 5 2881–2908.
- [210] S. Yang, D. Meng, H. Wang, Z. Chen, and B. Xu, "A comparative study for adaptive surrogate-model-based reliability evaluation method of automobile components." *International Journal of Structural Integrity* **14** (2023), no. 3 498–519.
- [211] R. G. McClarren, *Uncertainty Quantification and Predictive Computational Science*, vol. 1. Springer International Publishing, Cham (2018).
- [212] J. Zhang, S. Chowdhury, A. Mehmani, and A. Messac, "Characterizing Uncertainty Attributable to Surrogate Models." *Journal of Mechanical Design* **136** (3, 2014).

- [213] N. V. Queipo, R. T. Haftka, W. Shyy, T. Goel, R. Vaidyanathan, and P. Kevin Tucker, "Surrogate-based analysis and optimization." *Progress in Aerospace Sciences* **41** (1, 2005) 1–28.
- [214] S. Sakata, F. Ashida, and M. Zako, "Structural optimization using Kriging approximation." *Computer Methods in Applied Mechanics and Engineering* **192** (2003), no. 7 923–939.
- [215] B. Ankenman, B. L. Nelson, and J. Staum, "Stochastic Kriging for Simulation Metamodeling." *Operations Research* **58** (8, 2010) 371–382.
- [216] J. P. C. Kleijnen, "Kriging metamodeling in simulation: A review." *European Journal of Operational Research* **192** (2009), no. 3 707–716.
- [217] D. Krüger, B. Zeller-Plumhoff, B. Wiese, S. Yi, M. Zuber, D. C. Wieland, J. Moosmann, and R. Willumeit-Römer, "Assessing the microstructure and in vitro degradation behavior of Mg-xGd screw implants using μ CT." *Journal of Magnesium and Alloys* **9** (11, 2021) 2207–2222.
- [218] P. Kersaudy, B. Sudret, N. Varsier, O. Picon, and J. Wiart, "A new surrogate modeling technique combining Kriging and polynomial chaos expansions – Application to uncertainty analysis in computational dosimetry." *Journal of Computational Physics* **286** (4, 2015) 103–117.

Part II

Publications

***In silico* studies of Magnesium-based implants: a review of the current stage and challenges**

This chapter discusses how different *in silico* methods are implemented to study the biodegradation of Mg-based implants. *In silico* methods offer a powerful alternative to traditional testing of the materials in temporary orthopedic applications. Controlling the biodegradation of Mg-based implants is essential for designing implants that support bone during healing. It is imperative to identify and investigate the complex interactions between the various factors that play a crucial role in the degradation of biodegradable Mg-based implants. This investigation involves studying the effect of environmental conditions, such as temperature, pH, and flow rates, on degradation. By examining the interactions between these factors, a comprehensive understanding of the degradation mechanism can be achieved. This understanding will enhance the reliability and efficiency of degradation models. However, due to the complex nature of the biodegradation process, several modeling approaches have appeared in the literature. This raises the question of which of these approaches is the most effective at accurately modeling and simulating biodegradable implant degradation. To address this question, we conducted a thorough investigation and screening of the degradation models reported in the literature. We screened both *in vitro* and *in vivo* degradation systems, focusing on biodegradable implant degradation. Our discussion provides a comprehensive and critical analysis of the published models and their performance in capturing the complexity of the biodegradation process. Additionally, we explore different approaches to optimize the various sources of errors and quantify the uncertainties associated with the proposed models.

Publication details

Tamadur AlBaraghteh, Regine Willumeit-Römer, Berit Zeller-Plumhoff (2022). *In silico* studies of Magnesium-based implants: a review of the current stage and challenges. *Journal of Magnesium and Alloys*, 10(11) 2968-2996.
<https://doi.org/10.1016/j.jma.2022.09.029>.

Author's contribution

The author contributed to conceptualization, researching, discussion, writing and editing the original draft.

Copyright Notice

©This is an accepted version of the article originally published in the Journal of Magnesium and Alloys. The paper has been published under Creative Commons CC-BY 4.0 Licence. The copyright has been clarified in line with the publisher's guidelines.



Available online at www.sciencedirect.com

ScienceDirect

Journal of Magnesium and Alloys 10 (2022) 2968–2996



www.elsevier.com/locate/jma

Review

In silico studies of magnesium-based implants: A review of the current stage and challenges

Tamadur Albaraghteh*, Regine Willumeit-Römer, Berit Zeller-Plumhoff*

Helmholtz-Zentrum hereon GmbH, Institute of Metallic Biomaterials, Max-Planck-Str. 1, Geesthacht 21502, Germany

Received 18 February 2022; received in revised form 26 August 2022; accepted 21 September 2022

Available online 4 November 2022

Abstract

In silico methods to study biodegradable implants have recently received increasing attention due to their potential in reducing experimental time and cost. An important application case for *in silico* methods are magnesium (Mg)-based biodegradable implants, as they represent a powerful alternative to traditional materials used for temporary orthopaedic applications. Controlling Mg alloy degradation is critical to designing an implant that supports the bone healing process. To simulate different aspects of this biodegradation process, several mathematical models have been proposed with the ultimate aim of replacing laboratory experiments with computational modeling. In this review, we provide a comprehensive and critical discussion of the published models and their performance with respect to capturing the complexity of the biodegradation process. This complexity is presented initially. Additionally, the present review discusses the different approaches of optimizing and quantifying the different sources of errors and uncertainties within the proposed models.

© 2022 Chongqing University. Publishing services provided by Elsevier B.V. on behalf of KeAi Communications Co. Ltd.

This is an open access article under the CC BY-NC-ND license (<http://creativecommons.org/licenses/by-nc-nd/4.0/>)

Peer review under responsibility of Chongqing University

Keywords: Biodegradable implants; Degradation; *In silico*; Phenomenological approach; Physical approach; Validation; Verification; Uncertainty quantification; Mg.

1. Introduction

Biomedical implants can be traced back to ancient Egypt and South-Central American cultures [1]. These implants have been used in different medical applications, from replacing a missing tooth to building up a knee or a hip [1,2]. Different biomedical implant materials appear in the literature, *i.e.* polymers, calcium phosphate, bulk metallic glasses and metals (*e.g.* titanium, iron and magnesium) [3–5]. In the last two decades, innovations in the biomedical field played a leading role in increasing the quality, stability and biocompatibility of implants [6]. These continuous improvements in the field led to a new class of implants made of biodegradable metals, which broke the established paradigm that "metallic biomaterials must be corrosion resistant" [4,7,8]. Biodegradable

metal implants can be categorized into three classes; magnesium (Mg)-based, iron (Fe)-based and zinc (Zn)-based materials [5,9–11]. Biodegradable Mg-based implants are the main focus of this review.

As an element, Mg is one of the lightest engineering metals (density ~ 1.7 g) and one of the abundant elements in both earth's crust and human body [10]. Due to these unique properties of Mg, it has been subjected to different applications in different fields, for example in transport, energy for medical implants [2,4,12–19]. The increased importance of Mg-based implants in orthopaedic applications has been driven by its anti-inflammatory, antibacterial, and osteoinduction properties [20–23]. These properties promote Mg-based alloys to be used as short-term implants that will provide the required support during the bone healing process and ultimately dissolve completely in the complex physiological environment of the human body [2,10,17,24]. Different types and shapes of Mg-based biomedical implants have been developed to support different types of fractures. The schematic diagram in

* Corresponding authors.

E-mail addresses: tamadur.albaraghteh@hereon.de (T. Albaraghteh), berit.zeller-plumhoff@hereon.de (B. Zeller-Plumhoff).

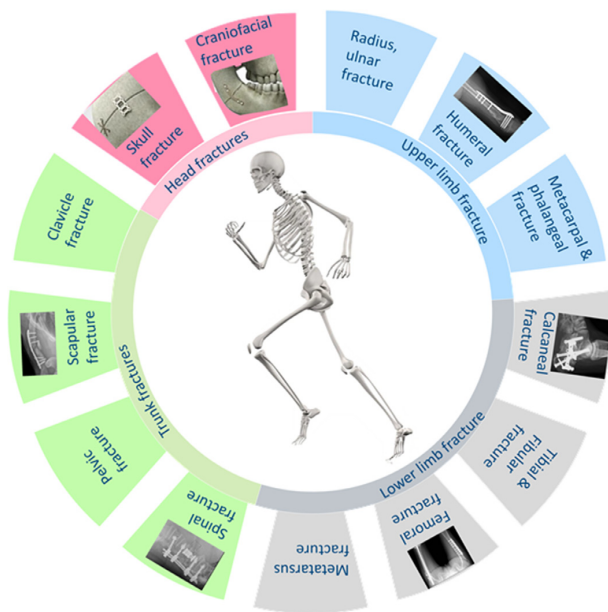


Fig. 1. Schematic illustration of different fracture sites in human body requiring various Mg-based biodegradable implants; For head fractures [36], upper limb fractures [37], lower limb fractures [38,39] and trunk fractures [40,41]. Fracture classification adapted from [25]. Skeleton image adapted (under free license from Freepik.com).

Fig. 1 illustrates some of these biomedical applications for Mg-based implants.

The matching degradation kinetics between biodegradable implants and the healing period of biological tissues is one of the key factors for a successful outcome and the degradation must take place with non-harmful residues [4,10,17,25–32]. In the development process of biodegradable implants based on Mg, controlling degradation is a challenge. In order to develop a clinically tested implant, several *in vivo* tests must be conducted. These tests are expensive and time consuming but most importantly they can cause harm and discomfort for the testing subjects. Thus, it is vital to pre-screen the implants through *in vitro* tests [27,32,33]. *In vitro* testing is an efficient approach to optimize the parameters needed to conduct *in vivo* studies. Furthermore, *in vitro* degradation mimics and evaluates specific subprocesses of *in vivo* degradation by series of methods and procedures [10,34]. Nevertheless, a gap between the predictions of these studies remains [35]. Computational modeling, which is also called *in silico* testing, can be used to fill in this gap, enhance the *in vitro* and *in vivo* predictions and speed up the development process. A recent review by Yang et al. [2] highlighted the important role of the mathematical approach in studying the dynamic degradation of Mg-based implants. Computational modeling captures and explains the dynamic physico-chemical interactions that occur in the system and their effects on the morphological and mechanical properties of the implants [2]. A key goal of computational modeling is to ultimately create a digital twin that can simulate both *in vivo* and *in vitro* degradation processes,

thus accelerating the material optimization process. However, modeling the degradation process of Mg-based implants is challenging, as it represents a complex multi-scale problem. Consequently, modeling the degradation process of Mg-based implants requires a thorough understanding of the degradation and the factors affecting it. The lack of accurate data to calibrate and optimize a model is another challenge in developing a reliable mathematical framework of degradation. In this regard, it is necessary to validate and verify all developed models through different test scenarios. This review provides a comprehensive overview of the different modeling approaches adopted to model the *in vitro* and *in vivo* degradation of magnesium-based biodegradable implants. The models will be reviewed critically in the context of the state-of-the-art knowledge on the biodegradation processes. In order to gain a deeper understanding of the system, we will begin by discussing the general concepts of Mg biodegradation and the key factors that affect it. Moreover, we demonstrate the challenges of modeling this complex process and the possible integration of validation and optimization techniques to enhance the development process of models. Finally, we comment on uncertainty quantification (UQ) methods and techniques, which are pivotal to yield reliable predictive models in the future.

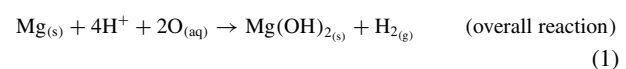
2. Degradation of biodegradable Mg-based implants

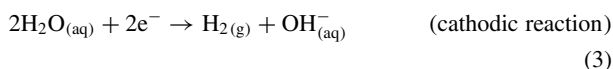
High degradation rates of Mg and its alloys are of major concern when assessing their applicability as implant materials [10,17,25,27–33,42–45]. Uncontrolled degradation of Mg-based implants may lead not only to implant failure but also may be a reason for producing a toxic environment within the body [5,10,20,33,46,47]. In principle, uncontrolled degradation could raise the pH value of the implant environment significantly, which can be toxic for living cells in any biological system [33,48]. Moreover, the uncontrolled degradation will produce higher amounts of hydrogen gas than the circulation system of the body can handle, leading an accumulation at the implantation site [5,10,20,27,32,33,49–51].

Various factors were reported to control the complex degradation process of biodegradable Mg-based alloys. In the next section, we will discuss the general concept of the degradation process of Mg-based alloys and the key factors affecting it in physiological media.

2.1. Basic concepts of degradation process

The degradation of Mg in water is an electrochemical reaction, where the overall reaction products are magnesium hydroxide and hydrogen gas, as seen by Eq. (1). This reaction involves anodic (for Mg) and cathodic (for H₂O) reactions, as seen in the following reactions:





The cathodic reaction in Eq. (3) states that each one mole of Mg degraded is corresponding to the production of one mole of H₂ [34]. Where the overall reaction reflects that the degradation process of Mg is a function of the pH of the system, which means that the dissolution of Mg is depending on the dissolution media. As the pH increases a passive layer of Mg(OH)₂ will start to form. This protective layer will increase the corrosion resistance of the metal [30,33,52–55]. But this layer is only stable under highly alkaline conditions (pH > 11), and loses its integrity under acidic conditions or in presence of aggressive ions (*i.e.* chloride, bromide, and sulphate ions), which induce pitting corrosion [33,50,56]. A tendency for galvanic corrosion is reported for Mg-based alloys due to the low standard electrode potential of Mg (−2.72 V) compared to other metals [52].

2.2. Key factors affecting the *in vitro* degradation process

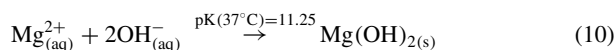
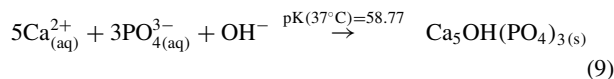
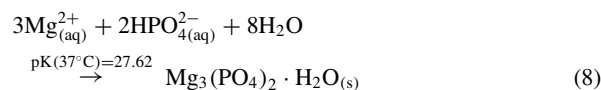
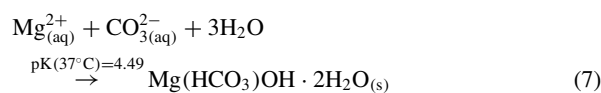
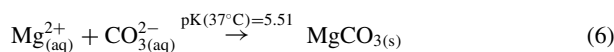
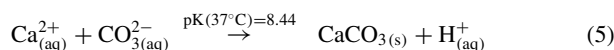
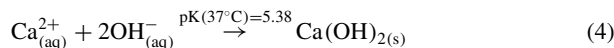
In general, the key factors controlling the degradation behavior of Mg-based implants in physiological media can be summarized as: medium composition, pH, temperature, CO₂ and O₂ concentrations, and medium flow rate, as well as alloying elements and materials processing routes [27,33]. The effect of these factors on the degradation process is not straight forward due to the interactions between them. Understanding these interactions is as important as recognizing the role of each individual factor within the degradation process. Fig. 2 presents schematic diagrams of the *in vitro* test and the key factors affecting its outcome. Fig. 2a presents the immersion test of Mg-based implants. In order to control the degradation test, the samples are placed into an incubator under physiological conditions (37 °C, 5% CO₂, pH of 7.4) (Fig. 2b).

2.2.1. The effect of the degradation medium

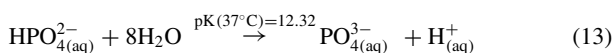
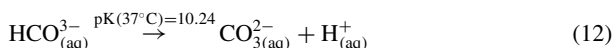
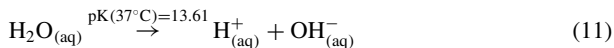
The degradation medium composition controls the nature of the degradation process and products, and therefore must be selected carefully to obtain comparable results to *in vivo* degradation tests [27,32]. Fig. 2d presents a schematic diagram of the effect of media composition over the degradation mechanism of Mg alloy. Different degradation media have been reported for studying the degradation of Mg and its alloys. These can be simple solutions, such as 0.9 wt.% NaCl, or a complex solution, such as Hanks' balanced salt solution (HBSS), simulated body fluid (SBF), phosphate buffered solutions, modified eagle medium, and Dulbecco's modified Eagle medium (DMEM) [11,27,32,10,11,27,35,57,58]. Recently, Mei et al. [59], reviewed the most common degradation media used in literature to test biomedical implants and the degradation mechanisms of Mg-based implants therein. A schematic illustration of degradation mechanisms from basic to highly complex is shown in Fig. 3. The complexity of degradation

media leads to more complex degradation mechanisms. Up to date, no universal medium has been declared to mimic *in vivo* conditions completely [11,27,35,57,58].

The effect of the medium's ionic composition. Due to the presence of additional ions in most of the degradation media used *in vitro* studies, the degradation layer or protective film that forms on the implant surface during degradation can contain several products in addition to Mg(OH)₂. Eqs. (4)–(10) list the main products predicted to form [30]. The presence of Ca²⁺ ions in particular has been shown to be highly important, as Lamaka et al. [60] reported a decrease of about 60% in the degradation rate when Ca²⁺ ions are added to HBSS, due to the formation of Ca-containing salts Eqs. (8)–(10) [32], as illustrated by Fig. 3 (Ringer's solution). In this case, the addition of Ca²⁺ ions was associated with a decrease in the near-surface pH during degradation and a corresponding decrease in the degradation rate [48,60]. If both Ca²⁺ and HCO₃[−] ions are present in the degradation medium, calcite formation Eq. (5) is observed, as shown in Fig. 3 (SBF and cell culture). In addition, the presence of anions HCO₃[−] and CO₃^{2−} have been shown to promote the formation of the precipitation layers of magnesite (Eq. (6)) and nesquehonite (Eq. (7)) [32]. Furthermore, the degradation of Mg in SBF medium is inhibited when a concentration of 27 mM or higher of HCO₃[−] is reported within the medium [48,61]. In early stages of degradation CO₃^{2−} ions are found to increase the degradation rate of Mg [48,62,63], while later they lead to the formation of a protective carbonate layer, due to the fact that most carbonate salts are insoluble under aqueous and physiological conditions (solubility constant of 10 × 10^{−8}). Another protective layer is induced by the phosphate ions (Eqs. (8) and (9)), which is most stable within a pH range of 4–7 [32,48] (Fig. 3, PBS and SBF).



rates [5,32]. Eq. (12) in particular depends on the presence of CO_2 in the atmosphere, which will dissolve to form carbonic acid in water and can then dissociate further.



The effect of organic components. In addition to the ionic composition of the medium, the presence of organic components plays an important role on the degradation process. A comprehensive review by Cai et al. [64], analyzed the effect of bioorganic compounds on the degradation and protection of Mg-based implants to gain a better understanding of how they influence the degradation process. In this review, the bioorganic molecules (glucose, amino acids, and protein) were shown to play a crucial role in the degradation behavior, mechanism, biomineralization, and surface modification of Mg-based implants. Nevertheless, not all experimental work yields a uniform picture. For example, different degradation behavior of high purity (HP)-Mg in the presence of proteins in different degradation medium was reported [65,66] and proteins were found to increase or decrease the degradation rate depending partly on the immersion time and on the alloy [64,65,67]. At the same time, other studies reported that proteins have a retardant effect on magnesium degradation and they alter the ion composition of the solutions [65–68]. During the degradation process, proteins are adsorbed onto the Mg surface resulting in insoluble layer acting as a barrier against degradation [34,64–66]. On the other hand, proteins, in particular bovine serum albumin, amino acids and organic chelating compounds may accelerate or slow the degradation of the implant by forming a complex with the metal cations [60,62,64,67,69,70]. Several studies reported that adding albumin to the degradation medium of Mg significantly changes its degradation environment and degradation behavior [71–75]. For example, in the early stage of degradation, the degradation rate of HP-Mg in HBSS solution containing fetal bovine serum (FBS) was found to increase. As with proteins, glucose can accelerate or retard the degradation of HP-Mg [62]. In saline solutions the transformation of glucose into gluconic acid, which rapidly interacts with the Mg oxides, decreases the pH of the solution, and promotes the absorption of chloride ions on the Mg surface. Due to this, the degradation rate of HP-Mg increases as the glucose content increases in saline solutions [62,76]. The opposite to this behavior is reported in Hank's solution, where the increased glucose content improves the formation of Ca-P compounds on the HP-Mg surface and hence enhances the degradation resistance [34,77].

The effect of pH and pH buffering. To control the environmental conditions pH and temperature, the well plates containing Mg specimen are placed into an incubator, schematic

diagram in Fig. 2b. Changes in pH shift the precipitation equilibrium during the degradation processes, which directly affects the degradation rate of Mg. The change in the pH of the media may move Mg from being immune to degradation to the degradation phase. Furthermore, the changes in pH directly affect the precipitation of salts within the degradation medium [48,60,78–80].

Based on our previous discussion, it is clear that controlling the pH is a major factor that controls the degradation process of Mg and the production rate of H_2 gas in the system [32,47,81,82]. The degradation process itself of Mg could increase the local pH because of the hydroxide ions produced during the cathodic reaction (Eq. (3)). Due to this the pH of media used in studying the degradation of Mg is controlled using buffer solutions and the CO_2 buffering system in incubators [10,81]. The effect of buffer systems used to regulate test media were highlighted in many studies [27,57,58,61,83]. A representative degradation medium should possess the similar buffering capacity to that of blood plasma [27]. Low concentrations of phosphate and plasma protein buffers (HPr/Pr) are important to regulate the pH values within the body. Additionally, both HCO_3^- and CO_2 are present in the body through the respiration process [27]. Gonzalez et al. [27] studied the effect of adjusting the SBF using most common buffers; 4-(2-hydroxyethyl)-1-piperazineethanesulfonic acid (HEPES), Tris-HCl, $\text{CO}_2/\text{NaHCO}_3$ and phosphate. A different degradation behavior than *in vivo* studies was reported under high concentrations of phosphate buffer. HP-Mg degraded four times faster in the presence of HEPES compared to CO_2 and NaHCO_3 , because HEPES inhibits the formation of the protective layer by lowering the pH and increases the diffusion of aggressive ions present within the media to the surface of the implant [27,33]. A similar effect over pH values was also reported when Tris-HCl was used, due to the fact that Tris-HCl consumes the hydroxide ions formed during the early stages of the degradation process (Eq. (3)) which leads to an increase in the degradation rates [27,61,84]. Based on the previous observations, researchers concluded that buffer systems should be carefully selected and only natural buffers should be used in order to reduce their effect on the degradation system. [27,60,69]. To clearly understand the interactions of the buffer ions and other ions during the degradation process, the variation of pH between bulk solution and the solution in the vicinity of the Mg surface must be interpreted carefully [48,60]. The concentration of CO_2 in the incubator was found to affect the pH and degradation rate. Note that the pH buffering within physiological medium is obtained by the presence of $p(\text{CO}_2) = 5\%$. The increased amount of CO_2 within the degradation media is found to elevate the pH of the system due to the formation of insoluble carbonates and hence suppress the degradation of Mg [48,64,76].

The effect of temperature. In addition to composition and pH of immersion media, the temperature of these fluids affects the degradation process of biodegradable Mg-based implants, Fig. 2b. The normal human body temperature is within the

range of 36.1–37.2 °C. In comparison to room temperature a temperature of 37 °C will slightly accelerate the degradation process [10,43] as temperature is one of the important factors that affect the solubility of different compounds. It is found for example to affect the precipitation of different calcium phosphates [85]. However, studying the effect of temperature over the degradation of Mg-based alloys is not possible without clarifying the connections and interactions between the temperature and other environmental factors, which includes pH and ion concentrations [27]. During *in vitro* tests the increased concentration of ions would lead to a slightly elevated temperature, which may affect the degradation rate by increasing the reaction constants [76].

The effect of hydrodynamic conditions. Because the degradation layer of Mg alloys is formed by dissolution-precipitation processes [10], any change in the surface chemistry of the implant will affect the degradation rate and the degradation process in general. Due to this, conducting the *in vitro* studies under dynamic or static conditions plays an important role in mimicking *in vivo* studies. The blood flow, for example, is one of the complex hydrodynamic conditions that can affect the degradation process *in vivo* studies. However, this case is not directly expressed within most *in vitro* studies [10,27,86]. The presence of hydrodynamic conditions affects the kinetics of the degradation reactions by changing the chemistry of the implant surface. Specifically, the mass transfer between the implant surface and the surrounding medium will be enhanced, which changes the concentrations of the degradation products, hydroxide ions, local chloride ion and cations by moving them away from the implant site [10,27,86–90]. These changes may result in changing the local pH of the implant surface by increasing the flow-induced shear stress (FISS) [27,42,89]. Due to the increased FISS, the deposition of the degradation products may be reduced, thus leading to an acceleration of the degradation of Mg alloys [34,65]. In addition, combining FISS and tensile stress was shown to slow the deterioration of strength and even reduce the variation in degradation rate. It is important to note that in this case, tensile stress has a much greater effect than FISS. As the tensile stress increases, degradation rates of Magnesium alloys are accelerated. Additionally, loss of mechanical properties and localized degradation morphology increased with the increase in tensile loading in different degradation media [91].

Most *in vitro* studies are still conducted under static or semi-static conditions [10,27], which means that the mass transfer process between the surface and the bulk medium is controlled by migration and diffusion. In this case, convection may only be present due to the H₂ evolution from the surface during the cathodic reactions (Eq. (3)) [10,27,88]. Under dynamic conditions, most reported studies were conducted under laminar flow with a moderate value of Reynold number (below 1000) [27]. Jia et al. [86], conducted dynamic immersion tests under cell culture conditions to investigate surface and internal degradation morphologies, porosity changes and degradation rates of three-dimensional porous Mg scaffolds. In terms of volume loss measurements under dynamic im-

mersion tests, scaffold degradation rates were significantly lower than under semi-static immersion tests for the same system [86,92]. Furthermore, the dynamic and statistic conditions were found to affect the adsorption of proteins within the degradation system, which affect the degradation of Mg-based implants. This was recently investigated by Hou et al. [70], where they studied the effect of BSA and FBS in HBSS under static and dynamic conditions. Both BSA and FBS resulted in a slight reduction of degradation rates due to protein adsorption and the formation of Ca/P salts on the top layer of the degradation layer under static conditions, while the reduction in the adsorption of proteins under dynamic conditions lead to a slight acceleration in the degradation rates.

The effect of the volume to area ratio (VA). It is also essential to discuss the volume to area ratio (VA), the implant's surface area to the immersion medium volume. Researchers reported that this ratio has a significant influence on degradation rates when it is lower than five [48,76,93,94]. Low VA ratios can result in a depletion of ions, resulting in the saturation of the medium with certain precipitates [48], with this case being mainly reported under static [27,93,94]. Further, controlling the VA ratio is of critical importance in the case of biodegradation of Mg-based implants to avoid changing the bulk pH and hence the *in vitro* degradation rates [27]. Conversely, the dynamic conditions would accelerate mass transfer between the surface and the bulk solution, resulting in forced participation and a reduction of the limiting diffusion layer. This explains why at the same VA ratio an increase in the FISS will increase the degradation rate under dynamic conditions compared to static conditions [27,91].

2.3. The effect of implant materials

Commercially available pure Mg cannot be used in load-bearing orthopaedic applications, due to its brittle properties, and insufficient corrosion resistance [9,20,49,95]. Accordingly, alloying systems are used to tailor these properties [96–99]. However, different grain sizes and intermetallic phases present in a Mg alloy, as well as metallic impurities, increase the challenge to understand the behavior of Mg-based implants. Localized degradation is observed within single-phase materials, which leads to pit formation on the surface of the metal [49,52]. However, the degradation reactions in aqueous environments are mostly dominated by microgalvanic coupling between magnesium and impurities or secondary phases, which are mostly present at the grain boundaries [49,50,52].

2.3.1. The effect of alloying elements and impurities

In biodegradable implants different alloying metals are introduced [10,100]. Fig. 2e presents a schematic diagram of the popular alloying elements used in magnesium alloys. The reactions of Mg alloys mainly depend on the alloy chemistry, due to this each Mg-based alloy should be tailored to meet the properties required by the target application position

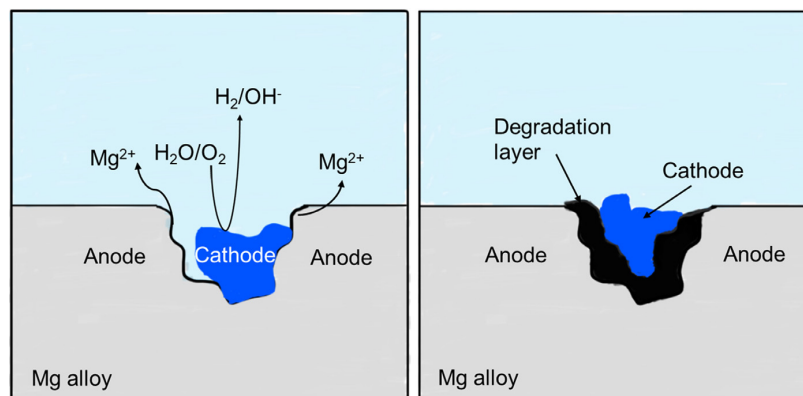


Fig. 3a. Schematic illustration of (a) galvanic degradation of Mg-based alloy, (b) the formation of the degradation layer.

[10,43,101]. It was reported that as Mg is alloyed with aluminium (Al) or zirconium (Zr) this will enhance the corrosion resistance. Note that for Al the concentration should be less than 6% in order to enhance both ductility and strength of the alloy [10,43]. However, studies showed that Al could cause nerve toxicity and may be related to Alzheimer due to the elevated concentrations of Al^{3+} in the brain [9,20,49,90], thus its use for implant materials should be avoided. When Mg is alloyed with Lithium (Li) it enhances the ductility of the alloy but may reduce the density and the strength of the alloy, which is solved by the ternary alloys with Al, or Mn (manganese) to form Mg-Li-x alloys [10]. Higher biocompatibility and enhancement in the bone healing process are clearly noticeable when Mg is alloyed with essential elements of the human body, such as calcium (Ca) and zinc (Zn), Bri.tech GmbH implants exhibit this characteristic [102,103]. Another example for Mg-based alloys is the alloys that contain rare earth elements (REE). The REE-Mg alloys are found to have high biocompatibility and better mechanical properties [20]. WE43-based implants (MAGNEZIX) from Syntellix (Hannover, Germany) are available in clinics [104,105]. Several published studies try to summarize the different alloying elements and their interactions, for example, summaries can be found in the reviews by Esmaily et al. [10], Chen et al. [9], and Song et al. [55]. Besides alloying, the coating of Mg-based implants has been investigated to enhance the mechanical properties and control the degradation process, where various coating techniques and surface modifications for the Mg-based implants [10,20,33,49,95,106].

The presence of impurities or intermetallic phases within the system of Mg alloys has been shown to lead to (micro)-galvanic corrosion, which can be accelerated through metallic re-deposition, as illustrated by the schematic diagrams in Fig. 3a. The galvanic corrosion takes place because of the low electrochemical potential of Mg. The alloying process leads to the presence of two or more metallic phases within the Mg-alloy, which will lead to a difference in the electrochemical potential and hence the Mg will be subjected to anodizing reactions [52,107]. Similarly, the presence of impurities such

as Fe, Ni or Cu will form micro-galvanic cells, due to the low solubility in Mg. These impurities not only increase the degradation rate of the Mg alloy but also severely effect its mechanical properties [10]. The standard theory of anodic dissolution of metals is not able to explain the strong hydrogen evolution reactions (HER) that take place in this case.

In the field of biodegradable Mg-based alloys, Höeche et al. [108] conducted a study highlighting this phenomenon within the field of the biodegradable Mg-based alloys. They correlated the HER with the electrochemical re-deposition of a thin iron film on the Mg surface. The re-deposition of Fe is found to accelerate the HER, due to the fact that the HER kinetics itself is strongly dependent on which impurities or the alloying element are present within the system [10,108,109]. As the reaction proceeds the re-deposition process becomes the determining process of the degradation system [108]. Höeche et al. [108] suggested that the HER kinetics is following the Heyrovsky mechanism, which is the preferred mechanism in an alkaline environment, based on different experimental studies of Mg-Fe systems. Hence the re-deposition mechanism combined with electrochemical desorption according to the Heyrovsky pathway will enhance the hydrogen generation during the degradation process of Mg in the presence of Fe, Ni, and Cu impurities. Based on this, within any system of Mg-based alloys containing Fe, Ni, or Cu, the metallic re-deposition must be restricted in order to control the degradation process [108]. However, recent studies by Kokubo and Takadama [58] and Zhang et al. [110] have demonstrated the presence of proteins and organic components as in DMEM+10%FBS increases the threshold at which Fe-impurities become detrimental to the degradation process. As noted in [67], the presumed micro-galvanic corrosion in simulated body fluid from impurities in the Mg led to a different degradation morphology, with sub-micrometer sized holes left within the degradation layer.

As a result of these findings and previous discussion, we can see that the degradation process of Mg-based implants is a highly complex multiscale process at the *in vitro* level. The process complexity increases at the *in vivo* level due

to the presence of additional factors, *e.g.* the presence of cells, and their complex interactions with the degradation process, as well as varying hydrodynamic and fluid properties [25,92,111]. Furthermore, different *in vivo* models need to be taken into account when studying degradation processes, such as rats, mice, and sheep [25,111]. Detailed experimental results regarding the *in vivo* and *in vitro* degradation behavior and rates of different Mg-based implants were summarized by Bairagi and Mandal [25], where Sekar et al. [111] focused on reviewing the latest development in studying the host response and degradation behavior of Mg-based implants in different animal models and clinical trials.

Understanding these factors and their correlations is crucial to build a reliable mathematical framework. In order to simplify the degradation process, several mathematical approaches appeared in literature, which resulted in having multiple models that are able to describe one or more but not all aspects of the degradation process. In the next section, we are presenting a comprehensive discussion of these approaches and the models derived under their assumptions and hypotheses.

3. Mathematical modeling and simulation studies of Mg-based biodegradable implants degradation

Mathematical models appear in the field of metal corrosion as early as the 1950s, mainly by a series of publications by Waber et al. [112–118] in which they provided mathematical representations and analyses of the galvanic corrosion of metals and the key factors affecting the process. Extended computational modeling has been applied to study different corrosion types of metals [119–123] and to predict their behavior under different conditions [124–128]. These early models helped in presenting the mathematical approach as a research tool aimed at improving the level of understanding of corrosion processes of metallic systems [119,120,123]. However, for biomedical implants, mathematical and computational modeling are relatively new concepts. The complexity of the system, *i.e.* unclear mechanisms underlying the degradation behavior, precipitate formation, interactions of ions and organic components, is large. Several computational models at both micro- and macroscopic levels have been applied to study the degradation of Mg-based alloys [121,129–135]. In the past few years, several researchers have reviewed the computational modeling of the degradation of Mg-based alloys [107,136,137]. A review by Boland et al. [136] presented a discussion of the degradation models of Mg-based stents and classified these models based on the degradation type as uniform, stress, pitting models. In a recent review by Abdallah et al. [107] the models were classified into phenomenological and physical models based on the basic principle of their derivation, a similar classification also proposed in a short review of bioabsorbable Mg-based stents by Zhang and Hao [137]. In this work, we are presenting an in-depth critical review of different degradation models developed to simulate the *in vitro* and *in vivo* degradation of Mg-based alloys. We elaborate the traditional classification of models into physi-

cal, phenomenological, analytical and machine learning-based models. Moreover, each of these models is classified into further subclasses. These subclasses clarify the different aspects covered by each model. Finally, the advantages and limitations of these models are thoroughly discussed.

3.1. Physical approach in modeling Mg degradation

The physical approach in modeling Mg degradation describes the models derived based on the Nernst–Planck equations (NPE). These models are able to capture several interactions within the system, *i.e.* the migration of ions, the formation of the degradation products and the dissolution reactions. The total flux (N_i , mol·s/m²) of ions in the immersion medium (electrolyte) is described by the NPE [131,138–143]

$$N_i = -D_i \nabla c_i - z_i F u_i c_i \nabla \phi + c_i U \quad (21)$$

where D_i is the diffusion coefficient, c_i denotes the concentration, z_i is the charge, F is Faraday's constant, U is the electrolyte velocity, and ϕ is the potential. The mobility, u_i , is estimated by the Nernst–Einstein equation

$$u_i = \frac{RT}{D_i} \quad (22)$$

here R is the universal gas constant and T is the absolute temperature. Under the assumption of a conserved flux of ionic species i , the mass balance of species flux including diffusion and migration at the beginning [131,141] is given by

$$\frac{\partial c_i}{\partial t} = -\nabla \cdot N_i = D_i \nabla^2 c_i - z_i F u_i c_i \nabla \cdot (c_i \nabla \phi) + \nabla \cdot (c_i U) \quad (23)$$

In order to solve the PDE system given in Eq. (23), further assumptions are required for each system. The degradation models derived from the physical approach can be classified into several subclasses according to assumptions proposed to simplify the PDE in Eq. (23). Several assumption were reported in literature, for example, to simplify the electrochemical reactions only Mg is assumed to be degraded [131,142]. Additional assumptions include the neglect of localized degradation, initially assuming a homogeneous surface, assuming that hydrogen bubbles do not react, and that re-dissolution of precipitates does not occur [131,141,144].

3.1.1. Activation controlled models

The activation control models are based on modeling the degradation of Mg-based implant as a function of the potential difference between the anodic Mg and the degradation media. This potential difference leads to accelerating the migration of Mg²⁺ ions from the degradation surface. And at this stage the migration will be faster than the formation of precipitate as presented by the overall degradation reaction (Eq. (1)) [131].

Deshpande [131] applied this approach to study Mg-Al alloy (AM30) system. A well-mixed (no concentration gradients) electroneutral, incompressible immersion medium was

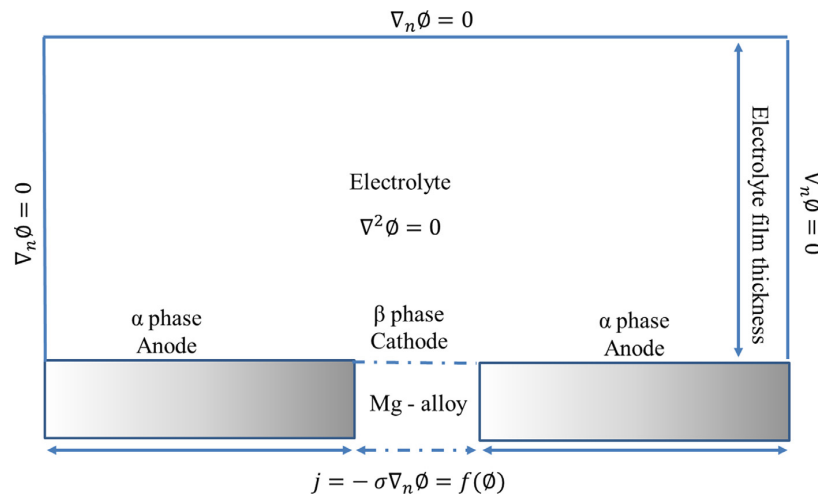


Fig. 4. The schematic of a computational domain along with the governing equation and the boundary conditions of Deshpande's model. The Mg-alloy was immersed in the electrolyte with an active exposure length of l . All other boundaries of the electrolyte were assumed to be insulated $\nabla_n\phi = 0$ (adapted with permission from Elsevier [131]).

assumed. Further, only the degradation of Mg-phase was considered by assuming that the degradation reaction only occurred at the anode surface (Mg-surface, α). Whereas the hydrogen evolution reaction took place at the cathode surface (Al-surface, β). These assumptions reduced Eq. (23) to

$$\nabla^2\phi = 0 \quad (24)$$

Insulation boundary conditions were applied to the electrolyte domain boundaries, presented in Fig. 4, to solve the potential Eq. (24). In this case, the degradation rate (DR) was measured as a function of the anode current (i_{anod}) based on Faraday's law:

$$DR = \frac{M}{zF\rho} i_{anod} \quad (25)$$

where M is the atomic mass of the degraded metal anode, ρ is the density, and F is Faraday's constant (96,485 C/mol).

Bharadwaj and Varadarajan [133] proposed an iterative method to solve the potential equation for a continuously changing computational domain with manually calculated coordinates based on the degradation rate/interface velocity. Deshpande [131] had coupled the model with adaptive meshing to investigate the effect of different metallic phases present. The application of the Arbitrary-Lagrangian-Eulerian (ALE) method enables the model to capture the moving interface during the degradation with high resolution [131,142,145]. Thus, Deshpande was able to capture the effect of the evolution of cross-sectional microstructure over the micro-galvanic degradation [131]. To validate the model, SVET experiments were conducted, where the current density was calculated based on Ohm's law [131,132]. Fig. 5 shows that the model was able to predict the spatial current density calculated from the SVET experiments. Both numerical model and SVET experiments indicated that the degradation rate increased as well as the anodic current density.

This could be explained by the enhanced degradation activity with the increased β -phase fraction. Note that the anodic current density was increased by an order of magnitude as the β -phase (cathode) increased from 10 to 90%. Also, the model was able to capture the increase in the degradation rate as the β -phase fraction increased, which was expected due to the increased cathode surface area. The deviation between the model prediction and SVET experiments could be explained by the fact that the model assumed no concentration gradient due to the unrealistic assumption of a well-mixed electrolyte. Also, the solution was assumed to be electroneutral, which is not the case in reality. Adding to that, the β -phase was not supported in this model, due to that it dissolved in the electrolyte solution as degradation progresses. Further validation of this approach was presented by Deshpande [132] for AE44–mild steel bimetallic couple system, where the degradation rates obtained by the model were within $\pm 7\%$ of the SVET experimental measurements.

Under the same assumption and using Eq. (24), Jia et al. [121] investigated the influence of geometrical factors on the degradation of magnesium AZ91D alloy in contact with mild steel. In this study, the Boundary Element Method (BEM) model predicted a similar distribution of the current density to the experimental measurements. However, the experimentally measured degradation rates were significantly higher. In order to achieve better agreement with experiments, Lacroix et al. [129] studied the galvanic coupling effect of Mg and Al, and calculated both the normal component and the radial component of the current distribution. Furthermore, a concentric geometry of two cylinders was used, which reduced the computational costs of the model. Montoya et al. [146], used this approach in modeling the effect of the electrolyte volume on the corrosion rate of an AZ31 implant *in vivo*. Based on the spatially explicit model derived here, a proportional relationship emerged between the electrolyte volume and the

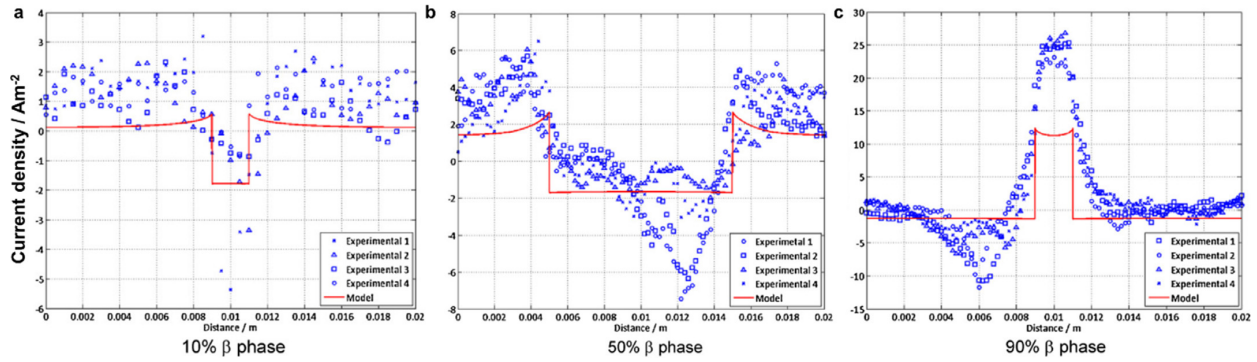


Fig. 5. The spatial current density variation predicted using the model and estimated from the SVET experiments for different phase fractions: (a) 10% (b) 50% and (c) 90%. (adapted with permission from Elsevier [131]).

degradation rate, with a higher degradation rate reported when the implants were covered with a thick layer of electrolyte. The study concluded that the thickness of the electrolyte was one of the key variables in understanding implant degradation *in vivo*. However, the model did not consider other important factors, such as grain size of the alloy, heat treatment, or the chemical environment and the evolution of hydrogen in the electrolyte, which resulted in the model being restricted to the conditions of the study. Additionally, a quantitative comparison with experimental data was not conducted.

The activation-controlled models were only able to estimate the galvanic current flow within an order of magnitude compared to the experimental values. Furthermore, these models could not predict the long-term current distribution, nor provide information regarding pitting corrosion [121,129,131,133]. These limitations of this subclass of physical models are due to the neglect of the effect of alloy composition, released Mg^{2+} ions, formation and nature of the degradation products, and the composition of the degradation medium. Furthermore, the assumption of stationary anode and cathode surfaces is unrealistic [131,142].

3.1.2. Diffusion-limited models

The second subclass of physical models of Mg alloy degradation are the diffusion-limited models, which are also known as the transport models. Diffusion-limited models assume the diffusion of Mg^{2+} and other ions as the rate-limiting in the transport process. This assumption neglects the influence of both fluid velocity and the migration of ions within the system. As a result, the PDE in Eq. (23) reduces to Fick's law

$$\frac{\partial c_i}{\partial t} = -\nabla \cdot (D_i \nabla c_i) \quad (26)$$

The diffusion-limited models also assume that the rates of chemical reactions associated with the degradation process are governed by the transport and solubility of metallic ions in the solution. So, the diffusion of Mg^{2+} ions can be described as:

$$\frac{\partial c_{Mg}}{\partial t} = \nabla \cdot (D_{Mg} \nabla c_{Mg}) \quad (27)$$

Grogan et al. [142], applied this approach to study the diffusion process of a pure Mg stent. This model used the moving boundary method to capture the movement of the degradation surface and investigated the degradation of the full stent geometries. However, there were no validation of this model with experimental data, which raised questions over its correctness. Furthermore, the Mg in this system was assumed to have no impurities, which limited the model validity to pure Mg with limited applicability to real experimental systems. Most applications use Mg-based alloys, which may be subject to micro-galvanic degradation. Also, this assumption created a challenge to track the evolution of the specimen geometry in case of high localized mass loss.

The same model was used by Shen et al. [147] to study the pitting degradation of Mg-1Ca and Mg-3Ge alloys. The parameters of the model were calibrated against the evolved hydrogen from the immersion experiments of a simplified pin geometry. Only the diffusion of Mg^{2+} ions in SBF was considered and the degradation layer was assumed to compose only of a dense layer of $Mg(OH)_2$. The degradation process was controlled by two main parameters: the diffusivity and the concentrations of Mg^{2+} ions.

To describe the moving interface, both Grogan and Shen used the a formula of the moving boundary velocity derived by Shen et al. and Scheiner and Hellmich [147,148] for pitting corrosion of stainless steel

$$\{-D \nabla c_{medium} (c_{alloy} - c_{deg}) \cdot \mathbf{n}\} \cdot \mathbf{n} = 0 \quad (33)$$

where \mathbf{v} is the velocity of the moving boundaries and the interface normal vector pointing to the degradation layer, is denoted by \mathbf{n} . The concentrations of Mg^{2+} ions were measured in the alloy (c_{alloy}), within the degradation media (c_{medium}) and the degradation layer (c_{deg} , denoted as the saturation concentration by Grogan et al.).

Grogan et al. [142] assumed the presence of a stable layer already covering the stent, note that there was no information about the composition of this layer, it was only used to sustain the assumption of diffusion-controlled degradation. Furthermore, there was no information about the degradation process before the formation of this layer. This limitation was

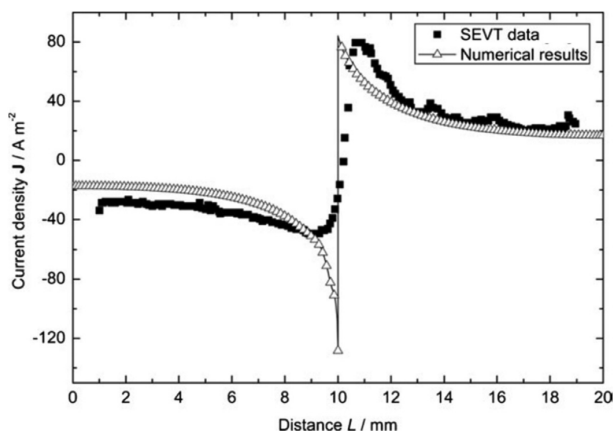


Fig. 6. Initial current density distributions predicted by Sun's model and obtained from the SVET experiments for AE44-mild steel bimetallic (adapted with permission from Springer [124]).

solved later by a further development of the model proposed by Sun et al. [124], which simulated the time-dependent deposition of degradation products on the metal surface by counting the changes in both electrical potential and mass transfer. Sun et al. [124] added the following assumption to this approach: (1) the deposits were porous with constant porosity, (2) there was no re-dissolution of the deposits after precipitation, (3) corrosion deposits are insulating. Based on these assumptions, in addition to being governed by Eq. (23) for mass transfer, the model accounted for electric potential variations according to

$$\frac{\partial}{\partial t} \nabla^2 \phi + \frac{\sigma}{\nu} \nabla^2 \phi = 0 \quad (28)$$

where σ is the conductivity of the electrolyte in S/m and ν is the relative permittivity. Sun's model thus included the electric potential of the deposits and the electrolyte in the electrical potential equation. Fig. 6 presents the initial current density distributions predicted by this model validated against validation data of SVET experiments [132].

Furthermore, Sun et al. [124] considered the porous nature of the degradation layer, which modified the diffusion coefficient in the mobility Eq. (22) as

$$D_{ie} = D_i(1 - \varepsilon) + \frac{D_i}{N_M} \varepsilon \quad (29)$$

where D_{ie} is the effective diffusion coefficient, N_M is the MacMullin number $N_M = \frac{\tau}{\varepsilon}$, where ε is the porosity and τ is the tortuosity factor of the degradation layer, respectively [149]. The outputs of Sun's model were in better agreement with experiments than the models presented by Deshpande [131] and Grogan et al. [142]. Further development was presented by Bajger et al. [139]. Bajger's model simulated the formation of the degradation layer in SBF media under physiological conditions. The level set method was implemented to capture the changing geometry of the implants during the degradation process [107,139]. HP-Mg with no initial protective layer was assumed. This assumption was justified in the case of in the

case of HP-Mg as a result of the lack of impurities a minimal ion transfer was ensured and the electrochemical degradation was negligible [142]. Bajger et al. assumed zero concentration of Mg^{2+} ions and only the presence of Cl^- ions in the electrolyte at the beginning of the reaction, based on this assumption the mass transfer in the electrolyte for both ions was measured as

$$\frac{\partial [Mg]}{\partial t} = \nabla(D_{Mg}^e \nabla[Mg]) - k_1[Mg] \left(1 - \frac{F}{F_{max}}\right) + k_2 F [Cl]^2 \quad (31a)$$

$$\frac{\partial F}{\partial t} = k_1[Mg] \left(1 - \frac{F}{F_{max}}\right) + k_2 F [Cl]^2 \quad (31b)$$

$$\frac{\partial [Cl]}{\partial t} = \nabla(D_{Cl}^e \nabla[Cl]) \quad (31c)$$

where k_1 , k_2 are the reaction rates pertaining to the formation and dissolution of the degradation layer. The model parameters were calibrated against HP-Mg experimental data, where the formation of hydrogen was used to measure the degradation rates. The calibration stage of the model enhanced the ability of the model to predict the degradation layer at different time points during the immersion test as presented in Fig. 7. No initial degradation layer at the initial time-step, Fig. 7a, where Fig. 7b shows that after 7 days a thin degradation layer was formed. However, the degradation layer was assumed uniform and no validation for its thickness was provided. Due to the lack of reported values in literature, the reaction rates were fitted using trial and error to the experimental data, which would increase the uncertainty in the model outcomes.

Recently, Barzegari et al. [150], developed Bajger's model for commercially-pure (CP) Mg biomaterials in simulated solutions; NaCl and SBF. The model considered the formation of a protective layer, the effects of the ions in the solution, and the changes in the pH due to the degradation phenomenon. Four scalar functions of space and time were developed to trace the changes in the ion concentrations of Mg^{2+} , chloride Cl^- ions and hydroxide OH^- ions, as well as the concentration of the protective film, which is mainly considered as $Mg(OH)_2$. Added to that, the level set method was implemented to trace the complex interface of the geometry. In order to simulate the pH changes in NaCl and SBF solutions, model parameters were calibrated using a Bayesian optimization algorithm. The model was able to simulate the pH change in NaCl and SBF solutions with an error of 5%. However, a drawback as with previous models arises from the fact that the model calibration was performed *via* tuning the diffusion rate in Eq. (31a), which does not account for physical phenomena.

Using this approach, Gartzke et al. [101], developed a FE model to investigate the formation of the degradation layer and the change in mechanical properties of the implant during *in vivo* degradation. In this model a 3D open-pored structure made of the magnesium alloy LAE442 was adopted to

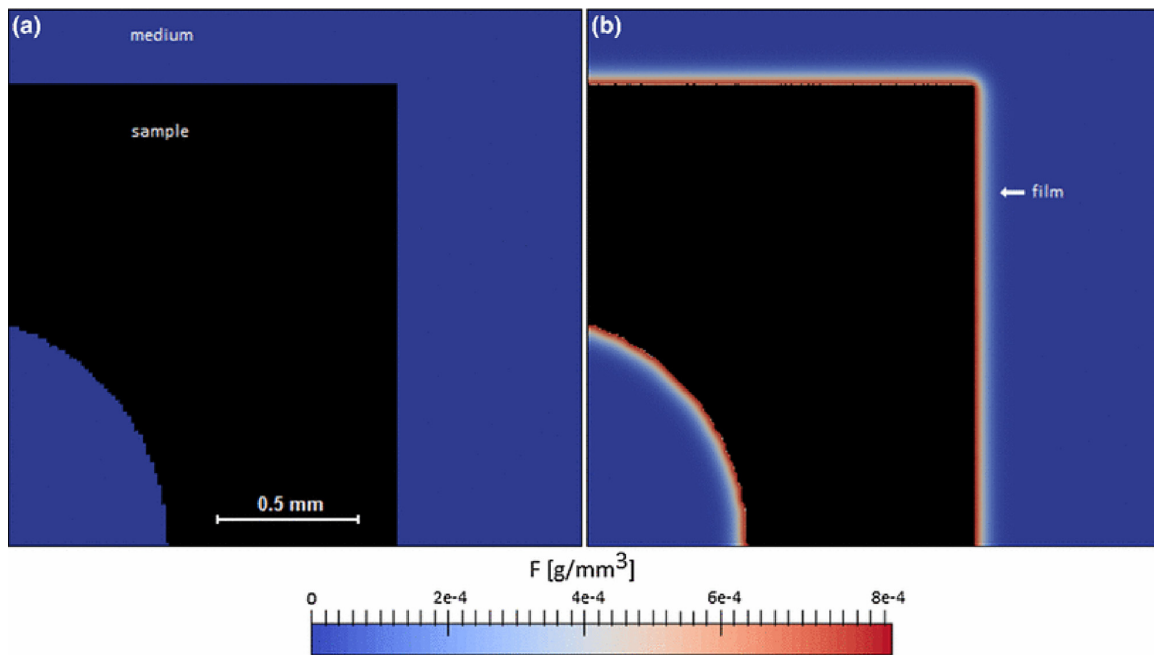


Fig. 7. The formation of a thin degradation layer predicted by the Bajger's model. (a) $t = 0$ days of immersion no degradation layer, (b) thin degradation layer after $t = 7$ days of immersion. (adapted from [139] under a CC-BY-4.0 license).

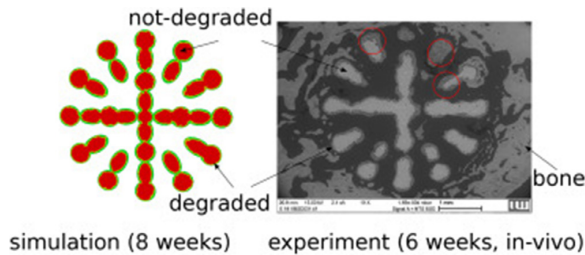


Fig. 8. FE model (left) and experimental results (right) of *in vivo* degradation on the implant structure at 8 weeks (simulation) and 6 weeks (μ CT image) (adapted from [101] under a CC-BY-4.0 license).

study the change in mechanical properties of the implant during the degradation process. Model calibration data was taken from *in vivo* experiments, where implants were inserted into rabbit femura and analyzed at 6, 12, 24 and 36 weeks post-implantation. The model was formulated to simulate a homogeneous material with a Mg concentration-dependent Young's modulus. To track the movement of the interface, the level set method was implemented. The model results regarding the dependence of Young's modulus on Mg concentration showed good agreement with an empirical solution for cubic open-cell foams. The model, however, failed to capture the inhomogeneous degradation behavior observed in the experiment (see Fig. 8), as the degradation was based on the diffusion of Mg^{2+} ions only. Further, a number of key factors were not considered, for example, the evolution of hydrogen and the formation of the degradation layer based on the precipitation of different salts based on the chemical environment.

3.1.3. Complex physical models

A more complex physical model was derived by Höche [141]. This model investigated the micro-galvanic degradation in a system of Mg coupled to Al. Several chemical reactions were included in this model; *i.e.* water disassociation (Eq. (11)), which were neglected in the previously presented models. The model further was able to simulate and quantitatively predicted the effect of degradation products on a time-dependent basis. Höche et al., modified Eq. (23) to

$$\frac{\partial c_i}{\partial t} + \nabla \cdot N_i = R_i \quad (32)$$

where R_i is the reaction rate of chemical species i . Furthermore, the impact of deposit porosity and pH development on the degradation rates were included in the simulations. However, this model assumed that the hydrogen gas bubbles were not interacting in the system, which was a challenge for the overall assumption of a non-degraded cathode. This would mean that the deposits were not affected by the gas bubbles. Also, the effects of gas dissolution in the electrolyte solution were neglected. Static conditions were assumed, which is not the case for *in vitro* testing of biomedical implants. The model also assumed that there were no localized corrosion effects, but it included some electrolyte species which would be responsible for the pitting degradation in the system. The model predictions were found in a good agreement with the validation experimental data.

Another complex model was introduced by Sanz-Herrera et al. [151] to simulate the effect of multiple chemical species on the *in vitro* degradation of Mg-based implant the model included a set of seven species; Mg (metal), H_2 , H_2O , Cl^- ,

MgO₂H₂ and MgCl₂. Fick's law (Eq. (26)) was used to predict the concentration gradient of each of these species. The current model was able to capture the trend of Mg degradation in calibration experiments but required different calibrations for every set of experimental data used. This model was calibrated to slow (0.05 mm/year) and fast degrading samples from the literature (0.3 mm/year), but no error metric was presented to compare model results to the literature. While the model included more ionic species than other models, it failed to incorporate the multitude of ionic species present in body fluids. Furthermore, this model was tested for *in vivo* application, where it was used to simulate the degradation of Mg-Zn-Zr screws implanted in Japanese white rabbits. The degradation process was determined by fitting the model key parameters, diffusion rate constant (D) and kinetic constant (k_d), to different scenarios of *in vivo* data, with the conclusion that the kinetic ratios influenced degradation rather than species diffusion. Note that the different fitting scenarios of the parameters reflected a ratio of four times faster degradation *in vivo*, however, the results for the *in vivo* case were fitted based only on a rough visual agreement of the degraded implant. Importantly, this model considered the pH evolution and hydrogen production, which are important factors not only for the degradation but also for the activity of the surrounding tissues. However, no comparison to experimental data was shown for these quantities and only a small number of relevant ions was included in the model. Therefore, while the presented model made an important step towards including some of the physico-chemical interactions in the system, it still contained a number of shortcomings when considering the biodegradation of Mg implants.

Recently, Zeller-Plumhoff and Albaraghteh et al. [152], developed a model that included all species pertaining to the reactions in Eqs. (4)–(10), as well as dissociation equations. This model simulated the degradation of pure Mg (99.92–99.95%) in SBF over four weeks and under semi-static immersion test. Data from weight loss and volume loss measurements was used to calibrate the degradation model. However, while the NPE was used to describe ion transport, the degradation rate itself was modeled using a data-derived equation. An error of 7% was reported for the simulation results of the anodic dissolution related degradation process of pure Mg in SBF. For the first time, the model presented a comparison to the literature of simulated precipitate formation, which was calibrated using data from energy-dispersive X-ray spectroscopy (EDX), as shown in Fig. 9.

Marvi-Mashhadi et al. [153], presented a simulation strategy to simulate the pitting degradation and the mechanical properties of WE43 scaffolds manufactured by laser power bed fusion after immersion in SBF. The strategy presented a phenomenological, diffusion-based model. The diffusion was modeled using FEM, where the values of the diffusion flux were randomly assigned based on the Weibull distribution. The Weibull distribution depends on two parameters: β determines the average degradation rate while γ controls the degree of localization of degradation, *i.e.* the lower values of γ would reflect higher pit formation. The values of β and

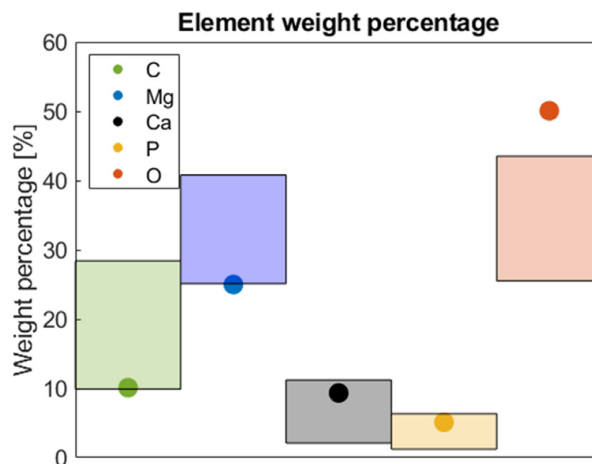


Fig. 9. The mean element weight percentages (wt.%) of elements in the degradation layer calculated based on the simulation and measurements using EDX. The scatter points are the predicted weight percentage from the simulation, while the shaded areas indicate the minimum and maximum mean values from the experiment (replotted from [152] under a CC-BY-4.0 license).

γ should be calibrated for each alloy and immersion environment, to define all the electrochemical and microstructural factors (pH, alloy composition, precipitates, etc.). The diffusion model was validated with X-ray computed tomography results of WE43 alloys immersed in SBF at different times. The geometric elements with a Mg concentration of less than 40% were considered forming precipitates (Mg(OH)₂) and were excluded from further mechanical simulations. The phenomenological part of the model was able to predict the reduction in the WE34 scaffold strength due to the progressive change in the deformation mechanisms with the immersion time. Overall, the simulation strategy was able to assess the effect of corrosion on the mechanical behavior of biodegradable scaffolds, which is critical for the design of biodegradable scaffolds for biomedical applications.

3.1.4. Simplified physical models

The physical approach is a well-established framework, but the need to update the domain of the system and the requirement for boundary tracking methods increases the complexity and computational costs of this approach. To reduce the complexity of the physical approach researchers have proposed simplified models. These models were simplified from computational and mathematical points of view but kept the physical principles of the physical approach. For example; Ahmed et al. [140] developed an advection-diffusion model of Mg-based alloy degradation in an aqueous environment with multiple moving boundaries to investigate the initial degradation process of pure Mg pellets. The simplified model was built by integrating triphasic models, which enabled the dimensionless presentation of different model parameters, which reduced the mathematical complexity of the model. Moreover, dimensionless studies were known to highlight the true effect of each parameter within the model. Despite the simplification of the model, the model was able to demonstrate the effect

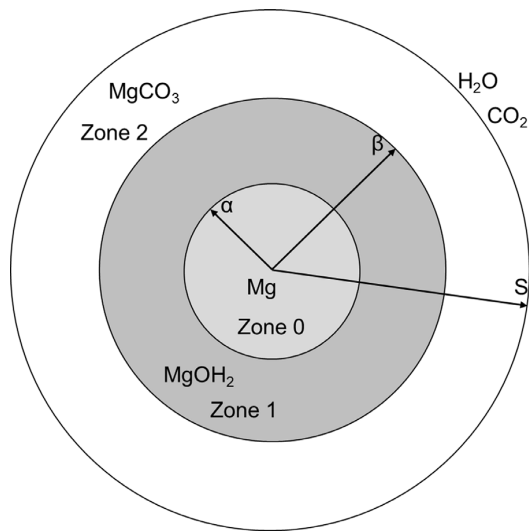


Fig. 10. Schematic diagram of triphasic model presented by Ahmed et al. [140], α , β and S are the interface distances of the different phases (redrawn from [140]).

of different chemical species over the *in vitro* degradation of Mg. Furthermore, the integration of the flow of liquid phases in porous media enhanced the model's ability to predict the dynamic change in the amount of Mg and the degradation products over time. The schematic diagram in Fig. 10 shows the map of Ahmed et al. model. By using the r as spatial coordinate, Ahmed et al. [140] modeled the initial degradation process as a function of the formulation of $\text{Mg}(\text{OH})_2$ in zone 1 (the region $\alpha < r < \beta$), MgCO_3 , in zone 2 (the region $r > \beta$) and neglected the presence of other species within the system. Furthermore, the porosity of the layers was neglected to ensure a smooth surface which is not the case observed in experiments.

Since solving the physical model can be computationally expensive, analytical functions can be fitted to the physical model predictions to reduce computation time. Adaptation of this approach was made by Shen et al. [147], where the physical model was solved only for the first 250 h of degradation. Then, a power function was used to fit the data and the degradation rate was calculated using the formula

$$\frac{d(\Delta v)}{dt} = A.Bt^{B-1} \quad (34)$$

where A and B are empirical parameters depending on the type of the alloy and the degradation media. In the case of Mg-1Ca alloy pin immersed in SBF solution, A had a value of 0.00198, where B equaled 0.52207. Where for Mg-3Ge alloy pin immersed in Hanks solution a value was 0.00011 and B was 0.98172. The integration of empirical fitting parameters enhanced the agreement with the experimental data for Shen et al. [147]. A similar approach was taken by Grogan et al. [142], who fitted the mass loss using $M = \alpha D^\beta c_{sat} \sqrt{t}$, with t the degradation time, D the diffusivity, c_{sat} the saturation concentration of Mg^{2+} ions in the medium and α , β fitting parameters.

Dahms et al. [154] immediately derived an analytical model based on the mass conservation law, which was considered a simple two-phase analytical model. The aim of this model was to predict the long-time degradation of Mg-0.3Ca implant material in defined physiological electrolyte environments. The model described the mean degradation depth *via* the analytical formula

$$h = h_0(1 - e^{-h/h_0}) + h_\infty t \quad (35)$$

here, h is the mean degradation depth obtained *via* fitting from mass loss experiments, h_0 is the initial degradation depth resulting from the rapid reactions and h_∞ is the long-time degradation depth. The time-dependent degradation rate DR was measured by differentiating the above equation with respect to time

$$DR = \frac{dh}{dt} = \frac{h_\infty t}{1 - e^{-h/h_0}} \quad (36)$$

While empirical models yield good results for fitting the experimental data, their lack of consideration with respect to the electrochemical processes occurring during Mg implant biodegradation limits their application to systems where enough experimental data is already available to calibrate the model empirical parameters. Therefore, predictive modeling cannot be achieved for differing alloy systems or environments. Furthermore, the accuracy of the model would depend directly on the accuracy of the calibration data, due to the use of the best fit method in the calibrations of model parameters.

3.2. Phenomenological approach in modeling of Mg degradation

The phenomenological approach is the second main approach in the modeling of Mg degradation. The models under the phenomenological approach are derived and developed based on the continuum damage theory (CD), which was introduced to calculate the effective stress in geometries with internal discontinuities [155–157]. The mathematical description of the degradation process under this approach includes the use of empirical models for surface erosion and their associated mass-loss rates, which integrate the description of the mechanical characteristics under multiple mechanical loads [12]. The transition between simplified physical models and phenomenological models is therefore fluid. CD theory models the degradation based on the damage evolution formula presented by Amerinatanzi et al. and Wenman et al. [138,158]. In general, Amerinatanzi et al. and Wenman et al. defined a scalar damage parameter D , which has a value between 0 and 1, which 0 represents a nondamaged, initial geometry, and 1 an element is fully damaged, fully degraded [156,157]. According to the literature, two main issues were reported to associated with the phenomenological approach; it is highly sensitive to mesh resolution as well as the calibration of D required experimental data for each test system [144,157,159,160]. Nevertheless, phenomenological models provide information on the interactions of im-

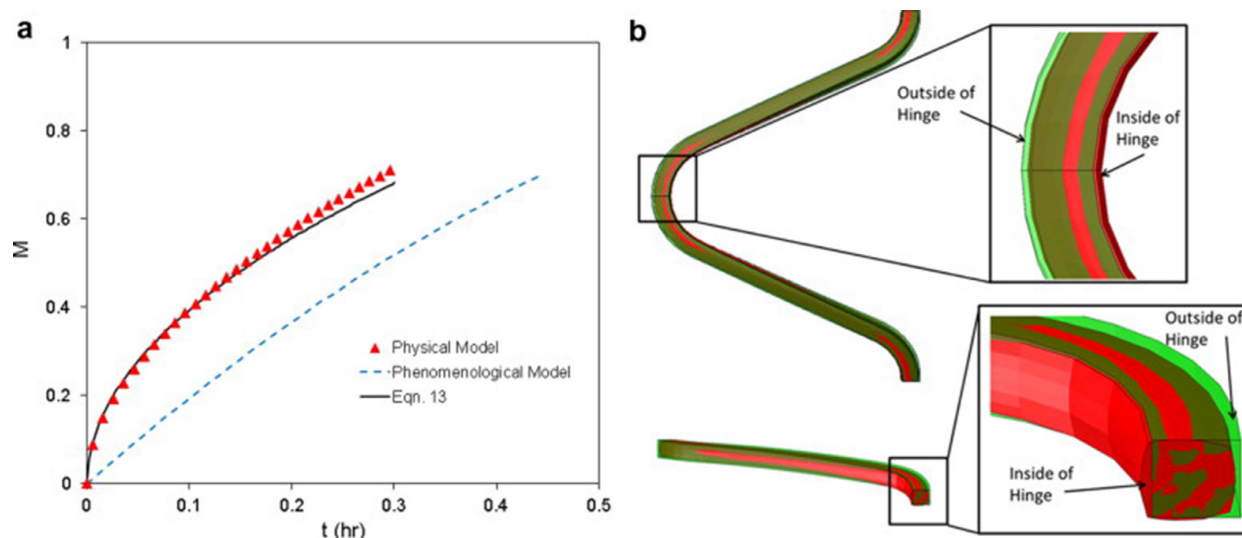


Fig. 11. (a) Comparison of percentage of mass loss over time predicted by the degradation models derived by Grogan, the physical model [142], phenomenological model [156] and analytical formula. (b) Comparison of the stent geometry at 70% mass loss for both models. The physical degradation model is shown in red and the phenomenological model is overlaid in transparent green (adapted with permission from Elsevier [142]).

plants with the surrounding environment and can be utilized to predict the mechanical functionality of implants under different conditions of physiological loading [2,107,156]. Due to this, models derived under the phenomenological approach are used in the optimization of manufacturing processes, material design and fabrication techniques of Mg-based alloys [12,142].

3.2.1. Uniform, pitting and stress cracks models

The damage evolution formula to reflect the status of the internal geometry over time for uniform degradation is

$$\sigma = (1 - D) \tilde{\sigma} \quad (37)$$

where $\tilde{\sigma}$ and σ are the effective stress and true stress, respectively. Combining the concept of the scalar damage parameter with the degradation mechanisms of Mg-based alloys, the mass loss during degradation over time can be calculated [107,156,161].

A CD model of Mg-based stent degradation was proposed by Gastaldi et al. [157], where the stent was assumed to experience two degradation mechanisms: the linear superposition of stress corrosion and uniform micro-galvanic corrosion. Gastaldi et al. therefore decomposed the damage parameter into two parts

$$D = D_U + D_{sc} \quad (38)$$

where D_U is the uniform degradation damage and D_{sc} the stress corrosion damage. In the current model, the rate of evolution of damage factor was modeled as

$$\frac{\partial D_U}{\partial t} = \frac{\delta U}{L_e} k_U \quad (39)$$

where δU and L_e are the characteristic dimension and k_U is the kinetics of the uniform corrosion process. While the D_{sc}

was assumed to follow the damage evolution law assumed for the stress degradation process in stainless-steel models

$$\frac{\partial D_{sc}}{\partial t} = \begin{cases} \frac{L_e}{\delta s} \left(\frac{S\sigma_{eq}^*}{1-D} \right)^R & \sigma_{eq}^* \geq \sigma_{th} > 0 \\ 0 & \sigma_{eq}^* < \sigma_{th} \end{cases} \quad (40)$$

where σ_{eq}^* is the equivalent stress affecting the entire stress degradation process, σ_{th} is the lowest stress value at which the stress degradation occurs. δs is the characteristic length of the stress degradation process, where S and R are parameters related to the degradation media, which are assumed constant over time. In Gastaldi's model σ_{th} was assumed to equal half of the yield stress of ZM21 alloy.

The calibration of the model with experiments showed that the developed model reproduced the behavior of different magnesium alloys subjected to static degradation conditions. Gastaldi's model parameters, S and R were calibrated to simulate the experimental response of uniform and stress degradation experiments and replicated the curve of global damage over degradation time. The model was implemented into a finite element (FE) framework where the damage increment was calculated and hence the degradation of Mg-based stent was measured [157].

Grogan et al. [156] derived a model under the CD approach to study the effect of degradation on the mechanical integrity of stents made of Mg-based alloy (AZ31). The model was able to predict the performance of the stent in an idealized arterial geometry during the degradation process. The use of CD allowed studying the induced micro-scale geometric discontinuities by degradation on overall specimen mechanical integrity without the need for their progression to be explicitly modeled. This was done by introducing the pitting parameter λ_U to the uniform degradation damage formula as in

the following equation

$$\frac{\partial D}{\partial t} = \frac{\delta U}{L_e} \lambda_U k_U \quad (41)$$

The pitting parameter was randomly assigned to each element of the degradation surface through the use of the Weibull distribution-based random number generator [136,156]. All the model parameters were calibrated and quantitatively validated by experiments. However, due to the random location of the pit nucleation, the model could not accurately detect pit location. [136,142,162].

Fig. 11 presents a comparison of the two models derived by Grogan et al., the physical [142] and the phenomenological [156]. Both models were tested for the same geometry and under the same conditions. As shown in Fig. 11a, differences between the physical model (and the derived analytical formulation) and the phenomenological model can be observed. Fig. 11b shows that the physical model predicted greater mass loss on the outside of the hinge and less mass loss on the inside of the hinge than the phenomenological model with comparison to the analytical formula derived based on the fitting of the experimental data [142]. The observation of non-local mass transfer, due to the pit formation, affected the degradation process and explained the difference in the predicting degradation rates between the physical [142] and the phenomenological [156] models.

Boland et al. [144] implemented Grogan's phenomenological model to simulate the localised pitting of a WE43 stent in a joint model of artery remodeling around the stent. The degradation parameters were recalibrated to fit the degradation of a Biotronik Magmaris stent. The aim of this model was to determine the material corrosion rate k_U , Weibull function parameter γ , and the growth rate parameter, β . These parameters were validated against independent *in vitro* degradation experiments. This simplified degradation model was considered sufficient to demonstrate the functionality of the biodegradable stent, although it did not consider the influence of the biological system on the degradation of the stent, in particular the remodeling of the artery around the stent struts. Moreover, no experimental validation of the model was provided.

3.2.2. Gurson-Tvergaard-Needleman (GTN) model

Vijayaraghavan et al. [123], presented a modified constitutive material damage model to study the stress corrosion cracking SCC of AZ31 alloy. The Gurson-Tvergaard-Needleman (GTN) model is a modification of the CD approach assuming that the damage occurring in the alloy is a result of the formation of the mild cracks and voids on the surface of the alloy under external stresses [123,137]. This model can predict the mechanical properties of AZ31 alloy under different temperatures and strain rate. Vijayaraghavan's approach provided better predictions of the failure and crack evolution of AZ31 alloys in different degradation media than Grogan's CD model. The governing equation of this model

was based on the GTN equation [123,137]

$$\phi = \frac{q^2}{\sigma_y^2} + 2q_1 D^* \cos h \left(\frac{-3q_2 p}{2\sigma_y} \right) - (1 + q_3 D^{*2}) = 0 \quad (42)$$

where σ_y , p , q are the equivalent, hydrostatic and effective stresses respectively, where q_1 , q_2 , and q_3 are fitting parameters to improve prediction of void interaction effects. The damage parameter D^* was expressed as a function of void volume fraction f , where the normal yield condition equals the GTN yield for $D^* = 0$ and the alloy fails when $D^* = 1$ [123].

To overcome the challenges associated with studying both pitting and stress crack degradation, researchers proposed other approaches, like peridynamic (PD), cellular automata (CA) and phase-field (PF) models. These approaches have been reviewed by Jafarzadeh et al. [163] for the material science field. Prior research suggests that these approaches may be implemented to study the degradation of Mg-based biodegradable implants and may be regarded as a development of the CD approach.

3.3. The cellular automata (CA) approach

The cellular automata (CA) approach has been used in different fields like public transport systems, forest fire spreading, biology, ecology and agriculture [163,164]. CA models simulate the evolution of multi-phase systems by simulating the behavior and interactions of the individual cell [163,164]. In degradation studies, the basic principle of this approach is to reduce the complexity of the system by simplifying the chemical reactions within the system based on the local simplified heuristics rules of the domain cells. The simplification of the reaction system captures the behavior of the large-scale reaction system based on the local interactions of the cells [164]. This reduction in complexity is related to the probabilistic nature of the CA technique, which represents the random properties of the electrochemical degradation reactions. Furthermore, the probabilistic nature of the CA approach eliminates the need for PDE-based mathematical formulation, thus reducing the computational cost [163]. CA models contain qualitative presentations of some basic physical and chemical processes [163,164]. However, CA models depend on the studied material systems, the rules enforced for the transition process, the determination methods of the CA model parameters and the model dimensions [164–167].

A recent paper by Shahmohmmadi et al. [168], implemented a three-dimensional CA model to study the degradation behavior of Poly-Lactic acid (PLA) and Mg alloy stents. The target of this model was to optimize the volume ratio of Mg within the stent. The optimal design of the stent was obtained by modeling different volume fractions of Mg and the CA model parameters were calibrated against experimental results of 10% of Mg volume fractions. The proposed CA model was able to calculate the degradation rate of Mg in Hank's buffer solution and to estimate the mechanical prop-

erties of the stent. The calibration of the model showed the optimal stent to have 5% of Mg volume fraction. According to the optimized CA model, 2.735% of magnesium was degraded after 30 days, whereas 2.716% were degraded in an experiment under the same conditions.

In metal degradation, CA models were found capable of including alloy microstructure in pitting corrosion [169]. Furthermore, the rules for the reaction-based restriction were found to obtain realistic looking and stochastic pit morphologies [165]. The main advantage of CA models is the simple computational framework that demonstrates the complex degradation system. A number of questions regarding the parametric nature of these models and the absence of quantitative comparisons to experiments remain to be addressed [163–165,167,170]. Further, solutions and methodologies are needed to overcome the limitation of the CA model dimensions [163,171,172]. This drawback is because the time magnitude and the spatial sizes are not derived based on any physical quantities, thus both require experimental data for calibration for all transition rules [163].

3.4. The peridynamic (PD) approach

The peridynamic (PD) approach is based on a recent theory that provides the possibility to handle material failure in solid structures [163]. In solid mechanics, PD models are based on the integrodifferential equations, the solution of these equations includes solving the discontinuities in a solid structure, which is known as fracture and damage [173,174]. The PD approach is a further development of the CD approach, where the PD models make use of a characteristic length scale "horizon", which determines the region of the nonlocal interactions. These nonlocal interactions occur between each point in the test domain and its neighborhoods [175]. Furthermore, these interactions are controlled with a response function, which includes all the constitutive information of the material [173,174]. This means the PD models predictions do not depend on the mesh as is the case in the FE-based models, which reduces the accuracy of the model [176]. Due to that, PD models are considered stable and they accurately predict the fracture and crack propagation in solid materials [173,174]. The application of this approach in studying the degradation of Mg-based implants may provide a solution to the deviation observed in the predictions between the phenomenological and physical approaches. This assumption could be explained by the fact that the PD approach captures the non-local mass transport, that occurs when the degradation is described by Fick's law (Eq. (27)) [131,139,142]. PD models view the degradation as a type of damage induced in the metal by dissolution, which is coupled with the diffusion problem in the electrolyte [163]. This non-local mass transfer was found to affect the degradation process as explained before when explaining the difference between the physical and the phenomenological models presented by Grogan et al. [142,156].

Chen and Bobaru [175] applied the PD approach to study the pitting corrosion damage in Mg-alloys, where only the an-

odic reaction was modeled as peridynamic diffusion process. Chen and Bobaru [175] coupled the phase-change mechanism to the system to allow the evaluation of the moving interface. This coupling eliminated the need for the flux continuity condition at the interface and allowed autonomous evolution of the moving interface. Furthermore, the complex chemical interactions were contained within the effective diffusion properties. A similar implementation to study the degradation-induced damage in Mg-Zn-Zr (ZK60A) alloy was done by Li et al. [177,178]. A diffusion degradation layer was introduced to describe the partial degradation domain and it was differentiated from the degradation product layer. The elemental analysis showed that the composition of the diffusion layer was mainly partially oxidized magnesium and diffused chloride ions. The governing PD equation is given by [175,177]

$$\rho(\mathbf{x}, t) \mathbf{u}(\ddot{\mathbf{x}}, t) = \int_{H_x} \mathbf{f}(\hat{\mathbf{x}} - \mathbf{x}, u(\hat{\mathbf{x}}, t) - u(\mathbf{x}, t)) dV_{\hat{\mathbf{x}}} + \mathbf{b}(\mathbf{x}, t) \quad (43)$$

where ρ is the mass density, \mathbf{u} is the displacement vector field, the horizon is H_x , \mathbf{f} is the pair-wise force function in the peridynamic bond connecting material points $\hat{\mathbf{x}}$ and \mathbf{x} and \mathbf{b} is the body density. In the case of ZK60A, the problem was considered as a static problem, which reduced the PD equation into

$$\int_{H_x} \mathbf{f}(\hat{\mathbf{x}} - \mathbf{x}, u(\hat{\mathbf{x}}) - u(\mathbf{x})) dV_{\hat{\mathbf{x}}} + \mathbf{b}(\mathbf{x}, t) = 0 \quad (44)$$

The energy minimization method was used to solve the PD static problem. The principle of energy minimization method was used to adapt the conjugate gradient method with secant line search, which minimized the energy in the system [177]. The above PD models showed that the degradation layer was not easily separable from the bulk, which would increase the initiation of the cracks and the possibility of them propagating into the bulk under external stresses [178]. These findings were supported by the experimental studies [177].

In a recent publication, Hermann et al. [179] proposed a computational framework to study the *in vitro* degradation of Mg-based biodegradable implants. This framework included two main models; 3D PD model to model the degradation of Mg-based alloys and FE model of the residual strength of the implant. The two models were connected *via* a damage variable. The PD degradation model was calibrated to volume loss experiments of Mg-5Gd and Mg-10Gd implants studied *in vitro* over the course of 8 weeks, as shown in Fig. 12. In this model, an adaptive multi-fine-grid discretization in space and an implicit time-stepping algorithm were implemented to enable the computationally efficient simulation of the complex screw geometry over the entire degradation time. The simulation domain was truncated in close proximity to the implant of interest by introducing non-local Dirichlet absorbing boundary conditions in order to maintain the accuracy of the method. An evolutionary algorithm was used to select non-local kernel functions and calibrate parameters based on volume loss over time experimental data. The model output

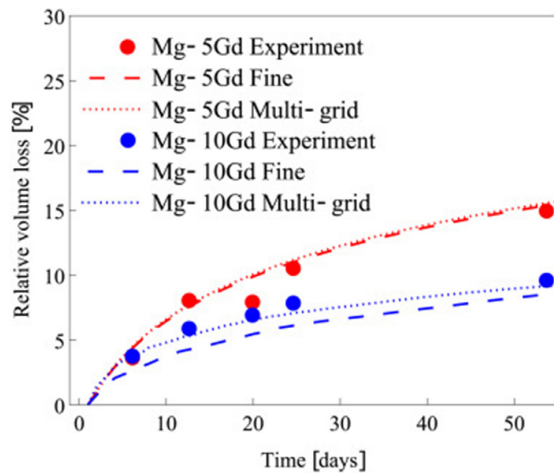


Fig. 12. Experimental and simulation volume loss for Mg-5Gd and Mg-10Gd, respectively (adapted from [179] under a CC-BY-4.0 license).

regarding the residual strength of the implant agreed with experimental observations.

In PD models the propagation of the degradation front does not depend on the discretization as it does for the CA approach. Because the PD theory itself does not require any assumption on the differentiability of the displacement field, no special treatments are needed for the displacement field due to the presence of crack [176]. Furthermore, the presence of the damage-dependent micro-diffusivity coefficient enables the PD models to incorporate different degradation types. Adding to that, PD can be extended to include the chemo-mechanical models, which enabled the analysis of stress-dependent corrosion and stress corrosion cracking [163,180]. In PD models, both mechanical and diffusion properties were found to change gradually within the degradation layer, which simulated the actual degradation process. The nonlocality of PD models increased the computational cost of the models because the volume integrals were required to be evaluated at each point in the domain. Parallel computing or the implementation using graphics processing unit-based computing could help in reducing the computational time, but this would increase the complexity of the implementation. Another drawback of the PD models was known as “the PD surface effect”, where the behavior of the model near the boundaries were different than the bulk, which required to apply boundary conditions [163,180].

3.5. The phase-field (PF) approach

Phase-field (PF) models were implemented to study the degradation of Mg-based implants. These models were applied to evaluate the interfaces between different phases [123]. The mathematical formulation of the PF model constructed by applying the Allen–Cahn and Cahn–Hilliard equations [181]. These equations were coupled to evaluate the phase-field $\varphi(\mathbf{X}, t)$, and the concentration field, which is also known as the

molar concentration of dissolved metal ions c , under the assumption of minimized free energy functional $\mathcal{F}(\varphi, c)$. The form of $\mathcal{F}(\varphi, c)$ depends on the type of degradation system [182]. Note that the value of φ is 1 in one domain and 0 in the other, where over the interface region it will have a value between 0 and 1. The PF models included a length scale due to the presence of the thickness of the interference (l). The material phase of transition described by the Allen–Cahn equation [120,163,181]

$$\frac{\partial \varphi}{\partial t} = -L \frac{\delta \mathcal{F}}{\delta \varphi} \quad (45)$$

where L is the interference kinetics parameter and $\delta \mathcal{F} / \delta \varphi$ is the variational differentiation of the energy functional with respect to the PF variable [182]. Cahn–Hilliard equation describes the evolution of the molar concentration of the metal atoms [120,163,181]

$$\frac{\partial c}{\partial t} = \nabla \cdot \left(\mathbf{D} \nabla \frac{\delta \mathcal{F}}{\delta c} \right) \quad (46)$$

where $\delta \mathcal{F} / \delta c$ is the variational differentiation of the energy functional with respect to concentration [182]. \mathbf{D} is the scalar diffusion mobility and it is a function of the diffusivity of the electrolyte, the free energy functional and the type of degradation.

Ma et al. [181] implemented the PF approach to simulate the impact of the stress assisted degradation of biodegradable Mg alloys with porous microstructures. In this investigation, Mg-based plates with and without pores were simulated. The phase-field variable φ was set to 0 for the electrolyte and 1 for the Mg. The total free energy of the system was given by

$$\mathcal{F} = \mathcal{F}_{el} + \mathcal{F}_{bulk} + \mathcal{F}_{int} \quad (47)$$

where \mathcal{F}_{el} represented the elastic strain energy stored in the system. \mathcal{F}_{bulk} and \mathcal{F}_{int} presented the electrochemical energy of the bulk phases and the interface energy required for material dissolutions, respectively [181]. As shown in Fig. 13, the PF model was able to simulate the evolution of the degradation surface during the stress assisted corrosion process of Mg-based alloys.

The mathematical nature of the PF models increases the computational cost of these models. The coupled PDEs introduces a dense mathematical framework to the system. Furthermore, PF models are strongly dependent on the selected free energy function, which would affect the ability of PF models to predict the damage evolution. A transition region was observed within the PF models at the degradation front similar to PD models. But in PF models this layer was found to depend on the selected free-energy function, where as in PD models this layer was found to depend on the nearby conditions around a test point. Due to this, PF models failed to predict the oscillatory behavior in thermally driven cracks but PD models were able to predict this behavior in high detail [183–186].

Table 1

Summary of the degradation models of biodegradable Mg-based implants investigated in this review, which were published between 2011 and 2022.

Authors	Model type	Study system	Brief description	Limitation
<i>In vivo</i> models				
Montoya et al. [146]	Physical – activation control model	AZ31 <i>in vivo</i> model: rat femurs	Studied the effect of electrolyte volume on the corrosion rate of an AZ31 implant <i>in vivo</i>	<ul style="list-style-type: none"> • No validation • Only considered the diameter and density of particles and the electrolyte volume
Gartzke et al. [101]. In	Physical – diffusion limited model	Magnesium alloy LAE442 <i>in vivo</i> model rabbit femurs	A 3D open-pored structure made of the magnesium alloy LAE442 was adopted to study the change in mechanical properties of the implant during the degradation process considering the different implantation locations (femur of rabbits)	<ul style="list-style-type: none"> • Qualitative results were obtained for the degradation due to the observed irregular behavior of the degradation • Only consider the diffusion of Mg ions and changes in Mg concentration and ignore all other influencing factors
Sanz-Herrera et al. [151]	Physical – semi-complex model	Mg-Zn-Zr screw <i>in vivo</i> model Japanese white rabbits femurs	The model simulated the degradation of Mg screw alloys (Mg-Zn-Zr) implanted in Japanese white rabbits	<ul style="list-style-type: none"> • Only qualitative measurements were reported
<i>In vitro</i> models				
Deshpande et al. [125]	Physical – activation control model	Mg-Al alloy (AM30)	The degradation of Mg-based alloy was described as a function of the potential difference between the anodic Mg and the degradation media. The ALE method was used to capture the moving interference during the degradation	<ul style="list-style-type: none"> • The concentration gradient was neglected under the assumption of well-mixed electrolyte • The solution was assumed to be electroneutral • Only considering the Mg-phase for the degradation process
Jia et al. [121]	Physical – activation control model	AZ91D alloy in contact with mild steel	Studied the influence of geometrical factors on the degradation process. The BEM was used to predict the distribution of the current densities	<ul style="list-style-type: none"> • The degradation rates were significantly lower than the experimental measurements
Grogan et al. [142]	Physical – diffusion limited model	Pure Mg stent	Presented a methodology to predict different saturation concentrations and diffusivities with full stent geometries. The model used the moving boundary method to capture the movement of the degradation surface	<ul style="list-style-type: none"> • Limited to pure Mg • Missing validation with experiments
Shen et al. [147]	Physical – diffusion limited model	Mg-1Ca and Mg-3Ge alloys.	Modeled the pitting degradation of Mg-1Ca and Mg-3Ge alloys, the model parameters were calibrated against the evolved hydrogen from the immersion experiments of a simplified pin geometry. The degradation process was controlled by two main parameters: the diffusivity and the concentrations of Mg ²⁺ ions	<ul style="list-style-type: none"> • Only the diffusion of Mg²⁺ ions in SBF was considered • the degradation layer was assumed to compose only of a dense layer of Mg(OH)₂
Sun et al. [124]	Physical – diffusion limited model	Pure Mg stent	Extension of Grogan's physical model. Introduced the time-dependent deposition of degradation products on the metal surface by counting the changes in both electrical potential and mass transfer	<ul style="list-style-type: none"> • Limited to pure Mg • Constant porosity of the degradation layer
Bajger et al. [139]	Physical – diffusion limited model	HP-Mg	Extension of Grogan's model. And simulated the formation of the degradation layer in SBF media under physiological conditions	<ul style="list-style-type: none"> • The electrochemical degradation was negligible • Trial and error to fit the model parameters
Barzegari et al. [150]	Physical – diffusion limited model	Commercially-pure (CP) Mg	Extension of Bajger's model. The model considered the formation of a protective layer, the effects of the ions in the solution, and the changes in the pH due to the degradation phenomenon. Furthermore, to simulate the pH changes in NaCl and SBF solutions, model parameters were calibrated using a Bayesian optimization algorithm	<ul style="list-style-type: none"> • The model calibration is performed <i>via</i> tuning the diffusion rate, which does not account for physical phenomena

(continued on next page)

Table 1 (continued)

Authors	Model type	Study system	Brief description	Limitation
Höche [141]	Physical – complex model	Mg-Al alloy	Investigated the micro-galvanic degradation in a system of Mg coupled to Al	<ul style="list-style-type: none"> • Neglected the effect of H₂ bubbles on the degradation process • The effects of gas dissolution in the electrolyte solution were neglected • Static conditions assumption was applied which is not the case in the lab.
Sanz-Herrera et al. [151]	Physical – semi-complex model	Mg- screw	Studied the physico-chemical interactions and the evolution of the phenomenon species. The effect of multiple chemical species included in the model by including a set of seven species in the study, where the concentration gradient	<ul style="list-style-type: none"> • Required experimental data for the calibration of each set • Boundary conditions required to consider the change in concentration at each stage of the model • Only qualitative measurements were reported within the order of magnitude of values in literature
Zeller-Plumhoff and Albaraghteh et al. [152]	Physical – complex model	Pure Mg (99.92 – 99.95%)	The model included all species of several reaction in SBF and resulted from the dissociation. And the data from weight loss and volume loss measurements was used to calibrate the degradation model. An error of 7% was reported for the simulation results of the anodic dissolution related degradation process of pure Mg in SBF. For the first time, the model presented a comparison to the literature of simulated precipitate formation, which was calibrated using data from energy-dispersive X-ray spectroscopy (EDX).	<ul style="list-style-type: none"> • The degradation rate itself was modeled using a data-derived equation • The model only valid for pure Mg • No pitting corrosion included
Marvi-Mashhadi et al. [153]	Physical – complex model	WE43 Mg scaffolds	Presented a simulation strategy to simulate the pitting degradation and the mechanical properties of WE43 Mg scaffolds. The simulation strategy was able to assess the effect of corrosion on the mechanical behavior of biodegradable scaffolds	<ul style="list-style-type: none"> • The values of Weibull distribution coefficients β and γ should be calibrated for each alloy and immersion environment
Ahmed et al. [140]	Physical – simplified model	Pure Mg	The model focus on studying the beginnings of the degradation process. Reduced the mathematical complexity of the model using the dimensionless presentation of different model parameters	<ul style="list-style-type: none"> • The degradation layer was assumed to only consist of Mg(OH)₂ and MgCO₃ • The model neglected the presence of other species • The porosity of layers was neglected
Shen et al. [147].	Physical – simplified model	Mg-1Ca, Mg-3Ge alloys	Studied the pitting degradation based on the diffusion mechanisms. The experimental data was used to calibrate the model parameters. Also, a simplified pin geometry was used	<ul style="list-style-type: none"> • The model contained empirical parameters that depends on the alloy and media • Limited to test systems due to the requirement of large sets of experimental data to calibrate the model parameters • Neglected the effect of the galvanic degradation and the presence of the impurities in the alloy
Dahms et al. [154]	Analytical model	Mg-0.3Ca	Simplified two-phase degradation model included empirical equations of mass conservation laws	<ul style="list-style-type: none"> • Chemical and electrochemical processes were not included
Gastaldi et al. [157]	Phenomenological-uniform degradation	Stents - ZM21 alloy	Introduced damage parameter for uniform degradation	<ul style="list-style-type: none"> • Assumed static conditions • Required experimental data for the calibration and fitting of model parameters

(continued on next page)

Table 1 (continued)

Authors	Model type	Study system	Brief description	Limitation
Grogan et al. [156]	Phenomenological-uniform and pitting degradation	Stent - AZ31 alloy	Introduced damage parameter and effective stress tensor for uniform and pitting degradation The FE mesh moved independently by implementing adaptive mesh using ALE Degradation rate was an input to the model as velocity of moving stent surface	<ul style="list-style-type: none"> Required experimental data for the calibration and fitting of model parameters No accurate detection of the pit location
Vijayaraghavan et al. [123]	Phenomenological-GTN model	AZ31 alloy	Adaptive GTN model to study the SCC of Mg-based alloy GTN model was able to predict the mechanical properties of AZ31 alloy under different temperatures and strain rate	<ul style="list-style-type: none"> Required experimental data for the fitting of model parameters
Shahmohmmadi et al. [168]	Phenomenological- CA model	PLA- 5% Mg alloy and PLA- 10% Mg alloy stents	Three-dimensional CA model to optimize the volume ratio of Mg within the stent	<ul style="list-style-type: none"> This model is only a parametric study without any quantitative comparisons to experiments Required experimental observations for each transition rules to calibrate the time magnitude and the spatial
Chen and Bobaru [175]	Phenomenological- PD model	Mg-Zn-Zr (ZK60A) alloy	Mathematically consistent simulation of the damage through coupling the concentration and the superposed mechanical bonds Do not need the interface conditions (Stefan conditions) in bi-material diffusion Don't required flux continuity conditions on the interface	<ul style="list-style-type: none"> The accuracy near the domain boundaries are reduced due to the neglecting domain nodes at the boundaries The degradation layer was not easily separable from the bulk
Hermann et al. [179]	Phenomenological- 3D PD model	Mg-5Gd and Mg-10Gd	A computational framework to study the degradation of Mg-based biodegradable implants, in which the degradation of Mg-alloys were modeled using 3D PD degradation model and a FE mechanical model	<ul style="list-style-type: none"> A validation study against <i>in vivo</i> Mg-based implants is needed to validate the provided framework
Ma et al. [181].	Phenomenological- PF model	Pure Mg – plates	Model was constructed based on Allen–Cahn and Cahn–Hilliard equations. The impact of stress assisted degradation of biodegradable Mg alloys with porous microstructures was simulated	<ul style="list-style-type: none"> High computational cost Models are depending on the selected free energy function Failed to predict the oscillatory behavior in thermally driven cracks

To summarize the models presented in this review, Table 1 presents a brief overview of the models applied to simulate the *in vivo* and the *in vitro* degradation of Mg-based implants.

Despite the important role that *in silico* testing of Mg implants can play in clarifying the overall process and propagation of the degradation process, there is no comprehensive computational framework that can predict the degradation behavior of Mg-based implants in both *in vivo* and *in vitro* environments. Each of the discussed approaches was built over several hypotheses and assumptions: simplified chemistry, considering a limited number of species within the system, simplified kinetic mechanisms, the electrochemical reactions are simplified to the basic anodic and cathodic reactions and few complex geometries are used. These simplified assumptions affect the reliability of the models and in many cases limit the model applicability to a certain system or conditions. Moreover, the lack of understanding and knowledge of the underlying processes of Mg biodegradation need to be improved to arrive at a point where a comprehensive and predictive computational framework for Mg degradation can be derived. Some of these remaining knowl-

edge gaps are related to the degradation process itself, such as the complex mechanisms of the degradation, unclear understanding of the degradation kinetics, the accumulation of H₂ in the system and the control of the pH [2,10]. Additionally, many values for the key parameters of the degradation process, such as reaction rate constants, diffusion coefficients and porosity remain unknown or are difficult to assess experimentally [48,113,136,138,139,141]. Furthermore, the degradation process of Mg is a multiscale problem, which increases the complexity of the mathematical representation and will require a multiscale computational framework to enable predictive modeling of the degradation of Mg-based implant [113,135,136,141,144,187]. Finally, the model calibration and the selection of the experimental data required for the validation of these models affect their reliability. Thus, these models require further optimization, calibration, and validation.

4. Reliability of the *in silico* approach

Highly informative models of the degradation of Mg-based alloys can only be achieved when the model is representing

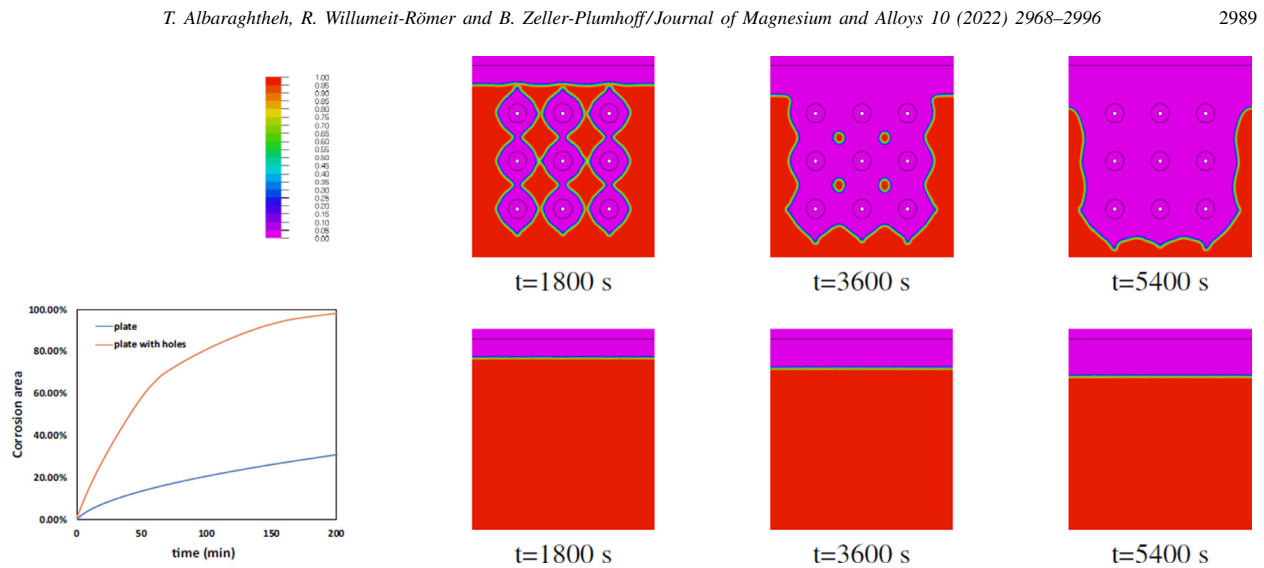


Fig. 13. Evolution of the morphology of the degradation surface at different times for the plates with and without pores (adapted with permission from John Wiley and Sons [181]).

a digital twin of the *in vitro* experiments, which means that the model outputs fit the experimental results qualitatively and quantitatively. Regardless of how comprehensive or accurate the degradation models of Mg-based alloys are, these models are a partial representation of the real system, due to several sources of uncertainties. These uncertainties accumulated within the system from the assumptions and hypothesis, which affect the development process of the model, the model parameters, the discretization techniques, and the experimental data that is used to calibrate and validate the model. To establish reliable models, it is therefore pivotal to identify and quantify the sources of uncertainties and errors in the model. At this stage, calibration, validation and verification play a large role.

4.1. Analysis techniques of *in vitro* studies of the degradation of Mg-based implants

To assess the validity of any degradation model, a comparison with experimental data is required. To this end, different parameters can be assessed, such as mass or volume loss, the potential of the electrolyte or the composition of the degradation layer. The degradation properties in electrochemical tests are evaluated by testing the open circuit potential (OCP), polarization curves and electrochemical impedance spectroscopy (EIS) via a three-electrode system [34,188]. In the immersion test, the study samples are immersed in a chemical solution in isolated wells and then either the mass loss or volume loss can be assessed or the degradation products are analyzed by a series of methods [33,34,52]. The immersion method is the common testing method for biodegradable materials, where the related testing protocols are published as: ISO 10993-15 (Biological evaluation of medical devices-Part 15: Identification and quantification of degradation products from metals and alloys) [189] and ASTM G31-

72 (Standard practice for laboratory immersion corrosion testing of metals) [190].

Different evaluation methods are used in the measurement and analysis of the degradation products, these methods are differing in their nature as physical or chemical tests, destructive or non-destructive for the test samples. Also, they can be categorized into unpolarized and polarized methods. Esmaily et al. [10] presented a comprehensive review over the different analysis techniques and methods that are used to study the degradation of Mg-alloys under different conditions. In this review we shortly summarize the most common methods used to evaluate the degradation rate of Mg alloys that can be used for calibration and validation of computational models.

4.1.1. Hydrogen evolution measurement

The degradation rate of Mg can be measured by measuring the volume of H_2 evolved, which is generally assumed to be equivalent to the mass loss of Mg (Eq. (1)) [34]. The volume of the gas is calculated *via* the gas law

$$PV = nRT \quad (14)$$

where P is the atmospheric pressure (Pa), V is the volume of H_2 (m^3), n is the substance amount of the gas (mol) and T is the temperature (K). This method is a real-time measurement of degradation with acceptable accuracy of calculating the alkalization in simple NaCl solutions. The measured degradation rate is not affected by the presence of degradation products but also gives no indication for them [34]. Consequently, this method gives limited information of the degradation mechanism and it is difficult to run concurrent to polarisation experiments [33]. The results of this experiment can be affected by changes in the atmospheric pressure and hydrogen leakage from the set-up [34]. Moreover, they are only valid if the oxygen reduction reaction is truly negligi-

ble during Mg biodegradation, despite recent evidence to the contrary [59].

4.1.2. pH monitoring

During the degradation of Mg, hydroxide ions are produced by the cathodic reaction (Eq. (3)), where the change in the concentration of OH^- will increase the pH of the media [52,83]. Measuring pH changes of the system can yield indirect information on the degradation rate of Mg alloys in simple immersion media and the influence of changing the media or alloying elements on the process [7,102,107,191]. pH monitoring is a low cost, easy to perform and continuous method. However, it is not an alternative to other methods, since the pH change will be influenced by buffer systems, difference between surface and bulk [59] and there is no quantitative measurement of the degradation rate [7,192].

4.1.3. Potentiodynamic polarization (PDP)

In potentiodynamic polarization, the degradation is studied through measuring the current by applying a single fixed potential, where the degradation rate is calculated by the formula [10,33].

$$\text{DR} = K \left(\frac{I_{\text{corr}}/\rho}{m_e} \right) \quad (15)$$

where K value is 3.273×10^{-3} mmg/ ($\mu\text{A cm a}$), I_{corr} is the current density, and m_e is the equivalent mass. This method is widely used to study the degradation [10,34,66], due to the relatively easy setup, easy preparation of samples and obtaining a dynamic profile of the degradation process [10]. The main disadvantages associated with this method are the requirement of specialized equipment, the need for assumptions of generalized corrosion and the high sensitivity to variations and errors [33]. Moreover, polarization measurements may be influenced by the dynamic process of the degradation layer formation and organic components may have a negative impact on the electrode behavior due to adsorption on its surface.

4.1.4. Electrochemical impedance spectroscopy

Electrochemical impedance spectroscopy (EIS) is a non-destructive method with a relatively easy setup and simple sample preparation. EIS provides continuous real time measurement and is able to quantify the formation of surface layers and the effect of these layers on the corrosion protection. In case of coating, EIS helps in determining the time-dependent breakdown, through calculating the current density of the degradation by Stern-Geary equation [33,107]. However, this method lacks the information over anodic/cathodic contribution and it is susceptible to corrosion that occurs over a period of time [10,33].

4.1.5. Mass loss

The mass loss method is based on measuring the change in the mass of the sample before and after the immersion test. To this end, the degradation layer that may form on the sample surface must be removed using chromic acid treatment [5,34].

Mass loss is an unpolarised method, where the degradation rate is calculated using the following formula [34]

$$\text{DR} = 8.76 \times 10^4 \frac{\Delta W}{At\rho} \quad (16)$$

where DR is the degradation rate, ΔW is the change in the weight, A is the original surface area and t is the exposure time. This method is low cost, simple to set up and perform. It is also easy to control the test environment. Furthermore, the output of these methods are accurate and clearly defined and concurrent polarization experiments are possible [33,34]. The main disadvantages of this method are the lack of information about the degradation mechanism, the absence of time-dependent degradation behavior thus requiring a large number of samples for a dynamic analysis of the degradation process [33,34].

4.1.6. X-ray microtomography (μCT)

Microfocus X-ray computed tomography (μCT) is a non-destructive 3D imaging method that can be used for analyzing the degradation of Mg alloy implants both *in situ* and in a static manner [98,193,194]. In a similar manner as for mass loss measurements, the degradation rate is calculated *via* the observed volume loss ΔV obtained from the images. As well as limitations associated with the used instrument, this method also has limitations that are related to the algorithm used to process the images and the values considered for the image parameters.

$$\text{DR} = \frac{\Delta V}{At} \quad (17)$$

In addition to studying the degradation rate of Mg alloys, understanding the formation of precipitates on the implant surface is required to accurately model the protective nature of the degradation layer. To analyze the precipitates, a number of methods can be used, most prominently, scanning electron microscopy and energy-dispersive spectroscopy, X-ray diffraction and Fourier-transform infrared spectroscopy.

4.2. Calibration, validation, and verification of *in silico* studies

To test the reliability of the model three main stages are well established within the computational fields, these stages are the calibration, validation, and verification [195]. In studying the *in vitro* degradation of Mg-based implants, model calibration plays a major role in determining the values of key parameters of the model based on the available experimental data of the same system or a similar system [124,132,192]. For example; Bajger et al. [139] reported that the values of the diffusion coefficients differ with one order of magnitude in literature. Also, the estimation of the key parameters of the system was done by trial and error fitting and due to that these parameters were limited for certain systems or study conditions [123,139,156,157]. The validation stage of *in vitro* degradation of the Mg-based alloys model involves validating the concepts of the electrochemical reactions, surface reactions, diffusion, forming and precipitation processes with

an actual *in vitro* experiment. At this stage, the degradation-rate values, the percentage of mass loss and hydrogen release are validated against experiments. The third stage of checking the reliability of a model is the verification, where the computational model and its implementation are correct [145,196,197]. In the degradation models of Mg-based implants the verification of the mesh is one of the important steps to accurately predict the implant shape and the movement of the degradation surface as presented by Wu et al. [198] and Deshpande [132].

Regardless of the ability of the current computational systems (hardware and algorithms) to simulate complex processes, the reliability of these models is sometimes questionable. Experimental data, model concepts, limitations of simulators and even the implementation of these models are sources of uncertainty and uncertainty propagation within the system. It is necessary to control and quantify the uncertainties associated with these sources and different parameters affecting the system. Calibration, validation and verification only target certain aspects of the system uncertainty but the total uncertainty in the system is still unquantified nor estimated [195] and a new approach is therefore needed to overcome this challenge.

Uncertainty Quantification (UQ) deals with the known unknowns of models. This field has grown in the last few decades due to the necessity to eliminate and quantify the uncertainties associated with different mathematical approaches. UQ quantitatively characterizes the proximity between both predictions and observations [199–201], through connecting the physical systems with the computational models simulating them, through tools and methodologies produced by combining different concepts from statistics, computational science, engineering and applied mathematics [195,202–204].

Recently, UQ has been integrated as an essential part of most computational studies due to the fact it makes the best use of the computational model by eliminating the uncertainties associated with them, pointing to the error sources and possible enhancements [200,205]. The available models simulating the degradation process of Mg-based implants are subject to various types of uncertainties. The epistemic uncertainty, appears due to the model assumption, the understanding of the system and the different observation and measurements [195,203,204]. The other type of uncertainty is the aleatory uncertainty, which is the non-reducible uncertainty of the system. These uncertainties are due to the natural variability in the model parameters, which can be quantified by defining different distribution within the probabilistic framework [200,202,203]. This building up of different uncertainties within each part of the degradation model results in the propagation of the uncertainty through the model and affects its predictions. The accumulated uncertainty within the system therefore plays an important role in the decisions made based on the model. The schematic diagram in Fig. 14 summarizes the uncertainty sources within the degradation system of Mg-based alloys. Consequently, quantifying the various uncertainties associated with the different aspects of the degradation process is highly important to produce a reliable mathemat-

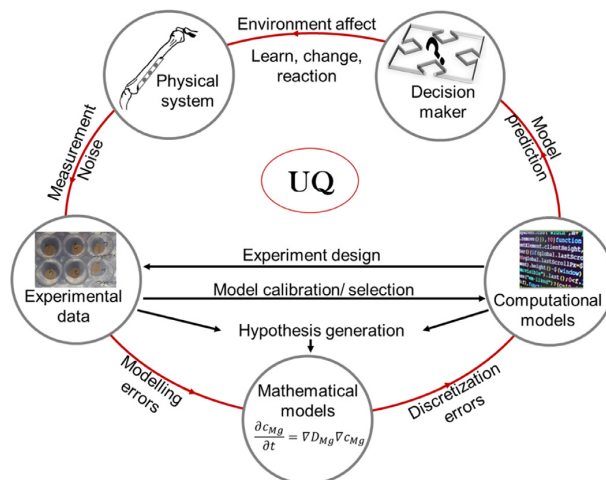


Fig. 14. Schematic diagram of uncertainty sources within the degradation process of Mg-based implants, the red arrows represents the building of uncertainty within the system. (Inspired by [206]).

ical framework that can accurately simulate the degradation process of Mg-based implants.

The degradation system of Mg-based implants is considered a large biochemical system, which is computationally expensive to evaluate. Furthermore, this system required the estimation of several missing key parameters. To estimate these parameters UQ provides several approaches and techniques [197,203,207]. Kriging algorithms, also known as Gaussian process modeling, is one of the techniques applied to optimize and estimate the missing model parameters. Kriging estimates the optimal parameter of the degradation model without requiring extensive runs for the original expensive model and hence play a major role in reducing the computational cost and size of study data sets [208].

In a recent study by Zeller-Plumhoff and Albaraghteh et al. [152], the key parameters of the degradation model of pure Mg in SBF were calibrated using a Kriging metamodel. These parameters were mainly reaction rate constants for the degradation and precipitation reactions. Using Kriging during the parameter estimation phase reduced the computational load from 5–23 min to 6–12 s and enhanced the model's reliability. Additionally, the Kriging metamodels-based sensitivity analysis identified a strong correlation between key parameters of the model, in particular precipitate formation on the surface of the implant.

Tak et al. [209] implemented Kriging algorithm to predict the corrosion rates of the metallic crude unit in a refinery process. The main challenge in this process was the inability of the available corrosion models to simulate the corrosion under the severe conditions. The Kriging model was developed to optimize the key parameters (pH, flow rates and concentration of Cl^- , Fe^{2+} , H_2S and NH_3) of the corrosion process. The Kriging model was compared to a multiple linear regression and an artificial neural network and provided the best results. The reduction of computational cost and the good

agreement of Kriging models are also reported by Kleijnen [210], where a qualitative and quantitative study of Kriging models of several systems was presented. In addition to parameter calibration, sensitivity analysis which identifies the parameters which affect the model the most is crucial in computational modeling, as it enhances the design of experiments of the studied system and serves to explain the behavior of this system. Sensitivity analysis provides a measure of confidence in the quantified model variables. Also, it identifies which parameters are contributing to the model behavior. This will help in generating accurate hypotheses about the system behavior [207,211,212]. The sensitivity analysis may present a solution to the dimensionality problem of the degradation system of the Mg-based implant. A recent study by Wang et al. [205] presented a multiphysics modeling of tribocorrosion in aluminium alloys under uncertainty quantification. Kriging was implemented to approximate and analyze the parameters and confidence intervals of the model. Each output of the FE model could be augmented by the confidence intervals corresponding to the UQ analysis. Furthermore, the Kriging model was tested against neural network (NN) model and the output of the Kriging model was in better agreement with the validation data than the NN model. The development of new methods for meta-modeling is ongoing, and in the future, more advanced meta-models, such as polynomial chaos Kriging and physics-informed neural networks should be evaluated for the use in implant degradation modeling.

Despite its obvious power and importance, UQ has not been fully recognised *in silico* studies of the degradation of biodegradable implants and remains far less understood in comparison with calibration, validation, and verification techniques. However, the UQ field is one of the richest and largest areas of computational research [213,214]. UQ methods and techniques are able to overcome the main challenges in material science such as the multiscale simulations, time scales and the lack of key parameters. Furthermore, UQ methods and techniques are able to handle the propagation of different types and sources of uncertainties and errors within the material science field. Therefore, we believe that UQ will in the future be used increasingly to support computational modeling of Mg degradation.

5. Summary and conclusions

In vitro studies of the degradation of Mg-based implants are highly important in understanding the underlying mechanisms, revealing the connections of different parameters affecting the degradation and presenting a picture of the implant behavior under different physiological conditions. In this review, we presented the different interactions between the key factors affecting the degradation process of Mg-based implants *in vitro*. The *in silico* approach will help in reducing the time and the cost of several experimental studies by presenting a theoretical understanding of the process and the interactions taking place within it. A large number of existing studies in the broader literature have examined several

computational approaches to model different aspects of the degradation process of Mg based alloys.

The literature review shows that the phenomenological approach provided the external visualization of the degradation process of the Mg-based implants, like the pits, cracks, and uniform degradation but these models were unable to capture the different interactions of Mg²⁺ ions, precipitates, and dissolution within the system, which can be predicted by the physical models. Physical models, however, were able to capture the complex movement of the degradation surface. PF, PD and CA provided additional possibilities to study more aspects of the degradation process without requiring complex PDE implementation and solution.

Despite the important role of these models in enhancing the understanding and studying of the implant systems, the majority of these models are still limited to certain systems or under certain conditions. Up to date, modeling of different degradation mechanisms accounting for all the electrochemical and mechanical phenomena represents a hard challenge. The developed models need to be calibrated and verified experimentally and theoretically. In the future, we recommend the integration of the uncertainty quantification (UQ) approach in studying the degradation process. This recommendation is driven by the various methods, techniques and algorithms provided by UQ, which not only enhance the model but also help, in a less complex form, in exploring the key factors affecting the system and its behavior. The application of UQ will increase the reliability of *in silico* approach and may help in filling the gap between the different studies of the degradation process of Mg-based implants and accelerate the development process.

Declaration of Competing Interest

The authors declare that they have no known competing financial interests or personal relationships that could have appeared to influence the work reported in this paper.

CRediT authorship contribution statement

Tamadur Albaraghteh: Conceptualization, Writing – original draft. **Regine Willumeit-Römer:** Writing – review & editing. **Berit Zeller-Plumhoff:** Conceptualization, Writing – original draft.

Acknowledgments

The authors would like to thank Dr. Stefan Bruns for the fruitful discussions. The authors acknowledge funding from the Helmholtz-Incubator project Uncertainty Quantification.

References

- [1] M. Saini, Y. Singh, P. Arora, V. Arora, K. Jain, World J. Clin. Cases 3 (2015) 52–57, doi:10.12998/wjcc.v3.i1.52.
- [2] Y. Yang, C. He, E. Dianyuan, W. Yang, F. Qi, D. Xie, L. Shen, S. Peng, C. Shuai, Mater. Des. 185 (2020) 108259, doi:10.1016/j.matdes.2019.108259.

- T. Albaraghteh, R. Willumeit-Römer and B. Zeller-Plumhoff/*Journal of Magnesium and Alloys* 10 (2022) 2968–2996 2993
- [3] B. Luthringer, F. Feyerabend, R. Willumeit, *Magnes. Res.* 27 (2014) 142–154, doi:[10.1684/mrh.2015.0375](https://doi.org/10.1684/mrh.2015.0375).
- [4] H. Li, Y. Zheng, L. Qin, *Prog. Nat. Sci. Mater. Int.* 24 (2014) 414–422, doi:[10.1016/j.pnsc.2014.08.014](https://doi.org/10.1016/j.pnsc.2014.08.014).
- [5] F. Witte, *Acta Biomater.* 6 (2010) 1680–1692, doi:[10.1016/j.actbio.2010.02.028](https://doi.org/10.1016/j.actbio.2010.02.028).
- [6] T.J. Webster, M. Lysaght, T.J. Webster, *Biomaterials for Artificial Organs*, Woodhead Publishing, 2011 xiii–xiv, doi:[10.1016/B978-1-84569-653-5.50014-5](https://doi.org/10.1016/B978-1-84569-653-5.50014-5).
- [7] Y.F. Zheng, X.N. Gu, F. Witte, *Mater. Sci. Eng. R Rep.* 77 (2014) 1–34, doi:[10.1016/j.mser.2014.01.001](https://doi.org/10.1016/j.mser.2014.01.001).
- [8] F. Witte, N. Hort, C. Vogt, S. Cohen, K.U. Kainer, R. Willumeit, F. Feyerabend, *Curr. Opin. Solid State Mater. Sci.* 12 (2008) 63–72, doi:[10.1016/j.cossms.2009.04.001](https://doi.org/10.1016/j.cossms.2009.04.001).
- [9] Z.R. Chen, Y. Xu, S. Pang, X. Zhao, Y. Zhao, *Hindawi Scanning* 2018 (2018) 15, doi:[10.1155/2018/9216314](https://doi.org/10.1155/2018/9216314).
- [10] M. Esmaily, J.E. Svensson, S. Fajardo, N. Birbilis, G.S. Frankel, S. Virtanen, R. Arrabal, S. Thomas, L.G. Johansson, *Prog. Mater. Sci.* 89 (2017) 92–193, doi:[10.1016/j.pmatsci.2017.04.011](https://doi.org/10.1016/j.pmatsci.2017.04.011).
- [11] L. Yang, N. Hort, R. Willumeit, F. Feyerabend, *Corros. Eng. Sci. Technol.* 47 (2012) 335–339, doi:[10.1179/1743278212Y.0000000024](https://doi.org/10.1179/1743278212Y.0000000024).
- [12] N. Sezer, Z. Evis, S.M. Kayhan, A. Tahmasebifar, M. Koç, *J. Magnes. Alloy.* 6 (2018) 23–43, doi:[10.1016/j.jma.2018.02.003](https://doi.org/10.1016/j.jma.2018.02.003).
- [13] M. Peuster, P. Wohlsein, M. Brüggemann, M. Ehlerding, K. Seidler, C. Fink, H. Brauer, A. Fischer, G. Hausdorf, *Heart* 86 (2001) 563–569 <https://www.scopus.com/inward/record.uri?eid=2-s2.0-0034778878&partnerID=40&md5=94130744ddc098ed20a05fd9c9017b78>.
- [14] M. Peuster, C. Hesse, T. Schlöo, C. Fink, P. Beerbaum, C. von Schnakenburg, *Biomaterials* 27 (2006) 4955–4962, doi:[10.1016/j.biomaterials.2006.05.029](https://doi.org/10.1016/j.biomaterials.2006.05.029).
- [15] J. Draxler, E. Martinelli, A.M. Weinberg, A. Zitek, J. Irrgeher, M. Meischel, S.E. Stanzl-Tschegg, B. Mingler, T. Prohaska, *Acta Biomater.* 51 (2017) 526–536, doi:[10.1016/j.actbio.2017.01.054](https://doi.org/10.1016/j.actbio.2017.01.054).
- [16] J.E. Coleman, *Curr. Opin. Chem. Biol.* 2 (1998) 222–234, doi:[10.1016/S1367-5931\(98\)80064-1](https://doi.org/10.1016/S1367-5931(98)80064-1).
- [17] G. Williams, N. Birbilis, H.N. McMurray, *Faraday Discuss.* 180 (2015) 313–330, doi:[10.1039/C4FD00268G](https://doi.org/10.1039/C4FD00268G).
- [18] C. Ruan, N. Hu, Y. Ma, Y. Li, J. Liu, X. Zhang, H. Pan, *Sci. Rep.* 7 (2017) 6794, doi:[10.1038/s41598-017-06354-1](https://doi.org/10.1038/s41598-017-06354-1).
- [19] O.M. Böstman, *J. Bone Jt. Surg. Am.* 73 (1991) 148–153.
- [20] J. Chen, L. Tan, X. Yu, I. Etim, M. Ibrahim, K. Yang, *J. Mech. Behav. Biomed. Mater.* 87 (2018) 68–79, doi:[10.1016/j.jmbbm.2018.07.022](https://doi.org/10.1016/j.jmbbm.2018.07.022).
- [21] J. Gallo, S.B. Goodman, Y.T. Kontinen, M. Raska, *Innate Immun.* 19 (2013) 213–224, doi:[10.1177/1753425912451779](https://doi.org/10.1177/1753425912451779).
- [22] C.A. St. Pierre, M. Chan, Y. Iwakura, D.C. Ayers, E.A. Kurt-Jones, R.W. Finberg, *J. Orthop. Res.* 28 (2010) 1418–1424, doi:[10.1002/jor.21149](https://doi.org/10.1002/jor.21149).
- [23] M. Geetha, A.K. Singh, R. Asokamani, A.K. Gogia, *Prog. Mater. Sci.* 54 (2009) 397–425, doi:[10.1016/j.pmatsci.2008.06.004](https://doi.org/10.1016/j.pmatsci.2008.06.004).
- [24] S.V.S. Prasad, S.B. Prasad, K. Verma, R.K. Mishra, V. Kumar, S. Singh, *J. Magnes. Alloy.* 10 (2022) 1–61, doi:[10.1016/J.JMA.2021.05.012](https://doi.org/10.1016/J.JMA.2021.05.012).
- [25] D. Bairagi, S. Mandal, *J. Magnes. Alloy.* 10 (2022) 627–669, doi:[10.1016/J.JMA.2021.09.005](https://doi.org/10.1016/J.JMA.2021.09.005).
- [26] H. Hermawan, *Biodegradable Metals: State of the Art*, Springer, Berlin, Heidelberg, 2012, doi:[10.1007/978-3-642-31170-3_2](https://doi.org/10.1007/978-3-642-31170-3_2).
- [27] J. Gonzalez, R.Q. Hou, E.P.S. Nidadavolu, R. Willumeit-Römer, F. Feyerabend, *Bioact. Mater.* 3 (2018) 174–185, doi:[10.1016/j.bioactmat.2018.01.003](https://doi.org/10.1016/j.bioactmat.2018.01.003).
- [28] E. Ghali, W. Dietzel, K.U. Kainer, *J. Mater. Eng. Perform.* 13 (2004) 7–23, doi:[10.1361/10599490417533](https://doi.org/10.1361/10599490417533).
- [29] F. Cecchinato, N.A. Agha, A.H. Martinez-Sanchez, B.J.C. Luthringer, F. Feyerabend, R. Jimbo, R. Willumeit-Römer, A. Wennerberg, *PLoS ONE* 10 (2015) e0142117, doi:[10.1371/journal.pone.0142117](https://doi.org/10.1371/journal.pone.0142117).
- [30] A. Atrens, G.L. Song, M. Liu, Z. Shi, F. Cao, M.S. Dargusch, *Adv. Eng. Mater.* 17 (2015) 400–453, doi:[10.1002/adem.201400434](https://doi.org/10.1002/adem.201400434).
- [31] N.A. Agha, F. Feyerabend, B. Mihailova, S. Heidrich, U. Bismayer, R. Willumeit-Römer, *Mater. Sci. Eng. C* 58 (2016) 817–825, doi:[10.1016/j.msec.2015.09.067](https://doi.org/10.1016/j.msec.2015.09.067).
- [32] M. Kieke, F. Feyerabend, J. Lemaitre, P. Behrens, R. Willumeit-Römer, *Biomaterials* 17 (2016) 131, doi:[10.1515/bnm-2015-0020](https://doi.org/10.1515/bnm-2015-0020).
- [33] N.T. Kirkland, N. Birbilis, M.P. Staiger, *Acta Biomater.* 8 (2012) 925–936, doi:[10.1016/j.actbio.2011.11.014](https://doi.org/10.1016/j.actbio.2011.11.014).
- [34] Z. Zhen, T. Xi, Y. Zheng, *Trans. Nonferr. Met. Soc. China* 23 (2013) 2283–2293, doi:[10.1016/S1003-6326\(13\)62730-2](https://doi.org/10.1016/S1003-6326(13)62730-2).
- [35] A.H.M. Sanchez, B.J.C. Luthringer, F. Feyerabend, R. Willumeit, *Acta Biomater.* 13 (2015) 16–31, doi:[10.1016/j.actbio.2014.11.048](https://doi.org/10.1016/j.actbio.2014.11.048).
- [36] H.S. Han, S. Loffredo, I. Jun, J. Edwards, Y.C. Kim, H.K. Seok, F. Witte, D. Mantovani, S. Glyn-Jones, *Mater. Today* 23 (2018), doi:[10.1016/j.mattod.2018.05.018](https://doi.org/10.1016/j.mattod.2018.05.018).
- [37] Z. Xue, H. Xu, H. Ding, H. Qin, Z. An, Comparison of the effect on bone healing process of different implants used in minimally invasive plate osteosynthesis: limited contact dynamic compression plate versus locking compression plate, *Scientific reports* 6 (2016) 1–9, doi:[10.1038/srep37902](https://doi.org/10.1038/srep37902).
- [38] Y.R. Jo, H.W. Kim, S.H. Moon, Y.J. Ko, *Ann. Rehabil. Med.* 37 (2013) 430–432.
- [39] T. Schepers, *Foot Ankle Clin.* 25 (2020) 683–695, doi:[10.1016/j.fcl.2020.08.008](https://doi.org/10.1016/j.fcl.2020.08.008).
- [40] P.C. Nolte, A.K. Tross, J. Studniorz, P.A. Grützner, T. Guehring, M. Schnetzke, *Sci. Rep.* 11 (123AD) (2022) 22101, doi:[10.1038/s41598-021-01625-4](https://doi.org/10.1038/s41598-021-01625-4).
- [41] M. Schwendner, S. Motov, Y.M. Ryang, B. Meyer, S.M. Krieg, S. Motov, Y.M. Ryang Yu-Mi, B. Meyer BernhardMeyer, *Eur. Spine J.* 31 (1234) (2022) 1138–1146, doi:[10.1007/s00586-021-07044-3](https://doi.org/10.1007/s00586-021-07044-3).
- [42] J. Wang, Y. Jang, G. Wan, V. Giridharan, G.L. Song, Z. Xu, Y. Koo, P. Qi, J. Sankar, N. Huang, Y. Yun, *Corros. Sci.* 104 (2016) 277–289, doi:[10.1016/j.corsci.2015.12.020](https://doi.org/10.1016/j.corsci.2015.12.020).
- [43] V. Tsakiris, C. Tardei, F.M. Clicinchi, *J. Magnes. Alloy.* 9 (2021) 1884–1905, doi:[10.1016/J.JMA.2021.06.024](https://doi.org/10.1016/J.JMA.2021.06.024).
- [44] J.M. Seitz, A. Lucas, M. Kirschner, *JOM* 68 (2016) 1177–1182, doi:[10.1007/S11837-015-1773-1](https://doi.org/10.1007/S11837-015-1773-1).
- [45] S. Amukarimi, M. Mozafari, *MedComm* 2 (2021) 123–144, doi:[10.1002/mco2.59](https://doi.org/10.1002/mco2.59).
- [46] M.P. Staiger, A.M. Pietak, J. Huadmai, G. Dias, *Biomaterials* 27 (2006) 1728–1734, doi:[10.1016/j.biomaterials.2005.10.003](https://doi.org/10.1016/j.biomaterials.2005.10.003).
- [47] S. Virtanen, *Mater. Sci. Eng. B* 176 (2011) 1600–1608, doi:[10.1016/j.mseb.2011.05.028](https://doi.org/10.1016/j.mseb.2011.05.028).
- [48] B. Zeller-Plumhoff, M. Gile, M. Priebe, H. Slominska, B. Boll, B. Wiese, T. Würger, R. Willumeit-Römer, R.H. Meißner, *Corros. Sci.* 182 (2021) 109272, doi:[10.1016/j.corsci.2021.109272](https://doi.org/10.1016/j.corsci.2021.109272).
- [49] J. Walker, S. Shadanbaz, T.B.F. Woodfield, M.P. Staiger, G.J. Dias, *J. Biomed. Mater. Res. Part B Appl. Biomater.* 102 (2014) 1316–1331, doi:[10.1002/jbm.b.33113](https://doi.org/10.1002/jbm.b.33113).
- [50] K. Gusieva, C.H.J. Davies, J.R. Scully, N. Birbilis, *Int. Mater. Rev.* 60 (2015) 169–194, doi:[10.1179/1743280414Y.0000000046](https://doi.org/10.1179/1743280414Y.0000000046).
- [51] L. Shi, Y. Huang, L. Yang, F. Feyerabend, C. Mendis, R. Willumeit, K. Ulrich Kainer, N. Hort, *J. Mech. Behav. Biomed. Mater.* 47 (2015) 38–48, doi:[10.1016/j.jmbbm.2015.03.003](https://doi.org/10.1016/j.jmbbm.2015.03.003).
- [52] G.L. Song, A. Atrens, *Adv. Eng. Mater.* 1 (1999) 11–33, doi:[10.1002/\(SICI\)1527-2648\(199909\)1:1<11::AID-ADEM11>3.0.CO;2-N](https://doi.org/10.1002/(SICI)1527-2648(199909)1:1<11::AID-ADEM11>3.0.CO;2-N).
- [53] G. Song, A. Atrens, *Adv. Eng. Mater.* 5 (2003) 837–858, doi:[10.1002/adem.200310405](https://doi.org/10.1002/adem.200310405).
- [54] G. Song, A. Atrens, *Adv. Eng. Mater.* 9 (2007) 177–183, doi:[10.1002/adem.200600221](https://doi.org/10.1002/adem.200600221).
- [55] J. Song, J. She, D. Chen, F. Pan, *J. Magnes. Alloy.* 8 (2020) 1–41, doi:[10.1016/j.jma.2020.02.003](https://doi.org/10.1016/j.jma.2020.02.003).
- [56] R. Ambat, N.N. Aung, W. Zhou, *J. Appl. Electrochem.* 30 (2000) 865–874, doi:[10.1023/A:1004011916609](https://doi.org/10.1023/A:1004011916609).
- [57] A. Oyane, H.M. Kim, T. Furuya, T. Kokubo, T. Miyazaki, T. Nakamura, *J. Biomed. Mater. Res. Part A* 65 (2003) 188–195, doi:[10.1002/jbm.a.10482](https://doi.org/10.1002/jbm.a.10482).
- [58] T. Kokubo, H. Takadama, *Biomaterials* 27 (2006) 2907–2915, doi:[10.1016/j.biomaterials.2006.01.017](https://doi.org/10.1016/j.biomaterials.2006.01.017).

- [59] D. Mei, S.V. Lamaka, X. Lu, M.L. Zheludkevich, *Corros. Sci.* 171 (2020) 108722, doi:10.1016/j.corsci.2020.108722.
- [60] S.V. Lamaka, J. Gonzalez, D. Mei, F. Feyerabend, R. Willumeit-Römer, M.L. Zheludkevich, *Adv. Mater. Interfaces* 5 (2018) 1800169, doi:10.1002/admi.201800169.
- [61] Y. Xin, K. Huo, H. Tao, G. Tang, P.K. Chu, *Acta Biomater.* 4 (2008) 2008–2015, doi:10.1016/j.actbio.2008.05.014.
- [62] R.C. Zeng, X.T. Li, S.Q. Li, F. Zhang, E.H. Han, *Sci. Rep.* 5 (2015) 13026, doi:10.1038/srep13026.
- [63] Y. Jang, B. Collins, J. Sankar, Y. Yun, *Acta Biomater.* 9 (2013) 8761–8770, doi:10.1016/j.actbio.2013.03.026.
- [64] L. Cai, D. Mei, Z.Q. Zhang, Y. Ding Huang, L.Y. Cui, S.K. Guan, D.C. Chen, M.B. Kannan, Y. Feng Zheng, R.C. Zeng, *J. Magnes. Alloy.* 10 (2022) 670–688, doi:10.1016/j.jma.2022.02.005.
- [65] A. Yamamoto, S. Hiromoto, *Mater. Sci. Eng. C* 29 (2009) 1559–1568, doi:10.1016/j.msec.2008.12.015.
- [66] L. Yang, E. Zhang, *Mater. Sci. Eng. C* 29 (2009) 1691–1696, doi:10.1016/j.msec.2009.01.014.
- [67] B. Zeller-Plumhoff, D. Laipple, H. Ćwieka, K. Iskhakova, E. Longo, A. Herrmann, S. Fleuner, I. Greving, M. Storm, R. Willumeit, *Bioact. Mater.* 6 (2021) 4368–4376, doi:10.1016/j.bioactmat.2021.04.009.
- [68] D. Tie, F. Feyerabend, N. Hort, R. Willumeit, D. Hoeche, *Adv. Eng. Mater.* 12 (2010) B699–B704, doi:10.1002/adem.201080070.
- [69] D. Mei, S.V. Lamaka, J. Gonzalez, F. Feyerabend, R. Willumeit-Römer, M.L. Zheludkevich, *Corros. Sci.* 147 (2019) 81–93, doi:10.1016/j.corsci.2018.11.011.
- [70] R. Hou, F. Feyerabend, H. Helmholz, V.M. Garamus, R. Willumeit-Römer, *J. Magnes. Alloy.* (2021), doi:10.1016/J.JMA.2021.07.021.
- [71] D. Mei, C. Wang, S.V. Lamaka, M.L. Zheludkevich, *J. Magnes. Alloy.* 9 (2021) 805–817, doi:10.1016/J.JMA.2020.07.002.
- [72] R.Q. Hou, N. Scharnagl, R. Willumeit-Römer, F. Feyerabend, *Acta Biomater.* 98 (2019) 256–268, doi:10.1016/J.ACTBIO.2019.02.013.
- [73] J. Huang, A. Gonzalez Orive, J.T. Krüger, K.P. Hoyer, A. Keller, G. Grundmeier, *Corros. Sci.* 200 (2022) 110186, doi:10.1016/J.CORSCI.2022.110186.
- [74] Z. Mardina, J. Venezuela, M.S. Dargusch, Z. Shi, A. Atrens, *Corros. Sci.* 199 (2022) 110160, doi:10.1016/j.corsci.2022.110160.
- [75] P. Du, D. Mei, T. Furushima, S. Zhu, L. Wang, Y. Zhou, S. Guan, *J. Magnes. Alloy.* 10 (2022) 1286–1295, doi:10.1016/J.JMA.2020.12.015.
- [76] R. Willumeit, F. Feyerabend, N. Huber, *Acta Biomater.* 9 (2013) 8722–8729, doi:10.1016/j.actbio.2013.02.042.
- [77] R. Zeng, W. Dietzel, F. Witte, N. Hort, C. Blawert, *Adv. Eng. Mater.* 10 (2008) B3–B14, doi:10.1002/adem.200800035.
- [78] C. Wang, C. Song, D. Mei, L. Wang, W. Wang, T. Wu, D. Snihirova, M.L. Zheludkevich, S.V. Lamaka, *Corros. Sci.* 197 (2022) 110059, doi:10.1016/J.CORSCI.2021.110059.
- [79] E.L. Silva, S.V. Lamaka, D. Mei, M.L. Zheludkevich, *ChemistryOpen* 7 (2018) 664–668, doi:10.1002/open.201800076.
- [80] A. Mohamed, H.G. Breiteringer, A.M. El-Aziz, *Corros. Rev.* 38 (2020) 489–495, doi:10.1515/correv-2020-0008.
- [81] E.P.S. González, S. Suriñach, M.D. Baró, J. Sort, R. Chamy, F. Rosenkranz, *Biodegradation: Engineering and Technology*, IntechOpen, London, UK, 2013, doi:10.5772/55584.
- [82] A.S. Gnedenkov, S.L. Sinebryukhov, V.S. Filonina, V.S. Egorkin, A.Y. Ustinov, V.I. Sergienko, S.V. Gnedenkov, *J. Magnes. Alloy.* 10 (2022) 1326–1350, doi:10.1016/J.JMA.2021.11.027.
- [83] R.C. Zeng, Y. Hu, S.K. Guan, H.Z. Cui, E.H. Han, *Corros. Sci.* 86 (2014) 171–182, doi:10.1016/j.corsci.2014.05.006.
- [84] Y. Xin, T. Hu, P.K. Chu, *Corros. Sci.* 53 (2011) 1522–1528, doi:10.1016/j.corsci.2011.01.015.
- [85] Y. Su, I. Cockerill, Y. Zheng, L. Tang, Y.X. Qin, D. Zhu, *Bioact. Mater.* 4 (2019) 196–206, doi:10.1016/j.bioactmat.2019.05.001.
- [86] G. Jia, M. Zhou, Y. Huang, C. Chen, L. Jin, Q. Wu, J. Weng, F. Yu, A. Xiong, G. Yuan, F. Feyerabend, H. Zeng, *J. Magnes. Alloy.* (2021), doi:10.1016/j.jma.2021.10.011.
- [87] A.P. Md Saad, A.T. Prakoso, M.A. Sulong, H. Basri, D.A. Wahjungrum, A. Syahrom, *Biomech. Model. Mechanobiol.* 18 (2019) 797–811, doi:10.1007/s10237-018-01115-z.
- [88] S. Johnston, Z. Shi, A. Atrens, *Corros. Sci.* 101 (2015) 182–192, doi:10.1016/j.corsci.2015.09.018.
- [89] N. Li, C. Guo, Y.H. Wu, Y.F. Zheng, L.Q. Ruan, *Corros. Eng. Sci. Technol.* 47 (2012) 346–351, doi:10.1179/1743278212Y.0000000006.
- [90] I. Marco, F. Feyerabend, R. Willumeit-Römer, O. Van der Biest, *Mater. Sci. Eng. C* 62 (2016) 68–78, doi:10.1016/j.msec.2016.01.039.
- [91] X.N. Gu, Y. Lu, F. Wang, W. Lin, P. Li, Y. Fan, *Bioact. Mater.* 3 (2018) 448–454, doi:10.1016/J.BIOACTMAT.2018.08.002.
- [92] M. Liu, Y. Zhang, Q. Zhang, Y. Wang, D. Mei, Y. Sun, L. Wang, S. Zhu, S. Guan, *J. Magnes. Alloy.* (2022), doi:10.1016/J.JMA.2022.05.004.
- [93] E.P.S. Nidadavolu, D. Krüger, B. Zeller-Plumhoff, D. Tolnai, B. Wiese, F. Feyerabend, T. Ebel, R. Willumeit-Römer, *J. Magnes. Alloy.* (2020), doi:10.1016/j.jma.2020.05.006.
- [94] K. Xie, N. Wang, Y. Guo, S. Zhao, J. Tan, L. Wang, G. Li, J. Wu, Y. Yang, W. Xu, J. Chen, W. Jiang, P. Fu, Y. Hao, *Bioact. Mater.* 8 (2022) 140–152, doi:10.1016/J.BIOACTMAT.2021.06.032.
- [95] A. Myrissa, N.A. Agha, Y. Lu, E. Martinelli, J. Eichler, G. Szakács, C. Kleinhans, R. Willumeit-Römer, U. Schäfer, A.M. Weinberg, *Mater. Sci. Eng. C* 61 (2016) 865–874, doi:10.1016/j.msec.2015.12.064.
- [96] J. Espiritu, M. Meier, J.M. Seitz, *Bioact. Mater.* 6 (2021) 4360–4367, doi:10.1016/J.BIOACTMAT.2021.04.012.
- [97] R. Willumeit-Römer, S. Bruns, H. Helmholz, D. Krüger, B. Wiese, S. Galli, J. Moosmann, B. Zeller-Plumhoff, P. Maier, S. Barela, V.M. Miller, N.R. Neelameggham, in: *The Comparability of in vitro and in vivo Experiments for Degradable Mg Implants*, Springer International Publishing, Cham, 2022, pp. 9–16.
- [98] B. Zeller-Plumhoff, D. Tolnai, M. Wolff, I. Greving, N. Hort, R. Willumeit-Römer, *Adv. Eng. Mater.* 23 (2021) 2100197, doi:10.1002/adem.202100197.
- [99] J.L. Wang, J.K. Xu, C. Hopkins, D.H.K. Chow, L. Qin, *Adv. Sci.* 7 (2020) 1902443, doi:10.1002/advs.201902443.
- [100] Y. Wang, P. Fu, N. Wang, L. Peng, B. Kang, H. Zeng, G. Yuan, W. Ding, *Engineering* 6 (2020) 1267–1275, doi:10.1016/J.ENG.2020.02.015.
- [101] A.K. Gartzke, S. Julmi, C. Klose, A.C. Waselau, A. Meyer-Lindenberg, H.J. Maier, S. Besdo, P. Wriggers, *J. Mech. Behav. Biomed. Mater.* 101 (2020) 103411, doi:10.1016/j.jmbbm.2019.103411.
- [102] Z. Li, X. Gu, S. Lou, Y. Zheng, *Biomaterials* 29 (2008) 1329–1344, doi:10.1016/j.biomaterials.2007.12.021.
- [103] X. Gu, Y. Zheng, Y. Cheng, S. Zhong, T. Xi, *Biomaterials* 30 (2009) 484–498, doi:10.1016/j.biomaterials.2008.10.021.
- [104] M.D. Costantino, A. Schuster, H. Helmholz, A. Meyer-Rachner, R. Willumeit-Römer, B.J.C. Luthringer-Feyerabend, *Acta Biomater.* 101 (2020) 598–608, doi:10.1016/J.ACTBIO.2019.10.014.
- [105] N. Anisimova, M. Kiselevskiy, N. Martynenko, B. Straumal, R. Willumeit-Römer, S. Dobatkin, Y. Estrin, *Cytotoxicity of biodegradable magnesium alloy WE43 to tumor cells in vitro: bioresorbable implants with antitumor activity?* *Journal of Biomedical Materials Research Part B: Applied Biomaterials* 108 (1) (2020) 167–173, doi:10.1002/jbm.b.34375.
- [106] Z.Z. Yin, W.C. Qi, R.C. Zeng, X.B. Chen, C.D. Gu, S.K. Guan, Y.F. Zheng, *J. Magnes. Alloy.* 8 (2020) 42–65, doi:10.1016/j.jma.2019.09.008.
- [107] M. Abdallah, A. Joplin, M. Elahinia, H. Ibrahim, *Corros. Mater. Degrad.* 1 (2020) 219–248, doi:10.3390/cmd1020011.
- [108] D. Hoeche, C. Blawert, S.V. Lamaka, N. Scharnagl, C.L. Mendis, M.L. Zheludkevich, *Phys. Chem. Chem. Phys.* 18 (2015), doi:10.1039/C5CP05577F.
- [109] E. Zhang, L. Yang, J. Xu, H. Chen, *Acta Biomater.* 6 (2010) 1756–1762, doi:10.1016/j.actbio.2009.11.024.
- [110] Y. Zhang, Y. Huang, X. Chen, B. Luthringer-Feyerabend, J. Xue, D. Zander, R. Willumeit-Römer, K.U. Kainer, N. Hort, *Scr. Mater.* 212 (2022) 114509, doi:10.1016/J.SCRIPTAMAT.2022.114509.
- [111] P. Sekar, N. S. V. Desai, *J. Magnes. Alloy.* 9 (2021) 1147–1163, doi:10.1016/J.JMA.2020.11.001.
- [112] J.T. Waber, *J. Electrochem. Soc.* 101 (1954) 271, doi:10.1149/1.2781244.

- T. Albaraghteh, R. Willumeit-Römer and B. Zeller-Plumhoff/*Journal of Magnesium and Alloys 10 (2022) 2968–2996* 2995
- [113] J.T. Waber, M. Rosenbluth, *J. Electrochem. Soc.* 102 (1955) 344, doi:10.1149/1.2430058.
- [114] J.T. Waber, *J. Electrochem. Soc.* 102 (1955) 420, doi:10.1149/1.2430111.
- [115] J.T. Waber, B. Fagan, *J. Electrochem. Soc.* 103 (1956) 64, doi:10.1149/1.2430234.
- [116] J.T. Waber, J. Mobersey, J. Ruth, *J. Electrochem. Soc.* 103 (1956) 138, doi:10.1149/1.2430245.
- [117] J.T. Waber, *J. Electrochem. Soc.* 103 (1956) 567, doi:10.1149/1.2430158.
- [118] E. Kennard, J.T. Waber, *J. Electrochem. Soc.* 117 (1970) 880, doi:10.1149/1.2407662.
- [119] J.C. Walton, *Corros. Sci.* 30 (1990) 915–928, doi:10.1016/0010-938X(90)90013-U.
- [120] T.Q. Ansari, J.L. Luo, S.Q. Shi, *Npj Mater. Degrad.* 3 (2019) 28, doi:10.1038/s41529-019-0090-5.
- [121] J.X. Jia, G. Song, A. Atrens, *Adv. Eng. Mater.* 9 (2007) 65–74, doi:10.1002/adem.200600206.
- [122] S.M. Sharland, P.W. Tasker, *Corros. Sci.* 28 (1988) 603–620, doi:10.1016/0010-938X(88)90027-3.
- [123] V. Vijayaraghavan, A. Garg, L. Gao, R. Vijayaraghavan, *Metals* 7 (2017) (Basel), doi:10.3390/met7030083.
- [124] W. Sun, G. Liu, L. Wang, T. Wu, Y. Liu, *J. Solid State Electrochem.* 17 (2013) 829–840, doi:10.1007/s10008-012-1935-9.
- [125] A. Muntean, M. Böhm, *J. Math. Anal. Appl.* 350 (2009) 234–251, doi:10.1016/j.jmaa.2008.09.044.
- [126] C. Chainais-Hillairet, *Discret. Contin. Dyn. Syst. B* 20 (2015) 77, doi:10.3934/dcdsb.2015.20.77.
- [127] F. Clarelli, B. De Filippo, R. Natalini, *Appl. Math. Model.* 38 (2014) 4804–4816, doi:10.1016/j.apm.2014.03.040.
- [128] R.S. Larson, *J. Electrochem. Soc.* 149 (2002) B40, doi:10.1149/1.1430716.
- [129] L. Lacroix, C. Blanc, N. Pèbère, B. Tribollet, V. Vivier, *J. Electrochem. Soc.* 156 (2009) C259, doi:10.1149/1.3148833.
- [130] K.B. Deshpande, *Corros. Sci.* 52 (2010) 2819–2826, doi:10.1016/j.corsci.2010.04.023.
- [131] K.B. Deshpande, *Electrochim. Acta* 56 (2011) 1737–1745, doi:10.1016/j.electacta.2010.09.044.
- [132] K.B. Deshpande, *Corros. Sci.* 52 (2010) 3514–3522, doi:10.1016/j.corsci.2010.06.031.
- [133] S.G. Bharadwaj, R. Varadarajan, in: *Proceedings of the 8th International Symposium on Advances in Electrochemical Science & Technology*, Goa, India, 2005, pp. 207–244, doi:10.1108/S1548-6435(2004)0000001009.
- [134] D. Höche, J. Isakovic, *Chem. Ing. Tech.* 85 (2013) 1951–1956, doi:10.1002/cite.201300033.
- [135] D. Trinh, P. Dauphin Ducharme, U. Mengesha Tefashe, J.R. Kish, J. Mauzeroll, *Anal. Chem.* 84 (2012) 9899–9906, doi:10.1021/ac3022955.
- [136] E.L. Boland, R. Shine, N. Kelly, C.A. Sweeney, P.E. McHugh, *Ann. Biomed. Eng.* 44 (2016) 341–356, doi:10.1007/s10439-015-1413-5.
- [137] X. Zhang, Z. Hao, *J. Phys. Conf. Ser.* 1838 (2021) 012012, doi:10.1088/1742-6596/1838/1/012012.
- [138] A. Amerinatanz, R. Mehrabi, H. Ibrahim, A. Dehghanhadikolaei, N. Shayesteh Moghaddam, M. Elahinia, *Bioengineering* 5 (2018) 105, doi:10.3390/bioengineering5040105.
- [139] P. Bajger, J.M.A. Ashbourn, V. Manhas, Y. Guyot, K. Lietaert, L. Geris, *Biomech. Model. Mechanobiol.* 16 (2017) 227–238, doi:10.1007/s10237-016-0812-3.
- [140] S.K. Ahmed, J.P. Ward, Y. Liu, *Materials* 11 (2018) (Basel), doi:10.3390/ma11010001.
- [141] D. Höche, *J. Electrochem. Soc.* 162 (2014) C1.
- [142] J.A. Grogan, S.B. Leen, P.E. McHugh, *Acta Biomater.* 10 (2014) 2313–2322, doi:10.1016/j.actbio.2013.12.059.
- [143] B.R. Murer N, N. Missert, in: *Proceedings of the OMSOL Users Conference, 2008*.
- [144] E.L. Boland, J.A. Grogan, P.E. McHugh, *Int. J. Numer. Method Biomed. Eng.* 35 (2019) e3247, doi:10.1002/cnm.3247.
- [145] J. Donea, A. Huerta, J.P. Ponthot, A. Rodriguez-Ferran, *Encyclopedia of Computational Mechanics*, John Wiley & Sons, Ltd, Chichester, UK, 2004, doi:10.1002/0470091355.ecm009.
- [146] R. Montoya, C. Iglesias, M.L. Escudero, M.C. García-Alonso, *Mater. Sci. Eng. C* 41 (2014) 127–133, doi:10.1016/j.msec.2014.04.033.
- [147] Z. Shen, M. Zhao, D. Bian, D. Shen, X. Zhou, J. Liu, Y. Liu, H. Guo, Y. Zheng, *J. Mater. Sci. Technol.* 35 (2019) 1393–1402, doi:10.1016/j.jmst.2019.02.004.
- [148] S. Scheiner, C. Hellmich, *Corros. Sci.* 49 (2007) 319–346, doi:10.1016/j.corsci.2006.03.019.
- [149] R.B. MacMullin, G.A. Muccini, *AIChE J.* 2 (1956) 393–403, doi:10.1002/aic.690020320.
- [150] M. Barzegari, D. Mei, S.V. Lamaka, L. Geris, *Corros. Sci.* 190 (2021) 109674, doi:10.1016/j.corsci.2021.109674.
- [151] J.A. Sanz-Herrera, E. Reina-Romo, A.R. Boccaccini, *J. Mech. Behav. Biomed. Mater.* 79 (2018) 181–188, doi:10.1016/j.jmbbm.2017.12.016.
- [152] B. Zeller-Plumhoff, T. AlBaraghteh, D. Höche, R. Willumeit-Römer, *J. Magnes. Alloy.* 10 (2022) 965–978, doi:10.1016/j.jma.2021.11.014.
- [153] M. Marvi-Mashhadi, W. Ali, M. Li, C. González, J. LLorca, *J. Mech. Behav. Biomed. Mater.* 126 (2022) 104881, doi:10.1016/j.jmbbm.2021.104881.
- [154] M. Dahms, D. Hoeche, N. Ahmad Agha, F. Feyerabend, R. Willumeit, *Mater. Corros.* (2017), doi:10.1002/maco.201709461.
- [155] A.H. Abdullah, M. Asri, N. Mohd, M.S. Alias, T. Giha, in: *Proceedings of the World Congress on Engineering, London, UK., International Association of Engineers, 2010*, pp. 2241–2246. July 4–6, 2012.
- [156] J.A. Grogan, B.J. O'Brien, S.B. Leen, P.E. McHugh, *Acta Biomater.* 7 (2011) 3523–3533, doi:10.1016/j.actbio.2011.05.032.
- [157] D. Gastaldi, V. Sassi, L. Petrini, M. Vedani, S. Trasatti, F. Migliavacca, *J. Mech. Behav. Biomed. Mater.* 4 (2011) 352–365, doi:10.1016/j.jmbbm.2010.11.003.
- [158] M. Wenman, K. Trethewey, S. Jarman, P. Chard-Tuckey, *Acta Mater.* 56 (2008) 4125–4136, doi:10.1016/j.actamat.2008.04.068.
- [159] W. Wu, D. Gastaldi, K. Yang, L. Tan, L. Petrini, F. Migliavacca, *Mater. Sci. Eng. B* 176 (2011) 1733–1740, doi:10.1016/j.mseb.2011.03.013.
- [160] J.A. Grogan, S.B. Leen, P.E. McHugh, *Biomaterials* 34 (2013) 8049–8060, doi:10.1016/j.biomaterials.2013.07.010.
- [161] J.R. Apps, J.C. Hutchinson, O.J. Arthurs, A. Virasami, A. Joshi, B. Zeller-Plumhoff, D. Moulding, T.S. Jacques, N.J. Sebire, J.P. Martinez-Barbera, *Acta Neuropathol. Commun.* 4 (2016) 57, doi:10.1186/s40478-016-0321-8.
- [162] W. Wu, S. Chen, D. Gastaldi, L. Petrini, D. Mantovani, K. Yang, L. Tan, F. Migliavacca, *Acta Biomater.* 9 (2013) 8730–8739, doi:10.1016/j.actbio.2012.10.035.
- [163] S. Jafarzadeh, Z. Chen, F. Bobaru, *Corros. Rev.* 37 (2019) 419–439, doi:10.1515/corrrev-2019-0049.
- [164] J. Stafiej, D. di Caprio, E. Bartosik, *J. Supercomput.* 65 (2013) 697–709, doi:10.1007/s11227-013-0933-8.
- [165] D. di Caprio, C. Vautrin-UI, J. Stafiej, J. Saunier, A. Chaussé, D. Féron, J.P. Badiali, *Corros. Sci.* 53 (2011) 418–425, doi:10.1016/j.corsci.2010.09.052.
- [166] N.V. Menshutina, A.V. Kolnoochenko, E.A. Lebedev, *Annu. Rev. Chem. Biomol. Eng.* 11 (2020) 87–108, doi:10.1146/annurev-chembioeng-093019-075250.
- [167] C.F. Pérez-Brokate, D. di Caprio, D. Féron, J. de Lamare, A. Chaussé, *Corros. Eng. Sci. Technol.* 52 (2017) 186–193, doi:10.1080/1478422X.2017.1300748.
- [168] A. Shahmohammadi, M. Baghani, M.S. Panahi, K. Wang, E. Hasanpur, M. Baniassadi, *Proc. Inst. Mech. Eng. Part L J. Mater. Des. Appl.* 235 (2021) 3–18, doi:10.1177/1464420720948253.
- [169] D. Di Caprio, J. Stafiej, G. Luciano, L. Arurault, *Corros. Sci.* 112 (2016) 438–450.
- [170] R. Liu, T. Li, L. Liu, Y. Cui, E.E. Oguzie, Y. Li, F. Wang, *J. Electrochem. Soc.* 166 (2019) C91.
- [171] C. Cui, R. Ma, A. Chen, Z. Pan, H. Tian, *Corros. Sci.* 154 (2019) 80–89.
- [172] P. Van der Weeën, A.M. Zimer, E.C. Pereira, L.H. Mascaro, O.M. Bruno, B. De Baets, *Corros. Sci.* 82 (2014) 133–144.

- [173] U. Galvanetto, T. Mudric, A. Shojaei, M. Zaccariotto, *Mech. Res. Commun.* 76 (2016) 41–47, doi:10.1016/j.mechrescom.2016.06.006.
- [174] A. Shojaei, A. Hermann, P. Seleson, C.J. Cyron, *Comput. Mech.* 66 (2020) 773–793, doi:10.1007/s00466-020-01879-1.
- [175] Z. Chen, F. Bobaru, *J. Mech. Phys. Solids* 78 (2015) 352–381, doi:10.1016/j.jmps.2015.02.015.
- [176] S.S. Kulkarni, A. Tabarraei, An ordinary state based peridynamic correspondence model for metal creep, *Engineering Fracture Mechanics* 233 (2020) 107042, doi:10.1016/j.engfracmech.2020.107042.
- [177] S. Li, Z. Chen, L. Tan, F. Bobaru, *Mater. Sci. Eng. A* 713 (2018) 7–17, doi:10.1016/j.msea.2017.12.053.
- [178] S. Li, Z. Chen, F. Wang, B. Cui, L. Tan, F. Bobaru, *J. Electrochem. Soc.* 163 (2016) C784–C790, doi:10.1149/2.1001613jes.
- [179] A. Hermann, A. Shojaei, D. Steglich, D. Höche, B. Zeller-Plumhoff, C.J. Cyron, *Int. J. Mech. Sci.* 220 (2022) 107143, doi:10.1016/j.jmesci.2022.107143.
- [180] Z. Chen, S. Jafarzadeh, J. Zhao, F. Bobaru, *J. Mech. Phys. Solids* 146 (2021) 104203, doi:10.1016/j.jmps.2020.104203.
- [181] S. Ma, D. Zhang, B. Markert, *PAMM* 19 (2019), doi:10.1002/pamm.201900442.
- [182] W. Mai, S. Soghrati, R.G. Buchheit, *Corros. Sci.* 110 (2016) 157–166.
- [183] Z. Xu, G. Zhang, Z. Chen, F. Bobaru, *Int. J. Fract.* 209 (2018) 203–222, doi:10.1007/s10704-017-0256-5.
- [184] M.J. Borden, C.V. Verhoosel, M.A. Scott, T.J.R. Hughes, C.M. Landis, *Comput. Methods Appl. Mech. Eng.* 217 (2012) 77–95.
- [185] M.J. Borden, T.J.R. Hughes, C.M. Landis, A. Anvari, I.J. Lee, *Comput. Methods Appl. Mech. Eng.* 312 (2016) 130–166.
- [186] R.J.M. Geelen, Y. Liu, T. Hu, M.R. Tupek, J.E. Dolbow, *Comput. Methods Appl. Mech. Eng.* 348 (2019) 680–711.
- [187] W. Bai, R. Sun, J. Leopold, *Procedia CIRP* 46 (2016) 428–431, doi:10.1016/j.procir.2016.03.122.
- [188] W. Badawy, N. Hilal, M. El-Rabee, N. El-Sayed, *Electrochim. Acta* 55 (2010) 1880–1887, doi:10.1016/j.electacta.2009.10.083.
- [189] ISO2019 Biological Evaluation of Medical Devices — Part 15: Identification and Quantification of Degradation Products from Metals and Alloys 10993-15, ISO, 2018 <https://www.iso.org/standard/68937.html>.
- [190] A.S.T.M.-72 Standard Standard Practice for Laboratory Immersion Corrosion Testing of Metals, ASTM International, West Conshohocken, PA., 2004, doi:10.1520/G0031-72R04.
- [191] Y. Liu, Y. Zheng, X.H. Chen, J.A. Yang, H. Pan, D. Chen, L. Wang, J. Zhang, D. Zhu, S. Wu, K.W.K. Yeung, R.C. Zeng, Y. Han, S. Guan, *Adv. Funct. Mater.* 29 (2019) 1805402, doi:10.1002/adfm.201805402.
- [192] H. Sun, C. Li, W. Fang, *Trans. Nonferr. Met. Soc. China* 21 (2011) s258–s261, doi:10.1016/S1003-6326(11)61588-4.
- [193] B. Zeller-Plumhoff, H. Helmholtz, F. Feyerabend, T. Dose, F. Wilde, A. Hipp, F. Beckmann, R. Willumeit-Römer, J.U. Hammel, *Mater. Corros.* 69 (2018) 298–306, doi:10.1002/maco.201709514.
- [194] E. Maire, P.J. Withers, *Int. Mater. Rev.* 59 (2014) 1–43, doi:10.1179/1743280413Y.0000000023.
- [195] C.J. Roy, W.L. Oberkampf, *Comput. Methods Appl. Mech. Eng.* 200 (2011) 2131–2144, doi:10.1016/j.cma.2011.03.016.
- [196] J. Xiao, S. Chaudhuri, *Electrochim. Acta* 56 (2011) 5630–5641, doi:10.1016/j.electacta.2011.04.019.
- [197] Y. Guyot, I. Papantoniou, Y.C. Chai, S. Van Bael, J. Schrooten, L. Geris, *Biomech. Model. Mechanobiol.* 13 (2014) 1361–1371, doi:10.1007/s10237-014-0577-5.
- [198] W. Wu, L. Petriani, D. Gastaldi, T. Villa, M. Vedani, E. Lesma, B. Previtali, F. Migliavacca, *Ann. Biomed. Eng.* 38 (2010) 2829–2840, doi:10.1007/s10439-010-0057-8.
- [199] R.G. Ghanem, *Int. J. Numer. Methods Eng.* 80 (2009) 671–672, doi:10.1002/nme.2751.
- [200] R. Ghanem, D. Higdon, H. Owahdi, *Handbook of Uncertainty Quantification*, Springer, 2017.
- [201] R.G. McClarren, *Uncertainty Quantification and Predictive Computational Science*, Springer International Publishing, Cham, 2018, doi:10.1007/978-3-319-99525-0.
- [202] F. Boukouvala, F.J. Muzzio, M.G. Ierapetritou, E.N. Pistikopoulos, M.C. Georgiadis, A.C. Kokossis, in: *Computer Aided Chemical Engineering*, Elsevier, 2011, pp. 432–436, doi:10.1016/B978-0-444-53711-9.50087-0.
- [203] R.G. Sargent, in: *Proceedings of the Winter Simulation Conference (WSC)*, 2015, pp. 1729–1740, doi:10.1109/WSC.2015.7408291.
- [204] A. Nicholls, *J. Comput. Aided Mol. Des.* 28 (2014) 887–918, doi:10.1007/s10822-014-9753-z.
- [205] K. Wang, Y. Wang, X. Yue, W. Cai, *Corros. Sci.* 178 (2021) 109095, doi:10.1016/j.corsci.2020.109095.
- [206] S. Hoffmann, F. Schönbrodt, R. Elsas, R. Wilson, U. Strasser, A.L. Boulesteix, *R. Soc. Open Sci.* 8 (2021) 201925.
- [207] M. Berenguel-Alonso, X. Granados, J. Faraudo, J. Alonso-Chamarro, M. Puyol, *Anal. Bioanal. Chem.* 406 (2014) 6607–6616, doi:10.1007/s00216-014-8100-5.
- [208] B. Ankenman, B.L. Nelson, J. Staum, *Oper. Res.* 58 (2010) 371–382 <http://www.jstor.org/stable/40605923>.
- [209] K. Tak, J. Kim, H. Kwon, J.H. Cho, I. Moon, *Korean J. Chem. Eng.* 33 (2016) 1999–2006, doi:10.1007/s11814-016-0083-9.
- [210] J.P.C. Kleijnen, *Eur. J. Oper. Res.* 192 (2009) 707–716, doi:10.1016/j.ejor.2007.10.013.
- [211] H.N. Najm, B.J. Debuschere, Y.M. Marzouk, S. Widmer, O.P. Le Maître, *Int. J. Numer. Methods Eng.* 80 (2009) 789–814, doi:10.1002/nme.2551.
- [212] T. Sumner, E. Shephard, I.D.L. Bogle, *J. R. Soc. Interface* 9 (2012) 2156–2166, doi:10.1098/rsif.2011.0891.
- [213] Y. Wang, D.L. McDowell, *Uncertainty Quantification in Multiscale Materials Modeling*, Elsevier, 2020, doi:10.1016/C2018-0-00364-3.
- [214] A. Chernatynskiy, S.R. Phillpot, R. LeSar, *Annu. Rev. Mater. Res.* 43 (2013) 157–182.

Computational modelling of magnesium degradation in simulated body fluid under physiological conditions

This chapter presents a novel computational model that simulates pure Mg biodegradation under physiological conditions. The biodegradation model captures the biodegradation behaviour of pure Mg and the formation of different precipitates on the implant surface in simulated body fluid over 28 days. This generalised model is implemented using COMSOL software and tracks biodegradation progression, providing insights into the mean biodegradation depth. Significantly, the model also simulates the precipitation process of various biodegradation product salts on the implant surface. However, the calibration process of this model is challenging due to the lack of reported values for the different key parameters, both for biodegradation and precipitation reactions. Moreover, this model is computationally expensive. To calibrate it, Kriging surrogate models are implemented to reduce simulation time and computational cost. The biodegradation model's accuracy is enhanced through simultaneous calibration based on the Kriging model and by using the mean biodegradation depth across multiple experimental datasets. This calibration process yields a notable alignment with the experimental data, with an uncertainty of 7%. Furthermore, in the case of salt precipitation within the biodegradation layer, Kriging models efficiently predict reaction rates. Additionally, the construction of Kriging surrogate models, incorporating the probabilistic nature of the parameters, which was not previously reported in the literature, facilitates advanced analyses such as sensitivity analysis. Sensitivity analysis offers an enhanced understanding of biodegradation system dynamics by identifying the most influential parameters affecting the biodegradation model predictions. Moreover, the sensitivity analysis reveals that the model parameters are correlated, which is related to the complexity and high computational costs of the model. Overall, the computational framework, including the biodegradation and Kriging models, provides a correlating fit to the experimental data from pure Mg samples of different geometries degrading in simulated body fluid, along with reliable error estimation.

Publication details

Berit Zeller-Plumhoff*, *Tamadur AlBaraghteh**, Daniel Höche, Regine Willumeit-Römer, (2022). Computational modelling of magnesium degradation in simulated body fluid under physiological conditions. *Journal of Magnesium and Alloys*, 10(4), 965–978. <https://doi.org/10.1016/j.jma.2021.11.014>.

* B. Zeller-Plumhoff and T. AlBaraghteh share first-authorship.

Author's contribution

The author contributed to software, implementation, discussion, writing and editing the original draft.

Copyright Notice

©This is an accepted version of the article originally published in the Journal of Magnesium and Alloys. The paper has been published under Creative Commons CC-BY 4.0 Licence. The copyright has been clarified in line with the publisher's guidelines.



Available online at www.sciencedirect.com

ScienceDirect

Journal of Magnesium and Alloys 10 (2022) 965–978



www.elsevier.com/locate/jma

Full Length Article

Computational modelling of magnesium degradation in simulated body fluid under physiological conditions

Berit Zeller-Plumhoff^{a,1,*}, Tamadur AlBaraghteh^{a,1}, Daniel Höche^b, Regine Willumeit-Römer^a

^a Helmholtz-Zentrum hereon GmbH, Institute of Metallic Biomaterials, Max-Planck-Straße 1, Geesthacht, 21502, Germany

^b Helmholtz-Zentrum hereon GmbH, Institute of Surface Science, Max-Planck-Straße 1, Geesthacht, 21502, Germany

Received 25 July 2021; received in revised form 29 October 2021; accepted 2 November 2021

Available online 26 December 2021

Abstract

Magnesium alloys are highly attractive for the use as temporary implant materials, due to their high biocompatibility and biodegradability. However, the prediction of the degradation rate of the implants is difficult, therefore, a large number of experiments are required. Computational modelling can aid in enabling the predictability, if sufficiently accurate models can be established. This work presents a generalized model of the degradation of pure magnesium in simulated body fluid over the course of 28 days considering uncertainty aspects. The model includes the computation of the metallic material thinning and is calibrated using the mean degradation depth of several experimental datasets simultaneously. Additionally, the formation and precipitation of relevant degradation products on the sample surface is modelled, based on the ionic composition of simulated body fluid. The computed mean degradation depth is in good agreement with the experimental data (NRMSE=0.07). However, the quality of the depth profile curves of the determined elemental weight percentage of the degradation products differs between elements (such as NRMSE=0.40 for phosphorus vs. NRMSE=1.03 for magnesium). This indicates that the implementation of precipitate formation may need further developments. The sensitivity analysis showed that the model parameters are correlated and which is related to the complexity and the high computational costs of the model. Overall, the model provides a correlating fit to the experimental data of pure Mg samples of different geometries degrading in simulated body fluid with reliable error estimation.

© 2021 Chongqing University. Publishing services provided by Elsevier B.V. on behalf of KeAi Communications Co. Ltd.

This is an open access article under the CC BY-NC-ND license (<http://creativecommons.org/licenses/by-nc-nd/4.0/>)

Peer review under responsibility of Chongqing University

Keywords: Biodegradation; Magnesium; Computational modelling; Corrosion; Uncertainty quantification; Kriging.

1. Introduction

Magnesium (Mg) and its alloys are emerging as promising alternatives to permanent implant materials, due to their biodegradability, low toxicity and ability to facilitate bone growth. There are numerous studies investigating the degradation of Mg-alloys *in vitro* in different cell culture media and *in vivo* in animal models. Due to the high complexity and sensitivity of the system a gap between the results of *in vitro* and *in vivo* studies remains [1]. Computational modelling can be used to facilitate closing the gap and enable

predictions based on *in vitro* experiments, and thus speed up the development process of new implants if reliable models are developed.

Different kinds of computational models of Mg degradation have been published until now; including physical, phenomenological, analytical and machine learning-based models. A simplified analytical model based on the mass conservation law was presented by Dahms et al. [2]. Chemical and electrochemical processes were not included in this model due to the analytical nature of the approach. Nevertheless, by capturing both long-term (degradation propagation) and short-term (initiation) characteristics, the degradation rate calculated by the analytical model was found to be in agreement with experimental data for up to 18 days. In other studies, continuum damage (CD) models are used to describe the degradation of Mg phenomenologically. Gastaldi et al. [3] and Grogan et al.

* Corresponding author.

E-mail addresses: berit.zeller-plumhoff@hereon.de, berit.zeller-plumhoff@hzg.de (B. Zeller-Plumhoff).

¹ These authors share first-authorship.

B. Zeller-Plumhoff, T. AlBaraghteh, D. Höche et al.

Journal of Magnesium and Alloys 10 (2022) 965–978

[4] used CD models to simulate the degradation of Mg-based stents. The CD approach enabled studying the micro-scale geometric discontinuities induced by the degradation on the mechanical integrity of the overall specimen without the need for the progression of the degradation to be modelled explicitly. Therein lies also the disadvantage of the CD approach, as it fails to incorporate the complex electrochemical processes during degradation, which change (locally) e.g. due to the composition of the degradation medium. Thus, a CD model will require calibration for each change in the corrosive environment or material composition.

Physical models based on the Nerst-Planck equation for Mg exposed to aqueous electrolytes were developed for example by Jia et al. [5], Deshpande [6] and Grogan et al. [7]. In these models, the geometric change of the computational domain due to the degradation was incorporated by applying an adaptive mesh. Grogan et al. [7] et al. applied this model to a stent geometry and additionally took the formation of a stable degradation layer into account. By doing so, they could sustain the assumption of a transport-controlled degradation across this layer. Sun et al. [8] et al. additionally introduced the time-dependent formation and deposition of corrosion products on the metal surface by including the changes in both electrical potential and mass transfer. Bajger et al. [9] et al. developed the model presented in [7] further by assuming the diffusion as the rate-limiting process and the absence of a protective layer. This model assumed a zero concentration of Mg^{2+} ions and only the presence of Cl^{-} ions in the electrolyte at the beginning of the reaction. The moving interface of the degrading metal Mg specimen was modelled implicitly using the level-set method. The model showed good agreement in terms of hydrogen evolution with published datasets. The physical model presented by Sanz-Herrera et al. [10] et al. incorporated the highest number of chemical species involved in the degradation process so far. This model included a set of seven species in the model; (metallic) Mg, H_2 , H_2O , Cl^{-} , $Mg(OH)_2$ and $MgCl_2$, where the concentration gradient of each of these species was modelled using reaction-diffusion equations. This model was reported to be valid for slow (0.05 mm/year) and fast (0.3 mm/year) degradation rates, but mostly qualitative comparisons were provided that were within the order of magnitude of experimental values in the literature. Ahmed et al. [11] et al. presented a simplified model, which was able to demonstrate the effect of different chemical species on the *in vitro* degradation of Mg. This model was simplified by using the dimensionless presentation of different model parameters, which reduced the mathematical complexity of the model.

A main drawback of most physical models is that they consider only the formation of magnesium hydroxide ($Mg(OH)_2$), which is however not the main degradation product forming during the degradation of Mg in simulated body fluids (SBFs) under physiological conditions [12,13]. Instead, the formation of a range of other precipitates must be taken into account. This is pivotal, as the forming precipitates and the evolving pH and H_2 gas influence the environment around the implant. Thus, if more complex models should be de-

veloped that include the cell-material interaction or any mechanical behaviour, it is important that both the degradation rate of Mg implants is modelled correctly, as well as the formation of the degradation layer that forms in SBF. Additionally, the published computational models are lacking three-dimensional (3D) input data on the degradation layer porosity as a key transport parameter, which limits their validity, as in many cases the degradation of Mg is modelled as a diffusion-limited problem.

A recent model by Höche [14] investigated the microgalvanic degradation in a system of Mg coupled to more noble materials. In addition to the formation of magnesium hydroxide, different chemical reactions occurring within the immersion medium were included in this model, such as water dissociation. This model considers deposit layer porosity and tortuosity and was able to simulate and quantitatively predict the effect of degradation products in a time-dependent manner. In this work, we are presenting a physical model that is an extension of the model presented in [14]. Specifically, we are modelling the degradation of pure Mg in SBF over four weeks in a semi-static immersion test. SBF was selected because it mimics the ionic composition of blood plasma more closely than NaCl. At the same time SBF does not contain organic components, which would increase the complexity of the ongoing interactions significantly. We assume a homogeneous degradation during which precipitates form at the Mg interface that do not re-dissolve. These precipitates form a porous degradation layer through which the chemical species diffuse. The degradation layer is assumed non-reactive and forming H_2 gas bubbles don't interact with any model components.

The model is calibrated using data from weight loss measurements and volume loss measurements based on 3D micro computed tomography (μ CT) data, as well as data from energy-dispersive X-ray spectroscopy (EDX) on the formation of certain precipitates. Moreover, experimental data from transmission X-ray microscopy was used to specify the porosity of the degradation layer. The estimation and calibration of different model parameters are one of the main challenges in the model development process due to the complex multiphysics nature of the current model and the high computational costs associated with it. Furthermore, most key parameters have no reported values in literature. For example, there are no reported values for any of the reaction rates of the system [9]. Uncertainty quantification (UQ) provides the methodologies to characterize the output uncertainties of a mathematical model based on variable inputs and to identify the different sources of the uncertainties within the model itself. For the parameter estimation we are employing the UQ approach by using a Kriging-based metamodeling (or surrogate modelling) methodology. Metamodels are constructed by generating a response of the model using a relatively small set of parameters and simulations. This reduces the computational costs and accelerates the calculation processes, but also allows for further advanced analyses, such as sensitivity analysis, reliability analysis and Bayesian model calibration, therefore enabling a better understanding of the system [15].

Table 1
Concentrations of ionic components in simulated body fluid [16].

Ion	Ion concentration [mM]
Na ⁺	142.00
Ca ²⁺	2.31
HCO ₃ ⁻	34.88
HPO ₄ ²⁻	1.39
Cl ⁻	109.90

To quantify the influence of model parameters over the model outputs, a global sensitivity analysis was performed.

2. Methodology

2.1. Modelling of electrochemistry and chemistry

We are modelling the degradation of pure Mg in SBF in a semi-static immersion test. The Mg specimen is assumed to be of a purity between 99.92% and 99.95%, but the influence of impurities is not directly modelled. The formulation of SBF that is modelled is taken from Bohner and Lemaitre [16] and contains the following chemical species: Na⁺, Ca²⁺, HCO₃⁻, HPO₄²⁻ and Cl⁻, in addition to H⁺ and OH⁻. Table 1 shows the different ionic concentrations in the medium.

We are considering the following (electro-)chemical reactions taking place at the implant surface, as suggested in [13]. Firstly, the magnesium is dissolving leading to the formation of hydrogen.



In the meantime, a number of precipitates form based on the ions contained in the degradation medium.

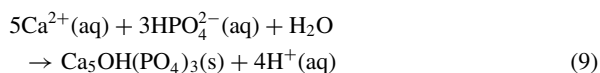
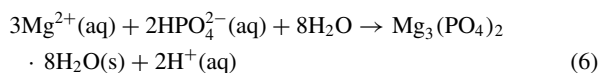
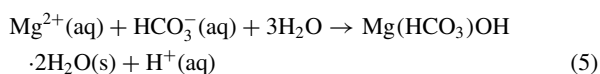
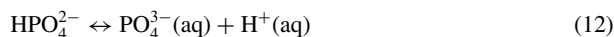
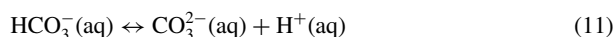
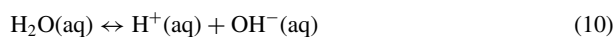


Table 2
Dissolution and dissociation constants as presented in [13].

Precipitate	Equation number	Precipitation constant pK
Brucite	(3)	15.97
Magnesite	(4)	4.73
Nesquehonite	(5)	-4.49
Bobierite	(6)	-2.98
Portlandite	(7)	-5.38
Calcite	(8)	-1.8
Hydroxyapatite	(9)	-35.42
Dissociation of		
Water	(10)	13.61
Hydrogen carbonate	(11)	10.24
Hydrogen phosphate	(12)	12.32

Additionally, we assume that water, hydrogen carbonate and hydrogen phosphate are dissociating in the media according to [13]:



While the oxygen reduction reaction was shown to be of importance during the degradation of pure Mg in NaCl, it is not incorporated into the model as its influence diminished after degradation over less than an hour for commercial purity Mg [17]. We therefore assume that it has little influence on the degradation process at the time scales considered in the present model.

The precipitation and dissolution constants (pK=-log₁₀K) at 37°C as presented in [13] and adjusted for the above chemical reactions are shown in Table 2.

2.2. Numerical model

A rectangular shape is used approximate a pure Mg sample that is covered with a degradation layer and degradation medium, see Fig. 1. An initial porous degradation layer of 10 nm is assumed to be on the sample surface. This equates to the thin MgO layer that forms on Mg samples immediately after exposure to air following the manufacturing of the sample [18]. In the following, Ω_{Mg} denotes the metal domain, Ω_{DL} the porous degradation layer of porosity ϵ and Ω_L the aqueous immersion medium. Fig 1 shows a schematic of the geometry, the included domains and modelled (electro-)chemical processes.

2.2.1. Transport of chemical species

The transport of the chemical species i of concentration c_i is described as

$$\frac{\partial c_i}{\partial t} + \nabla \cdot (D_i \nabla c_i - z_i \frac{D_i}{RT} F c_i \nabla V) = R_i \quad \text{in } \Omega_{DL} \cup \Omega_L \quad (13)$$

The first part of the species flux describes the diffusion of the species within the domain, whilst the second part describes

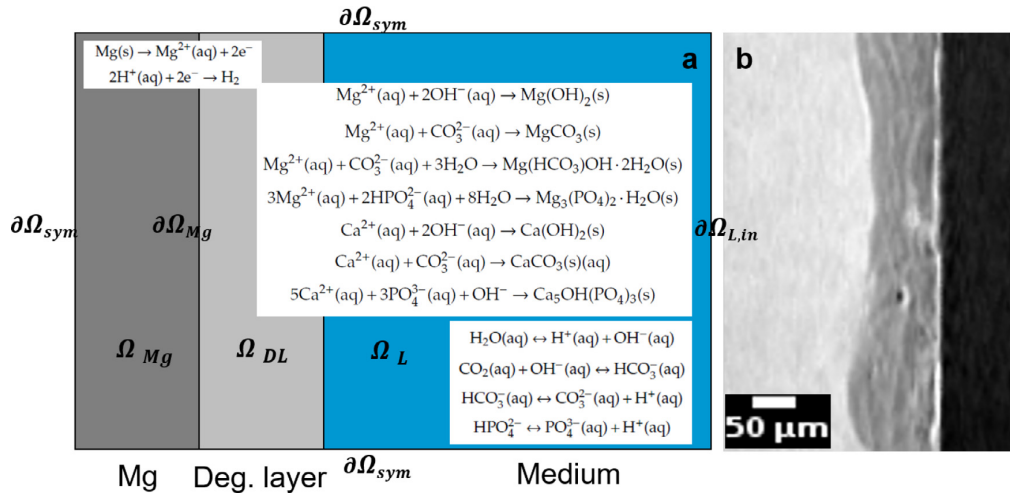


Fig. 1. (a) Schematic of the degradation process of pure Mg in simulated body fluid. The metallic Mg sample is assumed to be covered by a porous degradation layer from the start, with an initial thickness of 10 nm. The ions diffuse through the liquid medium and the liquid phase of the degradation layer towards the metal interface, where the Mg dissolution is taking place. Precipitates form within the degradation layer and the dissociation of different ionic species occurs in the liquid phase. Not to scale. (b) Slice through μ CT data of pure Mg disc degraded in SBF after 3 weeks for comparison.

the migration within the electric field. z_i denotes the species charge (e.g., for Mg^{2+} $z_{\text{Mg}} = 2$), V is the electric potential, $R \approx 8.314$ [J / (mol K)] the gas constant and T the temperature. $F \approx 96,485$ [C/mol] is the Faraday constant. The diffusion coefficient is given as

$$D_i = \frac{\epsilon}{\tau} D_{l,i} \quad \text{in } \Omega_{DL} \quad (14)$$

where τ is the tortuosity of the porous layer, ϵ the porosity and $D_{l,i}$ the diffusion coefficient of the chemical species in the liquid phase of the porous medium. For simplicity, it is assumed that the porosity can be described by ϵ only, i.e. $\tau = 1$. $\epsilon = 1$ in Ω_L therefore,

$$D_i = D_{l,i} \quad \text{in } \Omega_L. \quad (15)$$

Furthermore,

$$\frac{\partial c_i}{\partial t} = 0 \quad \text{in } \Omega_{Mg}. \quad (16)$$

The reaction rate R_i of chemical species i is described by

$$R_i = \epsilon \sum_j k_{l_j} (K_{eq,l_j} - c_i c_j) \quad \text{in } \Omega_{DL} \cup \Omega_L \quad (17)$$

with j denoting the chemical species with which i reacts under equilibrium constant K_{eq,l_j} and backward reaction constant k_{l_j} , i.e. in reaction l_j of Eqs (3)-(9). However, the formation of precipitates (Eqs. (3) to (9)) is assumed to take place only in the porous degradation layer.

Initial values $c_{0,i}$ of ionic species i in the liquid phase are determined from the medium composition and given in Table 1. $c_{0,i} = 0$ in the metal domain Ω_{Mg} .

A constant inflow is defined at boundary $\partial\Omega_{L,in}$, i.e. $c_i = c_{0,i}$ to model and approximate the semi-static immersion test.

Symmetry is assumed at $\partial\Omega_{sym}$. For the inner boundary between Ω_{Mg} and Ω_{DL} , denoted as $\partial\Omega_{Mg}$, flux discontinuity is assumed, as well as an electrode surface coupling, i.e., $-\mathbf{n} \cdot \mathbf{J}_i = \sum R_{i,m_m}$.

2.2.2. Formation of precipitates on mg surface

Precipitates are forming on the metal surface depending on the pH as highlighted in Fig. 2, according to Eqs. (3)-(9). The formation of precipitate p_l is given as

$$\frac{\partial c_{p_l}}{\partial t} = \epsilon k_l (K_{eq,l} - c_i c_j) \quad \text{in } \Omega_{DL} \cup \Omega_L \quad (18)$$

with the equilibrium constant $K_{eq,l}$ and backward reaction constant k_l for reaction l of the Eqs. (3)-(9) and i and j denoting the two species reacting in the respective reaction.

To determine if all chemical reactions presented in Section 2.1 have to be taken into account in the computational model, the freeware Hydra-Medusa [19] is used to determine the fractions of the above precipitates forming in SBF at 37°C depending on the pH. To this end, the solubility constants used in the software were adapted using the constants in Table 2. Fig. 2 shows the respective calculated fractions. Within the experimentally observed pH range, marked with vertical lines, neither nesquehonite ($\text{Mg}(\text{HCO}_3)\text{OH} \cdot 2\text{H}_2\text{O}(\text{s})$) nor portlandite ($\text{Ca}(\text{OH})_2(\text{s})$) are predicted form. However, nesquehonite has been observed within the degradation layer experimentally using X-ray diffraction in a previous study [12]. By contrast, the formation of portlandite hasn't been reported. Based upon this information, only Eq. (7) is removed from the model.

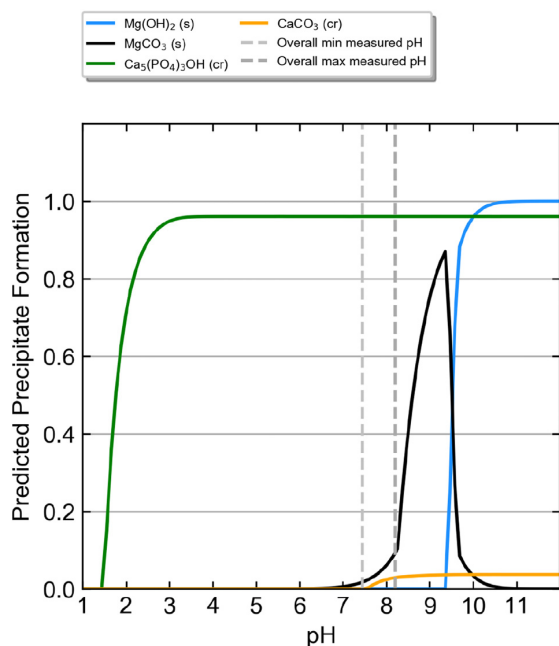


Fig. 2. Fractions of precipitates forming in SBF at 37°C depending on pH as computed from [19]. The figure is taken and adapted from [12] under a CC BY 4.0 license. Vertical lines indicate experimentally measured minimum and maximum pH values. The fractions are with respect to the precipitates based on Mg and Ca, respectively.

2.2.3. Magnesium degradation

As previous experiments have shown there is no easily quantifiable correlation between the electrochemical driven anodic dissolution related degradation of Mg and the ionic composition of the degradation medium [12]. Thus, we are mathematically uncoupling the formation of precipitates and the degradation of Mg. As the degradation behaviour shown in [20,21] followed a linear trend following an initial period of low degradation the degradation of metallic Mg (Eq. (1)) is modelled as:

$$\frac{\partial c_{Mg}}{\partial t} = \frac{\epsilon k_{deg}}{1 + \exp^{-(t-t_{init})}} \quad (19)$$

which equates to the effective rate of Mg^{2+} ion release at $\partial\Omega_{Mg}$, t_{init} denotes the starting time of degradation.

2.3. Experimental data for model input and calibration

Many model parameters are taken from the literature, such as the precipitate dissolution constants in Table 2. The initial concentration of the ionic species and their concentration at the boundaries is given by the SBF solution itself as stated in Table 1. Table 3 contains all other parameters involving the ionic species and forming precipitates.

For simplicity we will assume in the beginning that the current density in the electrolyte i_l is constant as measured experimentally for the corrosion potential. E_{corr} of Mg in SBF was

Table 3

Model parameters as taken from the literature.

Molecular weight	[g/mol]	Reference
Mg	1.739	
Density ρ	[kg/m ³]	
Mg	1.739	[8]
Diffusion coefficients D	[m ² /s]	
Na ⁺	1.33×10^{-9}	[14,23]
Cl ⁻	2.03×10^{-9}	[14,23]
H ⁺	9.31×10^{-9}	[14,23]
OH ⁻	5.27×10^{-9}	[8,14]
Mg ²⁺	7.05×10^{-9}	[8,14]
O ₂	2.4×10^{-9}	[14,24]
HCO ₃ ⁻	1.19×10^{-9}	[24,25]
CO ₃ ²⁻	0.923×10^{-9}	[24,25]
CO ₂	1.91×10^{-9}	[26]
HPO ₄ ²⁻	0.69×10^{-9}	[25,27]
PO ₄	0.612×10^{-9}	[25,27]
Ca ²⁺	0.793×10^{-9}	[28]

determined with respect to SHE as -1.66 V/cm² with a corresponding i_l of $31.6 \cdot 10^{-6}$ A/cm² [22]. The backward reaction constants of Eqs. (10)-(12) are all set to $1.4 \cdot 10^4$ m³mol⁻¹s⁻¹ for simplicity.

2.3.1. Degradation layer porosity

The porosity of the degradation layer evolving in SBF is determined using transmission X-ray microscopy, as published in [20]. In brief, pure magnesium (99.92%) discs were degraded in SBF in a semi-static immersion test for 1–4 weeks. Following degradation, the samples were dried and imaged using μ CT to determine the overall degradation morphology. Small samples were then extracted from the degradation layer using focussed-ion-beam (FIB) milling. These were imaged tomographically using TXM at a resolution down to 37 nm. The porosity of the degradation layer was determined based on the 3D image data. As the samples taken from 1 and 2 week specimen were imaged at higher resolution, we use the mean calculated porosity of 18.67% for these time points as input into the model. Fig. 3 gives an overview of the experimental data used in the current model for input and data calibration.

2.3.2. Model calibration data

The calibration of the model is performed by evaluating the mean degradation depth of the Mg specimen using both data from μ CT imaging and weight loss data. Data for 1–4 weeks is taken from [20], while additional μ CT data for 6–10 days is taken from [12] and from newly measured data. For a description of the data acquisition for the previously unpublished data please see the appendix. Moreover, the data from [20] and [12] differ, as discs of 99.92% purity were used and wires of 99.95% purity in the experiments, respectively. By calibrating the model to the data based on both geometries and materials simultaneously, it is possible to assess the generality of the model with respect to metal impurity within a certain range.

B. Zeller-Plumhoff, T. AlBaraghteh, D. Höche et al.

Journal of Magnesium and Alloys 10 (2022) 965–978

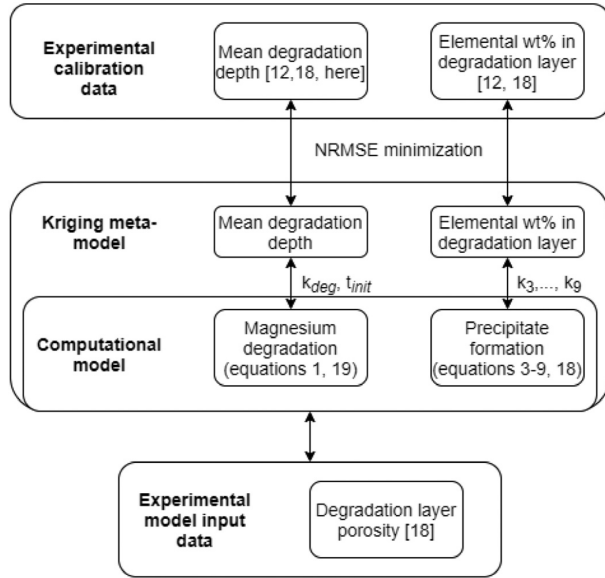


Fig. 3. Overview of the dataflow in the current model. The experimentally determined porosity of the degradation layer is given as input to the computational degradation model. The model simulates the Mg metal thinning and the formation of precipitates on the metal surface in an uncoupled manner. Based on the determined concentration changes, the Kriging meta-model determined the mean degradation depth and elemental wt% of the elements in the degradation layer, based on the different parameter settings. The results are compared with the experimental values on the basis of the NRMSE, which is minimized.

To calibrate the model for the formation of precipitates in the degradation layer, calibration data from EDX measurements is taken from [20] and [12]. In both cases, the mean elemental weight percentage (wt%) of each element in the degradation layer is calculated and used for the calibration. Again, by calibrating to experimental data from two experiments the model generality can be assessed with respect to the deviation of experimental results.

2.4. Implementation

The computational model is implemented in Comsol Multiphysics 5.6 (COMSOL AB, Stockholm, Sweden). The model geometry is a quasi-1D geometry. A schematic of the model geometry is given in Fig. 1, however, the Mg domain measures 0.2 mm in length, the initial degradation layer is 10 nm thick and the electrolyte domain is 0.2 mm long. The geometry is 1 μm high. The mesh is based on rectangular finite elements with a fixed height of 1 μm and a variable thickness, to refine the mesh near the degradation layer. Fig. 4 shows the extents of the initial mesh.

The arbitrary Lagrangian-Euler (ALE) method is used to capture the dynamic deformation of the model geometry and its moving boundaries. The ALE includes two frames: the reference frame, which has a fixed coordinates frame, and the spatial frame, which has coordinates moving with time, subject to boundary conditions [6,7]. Thus, utilizing ALE enables

explicitly tracking the moving interface of the degrading metal and it produces a smooth deformation of the mesh subjected to the constraints placed on the boundaries.

The normal velocity of the metal interface is calculated as

$$v_{deg} = \frac{M_{Mg}}{\rho_{Mg}} \frac{\partial c_{Mg}}{\partial t} \quad (20)$$

from which the mean degradation depth (MDD) is determined as a function of the degradation rate (DR) [29]:

$$MDD = r_{initial} - \int v_{deg} dt \quad (21)$$

Note that no displacement is considered for all other boundaries.

The mean elemental weight percentage of each element is calculated based on the concentration of each precipitated species c_{precj} and the molar mass. For example, for element i , we initially calculate the overall mass concentration in the degradation layer as:

$$\rho_{DL,elem_i} = \left(\sum_{j=1}^6 N_{precj,elem_i} c_{precj} \right) \cdot M_{elem_i} \quad (22)$$

with M_{elem_i} the molar mass of the element, and $N_{precj,elem_i}$ the stoichiometric factor for element i in precipitate j . The elemental weight percentage of the same element i is then

$$wt_{DL,elem_i} = \frac{\rho_{DL,elem_i}}{\sum_{k=1}^6 \rho_{DL,elem_k}} \cdot 100 \quad (23)$$

for elements C, Ca, P, H, O and Mg. H cannot be measured experimentally, therefore no calibration data is available for its wt%. The presence of H needs to be taken into account to calculate the mean element wt% of all other elements though.

2.4.1. Parameter estimation under uncertainty

Traditionally, the optimal model parameters are determined by running the computationally expensive simulation for a large number of possible parameters, followed by an error estimation. By employing metamodeling, the computational cost can be reduced while still covering the same range of possible parameter values. In this case, Kriging is used to quantify and optimize the reaction rates k_l for $l = 3, \dots, 9$, k_{deg} and t_{init} , by obtaining the optimal reaction rate constants to calibrate the model output with respect to the experimental data. In Kriging, the response of the model is constructed as the summation of the mean structure and a zero-mean stationary Gaussian stochastic process [15,30].

$$\mathcal{M}(x) = \beta^T f(x) + \sigma^2 Z(x, \omega), \quad (24)$$

for any $x = (k_{deg}, t_{init}, k_3, k_4, k_6, k_7, k_8, k_9)$. The first term of the right-hand side of the Eq. (24) is the mean value of the Gaussian process, which is also known as the trend, where P is the number of the random arbitrary functions f_j ; $j = 1, \dots, P$ and β is the corresponding coefficients β_j ; $j = 1, \dots, P$, which is obtained from the generalized least-squares method. The second term of the right-hand side of Eq. (24) is a realization of the stochastic process that is assumed to have a zero-mean, unit-variance $Z(x, \omega)$, where σ is

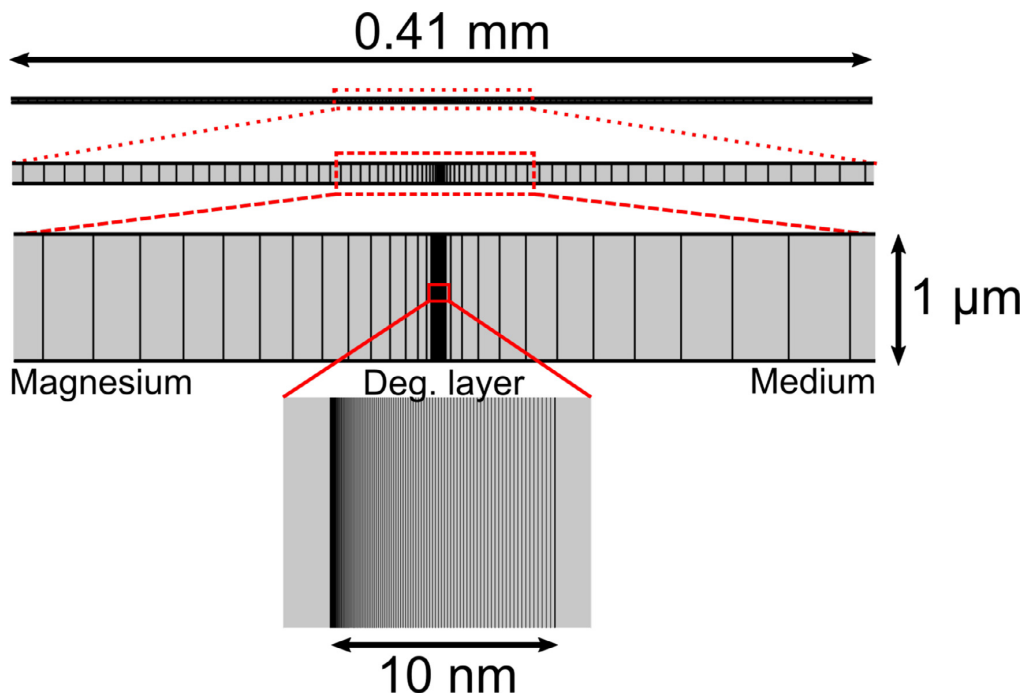


Fig. 4. Initial mesh used to model the magnesium corrosion. The overall extents of the mesh are denoted in the graph and the different regions are denoted in reference to Fig. 1 with several stages of zoom to enable the visualisation of the mesh within the initial 10 nm thick degradation layer.

the variance of the process and ω is the underlying probability space, which is defined in terms of the correlation function of the stochastic process $R(x, x', \theta)$ [15,31].

The mathematical presentation of the Kriging model to calculate the degradation rate constant would be

$$MDD = \mathcal{M}(k_{deg}, t_{init}) \quad (25)$$

and for the mean elemental weight percentage:

$$wt_{DL, elem_i} = \mathcal{M}(k_{deg}, t_{init}, k_3, k_4, k_5, k_6, k_8, k_9) \quad (26)$$

for elements i being C, Ca, P, O and Mg and j in k_j referring to the number of the precipitation reaction in Eqs. (3)-(9).

The Kriging algorithm was implemented in MATLAB (R2020b, The MathWorks, Inc., Massachusetts, United States) using the Kriging module of UQLab [32], a MATLAB-based Uncertainty Quantification framework. A wrapper script is used to convert data-format into a compatible format between COMSOL (via LiveLink) (true model output) and UQLab (data needed to create the input module). Later the output data of the true model was used to create the experimental design, which represent the initial known function values for the objective function in the Kriging metamodel. The observations of the true model are obtained by running the initial input samples in COMSOL through LiveLink and report the model response. The MDD and the elemental wt% of each chemical element in the true model are calculated then by the wrapper script. To describe the similarity between observations x and the new points x' generated by the Kriging metamodel, the Mate'r 5/2 correlation function was used, which is

given by [33]

$$R(x, x', v = 5/2) = \left(1 + \sqrt{5} \frac{|x - x'|}{\theta} + \frac{5}{3} \left(\frac{|x - x'|}{\theta} \right)^2 \right) \times \exp \left[-\sqrt{5} \frac{|x - x'|}{\theta} \right] \quad (27)$$

where the hyper-parameter θ was determined using the Maximum-likelihood (ML) estimation method.

Initial tests are performed to specify the testing ranges for each parameter. These tests are performed using the rate equation and guided by the experimental data (see Section 2.3.2). The maximum and minimum limits of the test intervals of each parameter were provided to the input module. Within the input module of the Kriging model, the Latin hypercube sampling (LHS) strategy is used to draw samples within the user-defined range. Random test sets within the input intervals were created using the LHS sampling strategy and tested based on the convergence of the model, the final input ranges are given in Table 4. Initially, 80 different sets of each tested parameters were generated using the random sampling strategy of LHS. These sets were randomly created under the assumption of a uniform distribution. After generating the test samples, a random selection of 25 sets out of the 80 sets was selected and run via LiveLink COMSOL to generate the true model response, which is needed to create the Kriging metamodel. In the current case, the true model object was directly defined as the Comsol model (via LiveLink), hence the experimental design test-matrices will be automatically de-

B. Zeller-Plumhoff, T. AlBaraghteh, D. Höche et al.

Journal of Magnesium and Alloys 10 (2022) 965–978

Table 4

Tested ranges for the model parameters and optimal parameters as estimated by Kriging. LOO-error for each parameter is given. As multi-output Kriging was performed for k_3 - k_9 , one LOO-error is given for these.

Parameter	Input range	Optimal value	LOO-error
k_{deg} [mol/m ² s]	$-1 \times 10^{-7} - -4 \times 10^{-5}$	-2.4321×10^{-5}	7.37133×10^{-7}
t_{init} [days]	0 - 4	1.935	4.4431×10^{-6}
k_3 [m ⁷ /mol ² s]	$-1 \times 10^{-19} - -1 \times 10^{-23}$	-9.0245×10^{-21}	
k_4 [m ⁷ /mol ² s]	$-1 \times 10^{-5} - -1 \times 10^{-12}$	-7.0332×10^{-9}	
k_5 [m ⁷ /mol ² s]	$-1 \times 10^{-5} - -1 \times 10^{-12}$	-7.0023×10^{-10}	
k_6 [m ⁷ /mol ² s]	$-1 \times 10^{-1} - -1 \times 10^{-12}$	-1.0798×10^{-2}	5.312×10^{-4}
k_8 [m ⁷ /mol ² s]	$-1 \times 10^{-19} - -1 \times 10^{-25}$	-8.0037×10^{-24}	
k_9 [m ⁷ /mol ² s]	$1 \times 10^{15} - 1 \times 10^{20}$	9.001×10^{16}	

finned within the UQLab through the wrapper function based on both model object and the input module.

The performance of the Kriging metamodel was estimated by the leave-one-out error (LOO-error) given by

$$LOO = \frac{1}{N_K} \left[\frac{\sum_{i=1}^{N_K} (\mathcal{M}(x_i) - \mathcal{M}_{(-i)}(x_i))^2}{Var[\mathcal{M}(\mathcal{X})]} \right] \quad (28)$$

with N_K the number of data points considered during Kriging and where $\mathcal{M}_{(-i)}(x_i)$ designates that the Kriging metamodel is obtained using all points of the experimental design except x_i and $\mathcal{M}(\mathcal{X})$ is the corresponding metamodel response of the initial experimental design [15,31].

The optimized value of each parameter based on the Kriging metamodel was found by the means of the normalized root mean squared error (NRMSE):

$$NRMSE_i = \frac{\sqrt{\frac{\sum_{j=1}^N (y_t - \hat{y}_j)^2}{N}}}{y_{max} - y_{min}} \quad (29)$$

with N the number of measurement points, y_t the (mean) experimental value at time t for output i at point j , i.e. either MDD or wt%, \hat{y}_j the Kriging metamodel response at point j , and y_{max} and y_{min} the maximum and minimum experimental values.

2.5. Sensitivity analysis of model parameters

In order to quantify the relative importance of each input parameter on the variability of the model output a global sensitivity analysis was performed. Global sensitivity analysis considers the inputs of the mathematical model as random variables and computes the relative importance of each parameter over the model output. In the metamodel we assumed that the model parameters were uniformly distributed. If all the input parameters for the sensitivity analysis are assumed independent and the parameter vector is given by $X_i = (k_{deg}, t_{init}, k_3, k_4, k_6, k_7, k_8, k_9)_i$ for $i \in \{1, \dots, P\}$, where P is the number of metamodel evaluations. X_u is a subset of metamodel inputs, i.e. $X_u = (X_{i1}, X_{i2}, \dots, X_{ik})$ for $u = \{i1, i2, \dots, ik\} \subset \{1, 2, \dots, P\}$ with corresponding outputs $\mathcal{M}(X_u)$. The metamodel results $\mathcal{M}(X)$ can be decomposed into contributions from each subset of input parameters according to the variance decomposition analysis

(ANOVA), with recursively defined contributions [34,35]

$$\mathcal{M}_u(X_u) = \sum_{v \subset u} (-1)^{|u|-|v|} \mathbb{E}[\mathcal{M}(X) | X_i, i \in v] \quad (30)$$

for $u \subset \{1, 2, \dots, P\}$

The Sobol' index for the corresponding subset u of metamodel runs was calculated as the variance of the subset over the total variance:

$$S_u = \frac{Var(\mathcal{M}_u(X_u))}{Var(\mathcal{M}(X))} \quad (31)$$

Consequently, the total Sobol' index for the entire set was calculated as:

$$S_k^T = \sum_{k \in u} S_u \quad \text{for } k = \{1, 2, \dots, P\} \quad (32)$$

In order to reduce the computational cost of the system, the sensitivity analysis was performed using the Kriging metamodels.

3. Results and discussion

3.1. Metamodel response

The visualization of the Kriging metamodel response at 28 days for different degradation rate constants (k_{deg}) is shown in Fig. 5. The y-axis is the MDD estimated by Kriging and the x-axis represents the different values of k_{deg} . The observation points are the true model response, i.e. the Comsol simulation output, where no Kriging estimation is done. The distribution over functions enables the Kriging metamodel to predict the mean degradation depth values at different time intervals and generate the confidence interval, which is important in systems with uncertain input parameters and parametric variability. The uncertainty in the model predictions is lower within the 95% confidence intervals, where the probability of finding the optimized value of the desired parameters is higher. Furthermore, large confidence intervals are related to systematic uncertainty, which indicates that assumptions underlying the physical model may need to be modified lateron [36].

The computational time of the Kriging metamodel was within the range of 6 - 12 second for each training matrix (25 test sets) for both MDD and wt% calculations. Within COMSOL, the average computational time for each training set of the same matrices is approximately 5–23 minutes. The

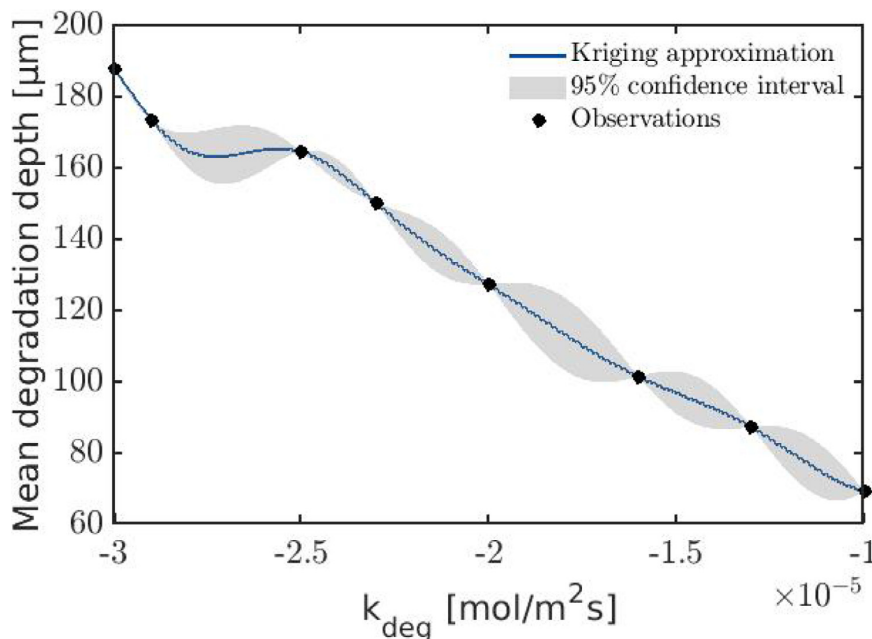


Fig. 5. The mean degradation depth estimated by the Kriging metamodel at different values of the degradation rate constant k_{deg} [$\text{mol}/\text{m}^2\text{s}$] at $t = 28$ days. The blue line presents the Kriging interpolation of the response at different values of k_{deg} , with 95% confidence intervals and no calculations at the observed points. The observations are the COMSOL model output. (For interpretation of the references to colour in this figure legend, the reader is referred to the web version of this article.)

reduction in the computational time didn't affect the accuracy of the system as can be seen in Table 4, which represents the optimized values for the model's parameters, with the input range and LOO error.

3.2. Calibrated degradation model

The mean degradation depth of the model is calculated using the optimized value of the degradation rate constant (k_{deg}), see Table 4, obtained based on the Kriging estimations. The simulation output in comparison to the experimental data is shown in Fig. 6a. The simulated MDD is in agreement with the experimental μCT imaging and weight loss data for 1–4 week with an overall NRMSE of 0.07. Detailed NRMSE values for each experimental data set can be found in Table B.5. The inset in Fig. 6a shows the confidence interval for MDD estimated by the Kriging model at approximately 14 days of degradation, which reflects the high certainty within the model predictions. The assumption of a linear degradation rate appears to approximate the degradation behaviour well, although it overestimates the degradation depth at earlier time points, both for datasets based on disc and wire degradation. Nevertheless, the variability of the experimental data is high at all time points, suggesting that a linear approximation is sufficient. Future experiments should aim at collecting additional long-term data to verify or refute this approach. At the current stage the model also does not differentiate between different levels of Mg purity, which influences the MDD. Future work should include the development of microgalvanic cells

for lower-purity Mg samples in SBF [20], e.g. by modelling the degradation of Mg using a non-linear law and adding an accelerating term dependent on the impurity level of the Mg in Eq. (19).

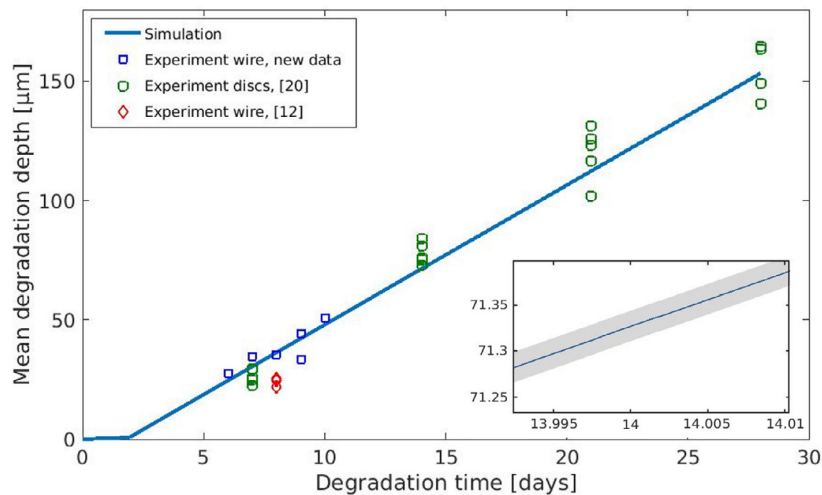
For comparison, we have computed the degradation rate for wires and discs respectively, based on the computed MDD, as shown in Fig. 6b. The results differ based on the specimen geometry, because the degradation rate is defined as

$$DR(t) = \frac{V(t) - V(0)}{A(0) \cdot t} [\text{mm}/\text{yr}] \quad (33)$$

and therefore depends both on the volume V and the surface area A of the sample, which are shape-dependent. In addition to the degradation of the pure Mg metal, the model estimated the mean elemental wt% of each element of the precipitated degradation products. The optimized values of the reaction rate constants of each of the precipitation reactions are given in Table 4.

Fig. 7 presents the solution of the model based on the optimized parameters for each element. The model response is found to fit the EDX measurements within the standard deviation of the experiments for Ca (NRMSE = 0.53), C (NRMSE = 0.59) and P (NRMSE = 0.40). For O (NRMSE = 0.99) and Mg (NRMSE = 1.03) the values differ more strongly. This could be due to the formation of other precipitates, which are not included in the current stage of the model, such as MgO or mixed $\text{Mg}_x\text{Ca}_y\text{-P}$ precipitates. Moreover, the difference in EDX measurements between different experimental conditions is larger than that for MDD. The 8-day measure-

(a) Mean degradation depth



(b) Degradation rate

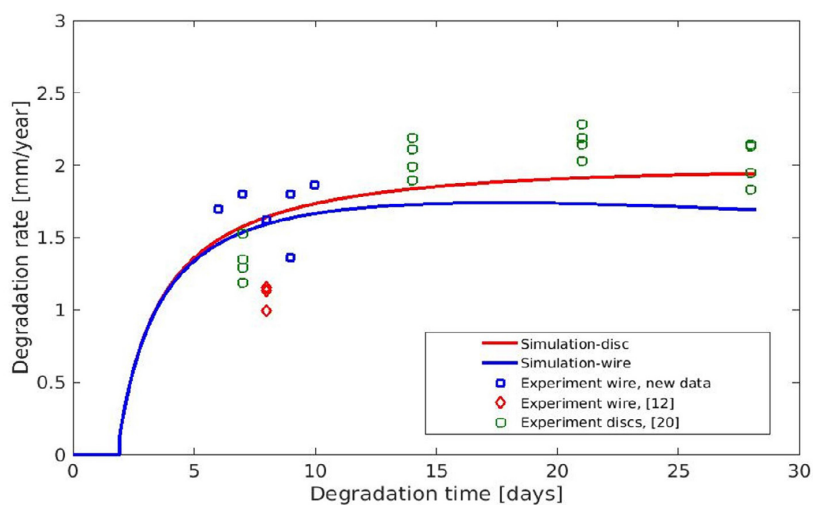


Fig. 6. The mean degradation depth (a) and corresponding degradation rate (b) calculated based on the simulation and experimental data obtained using μ CT. μ CT measurements were performed at 7, 14, 21 and 28 days [20], 8 days [12] and at 6, 7, 9 and 10 days (Appendix A). The sample geometry differed between wires and discs.

ment based on wire degradation differs strongly from that based on the degraded discs for 1–4 weeks. These differences may be due to different immersion volume to sample surface (VA) ratios in the experiments and other experimental uncertainties, such as the exact medium composition prepared by two different operators. Additionally, the current model has strongly simplified boundary conditions that do not take into account the change of the immersion medium every 2–4 days, as performed in the experiments. This simplification will be valid as long as the depletion of ions due to their precipitation during the degradation process is neglectable, which is

the case for high VA ratios and sufficiently frequent medium changes. Therefore, future models should entail a more detailed approach to integrate the experimental boundary conditions.

Finally, Fig. 8 shows the pH values determined in the liquid phase based on the OH^- concentration for different time points in comparison to experimental minimum and maximum values from [12]. A direct comparison with respect to time points is not sensible, due to the aforementioned discrepancy in boundary conditions. Nevertheless, the figure shows that the simulated pH is in the range of the experimental data.

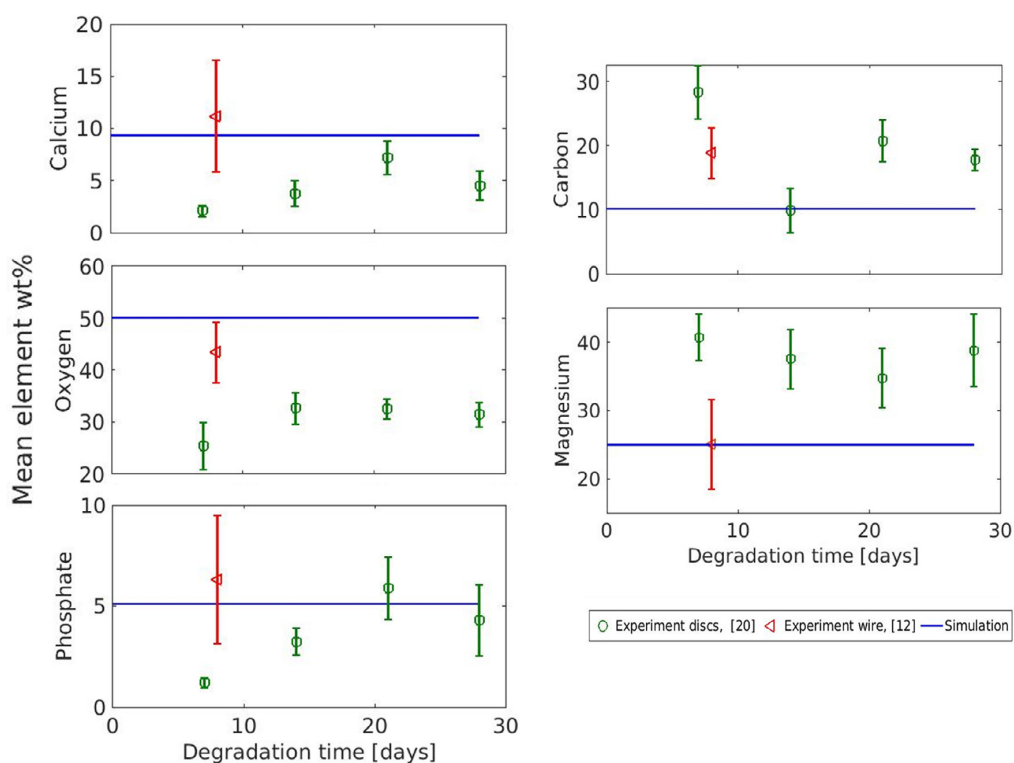


Fig. 7. The mean elemental weight percentage (wt%), calculated based on the simulation and measurements using energy-dispersive X-ray spectroscopy. EDX measurements were performed at 7,14,21 and 28 days [20] and 8 days [12].

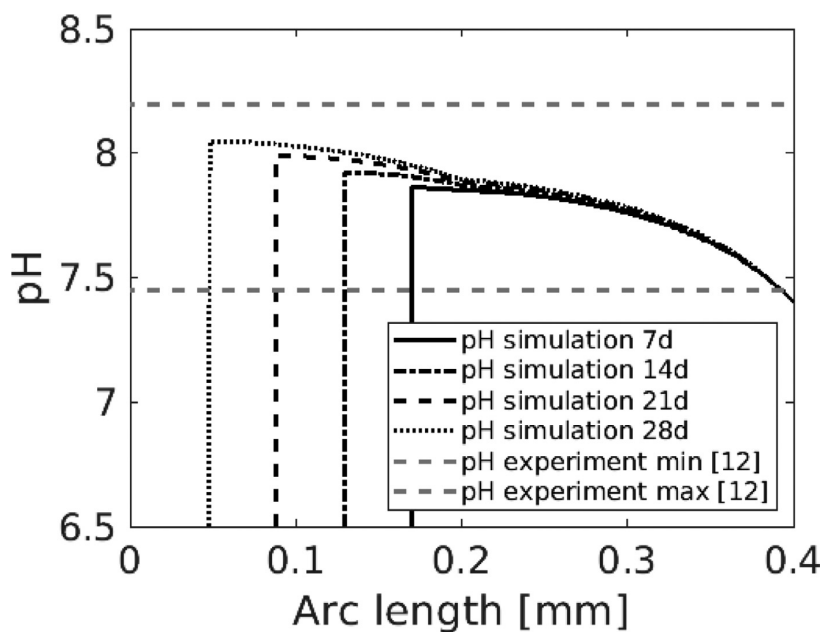


Fig. 8. pH value in liquid phase over the arc length of the domains determined by the simulation in comparison to experimental minimum and maximum data [12]. The simulated pH values are in the range of the experimental data. The sudden drop of the pH value is due to the liquid-metal interface, which moves over time.

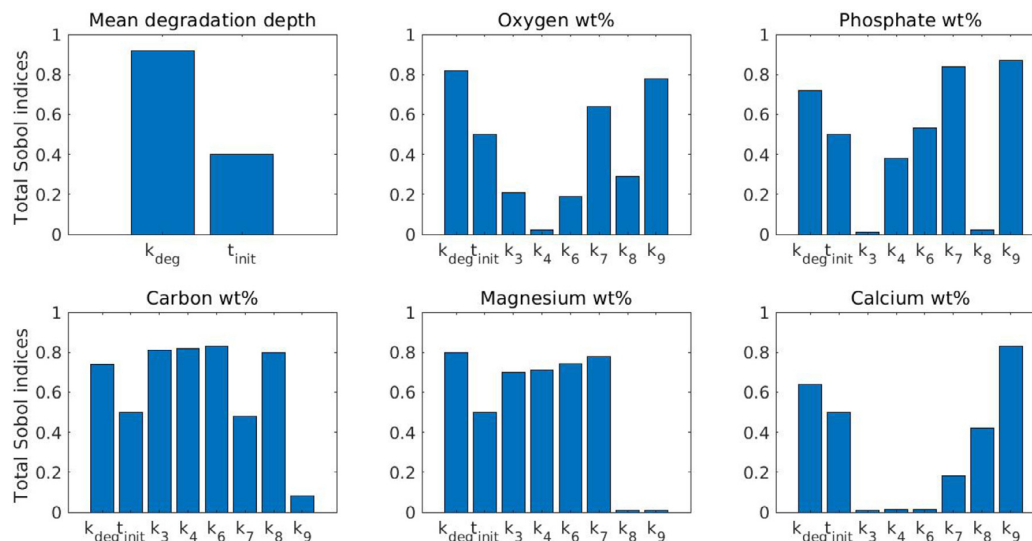


Fig. 9. Total Sobol indices of the calibrated model parameters calculated following the sensitivity analysis.

3.3. Sensitivity analysis of model parameters

Fig. 9 shows the global sensitivity analysis of each of the optimized parameters. The mean degradation depth is highly influenced by the degradation reaction rate constant (k_{deg}), while the sigmoid step initialization of the degradation (t_{init}) has only half the influence on the mean degradation depth. Due to numerical decoupling of the degradation model from the precipitation, the mean degradation depth only depends on these two parameters. By contrast, the salt precipitation is more complex. For example, the amount of precipitated carbon depends on all parameters that the model is calibrated for. Similarly, the amount of precipitated calcium depends not only on reaction rates k_6 and k_7 , which are directly related to Ca precipitation, but also on k_4 which models the formation of $Mg_3(PO_4)_2 \cdot 8H_2O(s)$, due to the competing reaction with phosphate ions for the formation of hydroxyapatite. The dependence of the elemental weight percentages on the reaction rates $k_{3,\dots,9}$ is highly correlated, therefore, the summation of the Sobol indices is higher than one [35,37]. The greater the correlation between parameters, the harder it will be to distinguish the influence of each individual parameter on the quantity of interest. As a result, a simplification of the precipitation reactions will be difficult.

Sensitivity analysis in general is an expensive approach that requires a large number of model runs under different conditions [35]. To overcome this problem, the total Sobol indices were calculated based on the Kriging metamodel, which reduced the computational cost of the sensitivity analysis to 40 - 60 seconds.

4. Conclusion

Overall, the presented model simulates the anodic dissolution related degradation process of pure Mg in SBF with an

error of 7%, which is similar to the experimental uncertainty. The model simulations provide the mean elemental wt% for each of the precipitated elements on the implant surface for the first time. This information is crucial to enable the prediction of the mechanical behaviour of the degraded specimen in the future. Furthermore, it will be of particular importance when modelling the interaction with cells who are sensitive to the implant surface mechanical properties. The presented model will be valid for Mg degradation in a medium with similar ionic composition in terms of the modelled precipitation and for solutions with a similar degradation profile. As the model has been calibrated for two shapes of Mg specimens with a purity between 99.92–99.95% it will be valid for pure Mg within this purity range. Thus, the degradation model presented needs to be enhanced in generality in the future by the formulation of a more general degradation reaction. The implementation of uncertainty quantification through the Kriging metamodel significantly reduced the computational load in the parameter estimation phase of the model and enhances the reliability of the model output. The performed sensitivity analysis reflected the correlation between the different parameters, which explains the complexity of the presented model. This was the case in particular for the salt formation on the sample surface.

Data availability

The datasets generated and analysed during the current study are available from the corresponding author on reasonable request.

Declaration of Competing Interest

The authors declare that they have no known competing financial interests or personal relationships that could have appeared to influence the work reported in this paper.

CRedit authorship contribution statement

Berit Zeller-Plumhoff: Conceptualization, Supervision, Writing – original draft. **Tamadur AlBaraghteh:** Formal analysis, Writing – original draft. **Daniel Höche:** Conceptualization, Writing – original draft. **Regine Willumeit-Römer:** Supervision, Writing – review & editing.

Acknowledgment

The authors TAB and BZP acknowledge funding from the Helmholtz-Incubator project Uncertainty Quantification. This research was supported in part through the Maxwell computational resources operated at Deutsches Elektronen-Synchrotron, Hamburg, Germany. We thank Dr. Julian Moosmann for his support at the P05 beamline and Helmholtz-Zentrum Hereon for providing beamtime. We thank Dr. Damar Wicaksono (HZDR) for the fruitful discussions regarding the UQLab software.

Appendix A. Determination of mean degradation depth for 6–10 days

Pure Mg (99.95%) wires with 1 mm diameter were degraded in SBF for 6–10 days. The degradation experiments were performed as described in [12,20]. Briefly, the wires were cut into rods of 2 cm length and cleaned and sterilized in a series of n-hexane, acetone, 100% ethanol and 70% ethanol in an ultrasonic bath. They were then laid into 12-well plates and immersed in 3 ml SBF solution. The well plates were stored in an incubator to ensure physiological conditions (5% CO₂, 37°C). The medium was changed every 3–4 days to avoid a saturation of ions. Following degradation, the wires were rinsed in double distilled water and ethanol and then dried. They were then imaged using μ CT at the P05 beamline at PETRA III, DESY, with a voxel size of 0.64 μ m or 1.28 μ m. The data was segmented and analysed as described in [12], and the mean degradation depth was then determined.

Appendix B. Model calibration errors per experiment data set

Table B.5 contains the detailed information on the NRMSE divided into the experiments and for the overall data.

Table B.5
NRMSE of the model output parameters w.r.t to the different experimental data sets and overall.

Calibration parameter	NRMSE w.r.t [20]	NRMSE w.r.t [12]	NRMSE w.r.t. unpublished wire data	overall NRMSE
MDD	0.08	3.52	0.13	0.07
Mg wt. %	2.19	24.98	-	1.03
C wt. %	1.28	0.193	-	0.59
O wt. %	2.77	2.55	-	0.99
Ca wt. %	1.03	1.87	-	0.53
P wt. %	0.48	1.22	-	0.40

References

- [1] A.H.M. Sanchez, B.J. Luthringer, F. Feyerabend, R. Willumeit, *Acta Biomater.* 13 (2015) 16–31, doi:10.1016/j.actbio.2014.11.048. URL: <https://www.sciencedirect.com/science/article/pii/S1742706114005510>.
- [2] M. Dahms, D. Höche, N. Ahmad Agha, F. Feyerabend, R. Willumeit-Römer, *Mater. Corros.* 69 (2) (2018) 191–196.
- [3] D. Gastaldi, V. Sassi, L. Petrini, M. Vedani, S. Trasatti, F. Migliavacca, *J. Mech. Behav. Biomed.Mater.* 4 (3) (2011) 352–365.
- [4] J. Grogan, B. O'Brien, S. Leen, P. McHugh, *Acta Biomater.* 7 (9) (2011) 3523–3533.
- [5] J.X. Jia, G. Song, A. Atrens, *Adv. Eng. Mater.* 9 (1–2) (2007) 65–74.
- [6] K.B. Deshpande, *Electrochim. Acta* 56 (4) (2011) 1737–1745.
- [7] J.A. Grogan, S.B. Leen, P.E. McHugh, *Acta Biomater.* 10 (5) (2014) 2313–2322.
- [8] W. Sun, G. Liu, L. Wang, Y. Li, *Electrochim. Acta* 78 (2012) 597–608.
- [9] P. Bajger, J. Ashbourn, V. Manhas, Y. Guyot, K. Lietaert, L. Geris, *Biomech. Model. Mechanobiol.* 16 (1) (2017) 227–238.
- [10] J. Sanz-Herrera, E. Reina-Romo, A. Boccacini, *Journal of the mechanical behavior of biomedical materials* 79 (2018) 181–188.
- [11] S.K. Ahmed, J.P. Ward, Y. Liu, *Materials* 11 (1) (2018) 1.
- [12] B. Zeller-Plumhoff, M. Gile, M. Priebe, H. Slominska, B. Boll, B. Wiese, T. Würger, R. Willumeit-Römer, R.H. Meißner, *Corros. Sci.* 182 (2021) 109272, doi:10.1016/j.corsci.2021.109272. URL: <https://www.sciencedirect.com/science/article/pii/S0010938X2100038X>.
- [13] M. Kieke, F. Feyerabend, J. Lemaitre, P. Behrens, R. Willumeit-Römer, *BioNanoMaterials* 17 (3–4) (2016) 131–143, doi:10.1515/bnm-2015-0020.
- [14] D. Höche, *J. Electrochem. Soc.* 162 (1) (2015) C1–C11, doi:10.1149/2.0071501jes.
- [15] L. Zhao, K. Choi, I. Lee, *AIAA J.* 49 (9) (2011) 2034–2046.
- [16] M. Bohner, J. Lemaitre, *Biomaterials* 30 (12) (2009) 2175–2179, doi:10.1016/j.biomaterials.2009.01.008.
- [17] C. Wang, D. Mei, G. Wiese, L. Wang, M. Deng, S.V. Lamaka, M.L. Zheludkevich, *npj Mater. Degrad.* 4 (1) (2020) 1–5, doi:10.1038/s41529-020-00146-1.
- [18] N. Wint, N. Cooze, J. Searle, J. Sullivan, G. Williams, H. McMurray, G. Luckeneder, C. Riener, *Corrosion of model Zn-Al-Mg alloy coatings on steel*
- [19] I. Puigdomenech, *Chemical Equilibrium Diagrams*, 2020, URL: <https://www.kth.se/che/medusa/chemeq-1.369367>.
- [20] B. Zeller-Plumhoff, et al., *Bioactive.Mater.* (2021). accepted at <https://doi.org/10.1016/j.bioactmat.2021.04.009>.
- [21] B. Zeller-Plumhoff, H. Helmholtz, F. Feyerabend, T. Dose, F. Wilde, A. Hipp, F. Beckmann, R. Willumeit-Römer, J.U. Hammel, *Mater. Corros.* 69 (3) (2018) 298–306, doi:10.1002/maco.201709514.
- [22] C. Ma, D. Xu, H. Yang, Z. Zhong, Z. Lu, *Corrosion Degradation Behavior of Forged Mg-Zn-Zr-Y Alloy in Simulated Body Fluid*, in: *Journal of Physics: Conference Series*, volume 1676, IOP Publishing Ltd, 2020, p. 12018, doi:10.1088/1742-6596/1676/1/012018.
- [23] O. Guseva, J. DeRose, P. Schmutz, *Electrochim. Acta* 88 (2013) 821–831.
- [24] F. Thébault, B. Vuillemin, R. Oltra, C. Allely, K. Ogle, *Electrochim. Acta* 82 (2012) 349–355.
- [25] D.R. Lide, *CRC Handbook of Chemistry and Physics* volume 85, CRC Press, 2004.
- [26] E.L. Cussler, E.L. Cussler, *Diffusion: Mass Transfer in Fluid Systems*, Cambridge University press, 2009.
- [27] A.C. Arulrajana, C. Renault, S.C. Lai, *Phys. Chem. Chem. Phys.* 20 (17) (2018) 11787–11793.
- [28] J.-F. Yan, T. Nguyen, R.E. White, R. Griffin, *Journal of the Electrochemical Society* 140 (3) (1993) 733.
- [29] E.P.S. Nidadavolu, F. Feyerabend, T. Ebel, R. Willumeit-Römer, M. Dahms, *Materials* 9 (8) (2016) 627.
- [30] T.J. Santner, B.J. Williams, W.I. Notz, B.J. Williams, *The Design and Analysis of Computer Experiments* volume 1, Springer, 2003.

B. Zeller-Plumhoff, T. AlBaraghtheh, D. Höche et al.

Journal of Magnesium and Alloys 10 (2022) 965–978

- [31] C. Lataniotis, D. Wicaksono, S. Marelli, B. Sudret, UQLab User Manual – Kriging (Gaussian process modeling), Technical Report, Chair of Risk, Safety and Uncertainty Quantification, ETH Zurich, Switzerland, 2019. Report n# UQLab-V1.3–105.
- [32] S. Marelli, B. Sudret, Uqlab: a framework for uncertainty quantification in Matlab, in: *Vulnerability, uncertainty, and risk: quantification, mitigation, and management*, 2014, pp. 2554–2563.
- [33] Z. Wang, A. Shafieezadeh, *Reliabil. Eng. Syst. Saf.* 182 (2019) 33–45.
- [34] R. Ghanem, D. Higdon, H. Owhadi, *Handbook of Uncertainty Quantification* volume 6, Springer, 2017.
- [35] J. Hart, P.A. Gremaud, *Int. J. Uncertain. Quantif.* 8 (6) (2018).
- [36] C.J. Roy, W.L. Oberkampf, *Computer methods in applied mechanics and engineering* 200 (25–28) (2011) 2131–2144.
- [37] G. Chastaing, F. Gamboa, C. Prieur, *J. Stat. Comput. Simul.* 85 (7) (2015) 1306–1333.

Utilizing computational modelling to bridge the gap between *in Vivo* and *in Vitro* degradation rates for Mg-xGd implants

The ability of surrogate models to map the biodegradation behavior of Mg-based implants, based on complex and computationally expensive computer models, without compromising accuracy while reducing computational cost and time, enables us to expand the parametric space of the 3D peridynamic model derived in [64]. This expansion allows prediction of the *in vivo* biodegradation of Mg-xGd implants. By relying on the similarity of the diffusion process of Mg^{2+} -ions in both biodegradation systems, it is possible to map the biodegradation between *in vitro* and *in vivo* depending on the diffusion rates of Mg^{2+} -ions in both biodegradation systems. The constructed Kriging models are calibrated to volume loss experimental datasets from *in vitro* and *in vivo* biodegradation of Mg-xGd screws. Moreover, based on these findings, Kriging models simulate the *in vivo* biodegradation of Mg-xGd with time-independent ratios of diffusion rates of Mg^{2+} -ions between 0.46 and 0.5, with MAE values between 0.31 and 0.44, respectively. Using these findings, in the future, it may become possible to estimate biodegradation rates *in vivo* by leveraging such links between diffusion rates derived from *in vitro* and *in vivo* experiments through surrogate models, in this manner, it will be possible to determine the rate of biodegradation of *in vivo* biodegradation rates solely based on *in vitro* experiments.

Publication details

(invited) Tamadur AlBaraghteh, Alexander Hermann, Arman Shojaei, Regine Willumeit-Römer, Christian J. Cyron, Berit Zeller-Plumhoff, (2023). Utilizing computational modelling to bridge the gap between *in vivo* and *in vitro* degradation rates for Mg-xGd implant. *Corros. Mater. Degrad.*, 4(2), 274-283. <https://doi.org/10.3390/cmd4020014>.

Author's contribution

The author contributed to methodology, software, formal analysis, writing, editing and original draft preparation.

Copyright Notice

©This is an accepted version of the article originally published in the Journal of Corrosion and Materials Degradation. The paper has been published under Creative Commons CC-BY 4.0 Licence. The copyright has been clarified in line with the publisher's guidelines.

Article

Utilizing Computational Modelling to Bridge the Gap between In Vivo and In Vitro Degradation Rates for Mg-xGd Implants

Tamadur Al Baraghteh ^{1,*}, Alexander Hermann ², Arman Shojaei ², Regine Willumeit-Römer ¹, Christian J. Cyron ^{2,3} and Berit Zeller-Plumhoff ¹ 

¹ Institute of Metallic Biomaterials, Helmholtz-Zentrum Hereon, Max-Planck-Str. 1, 21502 Geesthacht, Germany; berit.zeller-plumhoff@hereon.de (B.Z.-P.)

² Institute of Material Systems Modeling, Helmholtz-Zentrum Hereon, Max-Planck-Str. 1, 21502 Geesthacht, Germany

³ Institute for Continuum and Material Mechanics, Hamburg University of Technology, Eissendorfer Str. 42, 21073 Hamburg, Germany

* Correspondence: tamadur.albaraghteh@hereon.de

Abstract: Magnesium (Mg) and its alloys are promising materials for temporary bone implants due to their mechanical properties and biocompatibility. The most challenging aspect of Mg-based implants involves adapting the degradation rate to the human body, which requires extensive in vitro and in vivo testing. Given that in vivo tests are significantly more labour-intensive than in vitro and ethics prohibit direct experiments on animals or humans, attempts are commonly undertaken to infer conclusions on in vivo degradation behavior from in vitro experiments. However, there is a wide gap between these tests, and in vitro testing is often a poor predictor of in vivo outcomes. In the development of biodegradable Mg-based implants, considerable efforts are being made to reduce the overall time and cost of in vitro and in vivo testing. Finding a suitable alternative to predict the degradation of Mg alloys, however, remains challenging. We present computational modelling as a possible alternative to bridge the gap between in vitro and in vivo testing, thus reducing overall cost, duration and number of experiments. However, traditional modelling approaches for complex biodegradable systems are still rather time-consuming and require a clear definition of the relations between input parameters and the model result. In this study, Kriging surrogate models based on the peridynamic in vitro degradation model were developed to simulate the degradation behavior for two main alloys, Mg-5Gd and Mg-10Gd, for both in vitro and in vivo cases. Using Kriging surrogate models, the simulation parameters were calibrated to the volume loss data from in vitro and in vivo experiments. In vivo degradation of magnesium has one order of magnitude higher apparent diffusion coefficients than in vitro degradation, thus yielding the higher volume loss observed in vivo than in vitro. On the basis of the diffusivity of the Mg²⁺ ions modeled under in vitro degradation, Kriging surrogate models were able to simulate the in vivo degradation behavior of Mg-xGd with a ratio between 0.46 and 0.5, indicating that the surrogate-modelling approach is able to bridge the gap between in vitro and in vivo degradation rates for Mg-xGd implants.

Keywords: degradable magnesium; in vitro; in vivo; surrogate modelling; peridynamics; Kriging



Citation: Al Baraghteh, T.; Hermann, A.; Shojaei, A.; Willumeit-Römer, R.; Cyron, C.J.; Zeller-Plumhoff, B. Utilizing Computational Modelling to Bridge the Gap between In Vivo and In Vitro Degradation Rates for Mg-xGd Implants. *Corros. Mater. Degrad.* **2023**, *4*, 274–283. <https://doi.org/10.3390/cmd4020014>

Academic Editor: Daniel John Blackwood

Received: 30 September 2022

Revised: 28 February 2023

Accepted: 24 March 2023

Published: 31 March 2023



Copyright: © 2023 by the authors. Licensee MDPI, Basel, Switzerland. This article is an open access article distributed under the terms and conditions of the Creative Commons Attribution (CC BY) license (<https://creativecommons.org/licenses/by/4.0/>).

1. Introduction

Magnesium (Mg) and its alloys are under increasing investigation as temporary implant materials due to their non-toxicity, biocompatibility, and biodegradability properties [1,2]. In vitro and in vivo experiments are designed and conducted to study the degradation of Mg-based alloys in both cell culture media and animal models [3–6]. In the course of those studies, a substantial amount of experimentation is required to investigate the degradation rate of such implants in order to subsequently adapt them to be suitable for the human body. The analysis of several studies published in the field reflect the presence of a large gap between the predictions of in vitro and in vivo studies even for identical

degradation systems. The sensitivity of biodegradable systems to environmental conditions and their complexity have also contributed to this gap [5–11]. A detailed comparison of several published studies was conducted by Sanchez et al. in 2015 [7] to examine whether it is possible to correlate the *in vitro* and *in vivo* degradation behavior of Mg and Mg-based alloys. As a result, the study concluded that a clear correlation could not be established. This poor correlation between *in vitro* and *in vivo* degradation behavior remains a challenge until today, hence extensive studies are still required for the development of biodegradable Mg-based implants. Unfortunately, due to the expensive and time-consuming nature of such investigations, as well as ethical implications when considering animal experiments, an alternate strategy to comprehensive experimental trials is required. Computational modelling evolves as a powerful instrument for resolving this problem.

Mathematical modelling of biodegradable implant materials is a comparatively novel tool aimed at improving the understanding and prediction of degradation processes. In the respective literature, various mathematical models have been proposed to model certain aspects of the biodegradation process of Mg-based implants [12–17]. A more in-depth examination of the various modeling approaches and models of Mg-based implants in *in vivo* and *in vitro* environments may be found in recent reviews [18–21]. Due to the complexity of the system and its multiphysics nature, the available models are often limited and calibrated to specific *in vitro* or *in vivo* study systems only. Few comparisons between both environments have been made. For example, the model presented by Sanz-Herrera [22] provided qualitative measurements of the degradation of the Mg screw alloy (Mg-Zn-Zr) *in vitro* and implanted in a Japanese rabbit. The authors found a four-fold higher corrosion kinetics *in vivo* than *in vitro*. However, the modelling of *in vivo* degradation was limited to a 2D axisymmetric geometry.

A peridynamic model was recently developed to simulate the *in vitro* volume loss of Mg-5Gd and Mg-10Gd bone implant screws (in wt.%) in complex cell culture media [14]. Whereas in classical degradation modelling, e.g., by means of the Finite-Element-Method (FEM), additional effort is required to capture the evolution of the corrosion surface over the duration of simulated immersion [23], the corrosion model obtained from the nonlocal theory of peridynamics proposes a formulation using integro-differential equations, thus resulting in the evolution of the corrosion interface as a natural component of the solution of the governing equations [16,24]. In recent years, these models were extended to address several corrosion phenomena, e.g., passivation, salt layer formation, intergranular corrosion, stress-assisted corrosion, stress corrosion cracking and galvanic corrosion [25–29]. Using a peridynamic formulation, in [14] the degradation was modelled as a diffusive process depending on the diffusion of metal ions from the metal phase across a diffusive degradation layer into the surrounding medium. The model was demonstrated to accurately simulate the volume loss of the Mg-based implants in 3D and in turn served as input for the subsequent FEM model to predict the residual strength of the degraded implant. Considering that the peridynamic degradation model is diffusion-driven, by calibrating the model diffusivity parameters to both *in vitro* and *in vivo* data, it may be possible to elucidate correlations between the observed degradation behaviour. However, peridynamic models are relatively complex and computationally expensive. For such computation-intensive models, surrogate modelling has become an increasingly popular approach, introducing mathematical models that are more compact and faster to evaluate without compromising the accuracy of the original models.

Several techniques have been proposed to construct surrogate models using a minimum number of original model simulations [30–33]. Kriging, also known as Gaussian process modelling, has become a popular surrogate modeling technique in recent years, due to its accuracy and simplified mathematical construction. The quality of Kriging surrogate model predictions, however, is heavily influenced by the size and distribution of the input parameters as well as the original model response used to construct the surrogate model [34–37]. Recently, Zeller-Plumhoff and Albaraghteh et al. [12] implemented Kriging to calibrate and optimize the key parameters of a complex physical degradation model

of pure Mg under physiological conditions. The calibrated model was able to simulate the degradation with an accuracy of 7%, which is equal to the experimental error. Furthermore, the measured normalized root-mean-square deviation (NRMSE) of the simulated mean elemental weight percentage of precipitated salts reflected an acceptable agreement with the experimental data used in the calibration.

In this study, Kriging surrogate degradation models were developed based on in vitro peridynamic models that simulate the degradation of Mg-5Gd and Mg-10Gd bone implant screws. The optimized surrogate models were extended further to simulate the diffusion behavior of the aforementioned implants in vivo. The key model parameters describing the diffusion of Mg^{2+} ions within the electrolyte and the porous degradation layer forming on the metal surface were calibrated to in vitro and in vivo experiments thus providing the possibility to compare the diffusive behaviour with respect to the observed volume loss and degradation rates for both cases and alloys.

2. Materials and Methods

2.1. Model Calibration Data

The experimental data used for the calibration of the simulations were obtained by evaluating the relative volume loss (VL in %) of two magnesium gadolinium alloys, Mg-5 wt.%Gd and Mg-10 wt.%Gd screw implants (4 mm length, 2 mm diameter, M2 thread with 0.5×0.5 mm slotted screw head) in in vitro and in vivo tests. Details regarding the implant manufacturing and testing were published in [8,38]. In summary, in all cases, non-degraded screws were imaged using micro computed tomography (μ CT) to obtain their initial geometry. For the in vitro testing the screws were immersed in complex cell culture medium (α -Minimum Essential Medium or Dulbecco's Modified Eagle's Medium supplemented with 10% Fetal Bovine Serum and 1% Penicillin/Streptomycin) for 1, 2, 3, 4 and 8 weeks under cell culture conditions (37 °C, 5% CO_2 , 20% O_2 , and 95% rel. humidity). The immersion medium was changed every 2–4 days to avoid saturation of the medium with ions. To obtain the geometry after degradation the degradation layer was removed using chromic acid and the implants were again measured using μ CT. For details concerning methods, such as imaging parameters, see [38]. In vivo tests were carried out by implanting the screws into rat tibia with healing durations of 4, 8 and 12 weeks. Again, μ CT imaging, in this case synchrotron radiation-based, was used to study the morphology of the degraded screws. The experimental details can be found in [8]. Importantly, the data provided by (synchrotron radiation-based) μ CT yields highly resolved information on the screw morphology and can be used to determine the volume loss of the implants [39].

The volume loss [%] for Mg-xGd is calculated as

$$VL(t) = \frac{V(0) - V(t)}{V(0)} \cdot 100\%, \quad (1)$$

where $V(0)$ and $V(t)$ are the volume of residual metallic material before and after the degradation tests, respectively, as determined from μ CT images. The degradation rate (DR) [mm/yr] is calculated based on the volume loss as

$$DR(t) = \frac{V(0) - V(t)}{A(0) \cdot t}, \quad (2)$$

where $A(0)$ is the initial surface area of the sample and t is the degradation time.

2.2. Peridynamic Model and Implementation

In the present study, the peridynamic degradation model from [14] was employed to simulate the degradation behavior of Mg-based implant screws. Given that computational modelling of the electrochemical degradation processes associated with Mg-based alloys is generally very challenging, we adopt a bi-material solid-liquid interface description to efficiently capture the electrochemically driven dissolution and surface evolution. Con-

sidering a generic domain $\Omega \in \mathbb{R}^{n_d}$, where $n_d \equiv 3$ is the spatial dimension, the governing equation of the bi-material peridynamic degradation model is given by

$$\dot{C}(\mathbf{x}, t) - \int_{\mathcal{H}_x} c(t) \frac{C(\mathbf{x}', t) - C(\mathbf{x}, t)}{\|\mathbf{x}' - \mathbf{x}\|^{n_d - 2p}} dV_{\mathbf{x}'} = 0, \quad \mathbf{x} \in \Omega, \quad t > 0, \quad (3)$$

where $C(\mathbf{x}, t)$ is the (molar) concentration of the Mg-based alloy material associated with point \mathbf{x} at time t , \mathcal{H} is the spherical integration region or neighborhood with radius δ called horizon, $p \in (-1, \infty)$ is a scalar value assumed as $p \equiv 0$ and $c(t)$ is the proportionality coefficient called micro-diffusivity. The latter is a model parameter that depends on the regions (solid or liquid) in which the interacting points \mathbf{x}' and \mathbf{x} are located within the neighbourhood:

$$c(t) = \begin{cases} \frac{3\chi_s^2}{\pi\delta^2} 10^{\left(-\frac{V_L(t)}{l}\right)}, & \mathbf{x}' \text{ or } \mathbf{x} \text{ in solid part} \\ \frac{3\chi_l^2}{\pi\delta^2}, & \mathbf{x}' \text{ and } \mathbf{x} \text{ in liquid part,} \end{cases} \quad (4)$$

where χ_s^2 and χ_l^2 are the diffusivities of the classical local Fickian diffusion equation within the solid and liquid domains, respectively, $V_L(t)$ is the volume loss at time t of the Mg-based implant screw and $l > 0$ is an analytical non-negative model parameter, which represents the depth of the growing degradation layer and therefore leads to a dampening of the degradation with increasing values [40]. The values for l were found to be 1/4.25 and 1/15.53 for Mg-5Gd and Mg-10Gd, respectively. For the numerical implementation of (3) we employ the standard one-point Gaussian integration scheme and an adaptive multi-grid discretization method in space and an implicit Euler time-stepping algorithm [14,41]. The in-house high performance computing (HPC) cluster was utilized to perform the simulation on a computational node, that consists of two sockets, each with a 24-core 2.1 GHz Intel Xeon Scalable Platinum 8160 processor, thus providing a shared memory multiprocessing parallelism on 48 cores.

2.3. Kriging-Based Surrogate Model and Implementation

The implementation of Kriging techniques to construct a surrogate model for studying the degradation of Mg-based implants is described in detail in an earlier publication of ours [12]. In brief, the peridynamic degradation model is treated as a black-box and the Kriging-based surrogate model is built using a data-driven approach, as illustrated by the schematic diagram in Figure 1. The training data for the Kriging model are sampled from the input distribution in the parametric space of the input parameters. The sampled parameter combinations are evaluated using the expensive computational model (black-box) and the resulting observations are exploited to build the surrogate model on the whole domain of the input distribution.

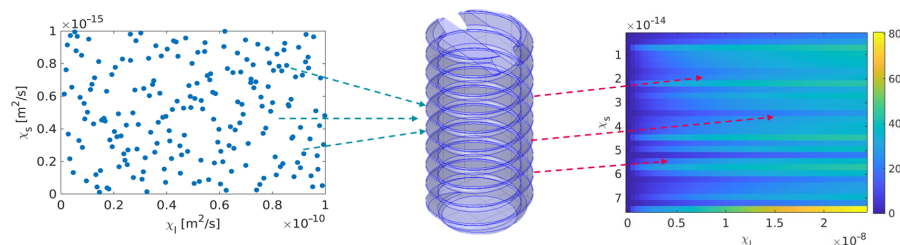


Figure 1. Schematic diagram of the construction of surrogate models.

The Latin hypercube sampling (LHS) method is used to draw thirty different sets of samples based on the assumed parameter distribution of the input parameters (χ_s^2 and χ_l^2) over a user-defined parametric space, similar to the sampling domain shown in Figure 2.

The sampling of the input variables ranges should be representative and capture all possible information about the original peridynamic model [42,43]. Due to the fact that the size and distribution of data points used in the numerical experiments have a major impact on the quality of surrogate model predictions [34,36]. In this case, the parametric space was extended from the range of optimized parameters proposed in [14].

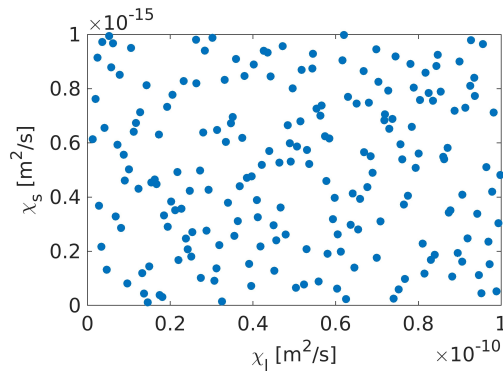


Figure 2. The sampling domain of χ_s^2 and χ_l^2 generated using the LHS technique.

The training data, also known as numerical experiment design (ED) $\{\mathcal{X}, \mathcal{Y}\}$, is generated by evaluating the peridynamic model output $\mathcal{Y} = [y_1, y_2, \dots, y_N]^T$ for N generated sample points of the input parameter vector $\mathcal{X} = [\chi_s^2, \chi_l^2]^T$, where \mathcal{Y} is the quantity of interest (QoI) simulated by the surrogate model, which for the model at hand is the volume loss VL of Mg-5Gd and Mg-10Gd implants. The general mathematical presentation of the surrogate model simulating the degradation of Mg-xGd implants is

$$\mathcal{M}(x) = \beta^T f(x) + \sigma^2 Z(x, \omega), \quad (5)$$

\mathcal{M} is the Kriging mapping function, which is the realization of the Gaussian process, that is used to calculate the volume loss \mathcal{Y} for any input parameter vector \mathcal{X} for a finite period of time. $\beta^T f(x)$ is the trend of the Kriging, which is the mean value of the Gaussian process, $\sigma^2 Z(x, \omega)$ is the realization of the stochastic process that is assumed to have a zero-mean, unit-variance $Z(x, \omega)$, where σ is the variance of the process and ω is the underlying probability space, which is defined in terms of the correlation function of the stochastic process $R(x, x', \theta)$ [44]. The performance of the Kriging-based surrogate model based on the training simulation data generated from the peridynamic model is estimated by the leave-out-error (ϵ_{LOO}), which is defined as

$$\epsilon_{LOO} = \frac{1}{N_e} \left[\frac{\sum_{i=1}^{N_e} (\mathcal{M}(x_i) - \mathcal{M}_{(-i)}(x_i))^2}{Var[\mathcal{M}(\mathcal{X})]} \right], \quad (6)$$

where N_e is the number of data points considered during Kriging, $\mathcal{M}_{(-i)}(x_i)$ designates that the Kriging surrogate model is obtained using all points of the numerical experimental design except x_i and $\mathcal{M}(\mathcal{X})$ is the corresponding surrogate model response of the initial numerical experimental design generated using the original model [44]. The generated Kriging-based surrogate model is calibrated based on the experimental data of both in vitro and in vivo degradation tests of Mg-xGd biodegradable implants. The calibration process was performed by dividing the model domain into equal intervals and then re-sampling each of the intervals using LHS. Intervals with higher uncertainty were further divided and sampled. The goodness of the calibration was measured by the means of the mean absolute error (MAE), which is calculated via

$$MAE = \frac{\sum_{j=1}^N |y_t - \hat{y}_j|}{N}, \quad (7)$$

with N the number of measurement points, y_t the (mean) experimental value at time t for the volume loss at point j , \hat{y}_j the Kriging surrogate model response at point j . The Kriging-based surrogate model is implemented using the Kriging module within the UQLab framework [45], which is installed and integrated under BSD 3-clause license in MATLAB 2021b (The MathWorks, Inc., Natick, MA, USA).

3. Results and Discussion

Surrogate models were trained to predict the volume loss based on the computational experimental design (ED), which was collected from random samples of the target parameters using LHS. The ranges for the input parameters were set similarly to the ranges assumed during the parameter optimization for the PD models. Thus, the ranges were assumed between 1×10^{-17} m²/s to 1×10^{-12} m²/s and 1×10^{-12} m²/s to 1×10^{-7} m²/s for χ_s^2 and χ_l^2 , respectively.

The developed surrogate models can capture the QoI for both implant alloys, Mg-5Gd and Mg-10Gd, for in vitro degradation sufficiently well, as can be inferred from the performance of the surrogate model with respect to the peridynamic model shown in Figure 3. It should be noted that the response of the PD model for the in vivo case was assessed based on pure numerical findings of the PD model, the ranges of the numerical test were confirmed based on the experimental data from [38]. The error of the surrogate models, represented by ε_{LOO} was between 2.1×10^{-3} and 5.5×10^{-3} for Mg-5Gd and 1.7×10^{-3} and 3.1×10^{-3} for Mg-10Gd. Furthermore, the Kriging surrogate model reduces the computational time required to run the training matrix, which contains the training sets of parameters, down to 23.6 s in order to simulate the entire domain over the respective simulated immersion time compared to approximately 3 h for the peridynamic model with the same set of parameters.

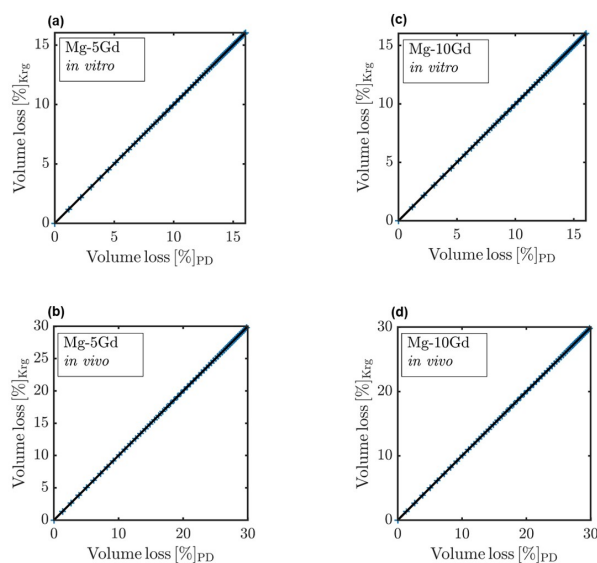


Figure 3. Comparison between the QoI (VL) computed by the PD model and corresponding Kriging surrogate models predictions (a) Mg-5Gd in vitro, (b) Mg-5Gd in vivo. (c) Mg-10Gd in vitro and (d) Mg-10Gd in vivo.

Generally, surrogate models have a wider range of applications due to their ability for mapping the response domain with respect to the full input distribution. The model key parameters χ_s^2 [m²/s] and χ_l^2 [m²/s] were calibrated and optimized using the predictions of the surrogate model and later the model response was validated against VL determined from μ CT measurements obtained for in vitro degradation [38] and for in vivo degradation [8]. The optimized values of χ_s^2 and χ_l^2 for Mg-5Gd and Mg-10Gd for both in vitro and

in vivo cases are given in Table 1. The PD model responses were collected over 56 days (8 weeks), so the Kriging models of the in vitro case were initially trained and calibrated over 56 days. Surrogate model responses were numerically extrapolated to 100 days in order to capture the time points from in vivo experiments. The diffusivity of Mg^{2+} ions was found to be one order of magnitude higher in the in vivo case with respect to in vitro, which is expected based on the reported degradation behaviour of the current implants by [8,38].

Table 1. The optimized parameters of in vitro and in vivo measured via the Kriging-based surrogate models and the MAE with respect to the experimental data.

	In Vitro		In Vivo	
	Mg-5Gd	Mg-10Gd	Mg-5Gd	Mg-10Gd
χ_S^2 [m^2/s]	2.9×10^{-15}	1.78×10^{-15}	7.8×10^{-14}	9.6×10^{-14}
χ_I^2 [m^2/s]	8.7×10^{-9}	1.44×10^{-9}	5.4×10^{-8}	8.4×10^{-8}
MAE	0.03	0.08	0.31	0.44

The visualization of the calibrated surrogate models' responses in comparison to the experimental data for 100 days of degradation for Mg-5Gd and Mg-10Gd implants for both in vitro and in vivo are shown in Figure 4a. For the in vitro degradation the simulated VL are in agreement with VL determined from μ CT measurements (scatter plots in Figure 4a,b [38], with MAE of 0.03 for Mg-5Gd and 0.08 Mg-10Gd. The same observation is also valid for the simulated in vivo VL, where the simulated values agree with VL determined from μ CT measurements [8] (scatter plots in Figure 4a,b), with MAE values of 0.31 and 0.44 for Mg-5Gd and Mg-10Gd, respectively. The accuracy of the calibration process of the key parameters of the surrogate models was slightly compromised by the uncertainties associated with the experimental data. The relatively high standard deviation of the experimental measurements, as can be seen in Figure 4a, was one of the main challenges of the calibration process. There were also limitations in the number of available data, i.e., the in vitro degradation was limited to five time points between one week and eight weeks, while the in vivo degradation was limited to three time points: four, eight, and twelve weeks. The calibration process would be improved by including more degradation time points, which would also reduce numerical overfitting and underfitting. In addition, it is important to increase the number of samples at each point in order to maintain lower standard errors.

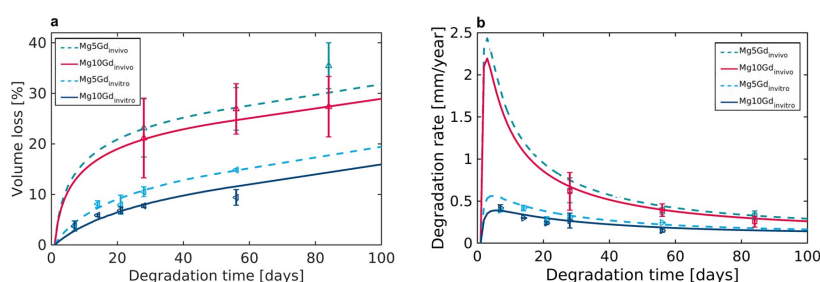


Figure 4. (a) Experimental (single data points displaying mean \pm standard deviation) and Kriging-based surrogate model simulations of volume loss of in vitro and in vivo for Mg-5Gd and Mg-10Gd, respectively. (b) The degradation rate calculated based on the volume loss. The VL was determined from μ CT measurements as published in [8,38].

In general, based on in vitro surrogate models for the same implants, the current approach of surrogate modeling provided an opportunity to model the in vivo degradation behaviour of Mg-5Gd and Mg-10Gd. It has also been shown that the surrogate models are capable of simulating the degradation of Mg-xGd implants for over 100 days, for both in vitro and in vivo degradation; however, further experiments are needed to validate

the results. For comparison the degradation rates (DR) of Mg-5Gd and Mg-10Gd were calculated in both in vitro and in vivo systems, Figure 4b. The surrogate model-based DR were found to follow the experimental data for both the cases.

As the simulation results for the DR suggest, calculating a ratio between DR for in vitro and in vivo as performed by [7] will yield different values, depending on the degradation time. By contrast, using computational modelling, it is possible to derive a time-independent ratio between the DR based on the diffusivity of the Mg^{2+} ions. For Mg-5Gd, the mean ratio of χ_s^2 and χ_l^2 between in vitro and in vivo experiments was calculated as 0.5, while for Mg-10Gd the mean ratio was calculated as 0.46. By establishing such ratios for different material systems, it will be possible to predict the degradation behaviour in vivo based on that observed in vitro in the future, thus reducing the effort required by performing a large number of experiments.

4. Conclusions

In this study, Kriging surrogate models were developed to simulate degradation behavior as a function of Mg^{2+} ion diffusivity. Peridynamic in vitro degradation models were used to generate observations in order to construct Kriging surrogate models. These models were shown to simulate the in vitro degradation behaviour of Mg-5Gd and Mg-10Gd implants with MAE-values of 0.03 and 0.08, respectively. The Kriging surrogate models with optimized key parameters, χ_s^2 and χ_l^2 , were able to simulate in vivo degradation behavior for Mg-5Gd and Mg-10Gd at MAE values of 0.31 and 0.44, respectively. Additionally, the computational approach employed was able to significantly reduce the computational time and cost as compared to the original peridynamic degradation model. More importantly, the proposed approach provided time-independent ratios based on the variation in Mg^{2+} ion diffusivities within the degradation system. Using the time-independent ratios established between in vitro and in vivo experiments by means of Kriging surrogate models, we may in the future be able to infer in vivo degradation rates based on in vitro experiments.

Author Contributions: T.A.B.: methodology, software, formal analysis, writing—original draft preparation. A.H.: peridynamic modelling, writing—original draft, editing—original draft. A.S.: Supervision, review and editing—original. R.W.-R.: supervision, review and editing—original draft. C.J.C.: supervision, review and editing—original draft. B.Z.-P.: conceptualization, supervision, review and editing—original draft. All authors have read and agreed to the published version of the manuscript.

Funding: TAB and BZP acknowledge the funding from the Helmholtz-Incubator project Uncertainty Quantification and the German Ministry for Education and Research (16DKWN112C) and the NextGenerationEU program. AH, AS and CJC acknowledge the funding by the Deutsche Forschungsgemeinschaft (DFG, German Research Foundation)—470246804.

Data Availability Statement: The experimental data for the validation can be found in [8,38]. The data sets generated and analyzed during the current study are available from the authors on reasonable request.

Acknowledgments: This research was supported in part through the Maxwell computational resources operated at Deutsches Elektronen- Synchrotron, Hamburg, Germany.

Conflicts of Interest: The authors declare no conflict of interest.

References

1. Gonzalez, J.; Hou, R.Q.; Nidadavolu, E.P.S.; Willumeit-Römer, R.; Feyerabend, F. Magnesium degradation under physiological conditions—Best practice. *Bioact. Mater.* **2018**, *3*, 174–185. [[CrossRef](#)] [[PubMed](#)]
2. Luthringer, B.; Feyerabend, F.; Willumeit, R. Magnesium-Based Implants: A Mini-Review. *Magnes. Res.* **2014**, *27*, 142–154. [[CrossRef](#)] [[PubMed](#)]
3. Su, Y.; Cockerill, I.; Zheng, Y.; Tang, L.; Qin, Y.X.; Zhu, D. Biofunctionalization of metallic implants by calcium phosphate coatings. *Bioact. Mater.* **2019**, *4*, 196–206. [[CrossRef](#)]

4. Myrissa, A.; Agha, N.A.; Lu, Y.; Martinelli, E.; Eichler, J.; Szakács, G.; Kleinhans, C.; Willumeit-Römer, R.; Schäfer, U.; Weinberg, A.M. In vitro and in vivo comparison of binary Mg alloys and pure Mg. *Mater. Sci. Eng. C* **2016**, *61*, 865–874. [[CrossRef](#)]
5. Willumeit-Römer, R.; Bruns, S.; Helmholz, H.; Krüger, D.; Wiese, B.; Galli, S.; Moosmann, J.; Zeller-Plumhoff, B. *The Comparability of In Vitro and In Vivo Experiments for Degradable Mg Implants*; Springer International Publishing: Cham, Switzerland, 2022; pp. 9–16.
6. Negrescu, A.M.; Necula, M.G.; Costache, M.; Cimpean, A. In vitro and in vivo biological performance of Mg-based bone implants. *Rev. Biol. Biomed. Sci.* **2020**, *3*, 11–41. [[CrossRef](#)]
7. Sanchez, A.H.M.; Luthringer, B.J.C.; Feyereabend, F.; Willumeit, R. Mg and Mg alloys: How comparable are in vitro and in vivo corrosion rates? A review. *Acta Biomater.* **2015**, *13*, 16–31. [[CrossRef](#)]
8. Krüger, D.; Galli, S.; Zeller-Plumhoff, B.; Wieland, D.F.; Peruzzi, N.; Wiese, B.; Heuser, P.; Moosmann, J.; Wennerberg, A.; Willumeit-Römer, R. High-resolution ex vivo analysis of the degradation and osseointegration of Mg-xGd implant screws in 3D. *Bioact. Mater.* **2022**, *13*, 37–52. [[CrossRef](#)]
9. Kokubo, T.; Takadama, H. How useful is SBF in predicting in vivo bone bioactivity? *Biomaterials* **2006**, *27*, 2907–2915. [[CrossRef](#)]
10. Zheng, Y.F.; Gu, X.N.; Witte, F. Biodegradable metals. *Mater. Sci. Eng. R Rep.* **2014**, *77*, 1–34. [[CrossRef](#)]
11. Amukarimi, S.; Mozafari, M. Biodegradable magnesium-based biomaterials: An overview of challenges and opportunities. *MedComm* **2021**, *2*, 123–144. [[CrossRef](#)]
12. Zeller-Plumhoff, B.; AlBaraghteh, T.; Höche, D.; Willumeit-Römer, R. Computational modelling of magnesium degradation in simulated body fluid under physiological conditions. *J. Magnes. Alloys* **2022**, *10*, 965–978. [[CrossRef](#)]
13. Grogan, J.A.; Leen, S.B.; McHugh, P.E. A physical corrosion model for bioabsorbable metal stents. *Acta Biomater.* **2014**, *10*, 2313–2322. [[CrossRef](#)] [[PubMed](#)]
14. Hermann, A.; Shojaei, A.; Steglich, D.; Höche, D.; Zeller-Plumhoff, B.; Cyron, C.J. Combining peridynamic and finite element simulations to capture the corrosion of degradable bone implants and to predict their residual strength. *Int. J. Mech. Sci.* **2022**, *220*, 107143. [[CrossRef](#)]
15. Deshpande, K.B. Numerical modeling of micro-galvanic corrosion. *Electrochim. Acta* **2011**, *56*, 1737–1745. [[CrossRef](#)]
16. Chen, Z.; Bobaru, F. Peridynamic modeling of pitting corrosion damage. *J. Mech. Phys. Solids* **2015**, *78*, 352–381. [[CrossRef](#)]
17. Marvi-Mashhadi, M.; Ali, W.; Li, M.; González, C.; LLorca, J. Simulation of corrosion and mechanical degradation of additively manufactured Mg scaffolds in simulated body fluid. *J. Mech. Behav. Biomed. Mater.* **2022**, *126*, 104881. [[CrossRef](#)] [[PubMed](#)]
18. Boland, E.L.; Shine, R.; Kelly, N.; Sweeney, C.A.; McHugh, P.E. A Review of Material Degradation Modelling for the Analysis and Design of Bioabsorbable Stents. *Ann. Biomed. Eng.* **2016**, *44*, 341–356. [[CrossRef](#)] [[PubMed](#)]
19. Albaraghteh, T.; Willumeit-Römer, R.; Zeller-Plumhoff, B. In silico studies of magnesium-based implants: A review of the current stage and challenges. *J. Magnes. Alloys* **2022**, *10*, 2968–2996. [[CrossRef](#)]
20. Abdallah, M.; Joplin, A.; Elahinia, M.; Ibrahim, H. Corrosion Modeling of Magnesium and Its Alloys for Biomedical Applications: Review. *Corros. Mater. Degrad.* **2020**, *1*, 219–248. [[CrossRef](#)]
21. Zhang, Z.; Lu, X.; Yan, Y. A novel pathway for the preparation of Mg metal from magnesia. *J. Magnes. Alloys* **2021**, *10*, 2847–2856. [[CrossRef](#)]
22. Sanz-Herrera, J.A.; Reina-Romo, E.; Boccaccini, A.R. In silico design of magnesium implants: Macroscopic modeling. *J. Mech. Behav. Biomed. Mater.* **2018**, *79*, 181–188. [[CrossRef](#)] [[PubMed](#)]
23. Gartzke, A.K.; Julmi, S.; Klose, C.; Waselau, A.C.; Meyer-Lindenberg, A.; Maier, H.J.; Besdo, S.; Wriggers, P. A simulation model for the degradation of magnesium-based bone implants. *J. Mech. Behav. Biomed. Mater.* **2020**, *101*, 103411. [[CrossRef](#)] [[PubMed](#)]
24. Shojaei, A.; Hermann, A.; Seleson, P.; Cyron, C.J. Dirichlet absorbing boundary conditions for classical and peridynamic diffusion-type models. *Comput. Mech.* **2020**, *66*, 773–793. [[CrossRef](#)]
25. Jafarzadeh, S.; Chen, Z.; Bobaru, F. Peridynamic Modeling of Repassivation in Pitting Corrosion of Stainless Steel. *Corrosion* **2018**, *74*, 393–414. [[CrossRef](#)]
26. Jafarzadeh, S.; Chen, Z.; Bobaru, F. Peridynamic Modeling of Intergranular Corrosion Damage. *J. Electrochem. Soc.* **2018**, *165*, C362–C374. [[CrossRef](#)]
27. Jafarzadeh, S.; Chen, Z.; Bobaru, F. Computational modeling of pitting corrosion. *Corros. Rev.* **2019**, *37*, 419–439. [[CrossRef](#)]
28. Chen, Z.; Jafarzadeh, S.; Zhao, J.; Bobaru, F. A coupled mechano-chemical peridynamic model for pit-to-crack transition in stress-corrosion cracking. *J. Mech. Phys. Solids* **2021**, *146*, 104203. [[CrossRef](#)]
29. Zhao, J.; Jafarzadeh, S.; Rahmani, M.; Chen, Z.; Kim, Y.R.; Bobaru, F. A peridynamic model for galvanic corrosion and fracture. *Electrochim. Acta* **2021**, *391*, 138968. [[CrossRef](#)]
30. Zhang, J.; Yin, J.; Wang, R. Basic Framework and Main Methods of Uncertainty Quantification. *Math. Probl. Eng.* **2020**, *2020*, 6068203. [[CrossRef](#)]
31. Sudret, B.; Marelli, S.; Wiart, J. Surrogate Models for Uncertainty Quantification: An Overview. In Proceedings of the 2017 11th European Conference on Antennas and Propagation (EUCAP), Paris, France, 19–24 March 2017. [[CrossRef](#)]
32. Wu, X.; Wang, C.; Kozłowski, T. Kriging-Based Surrogate Models for Uncertainty Quantification and Sensitivity Analysis. In Proceedings of the International Conference on Mathematics and Computational Methods Applied to Nuclear Science and Engineering, Jeju, Republic of Korea, 16–20 April 2017.
33. Wang, K.; Wang, Y.; Yue, X.; Cai, W. Multiphysics modeling and uncertainty quantification of tribocorrosion in aluminum alloys. *Corros. Sci.* **2021**, *178*, 109095. [[CrossRef](#)]

34. Liu, Y.; Li, L.; Zhao, S.; Song, S. A global surrogate model technique based on principal component analysis and Kriging for uncertainty propagation of dynamic systems. *Reliab. Eng. Syst. Saf.* **2021**, *207*, 107365. [[CrossRef](#)]
35. Bhoosekar, A.; Ierapetritou, M. Advances in surrogate based modeling, feasibility analysis, and optimization: A review. *Comput. Chem. Eng.* **2018**, *108*, 250–267. [[CrossRef](#)]
36. Fuhg, J.N.; Fau, A.; Nackenhorst, U. State-of-the-Art and Comparative Review of Adaptive Sampling Methods for Kriging. *Arch. Comput. Methods Eng.* **2021**, *28*, 2689–2747. [[CrossRef](#)]
37. Cole, D.A.; Christianson, R.B.; Gramacy, R.B. Locally induced Gaussian processes for large-scale simulation experiments. *Stat. Comput.* **2021**, *31*, 33. [[CrossRef](#)]
38. Krüger, D.; Zeller-Plumhoff, B.; Wiese, B.; Yi, S.; Zuber, M.; Wieland, D.C.; Moosmann, J.; Willumeit-Römer, R. Assessing the microstructure and in vitro degradation behavior of Mg-xGd screw implants using μ CT. *J. Magnes. Alloys* **2021**, *9*, 2207–2222. [[CrossRef](#)]
39. Zeller-Plumhoff, B.; Tolnai, D.; Wolff, M.; Greving, I.; Hort, N.; Willumeit-Römer, R. Utilizing Synchrotron Radiation for the Characterization of Biodegradable Magnesium Alloys-From Alloy Development to the Application as Implant Material. *Adv. Eng. Mater.* **2021**, *23*, 2100197. [[CrossRef](#)]
40. Gießgen, T.; Mittelbach, A.; Höche, D.; Zheludkevich, M.; Kainer, K.U. Enhanced predictive corrosion modeling with implicit corrosion products. *Mater. Corros.* **2019**, *70*, 2247–2255. [[CrossRef](#)]
41. Shojaei, A.; Hermann, A.; Cyron, C.J.; Seleson, P.; Silling, S.A. A hybrid meshfree discretization to improve the numerical performance of peridynamic models. *Comput. Methods Appl. Mech. Eng.* **2022**, *391*, 114544. [[CrossRef](#)]
42. Cheng, K.; Lu, Z.; Ling, C.; Zhou, S. Surrogate-assisted global sensitivity analysis: An overview. *Struct. Multidiscip. Optim.* **2020**, *61*, 1187–1213. [[CrossRef](#)]
43. Wang, C.; Duan, Q.; Tong, C.H.; Di, Z.; Gong, W. A GUI platform for uncertainty quantification of complex dynamical models. *Environ. Model. Softw.* **2016**, *76*, 1–12. [[CrossRef](#)]
44. Zhao, L.; Choi, K.; Lee, I. Metamodeling Method Using Dynamic Kriging for Design Optimization. *AIAA J.* **2011**, *49*, 2034–2046. [[CrossRef](#)]
45. Marelli, S.; Sudret, B. UQLab: A Framework for Uncertainty Quantification in Matlab. In *Vulnerability, Uncertainty, and Risk*; American Society of Civil Engineers: Reston, VA, USA, 2014; pp. 2554–2563. [[CrossRef](#)]

Disclaimer/Publisher's Note: The statements, opinions and data contained in all publications are solely those of the individual author(s) and contributor(s) and not of MDPI and/or the editor(s). MDPI and/or the editor(s) disclaim responsibility for any injury to people or property resulting from any ideas, methods, instructions or products referred to in the content.

Best practices in developing a UQ-workflow for modelling the biodegradation of Mg-based implants

This chapter investigates the crucial aspect of surrogate models implemented to study biodegradable implants' degradation and addresses the uncertainty challenge. Effective quantification of uncertainty and enhancement of computational models necessitate repeated evaluation. Nevertheless, complex numerical models, such as those simulating the electrochemical biodegradation of Mg-based implants, present a significant challenge. The solution lies in evaluating a model that can approximate these complex and resource-intensive models. Despite being viable, applying this approach to studying complex degradation models remains limited and needs more development.

Furthermore, the degradation of Mg-based implants under physiological conditions introduces various sources of uncertainty, demanding careful consideration during surrogate model selection. This chapter comprehensively examines the suitability of different surrogate models for varying degradation models. Here, three techniques, Kriging, polynomial chaos expansion and polynomial chaos Kriging, are constructed for three distinct computational models representing the biodegradation of Mg-based implants. Moreover, this study unveils the uncertainties inherent in different models through comprehensive analyses of global sensitivity and uncertainty propagation in diverse scenarios. Kriging is an effective method for calibrating various models with minimal computational time and cost. PCE and PCK, on the other hand, demonstrate greater abilities in predicting uncertainties within degradation systems, particularly for further UQ and sensitivity analyses.

Publication details

Tamadur AlBaraghteh, Regine Willumeit-Römer, Berit Zeller-Plumhoff (2024). Best practices in developing a UQ-workflow for modelling the biodegradation of Mg-based implants. *Advanced Science*, 2403543. <https://doi.org/10.1002/advs.202403543>.

Author's contribution

The author contributed to conceptualization, methodology, software, formal analysis, writing, editing and original draft preparation.

Copyright Notice

©This is the accepted version of the article originally published in the Journal of Advanced Science. The paper has been published under the Creative Commons CC-BY 4.0 License. Copyright has been clarified in accordance with the publisher's guidelines.

Best Practices in Developing a Workflow for Uncertainty Quantification for Modeling the Biodegradation of Mg-Based Implants

Tamadur AlBaraghteh,* Regine Willumeit-Römer, and Berit Zeller-Plumhoff*

Computational models of electrochemical biodegradation of magnesium (Mg)-based implants are uncertain. To quantify the model uncertainty, iterative evaluations are needed. This presents a challenge, especially for complex, multiscale models as is the case here. Approximating high-cost and complex models with easy-to-evaluate surrogate models can reduce the computational burden. However, the application of this approach to complex degradation models remains limited and understudied. This work provides a workflow to quantify different types of uncertainty within biodegradation models. Three surrogate models—Kriging, polynomial chaos expansion, and polynomial chaos Kriging—are compared based on the minimum number of samples required for surrogate model construction, surrogate model accuracy, and computational time. The surrogate models are tested for three computational models representing Mg-based implant biodegradation. Global sensitivity analysis and uncertainty propagation are used to analyze the uncertainties associated with the different models. The findings indicate that Kriging proves effective for calibrating diverse computational models with minimal computational time and cost, while polynomial chaos expansion and polynomial chaos Kriging exhibit greater capability in predicting propagated uncertainties within the computational models.

1. Introduction

Magnesium (Mg) and its alloys are being investigated increasingly as temporary bone implant materials due to their non-toxicity, biocompatibility, and biodegradability.^[1] However, numerous in vitro and in vivo experiments are needed to tailor the degradation rates of these implants to be suitable for the human body.^[2,3] A growing interest in digital twins, which use computational models to imitate and predict these experiments, has been stimulated by the increasing digitization of data and processes.^[4-6] As such, digital twins are expected to bridge the gap between the in vitro and in vivo experiments, while also reducing costs, experimental time, and the number of animal tests.^[7,8]

Degradation models, which will form the basis for the digital twin, possess a multi-dimensional and multi-scale nature, thereby resulting in a substantial computational load during their solution.^[9-11] Moreover, these models are inherently uncertain.

While state-of-the-art degradation models include a wide variety of complexities and can be used for certain applications, these models cannot be generalized to estimate the degradation of implants under different environmental conditions.^[9,11-13] Uncertainty is an inherent characteristic of complex systems in mathematical models. This uncertainty arises from multiple sources, including uncertain input parameters, mathematical approximations, and the assumptions and hypotheses used to construct the model.^[14] Furthermore, limitations in computing resources contribute to these uncertainties by constraining numerical computation precision, the number of feasible model evaluations, and the scope of computations available for supporting analyses.^[15,16] It is important to note that the reliability of a degradation model is influenced both by the uncertainty associated with the estimations of the computational model and the uncertainty associated with the observations of the physical system, which must be quantified in order to build a digital twin of in vivo and in vitro experiments.^[4,6,8,13]

In uncertainty quantification (UQ), models are analyzed within an uncertainty framework that assesses and quantifies the impact of uncertainties on model predictions. Such analysis involves assessing the impacts of uncertainty on reliability and

T. AlBaraghteh, R. Willumeit-Römer, B. Zeller-Plumhoff
 Institute of Metallic Biomaterials
 Helmholtz-Zentrum hereon GmbH
 Max-Planck-Straße 1, 21502 Geesthacht, Germany
 E-mail: tamadur.albaraghteh@hereon.de;
berit.zeller-plumhoff@hereon.de

T. AlBaraghteh
 Institute of Surface Science
 Helmholtz-Zentrum hereon GmbH
 Max-Planck-Straße 1, 21502 Geesthacht, Germany
 B. Zeller-Plumhoff
 Data-driven Analysis and Design of Materials
 Mechanical Engineering and Marine Technologies
 University of Rostock
 Albert-Einstein-Straße 2, 18059 Rostock, Germany

 The ORCID identification number(s) for the author(s) of this article can be found under <https://doi.org/10.1002/advs.202403543>

© 2024 The Author(s). Advanced Science published by Wiley-VCH GmbH. This is an open access article under the terms of the [Creative Commons Attribution](#) License, which permits use, distribution and reproduction in any medium, provided the original work is properly cited.

DOI: [10.1002/advs.202403543](https://doi.org/10.1002/advs.202403543)

robustness, calibration using experimental data, or conducting global sensitivity analysis.^[13,17] Two main approaches exist for UQ techniques: intrusive and non-intrusive techniques. The intrusive approach involves incorporating uncertain variables into the governing equations of the mathematical model and modifying the source codes of the numerical models.^[18–20] However, these modifications become challenging as the mathematical complexity of the computational model increases, leading to increased CPU usage and computational times.^[19,21] Moreover, these techniques are not feasible when source codes are unavailable to end-users, e.g., when using commercial software. On the other hand, non-intrusive techniques treat the original model as a black box and rely on sampling techniques to explore the model's input space and evaluate the model's responses without altering its internal structure.^[19,21–23] In general, the uncertainty inherent in the degradation models of Mg-based implants can be assessed through non-intrusive UQ methods. However, although non-intrusive UQ techniques are straightforward from a methodological point of view, they are computationally demanding even with high-performance computing resources.^[6,19] To address this challenge, surrogate modeling is employed, wherein complex models are approximated by fast-to-evaluate analytical functions based on an input/output mapping of the original model.^[24,25]

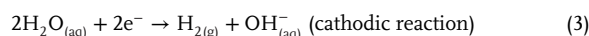
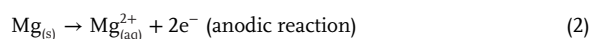
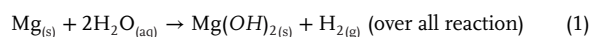
In recent years, surrogate modeling has gained significant interest, as these models can be trained using limited data obtained from the complex multi-scale model.^[24–26] This development in the approach has led to the creation of various classes of surrogate models; a detailed review can be found in ref. [25]. These classes are differentiated based on type, training strategies, data requirements and application-specific criteria. Consequently, selecting the appropriate surrogate model for the system under study becomes crucial.^[6,15,27–29] A surrogate model's effectiveness and accuracy are determined by a combination of several factors, each of which plays an important role in its reliability and performance. Among these factors are the mathematical nature of the original model functions, the selection of a surrogate model type tailored to the specific domain of the problem, and its capability to enhance understanding of the model's input-output relationships.^[30] One of the most influential factors affecting surrogate model performance is the quality and quantity of training data used during its construction, as well as the choice of the set of input variables and the control of the noise inherent in these variables.^[28,31] Equally significant is the level of complexity of the surrogate model itself. Excessively simplified surrogate models might not have the capacity to capture the underlying behavior of the system, while an overly complex one risks overfitting and subsequent poor generalization to unseen data.^[6,28] Additionally, accurately tuning the surrogate model's parameters is essential for achieving accuracy and high performance.^[24] Incorporating domain knowledge enhances the performance of surrogate models by providing a comprehensive understanding of the underlying phenomenon of the system. Also, proper pre-processing of the data, coupled with the use of independent datasets to validate and test the surrogate models, can significantly boost their performance and accuracy.^[15,27,28] Furthermore, it is imperative to reconstruct the surrogate models to align with advancements in the original models they represent as well as keeping a balance between accuracy and computational efficiency is a crucial issue for optimal performance.^[15,29]

In simulating the degradation of biodegradable implants, surrogate models play a promising role. Therefore, the focus of this manuscript is to present a best-practice workflow for constructing and applying such surrogate models to different degradation models. Although the demonstration of these methods is performed using simpler in vitro models, the proposed workflow is also applicable to more complex models. As we have demonstrated previously, under certain conditions, it is possible to utilize surrogate models to expand the parametric space and simulate in vivo corrosion based on in vitro corrosion.^[8] Furthermore, the paper assesses the impact of three surrogate modeling techniques, namely Kriging, Polynomial Chaos Expansion (PCE) and polynomial chaos Kriging (PCK) on the uncertainty analysis of the degradation models. These techniques are evaluated using three different mathematical models that characterize various aspects and phenomena related to the degradation of biodegradable Mg-based alloys. The degradation models vary in terms of mathematical complexity, dimensionality and model construction hypotheses and assumptions. During the development of these surrogate models, we will examine the influence of parameter sampling strategies, including adaptive sampling. A further objective of the study is to test and analyze the performance of these surrogate models for two fundamental forward UQ tasks: sensitivity analysis and uncertainty propagation.

2. Experimental Section

2.1. Overview of the Degradation Process

The general concept of the degradation and the main factors affecting it have been presented in refs. [1, 13, 32]. As a summary, the degradation of Mg in aqueous media is an electrochemical reaction (Equation 1), which involves an anodic reaction for Mg (Equation 2), while water goes through a cathodic reaction (Equation 3). Ultimately, magnesium hydroxide and hydrogen gas (H₂) are produced.



Equation (3), one mole of Mg must be degraded in order to produce one mole of H₂. While according to Equation (1), the overall degradation reaction depends on the degradation medium as a function of the pH.^[32,33] It is anticipated that a passive layer of magnesium hydroxide, Mg(OH)₂, will develop in response to an increasing pH value. This layer will act as a protective layer to increase the corrosion resistance of the metal. However, this layer is only stable when the pH level is highly alkaline (pH > 11).^[32,34,35] A more stable thin, porous MgO layer (less than 10 nm) was observed to form due to interactions with air.^[36] Corrosion of metal is an electrochemical process that occurs when a metal interacts with an aqueous electrolyte and changes its oxidation state, as demonstrated by Equation (2). During this process, electrons are transferred between the electrode's interface and metal atoms are oxidized to form ionic species, with electrons being liberated at the same time.^[34,37]

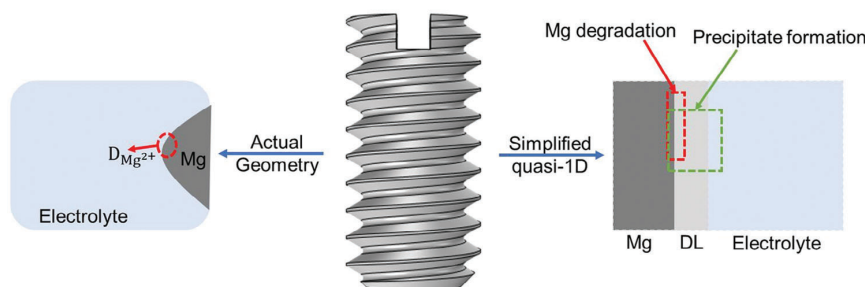
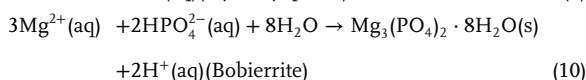
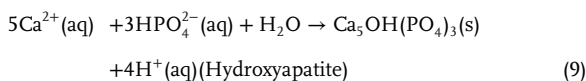
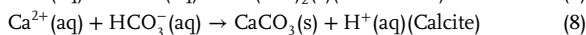
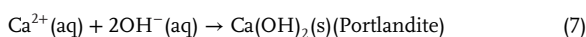
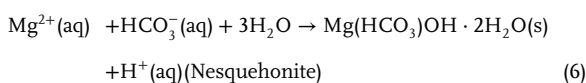


Figure 1. Schematic illustration of the approximated numerical geometries of Mg-based implants for the three degradation models. To the right, the implant geometry is simplified using quasi-1D geometry for both the degradation model of pure Mg and the formation of precipitate.^[39] Left schematic shows the focus on the diffusion of Mg^{2+} -ions from the implant surface to the electrolyte.

Generally, degradation systems of biodegradable bone implants operate within a pH range of 7.4 ± 0.4 ,^[38] allowing the formation of several precipitates based on the ions present in the degradation medium. The chemical reactions of the precipitates in this study are presented in the following equations, with the name of each precipitate indicated alongside its corresponding equation.^[37] Note that the precipitation of Bobierite, Equation (10), was not considered in any of the degradation models.



2.1.1. Numerical Simulation and Model Development of the Degradation Process

In the current study, three finite element models were conducted to simulate different aspects of the degradation behavior of Mg-based implants.

The first model is a generalized quasi-1D FE model of pure Mg degradation in simulated body fluid (SBF) over the course of 28 days, which was taken from ref. [39]. In the second FE model, a second aspect of the model derived in ref. [39] was considered, which is the simulation of the formation and precipitation of relevant degradation products on the surface of the implant over the course of 28 days. For the third FE model, a simplified 3D degradation model of an actual implant geometry based on diffusion was derived. For this model, experimental data of Mg-xGd (Mg-5 wt.% Gd and Mg-10 wt.% Gd) over the course

of 56 days were used for the calibration process. The schematic diagram in Figure 1 illustrates the models' basic principles and geometries.

In a brief summary of the degradation models, the generalized quasi-1D model of pure Mg degradation in SBF, illustrated in Figure 1, marked with a red box on the right of the implant rendering, was derived based on experimental observations by refs. [40, 41]. In this model, Mg degradation was found to have an initial period of low degradation followed by a linear trend. The mathematical presentation of the effective rate of Mg^{2+} ions released at the metallic-liquid interface is given by

$$\frac{\partial c_{Mg}}{\partial t} = \frac{\epsilon k_{deg}}{1 + \exp^{-(t-t_{init})}} \quad (11)$$

where $\partial c_{Mg}/\partial t$ is the change in the concentration profile of Mg (c_{Mg}) over time and t_{init} denotes the starting time of degradation, taking into account the initial thin degradation layer of MgO. ϵ and k_{deg} are the porosity of the degradation layer and the degradation rate constant, respectively. The dynamic deformation of the model geometry was captured using the arbitrary Lagrangian–Euler (ALE) method, which was utilized to explicitly track the moving interface of the degraded Mg.^[39,42–44] The degradation of Mg was then calculated in terms of the mean degradation depth (MDD) as

$$MDD = r_{initial} - \int v_{deg} dt \quad (12)$$

where $r_{initial}$ is the length of the Mg-domain and v_{deg} is the normal velocity of the metal interface and it is computed based on the concentration gradient of the Mg as

$$v_{deg} = \frac{M_{Mg}}{\rho_{Mg}} \frac{\partial c_{Mg}}{\partial t} \quad (13)$$

where M_{Mg} and ρ_{Mg} are the molecular weight and the density of Mg, respectively.

The formation of precipitates on the surface of the implant from different chemical species in the medium, marked with a green box on the right of the implant rendering, is modeled using the Nernst–Planck Equation (NPE) (14). NPE is implemented

to mathematically describe the transport of chemical species i of concentration c_i and it is given by

$$\frac{\partial c_i}{\partial t} + \nabla \cdot (D_i \nabla c_i - z_i \frac{D_i}{RT} F c_i \nabla V) = R_i \quad (14)$$

The left-hand side of the NPE represents the species flux, where the first part describes the diffusion of species within the porous degradation layer (DL) and the electrolyte. While the migration of species within the electric field is described in the second part of NPE (14). D_i denotes the diffusion coefficient of the chemical species in the liquid phase of the porous medium, z_i is the species charge, V is the electric potential, $R \approx 8.314$ J (mol K)⁻¹ is the gas constant and T is the temperature. $F \approx 96485$ C mol⁻¹ is the Faraday constant. The right-hand side of NPE, R_i , is the chemical reaction rate of species i . The analysis of the degradation layer showed that it contained a number of different precipitates.^[38] Under the assumption that the formation of precipitates on Mg surface can only take place in the porous degradation layer, the formation of precipitate p_l , according to the chemical Equations (4)–(9), can be mathematically modeled as^[39]

$$\frac{\partial c_{p_l}}{\partial t} = \epsilon k_l (K_{eq,l} - c_i c_j) \quad (15)$$

where $K_{eq,l}$ is the equilibrium constant and k_l is the backward reaction constant for reaction l of the Equations (4)–(9) and i and j denote the two species reacting in the respective reaction. Based on the concentration of each precipitated species c_{p_l} , the elemental wt% of each chemical element within the degradation layer as

$$wt_{DL,elem_i} = \frac{\rho_{DL,elem_i}}{\sum_{k=1}^6 \rho_{DL,elem_k}} \cdot 100 \quad (16)$$

where $elem_i$ stands for the chemical elements C, Ca, P, H, O, and Mg. $\rho_{DL,elem_i}$ is overall mass concentration in the degradation layer of element i .

The simplified 3D degradation model is derived from NPE (14) under the assumption that the diffusion of Mg²⁺ and other ions is the rate-limiting step for degradation. Under the assumption that degradation is governed by the diffusion of Mg²⁺ ions from the implant surface within the degradation medium.^[42,43,45] Under this assumption, the NPE (14) reduces into Fick's law^[46] and the diffusion of Mg²⁺ ions is modeled as

$$\frac{\partial c_{Mg}}{\partial t} = -\nabla \cdot (D_{Mg} \nabla c_{Mg}) \quad (17)$$

where D_{Mg} is the diffusion coefficient of Mg²⁺ ions from the implant surface into the degradation medium. In the study of Mg-based alloys, diffusion-only models assume the formation of a uniform corrosion layer on the alloy's surface, with degradation progressing uniformly as Mg²⁺ ions diffuse through this layer. However, these models face limitations in accurately capturing the non-uniform degradation behavior observed in experimental settings. Despite this limitation, the application of diffusion-only models to study alloy degradation remains valid. These models can adjust key parameters, such as the diffusion coefficient and degradation layer thickness, to align with experimental data.

While these parameters may not directly reflect the alloy's heterogeneous microstructure and surface morphology, they still offer a macroscopic perspective on the degradation process.^[39,47] The quasi-1D FE model of pure Mg degradation in SBF, which simulates degradation and precipitate formation, is discretized using rectangular FE and implemented in COMSOL Multiphysics 6.2 (COMSOL AB, Stockholm, Sweden). A symmetric quasi-1D geometry with a height of 1 μm and equal domains of 0.2 mm for both the Mg and electrolyte domains is employed. Additionally, an initial degradation layer of 10 nm is considered, utilizing a variable thickness mesh that is refined near the degradation layer.^[39] For the simplified 3D degradation model, a realistic 3D screw identical to the geometry of the experimental screws used in ref. [48] is used. A CAD mesh is imported into COMSOL Multiphysics 6.2, then a free tetrahedral mesh of the implant, which measures 4 mm in length, 2 mm in diameter with a M2 thread and a 0.5 × 0.5 mm slotted screw head, is created surrounded by the geometry of the electrolyte, which has a dimension of 3x3x5 mm. The mesh is smoothed through four iterations and it is bound by 0.03 and 0.05 mm to avoid staircase effects. Zero initial concentration of Mg²⁺ ions within the electrolyte is assumed. A constant diffusion coefficient of the chemical species in the liquid phase of the porous medium is set to equal 1.4×10^{-16} m² s⁻¹.

The three biodegradation models mentioned above were selected to ensure the flexibility and generalization of the proposed UQ-workflow. Although these models may seem simple from a computational and mathematical standpoint, their straightforward nature is intentional. It highlights the surrogate model's ability to be tailored to the unique characteristics of different degradation systems without unnecessary complexity. Furthermore, by employing models with varying levels of complexity, we effectively harness the strengths of both simple and intricate surrogate models, ensuring that our approach remains broadly applicable and generalizable to more complex degradation scenarios.

2.1.2. Calibration Data

The degradation models are calibrated against in-house experimental data. The calibration data for the generalized quasi-1D FE model of pure Mg degradation is obtained by evaluating the mean degradation depth of the Mg specimen using both data from μCT imaging and weight loss data. The calibration data were taken from the original model publication.^[39] The formation of precipitates data is obtained from EDX measurements, originally published in refs. [40, 49], in which the mean elemental weight percentage (wt%) of each element in the degradation layer is calculated. For both models a 28-day degradation period is covered by experimental data. The simplified 3D degradation model is calibrated using volume loss (VL in %) data of Mg-5 wt.% Gd and Mg-10 wt.% Gd, which is obtained from in vitro tests conducted and published in ref. [50]. The volume loss % is measuring the difference in the implant volume over the degradation time, within the degradation model. The volume loss is measured as a function of the concentration changed along the degradation time. Since the concentration of Mg can be expressed as a function of number of Mg moles (N_{Mg}) and the volume of Mg

Table 1. The surrogate model presentation of the QoI (\mathcal{Y}) and the input parameter vector (\mathcal{X}) for the three case studies of the degradation models of Mg-based alloys.

Degradation model	\mathcal{X}	\mathcal{Y}
quasi-1D degradation model of pure Mg	k_{deg}, t_{init}	MDD
Formation of precipitation on implant surface	$k_{deg}, t_{init}, k_1, k_2, k_3, k_4, k_5, k_6, k_7, k_8$	$w_{DL, Mg}^t, w_{DL, O}^t, w_{DL, P}^t, w_{DL, C}^t, w_{DL, Ca}^t$
3D degradation model of Mg-alloy	D_{Mg}	VL

where: k_{deg} is the degradation rate constant, t_{init} is the starting time of degradation/days, the reaction rate constants $k_1, k_2, k_3, k_4, k_5, k_6, k_7$, and k_8 correspond to the precipitation reactions represented by Equations (4)–(9), D_{Mg} = diffusion coefficient of Mg^{2+} ions, MDD = mean degradation depth, w^t = weight percentage of elements, where DL denotes the degradation layer and Mg, Ca, O, P, and C are the chemical elements in DL. VL is the volume loss

within the implant $c_{Mg} = N_{Mg}/V_{Mg}$, Equation (17) can be written as:

$$\frac{\partial(\rho_{Mg} \cdot V_{Mg})}{\partial t} = -V \cdot (D_{Mg} \nabla(\rho_{Mg} \cdot V_{Mg})) \quad (18)$$

where ρ_{Mg} is the density of Mg within the implant, which is 1.81 and 1.87/g cm^{-3} for Mg-5 wt.% Gd and Mg-10 wt.% Gd, respectively. V_{Mg} is the volume of Mg at time t, based on Equation (18), the volume loss % is calculated as:

$$VL(t) = \frac{V(0) - V(t)}{V(0)} \cdot 100\% \quad (19)$$

where $V(0)$ is the initial volume of the implant and $V(t)$ is the residual volume calculated by Equation (18). Note that the initial concentrations of Mg within the implants are adapted from the experiment; 7.13×10^{-5} and 7.07×10^{-5} mol mm^{-3} for Mg-5 wt.% Gd and Mg-10 wt.% Gd, respectively. The degradation rate (DR) in $mm\ yr^{-1}$ is calculated based on volume loss as

$$DR(t) = \frac{V(0) - V(t)}{A(0) \cdot t} \quad (20)$$

where $A(0)$ is the initial surface area of the sample and t is the degradation time.

2.2. Overview of Surrogate Modeling

Several surrogate models have been developed and tested for different engineering problems. However, there is no consensus or clear-cut guidelines on the selection process in the literature.^[30] In the present study, the focus was on surrogate models that treat the computational model as a black box which means these models only need the input values of model parameters and the corresponding output values of the quantity of interest (QoI). Here, a comparative analysis of three surrogate models was conducted, specifically Kriging (Krg), Polynomial Chaos Expansion (PCE), and Polynomial Chaos Kriging (PCK). Their performance and capacity were assessed to accurately represent degradation behavior. These surrogate models are evaluated throughout three specific tasks: parameter estimation, prediction of the original model's outcomes and sensitivity analysis within the context of degradation models. A general overview of surrogate models is provided in this section, including their construction and mathematical presentation.

The general mathematical format of the surrogate models is

$$\mathcal{Y} = \mathcal{M}^S(\mathcal{X}) \quad (21)$$

where S represents the surrogate model method, in the current mathematical presentations S will be substituted with *Krg*, *PCE* and *PCK* for three different techniques. \mathcal{Y} is the QoI for which the models are solved, \mathcal{M} is the surrogate shape/mapping function, which can be a system of equations, a code or any corresponding functions that can be used to calculate \mathcal{Y} values for any input parameters vector \mathcal{X} for a finite period of time. \mathcal{Y} and \mathcal{X} for the current test cases are given in Table 1.

2.2.1. A Brief Review Surrogate Modeling Techniques

In this section a brief description of the three surrogate modeling techniques implemented in this study is presented.

Polynomial Chaos Expansion: The main idea of PCE is to expand the model response onto multivariate polynomial bases that are orthogonal to joint distributions of input variables. Consequently, evaluating the PCE coefficients is equivalent to characterizing the probability density function of the model response.^[25,51] The QoI of the original model can be approximated by a finite, truncated set of polynomials

$$\mathcal{Y} = \mathcal{M}^{PCE}(\mathcal{X}) = \sum_{\substack{\alpha \in \mathbb{N}^M \\ 0 \leq |\alpha| \leq p}} \gamma_{\alpha} \Psi_{\alpha}(\mathcal{X}) \quad (22)$$

where $\Psi_{\alpha}(\mathcal{X})$ are multivariate polynomials orthonormal with respect to the joint probability density function $f(\mathcal{X})$. $\gamma_{\alpha} \in \mathbb{R}$ are the expansion coefficients of the multivariate polynomials, which is estimated by a least-square minimization method, and $\alpha \in \mathbb{N}^M$ is a multi-index that identifies the components of the multivariate polynomials Ψ_{α} . The product of univariate polynomials is used to evaluate and build the multivariate polynomials as $\Psi_{\alpha}(\mathcal{X}) = \prod_{i=1}^n \Psi_{\alpha_i}^{(i)}(\mathcal{X}_i)$,^[52,53] where $\Psi_{\alpha_i}^{(i)}$ is the polynomial in the i -th variable of degree α_i . The total degree of multivariate polynomials is defined as $|\alpha| = \sum_{i=1}^n \alpha_i$. The total number of the expansion terms for the summation is $((p+n)!/p!n!)$, which is depending on the adopted truncation scheme.^[52,53] Here, the hyperbolic index set based on q-norms is implemented, where $\alpha \in \mathbb{N} : \|\alpha\|_q \leq p$ and p is the maximal total polynomial degree and the norm $\|\alpha\|_q \leq p$ is defined as $\|\alpha\|_q = (\sum_{i=1}^n \alpha_i^q)^{1/q}$.^[52] The basis function of PCE can be described by several types of the orthogonal polynomials, e.g., Hermite, Laguerre, Jacobi, Legendre, Krawtchouk, Meixner, and

Hahn.^[25] In the current study, a PCE degree-adaptive calculation of the PCE coefficients, in particular the degree of polynomials, is implemented using the algorithm developed by ref. [54]. In other words, if an array of a specific range of possible degrees is given, the degree with the lowest ϵ_{LOO} error is selected automatically.

Kriging: The main idea behind Kriging, which is also known as Gaussian processing (GP), is to find the best linear unbiased prediction by minimizing the mean square error of the predictions.^[25,55] The Kriging predictor, Equation (23), consists of two main parts: the deterministic polynomial term, which describes the global trend of the data. While the second part is the realization of a stochastic process that accounts for the lack of fit in the first part.^[30]

$$\mathcal{Y} = \mathcal{M}^{Krg}(\mathcal{X}) = \beta^T f(\mathcal{X}) + \sigma^2 Z(\mathcal{X}, \omega) \quad (23)$$

where $\beta^T f(\mathcal{X})$ is the mean value (trend) of GP, $f(\mathcal{X})$ are arbitrary functions $f_j, j = 1, \dots, P$ that define the trend of the mean prediction at location \mathcal{X} and β is the corresponding vector of unknown regression coefficients $\beta_j, j = 1, \dots, P$, it should be selected precisely and it specifies the type of Kriging.^[30,56] σ^2 is the constant variance of GP and $Z(\mathcal{X}, \omega)$ is a zero-mean unit variance, stationary to the Gaussian process. ω is the probability space that is defined by a correlation function $R(x_i, x_j, \theta)$ and its hyperparameter θ , which is estimated by solving an optimization problem.^[30]

The stochastic part of the Kriging equation requires the selection of the kernel, also known as the correlation function. The kernel describes the correlation between two sample points x_i, x_j in the output space. In the current study the Matérn 5/2 kernel, Equation (24), is used.^[57]

$$R(x, x', \nu = 5/2) = \left(1 + \sqrt{5} \frac{|x - x'|}{\theta} + \frac{5}{3} \left(\frac{|x - x'|}{\theta} \right)^2 \right) \times \exp \left[-\sqrt{5} \frac{|x - x'|}{\theta} \right] \quad (24)$$

The Matérn 5/2 kernel functions offer multiple hyperparameters, providing enhanced flexibility when fitting complex mathematical functions. Furthermore, the differentiability of the Kriging model depends on the smoothness of the kernel.^[58,59] Smooth functions like Gaussian kernels produce very smooth interpolations, while the Matérn family, which is less smooth, can better capture non-smooth functions.^[59,60] Additionally, anisotropic kernels can model functions with varying degrees of importance across input variables because they have different length scales along different input dimensions.^[60,61] Moreover, faster evaluations are ensured with fewer non-zero coefficient Kriging models, which can be achieved by constructing sparse Kriging models, a capability provided by Matérn kernels.^[61] The characteristics of this kernel family enabled them to successfully fit all tested degradation models.

Polynomial Chaos Kriging: The PCK technique combines the two previous approaches in a simple way, leveraging each technique's strength.^[62] The PCK identifies the most relevant basis functions of model response adaptively. Moreover, it uses PCE as a regression-based approach to capture global behavior of the computational model and uses Kriging as an interpolation-based technique to capture local variation.^[63] In this sense, PCK can be

seen as a universal Kriging model with a specific trend described by PCE.^[25,55] The general formula of PCK is^[55]

$$\mathcal{Y} = \mathcal{M}^{PCK}(\mathcal{X}) = \sum_{\substack{\alpha \in \mathbb{N}^M \\ 0 \leq |\alpha| \leq p}} \gamma_\alpha \Psi_\alpha(\mathcal{X}) + \sigma^2 Z(\mathcal{X}, \omega) \quad (25)$$

The PCK surrogate model was constructed sequentially, i.e., the set of optimal polynomials is found first and then the PCK model is calibrated to find the parameters of Kriging. This results in lower computational costs for the degree-adaptive calculation of the PCE coefficients.

2.2.2. Surrogate Models Performance

The surrogate models in this study are constructed using k -fold cross validation (CV).^[25,64–66] In CV, the training data is randomly divided into k equal sized subsets. One of these subsets is considered the validation set and it is used for model assessment, while all other sets are used as training sets, which helps avoid both underfitting and overfitting of the training data.^[65,67,68] Moreover, CV helps assess the generalization of the constructed surrogate models. This is because CV involves repeatedly training the surrogate models on subsets of the data and evaluating their performance on the remaining held-out folds. The consistent performance of the surrogate models across the CV folds confirms their robustness and generalization capabilities. In particular, this means that a surrogate model is built k times, and its accuracy is measured by the total error in the predictions from each of these models, specifically by calculating the leave-one-out error (ϵ_{LOO}) for each sample of size N .^[15,64,69]

$$\epsilon_{LOO} = \frac{1}{N_k} \left[\frac{\sum_{i=1}^{N_k} (\mathcal{M}(x_i) - \mathcal{M}_{(-i)}(x_i))^2}{\text{Var}[\mathcal{M}(\mathcal{X})]} \right] \quad (26)$$

where N is the number of data points considered during building the surrogate model, $\mathcal{M}(X_i) - \mathcal{M}_{(-i)}(X_i)$ is the difference in prediction between the original observation and surrogate model observation for all training sets except x_i .

The best surrogate model is determined by evaluating performance metrics. The normalized root mean square error (NRMSE) is used as a performance metric. In terms of using N as the number of measurement points, \hat{y}_j is the surrogate model response at point j and y_i is the (mean) experimental value at time t for output i at point j . The NRMSE is calculated using Equation (27) with respect to the experimental data (y_i).

$$NRMSE_i = \frac{\sqrt{\frac{\sum_{j=1}^N (y_i - \hat{y}_j)^2}{N}}}{\gamma_{max} - \gamma_{min}} \quad (27)$$

with γ_{max} and γ_{min} the maximum and minimum experimental values.

Furthermore, the computational time for the construction of each of the surrogate models is reported for all stages, including sampling, parameter estimation, and optimization stages.

2.2.3. Surrogate Modeling Implementation

The surrogate models were constructed using the modules of the surrogate models in UQLab,^[70] which is a MATLAB-based uncertainty quantification framework. Two wrapper scripts were used; the first, the COMSOL-UQLab wrapper, to connect and convert data-formats between COMSOL (via LiveLink) and UQLab-MATLAB (R2022a, The MathWorks, Inc., Massachusetts, United States). Second, a wrapper script was implemented to construct surrogate models using adaptive sampling sets. Here, the original UQLab modules (Input, active learning reliability, surrogate models) were updated to incorporate the sampling algorithm. The computational time is divided into three phases: the sampling phase to generate training data, the construction and optimization of the surrogate model, and then the parameter estimation of the degradation model based on the surrogate model. The overall simulation time T_{sim} is given by

$$T_{sim} = T_{BBN} + T_{SM} + T_{opt} + T_C + T_I \quad (28)$$

where T_{BB} is the time of execution of the black-box model for N samples, T_{SM} is the training time required to construct the surrogate model, T_{opt} time required for parameter estimation. T_C and T_I are the total time of communication between workflow steps and the idle time of the corresponding computational unit, both of which can be neglected here because they do not impact the overall simulation time.

2.3. Design of Computer Experiments (DOEs) for Surrogate Models

The accuracy and performance of surrogate models are significantly impacted by the quality of the training data used to map the input–output relationship of the original model, sample size and the surrogate techniques.^[25,30,71,72] Within the scope of surrogate models, two types of sampling strategies are implemented: one-shot and adaptive strategies.^[73–75] One-shot sampling methods are static, domain-based and non-adaptive. These methods are designed for deterministic numerical experiments, in which the same input always yields the same response. Using these methods, a surrogate model is constructed in a single stage with a fixed set of samples. The minimum sample size required is ten times the number of uncertain parameters ($10N + 2$). These samples are distributed as evenly as possible over the sampling space, without considering prior knowledge of the original model or physical system.^[30] The main challenge associated with these methods is the unknown number of training points needed to achieve an acceptable accuracy of the constructed model.^[71,76] On the other hand, adaptive sampling methods construct the surrogate model sequentially. With these strategies, a surrogate model is initially built using a set number of training points. As an initial sample size for training data, ten times the number of the key parameters of the degradation model are selected following the recommendation of Jonas et al.,^[77] for expensive black-box models. By incorporating additional data points into the initial training set, the accuracy of the surrogate model is improved. As soon as the required accuracy is achieved the sampling process stops.^[76] Adaptive sampling algorithms are designed to strategi-

Algorithm 1 An adaptive sampling algorithm for the construction of surrogate models.

Require: Input parameter vector (\mathcal{X})
Ensure: Parameter distribution is uniform distribution $Z \sim \mathcal{U}[0, 1]^M$
Ensure: Number of key parameters N_p and total sampling set N_T
 Bonded design space of \mathcal{X} as [lower limit, higher limit]
 Number of initial sampling set using LHS, $N = 10N_p$
 Initial sampling set using LHS, N_i
 Initial experimental $\mathcal{X} = x_1^{(1)}, \dots, x_1^{(N)}$
 corresponding original model response $\mathcal{Y}^{original} = \mathcal{M}^{original}(\mathcal{X}) = y_1^{(1)}, \dots, y_1^{(N)}$
 Create the surrogate model \mathcal{M}^{SM}
 Set threshold $\theta = 10^{-4}$ set threshold
if $\epsilon_{LOO} < \theta$ **then**
 $N_{new} = N$
 \mathcal{M}^S is accepted
else if $\epsilon_{LOO} = \theta$ **then**
 minimum accuracy is reached
 $N_{new} = N$
 \mathcal{M}^S is accepted
else if $\epsilon_{LOO} > \theta$ **then**
 $N^* = \max_{i \in \{1, \dots, N\}} \min_{j \in \{1, \dots, N\}} \|N_T - N_j\|$
 find $N^{new} = N \in N_T : \mathcal{Y}^{SM}(N) < q$
end if

cally introduce new training points into areas characterized by high uncertainty in the surrogate model's response.

To study the effect of choosing the sampling strategy on the performance of surrogate models, we tested four one-shot sampling methods: Monte Carlo sampling (MC), Latin Hypercube sampling (LHS), Sobol sequence sampling (Sobol) and Halton sequence sampling (Halton). A brief comparison is presented in appendix A. These methods were tested across the three models to assess their performance in handling different dimensions of degradation models. Generally, these methods are characterized by their ability to draw random samples from the parametric space. However, the number of samples, the tendency for random clustering and the effectiveness of these methods are influenced by the complexity of the original model and the number of parameters.^[30,71,75] The comparison between on-shot sampling methods was performed and implemented using the UQLab input module and COMSOL-UQLab wrapper scripts.

An adaptive sampling **Algorithm 1** based on LHS was implemented to locate new samples in regions within the parametric space that were characterized by high uncertainty.^[78] The characteristics of these regions are determined in accordance with the calculated ϵ_{LOO} of the surrogate models. This algorithm was implemented using a customized script, which used the predefined UQLab-MATLAB constrained min-max (CMM) learning function. If adding new sample points does not improve the model's performance, the sample size is considered sufficient according to the predefined stopping criteria, $\epsilon_{LOO} < \theta$, with a predefined threshold θ .^[79,80]

For the parameter estimation of the degradation models, all the parameters are assumed to be uniformly distributed within the testing ranges. Moreover, initial tests using the rate equation and

Table 2. The ranges of parameters for the degradation models, and the optimal parameters estimated by Kriging, PCE, and PCK models.

Parameter	Input range	Optimal value			Ref.
		Krg	PCE	PCK	
Model 1 - Equations 11					
$k_{deg} / \text{mol m}^{-2}\text{s}$	$-1 \cdot 10^{-4} - 1 \cdot 10^{-9}$	$-2.4321 \cdot 10^{-5}$	$-2.4332 \cdot 10^{-5}$	$-2.4343 \cdot 10^{-5}$	[39]
t_{init} / day	0 - 3	1.932	1.933	1.929	
Model 2 - Equations 4 - 9					
$k_1 / \text{m}^7 \text{mol}^{-2}$	$-1 \cdot 10^{-19} - 1 \cdot 10^{-23}$	$-9.0245 \cdot 10^{-21}$	$-9.0302 \cdot 10^{-21}$	$-9.05301 \cdot 10^{-21}$	[39]
$k_2 / \text{m}^7 \text{mol}^{-2}$	$-1 \cdot 10^{-5} - 1 \cdot 10^{-12}$	$-7.0332 \cdot 10^{-9}$	$-7.0502 \cdot 10^{-9}$	$-7.0180 \cdot 10^{-9}$	
$k_3 / \text{m}^7 \text{mol}^{-2}$	$-1 \cdot 10^{-5} - 1 \cdot 10^{-12}$	$-7.0023 \cdot 10^{-10}$	$-7.0045 \cdot 10^{-10}$	$-7.0038 \cdot 10^{-10}$	
$k_4 / \text{m}^7 \text{mol}^{-2}$	$-1 \cdot 10^{-1} - 1 \cdot 10^{-12}$	$-1.0798 \cdot 10^{-2}$	$-1.096 \cdot 10^{-2}$	$-1.0878 \cdot 10^{-2}$	
$k_5 / \text{m}^7 \text{mol}^{-2}$	$-1 \cdot 10^{-19} - 1 \cdot 10^{-25}$	$-8.0037 \cdot 10^{-24}$	$-8.0065 \cdot 10^{-24}$	$-8.0029 \cdot 10^{-24}$	
$k_6 / \text{m}^7 \text{mol}^{-2}$	$-1 \cdot 10^{15} - 1 \cdot 10^{20}$	$9.001 \cdot 10^{16}$	$9.01 \cdot 10^{16}$	$9.0024 \cdot 10^{16}$	
Model 3 - Equations 17					
$D_{Mg^{2+}} \text{ Mg-5Gd}$	$1 \cdot 10^{-12} - 1 \cdot 10^{-4}$	$6.05 \cdot 10^{-9}$	$6.125 \cdot 10^{-9}$	$6.053 \cdot 10^{-9}$	[8]
$D_{Mg^{2+}} \text{ Mg-10Gd}$	$1 \cdot 10^{-12} - 1 \cdot 10^{-4}$	$9.53 \cdot 10^{-10}$	$9.721 \cdot 10^{-10}$	$9.608 \cdot 10^{-10}$	

guided by the experimental data are performed to specify the testing ranges for each of the uncertain parameter. The parametric space of the uncertain parameters are constructed for each model using the maximum and minimum limits of the test intervals, these values are given in Table 2.

2.4. Uncertainty Quantification Workflow

The following workflow is proposed for conducting UQ analyses for degradation models of Mg-based biodegradable implants. The workflow is illustrated in Figure 2, where four main steps are presented. The first step involves designing the computer experiments, as detailed in Section 2.3. This step includes defining the parametric space of the model's key parameters, determining sampling strategies and creating the sampling set. It is crucial to define the distribution of the key parameters and to specify

the Quantities of Interest (QoI) that need to be quantified, as presented in Table 1 for the three cases under consideration. Additionally, if adaptive sampling is used, the initial sampling set $\mathcal{X}_{train,init}$ must be defined in this step. Moving on to the second step of the workflow, which is how to deal with the original models. At this step, observations $\mathcal{Y}_{train,init}$ of the original models are gathered by evaluating the degradation models for the sampling sets generated during the DOE step. The construction of a surrogate model \mathcal{M}^S (Equation 21) is the focus of the third step. Here, the surrogate model functions are mapped onto the user-defined parametric space using observations from the original model. The surrogate models are trained and their parameters are optimized. In the case of adaptive sampling, this step will involve iteratively training the surrogate model until achieving the best surrogate model with the lowest (ϵ_{LOO}) (Equation 26). The optimal surrogate model, whether it be Kriging, PCE or PCK, is subsequently used for further UQ analysis. These analyses

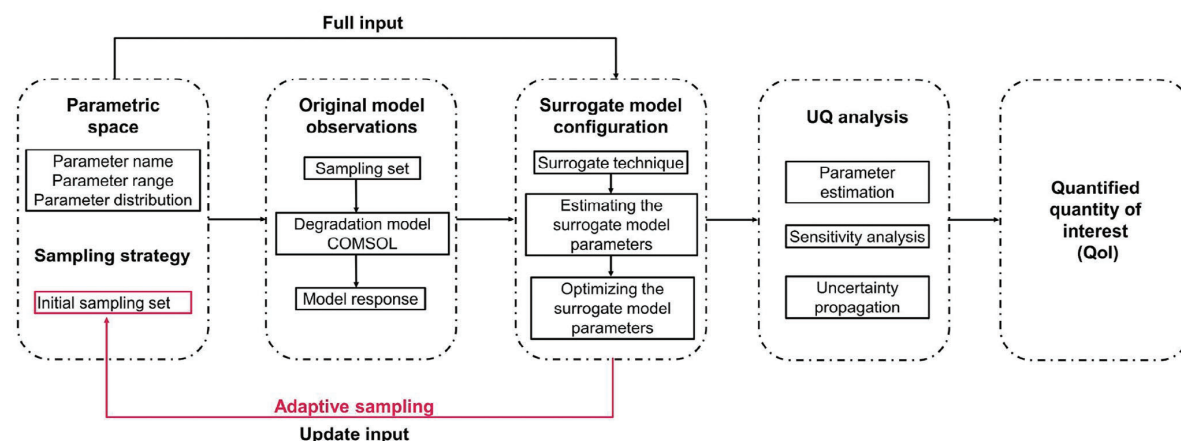


Figure 2. Workflow for quantifying the uncertainty associated with degradation models of Mg-based biodegradable implants using the surrogate modeling approach.

include parameter estimation, uncertainty propagation and sensitivity analysis. As the UQ analysis progresses, the original models are characterized, leading to the quantification of QoIs. As a result, the uncertainties associated with these quantities are taken into account during their presentation.

2.4.1. Sensitivity Analysis

Sobol' sensitivity analyses were performed to evaluate the variance contribution of each individual and combination of key parameters to the variance of the degradation model output.^[81–83] Throughout this study, how the variation in k_{deg} and t_{init} affects the degradation of pure Mg was examined, whereas the effect of varying k_{deg} , t_{init} and k_i on the precipitation model response is tested. Results for the variance-based sensitivity analysis are expressed by two sensitivity indices: the Sobol' first order sensitivity indices S_i , Equation (29a), indicate the importance of each parameter considered individually, while the total sensitivity indices S_{T_i} , Equation (29b), account for both the importance of individual parameters and interactions between parameter pairs.^[81]

$$S_i = \frac{\text{Var}(\mathcal{M}_i(X_i))}{\text{Var}(\mathcal{M}(X))} \quad (29a)$$

$$S_k^T = \sum_{k \in u} S_u \quad \text{for } k = \{1, 2, \dots, P\} \quad (29b)$$

where X is the parameter vector, X_i is a subset of surrogate model inputs with corresponding outputs M_i and P is the number of surrogate model evaluations. M_i is the surrogate model shape function defined by Equation (21).

2.4.2. Propagation of Uncertainty

Uncertainty propagation is the process of predicting the influence of uncertainties (e.g., measurement errors, model defects, etc.) in input variables on the uncertainty of output variables in a system or process,^[84,85] which can then be utilized to improve decision-making and risk assessment. To assess the propagation of uncertainty within the surrogate models the variation in the input parameters was reported in terms of ϵ_{LOO} (Equation 26). Here, we tested the change in ϵ_{LOO} between the single-shot and adaptive sampling. Moreover, the effect of changing the number of uncertain parameters over the surrogate models was also reported.

3. Results and Discussion

3.1. The Construction of Surrogate Models

The four different sampling methods tested in this study compared in terms of the average ϵ_{LOO} values of the constructed surrogate models based on ten random one-shot sample runs. The construction of each surrogate model was performed using the same test samples. Therefore, for the testing purpose of the single-shot sampling methods, it was necessary to gather

ten sample sets, with each set containing 22, 82, and 12 samples for models 1, 2, and 3, respectively. For single-shot sampling, Figure 3a–c shows that surrogate models constructed with training data sampled using LHS have the lowest ϵ_{LOO} values for all degradation models. Furthermore, LHS reduces the number of samples required while maintaining inference accuracy, with a conversion error given by $O((i-1)/N, i/N)$, where N represent the equally probable intervals between each input variable, and i represent a variable corresponding to one of these intervals, where $i \in [1, N]$. This can be attributed to the space-filling nature of LHS.^[74] In general, LHS generates random samples by dividing the range of input variables into equally probable intervals. In each dimension, each interval is sampled only once, which helps prevent random clustering issues as is the case with MC sampling. Nonetheless, surrogate models constructed using MC sampling have ϵ_{LOO} values close to LHS, as can be seen for model 1 and model 2, Figure 3a,b, respectively.

As the number of uncertain parameters increases, the degradation model becomes increasingly complex. This is illustrated in Figure 3b for model 2. Using single-shot sampling, more data sets are needed to enhance the accuracy of the constructed surrogate models for model 2. Moreover, the relatively high ϵ_{LOO} values for all single-shot sampling strategies presented in Figure 3a–c suggest that these strategies were unsuccessful in producing representative data sets that could be used to construct surrogate models with sufficient accuracy. Both Sobol and Halton sampling exhibit relatively high ϵ_{LOO} due to the strong correlation between generated samples resulting from the low dimensionality of the parametric space (d) of the three degradation models ($1 \leq d \leq 10$).^[22] Low dimensionality of the degradation model results in higher variation in ϵ_{LOO} values as can be observed for model 1, $d = 2$ and model 3, $d = 1$. While, for model 2, which has $d = 8$ less variation is observed. However, a large number of samples is necessary to ensure convergence due to the dependency of error conversion on both number of samples and dimensionality, namely $O(\log(N)^d/N)$ for Halton sampling, while it is $O(\log(N)^d/N)$ for Sobol sampling.

In general, as the dimensionality of the degradation model increases more samples are required to construct the surrogate model.^[30,80] As shown in Figure 3c, using the same sampling set constructed with LHS results in the same accuracy for all surrogate models of Model 3 with $d = 1$. This is because the dimensionality of a surrogate model is determined by the number of input parameters it needs to represent, which, in this case, is the diffusion coefficient of Mg^{2+} ions. For model 1 and 2 both PCE and PCK require more samples to improve their convergence and reduce ϵ_{LOO} values. On the other hand, Kriging models outperform the other surrogate models due to their ability to handle limited data sets since they were designed to utilize minimal sampling. This can be explained by the fact that the Kriging-based technique interpolates the simulation results and fits the Maximum Likelihood Estimation as well as the unbiased Linear Predictor-criterion on the results. Hence, it is recommended to use Kriging for cases where the dimensionality is less than 20.^[30,80]

The problem of training data size arises as the number of original model parameters increases, leading to increase the number of required samples. As evident from the results of one-shot sampling, as the size of the sampling set influence

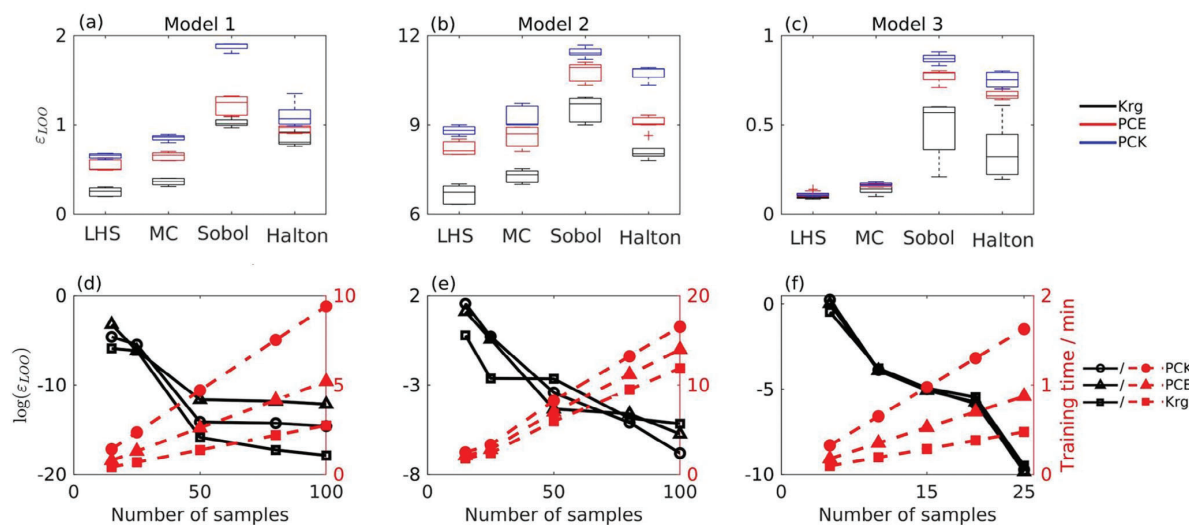


Figure 3. DOE comparison across the three degradation models, each represented by a column. Row 1 (panels a–c) illustrates the effect of different sampling methods on the ϵ_{LOO} error across the surrogate models. Row 2 (panels d–f) depicts the number of adaptive samples obtained using Algorithm 1, as functions of accuracy (ϵ_{LOO}), training time, and the type of surrogate model.

the cost associated with training and constructing these models. Figure 3(d–f) summarizes the ability of adaptive sampling algorithm based on LHS and using the semi-supervised CMM learning function on optimizing the number of samples, based on function of accuracy (ϵ_{LOO}) and training time to construct the surrogate models for the three degradation models. It is clear that as the sample size increases the training time increases for all surrogate models. Furthermore, the implementation of the adaptive sampling approach indicates that constructing surrogate model with an accuracy of 10^{-3} in terms of ϵ_{LOO} is possible with fewer number of samples even for model 2, which contains 8 uncertain parameters.

Adaptive sampling decreases the number of samples required to construct the surrogate models without affecting the accuracy of the models, as can be seen for the three degradation models in Figure 4a,b. The subplot in Figure 4a shows that for single-shot sampling with LHS, the curves of Kriging and PCE tend to coincide as the number of samples is above 30, while 58 samples are needed for PCK curve to converge to the same value. For adaptive sampling algorithm, Figure 4d, the three curves are coinciding after only 15 samples, which drastically reduces the computational cost and time. A comparable trend is observed for the other degradation models presented in the subplots in Figure 4b,e and c,f. For model 3, panels c, and f all surrogate curves coincide after ten samples. Overall, as the number of samples increases both single-shot LHS and adaptive sampling algorithm are converging to constant ϵ_{LOO} values. The effect of the number of parameters is presented in the third row of Figure 4g–i. Overall, the implementation of adaptive sampling algorithm reduces the propagation of error within the surrogate models. However, it is clear that for low dimensional models, specifically model 1 with $d < 3$, both PCE and PCK propagate higher error, while Kriging is more efficient due to its ability to deal with small data sets and lower dimensionality. However, for the case with 8 uncertain parameters,

model 2, the propagation of error within Kriging is higher with respect to other surrogates due to the tendency of Kriging to form ill-conditioned matrices under high dimensional models.^[86,87] In general, as the number of uncertain parameters increases the propagation of uncertainty, in terms of ϵ_{LOO} values, within the models increases too.

Figure 5 illustrates the breakdown of CPU-time. Collecting the training data, or the sampling phase, is the most CPU-intensive as illustrated in Figure 5a. We anticipate and attribute the extended duration of the sampling stage to the need to execute the original degradation models, which take, on average, 8, 25, and 90 min for each run for each of the three degradation models, respectively. Figure 5a shows that adaptive sampling reduces the CPU-time for the sampling stage, which is T_{BBN} in Equation (28). Overall, adaptive sampling reduces the T_{BBN} for the three degradation models. For model 2, it T_{BBN} takes twice as long as adaptive sampling, including the initial sampling and searching for new samples. In this case the higher T_{BBN} is attributed to the increased number of uncertain parameters. The CPU-time for constructing surrogate models, T_{SM} presented in Figure 5b showed that for the three degradation models PCK required higher time, which contributed to the fact that PCK involves the integration of two different techniques; PCE and Kriging. T_{SM} for the first and third FE degradation models are less than 1 min and this is due to the low number of uncertain parameters. On the other hand, T_{SM} increases for model 2 due to the complexity of the degradation model itself and the increased number of uncertain parameters. Figure 5c illustrates the parameter estimation time, T_{opt} , which is required by each surrogate model to estimate the key parameters for each of the degradation models. At this stage, surrogate models are used to speed up the calibration process. Figure 5c highlights that Kriging demands higher T_{opt} primarily due to the need for estimating the hyperparameters of Kriging. Further, Kriging's determination of the spatial covariance structure of the sampled

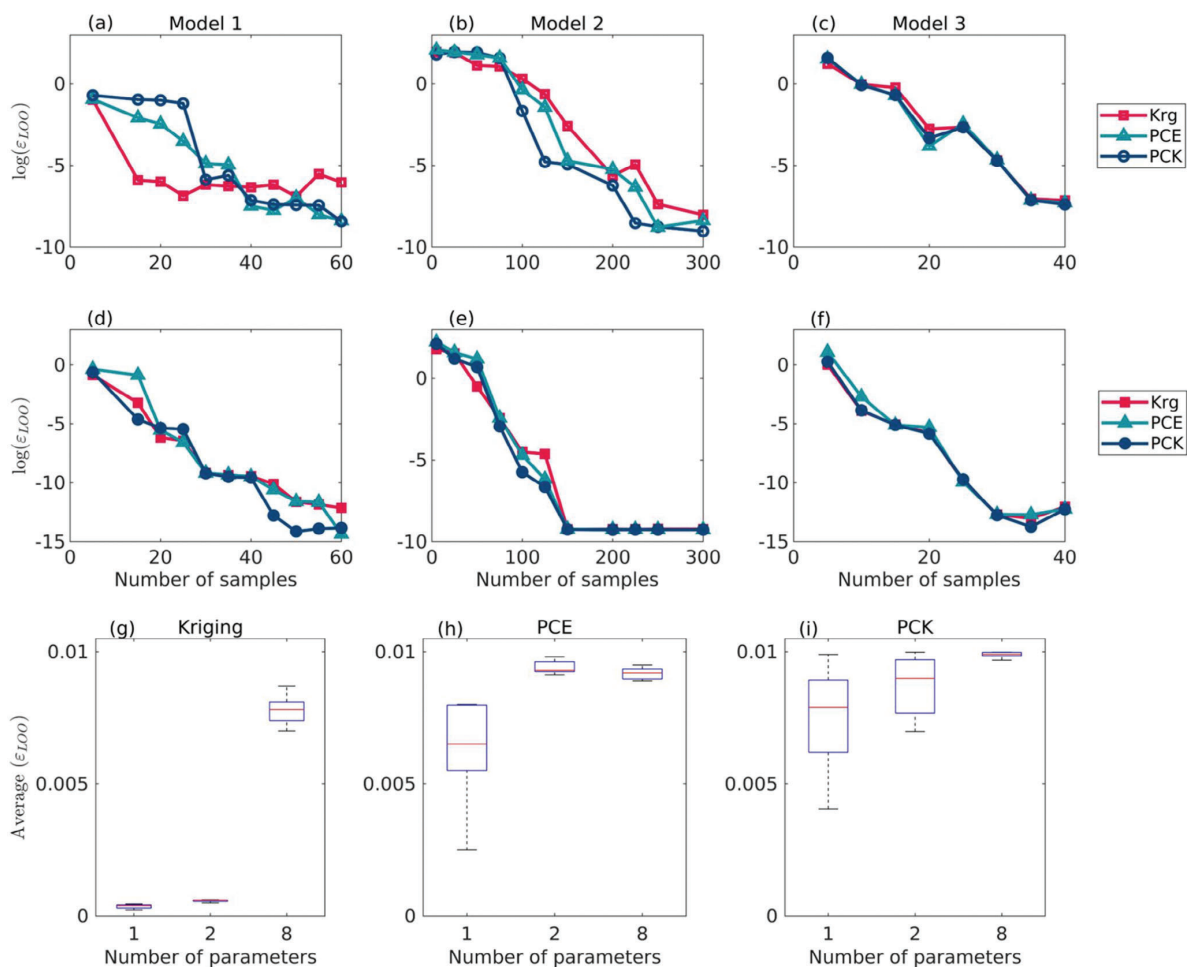


Figure 4. The effect of changing the number of samples and the number of parameters on error propagation. Row 1, panels a–c, illustrate the propagation of error as a function of the number of samples using single-shot sampling (LHS). Row 2, panels d–f, illustrate the propagation of error as a function of the number of samples using adaptive sampling (Algorithm 1). Row 3, panels g–i, present box plots of the average ϵ_{LOO} for surrogate models as a function of the number of parameters: g) Kriging, h) PCE, and i) PCK.

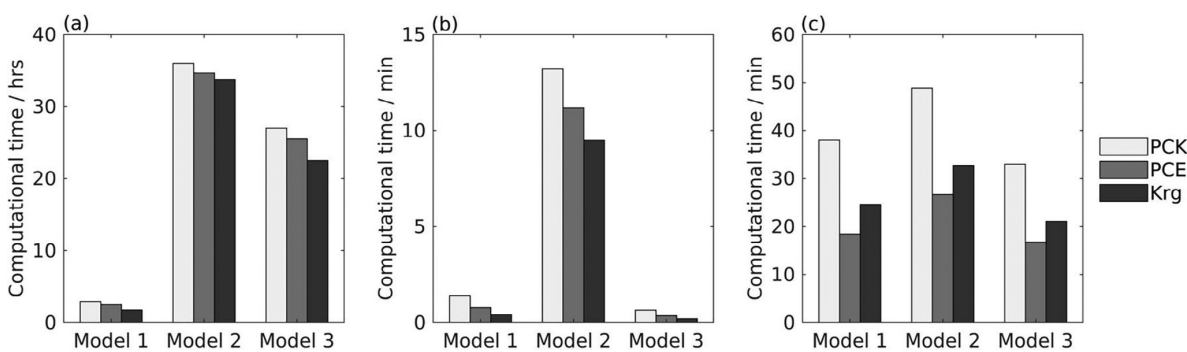


Figure 5. CPU-time for the three degradation models, a) T_{BB_N} : total sampling time b) T_{SM} : time to construct a surrogate model, c) T_{opt} : time to perform the parameter estimation based on surrogate models.

points contributes to the increased T_{opt} . The ability to analytically compute PCE coefficients significantly contributes to reducing the optimization time for PCE models across all cases,^[72] which also contributes to decreasing the computational costs of PCK.

In summary, the choice of sampling strategy and the size of the training sample set are critical for constructing accurate, robust, and efficient surrogate models, as well as for overcoming issues of underfitting. The findings underscore that as the dimensionality of the degradation model increases (model 3 < model 1 < model 2), a larger number of samples is necessary for accurate surrogate model construction. However, the proposed adaptive sampling algorithm reduced the required number of samples without compromising accuracy. Furthermore, PCE and PCK demonstrated lower error propagation in models with dimensions greater than two (model 2). CPU time analysis revealed that adaptive sampling significantly reduced the CPU time required for the sampling phase, particularly in high-dimensional models. PCE had the lowest time required to construct the surrogate models, while Kriging required more time for parameter estimation due to hyperparameter (*kernel*) optimization, and PCK had higher model construction times due to its integration of PCE and Kriging techniques.

To construct the surrogate models, initially, five sets of samples for each key parameter were randomly generated using LHS method and refined according to the adaptive sampling Algorithm 1. In total, three sets of sample groups were generated for each surrogate model. Kriging required 15, 50, and 7 samples for the three respective FE degradation models. For PCE and PCK, 25 samples were needed for models 1 and 2, while 10 samples were generated for model 3.

3.2. Performance of the Different Surrogate Models

Tested ranges for the key parameters of the degradation models and the optimal parameters as estimated by Kriging, PCE, and PCK for each model are given in Table 2. The key parameters estimated by the three surrogate models for all the degradation models have relatively close values. Based on this observation and considering the critical characteristics of size, time and accuracy, Kriging models are more suitable for parameter estimation tasks requiring lower computational time and higher accuracy. This observation is supported by the small reduction in the ϵ_{LOO} for the three surrogate models as presented in Table 3, for example for model 1, ϵ_{LOO} value, based on adaptive sampling, is $1.296 \cdot 10^{-4}$ for PCE and $1.308 \cdot 10^{-5}$ for PCK compared to $2.03 \cdot 10^{-4}$ for Kriging.

At each step, the performance of the surrogate models is evaluated in terms of ϵ_{LOO} , which measures the accuracy of the predictions of the surrogate model. During this stage, the key parameters outlined in Table 2, along with their respective ranges for constructing the parametric space, are estimated and quantified using surrogate models. The agreement between surrogate and original models are visualized in the QQ-plots in Appendix B. All the points on the QQ-plots of all surrogate models and tested degradation models fall near the 45-degree line, which indicates that the surrogate models are capturing the same underlying patterns in the data as the original degradation model.^[88,89]

Table 3. Validation of the performance of three surrogate models at the optimized number of samples, based on adaptive sampling, for degradation models. The performance is evaluated in terms of ϵ_{LOO} for surrogate model accuracy and NRMSE with respect to experimental data.

Model	ϵ_{LOO}			NRMSE		
	Kriging	PCE	PCK	Kriging	PCE	PCK
Model 1						
MMD	$2.03 \cdot 10^{-4}$	$1.296 \cdot 10^{-4}$	$1.308 \cdot 10^{-5}$	0.07	0.05	0.051
Model 2						
Mg	$5.312 \cdot 10^{-4}$	$3.703 \cdot 10^{-5}$	$1.082 \cdot 10^{-5}$	0.99	1.003	1.006
Ca				0.53	0.40	0.62
C				0.59	0.56	0.60
P				0.38	0.36	0.362
O				1.03	0.98	1.01
Model 3						
VL% _{Mg-5Gd}	$3.01 \cdot 10^{-4}$	$2.13 \cdot 10^{-6}$	$4.861 \cdot 10^{-6}$	0.03	0.07	0.08
VL% _{Mg-10Gd}	$7.04 \cdot 10^{-4}$	$3.71 \cdot 10^{-6}$	$6.089 \cdot 10^{-6}$	0.02	0.08	0.09

Subsequently, the optimal values of the key parameters are used to calibrate the output of the degradation models with respect to the in-house experimental data (Section. 2.1.2).

In view of the NRMSE values provided in Table 3, small deviation in the results can be observed for the performance of the surrogate models with respect to experimental data. This difference is due to the mathematical nature of the surrogate models, which controls the creation of the surrogate mapping function, explained in Table 1. The different mapping function of surrogate models enables Kriging to interpolate local variations of the output of the degradation model. Polynomial surrogates (e.g., PCE), on the other hand, are generally approximated by the global behaviors of degradation models. In this way, PCK can explain the better agreement with experimental data, as it combines local and global approximations. However, the efficiency of the adaptive-sampling leads to enhance the quality of the training data, hence, the surrogate models, Kriging, PCE and PCK are able to characterize the three degradation models accurately, as can be seen in Figure 6 for PCK model. The performance of PCE and Kriging for the three degradation models figures are presented in Appendix B. However, it is crucial to note that the generalization of any of these constructed surrogate models to simulate other implants under different conditions or degradation phenomena necessitates further validation and training.

All surrogate models performed robustly and captured the underlying data patterns, with PCK offering the best agreement by incorporate both interpolation of local variations (from Kriging) and approximate the global behaviors of degradation models by the polynomial trend (PCE). However, Kriging demonstrated slightly higher computational efficiency (less CPU time) with acceptable accuracy (based on NRMSE) for parameter estimation.

3.3. Sensitivity Analysis (SA)

To assess the sensitivity of model responses to uncertainties in input parameters, Sobol' indices were computed and compared for the multi-parameter models (models 1 and 2). The first-order

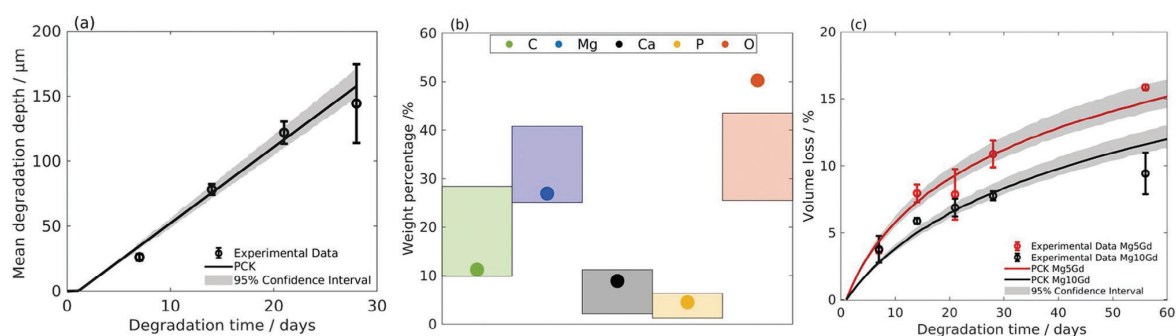


Figure 6. The performance of PCK for the three degradation models: a) model 1, b) model 2, the weight percentage plot, the scatter points are the predicted weight percentage from the PCK model, while the shaded areas indicate the minimum and maximum mean values from the experiment c) model 3.

Sobol' indices (S_i) quantify the direct effect of each individual parameter, while the total Sobol' indices (S_{T_i}) capture all interactions involving that parameter. For clarity, the Sobol' indices for the three surrogate models constructed for the degradation model 1 are presented in a bar chart in **Figure 7**. The indices were visualized for the first ten days of degradation, as the values stabilized beyond this point. For the Kriging surrogate model of model 1, S_i indicates that the two parameters k_{deg} and t_{init} primarily compete during the first ten days, with t_{init} being the most influential over MDD. After the eighth day, both parameters exert nearly equal influence. This pattern is mirrored in the total Sobol' indices (S_{T_i}). In contrast, the Sobol' indices derived from the PCE and PCK models suggest that t_{init} mainly affects the initial sigmoid activation during the early stages (2 days) of the degradation process, after which k_{deg} becomes dominant as the degradation process is governed by the degradation reaction. This

finding aligns with the mathematical expression of MDD (Equation 11). Moreover, the small differences between S_i and S_{T_i} suggest that the interaction between k_{deg} and t_{init} is relatively minor on the long term and can be disregarded without significantly affecting the model's predictions if a proper optimization step is introduced for t_{init} . Consequently, the model complexity can be reduced by running the model for only up to three days and optimizing and setting a constant value for t_{init} . With the simplified model, the other parameters can then be calibrated. However, the Sobol' indices based on the Kriging surrogate model suggest that both parameters have relatively equal influence over MDD, indicating a correlation between them. This finding appears contradictory, given that the negligible difference between S_i and S_{T_i} , except on day 1, supports the same conclusion as the PCE and PCK models: there is no significant interaction between these two parameters. The observed differences in the interpretation

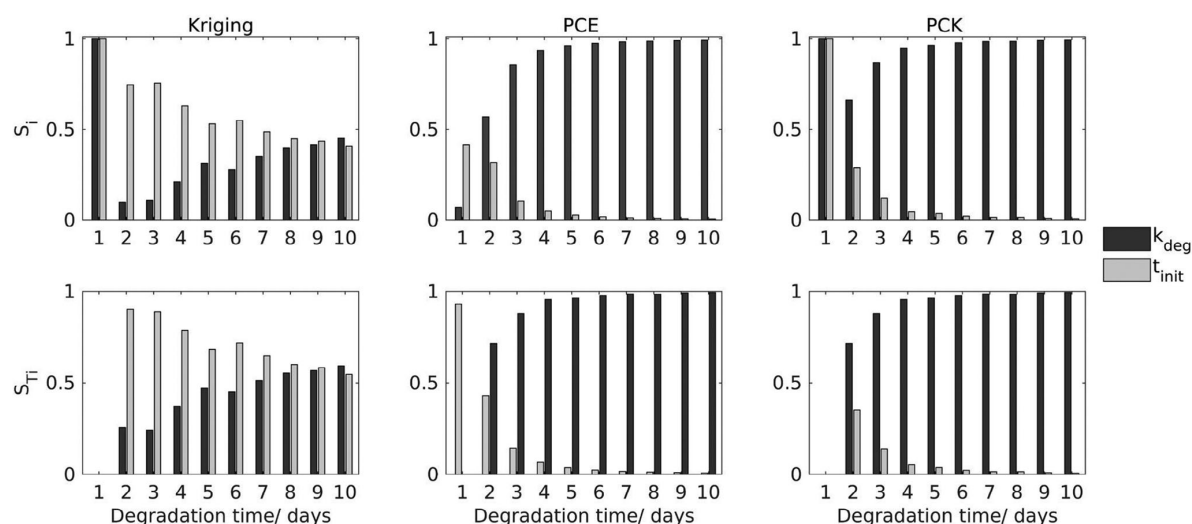


Figure 7. Global sensitivity analysis of case 1 for the first ten days of degradation. The Sobol' indices (for uncertain parameters of the degradation model. The first Sobol' indices (S_i) and total effect indices (S_{T_i}) measured following surrogate-based global sensitivity analysis for the degradation reaction, where the uncertain input variables are k_{deg} and t_{init} and the QoI is MDD.

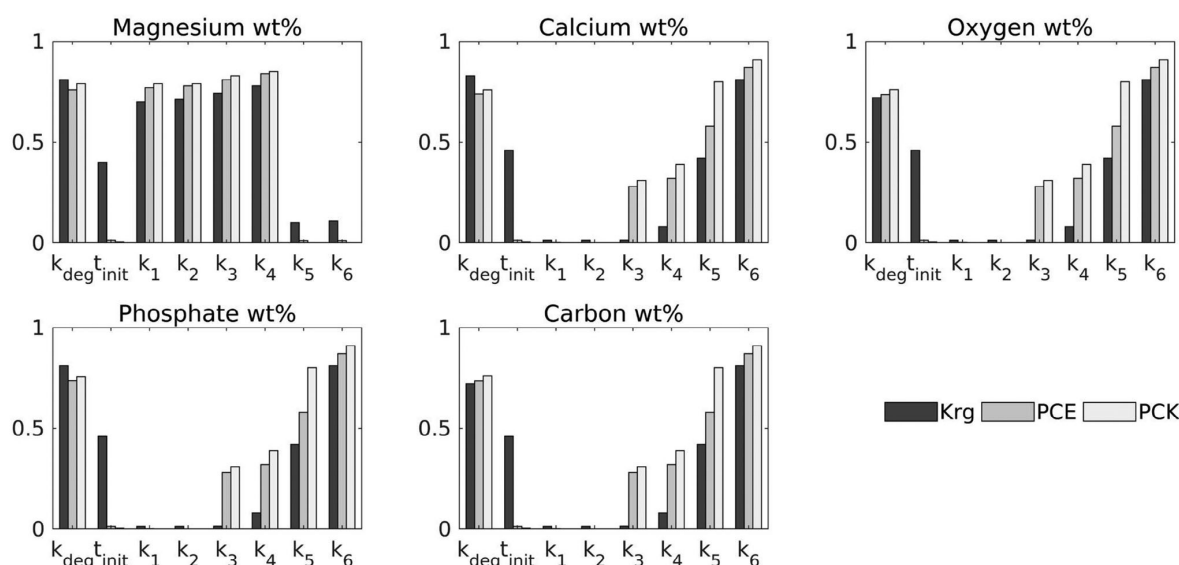


Figure 8. Sobol' indices (S_{T_i}) for key parameters of precipitate formation on the surface of Mg implant model, a) Oxygen, b) Magnesium c) Carbon, d) Calcium, and e) Phosphate. The total effect indices (S_{T_i}) were measured following surrogate-based global sensitivity analysis. The sum of (S_{T_i}) can exceed one. In the absence of interactions, equality is obtained.

of Sobol' indices across surrogate models can be attributed to the methods used to compute these indices. In the case of PCE and PCK, the Sobol' indices are calculated analytically by evaluating the integrals in the model decomposition, which significantly reduces computational costs. On the other hand, Kriging struggles to reflect these interactions due to the stochastic uncertainty introduced by the Monte Carlo methods typically used to evaluate Sobol' indices. This discrepancy highlights the importance of clearly defining the objectives of using surrogate models, i.e., whether they are applied only to accelerate tasks such as parameter calibration, or whether they are used for understanding the underlying system and the influence of certain parameters thereon as in sensitivity analysis.

For model 2, which simulates the precipitation reactions during Mg degradation, the calculated Sobol' indices were found to be nearly equal ($S_{T_i} - S_i < 0.005$) for all surrogate models, so only S_{T_i} are presented in Figure 8. The sensitivity analysis showed similar results between the PCE and PCK models, but significant differences were observed when compared to the Sobol' indices derived from the Kriging surrogate. Specifically, when assessing the influence of the degradation kinetic parameters, k_{deg} and t_{init} , on the wt% of Mg, Ca, O, P, and C, the Kriging model indicated that t_{init} has a significant effect. In contrast, both PCE and PCK showed that t_{init} has a negligible impact, which aligns with the formulation of model 2 where t_{init} had limited influence on precipitate formation in the degradation layer. Thus, t_{init} can be excluded from further analysis and assigned a constant value to reduce the dimensionality of the analysis. Meanwhile, k_{deg} is found to influence the formation of all precipitates, which means it is crucial to include the kinetic of the degradation during the analysis of the precipitation process. All three surrogate models consistently indicated that parameters k_1 and k_2 have a minimal effect on wt% of

Ca, O, P, and C, suggesting that these parameters can be treated as constants for modeling these elements. This is surprising, as both brucite (Equation 4, k_{-1}) and magnesite (Equation 5, k_{-2}) contain O and the latter also C. In contrast, the models revealed a significant influence of k_1 and k_2 on wt% of Mg, indicating that calibration for both parameters should focus primarily on the wt% of Mg. Interestingly, k_3 and k_4 had uniform effects over all elemental weight percentages except Mg, which suggests that both parameters might be considered as global parameters that affect all elemental wt% equally except wt% of Mg. The exception for Mg in relation to k_3 and k_4 likely stems from correlations between precipitate reactions. Moreover, except for Mg, all elemental wt% are strongly influenced by k_5 and k_6 , which are mainly associated with the precipitation of two precipitation calcite and hydroxyapatite. The strong correlation shown by S_{T_i} indicates the presence of competing reactions between calcium and phosphate ions in the formation of hydroxyapatite. Furthermore, similar dependencies were observed for oxygen, magnesium, and carbon. These findings not only streamline the modeling process but also highlight potential mechanistic differences in elemental behaviors, particularly for Mg, offering directions for further investigation into the system's underlying chemistry. Note that both PCE and PCK effectively captured these correlations, whereas the Sobol' indices derived from Kriging did not reflect all the interactions. This disparity may be due to the tendency of Sobol' indices derived from Kriging to emphasize underlying global trends in the data samples. Additionally, the mathematical assumption of a constant mean (Equation 23) limits the precision of the Kriging models' predictive ability.

The Sobol' indices derived based on PCE and PCK reflected the influence of the key parameters and their interactions on the degradation models more accurately than Kriging. The results of

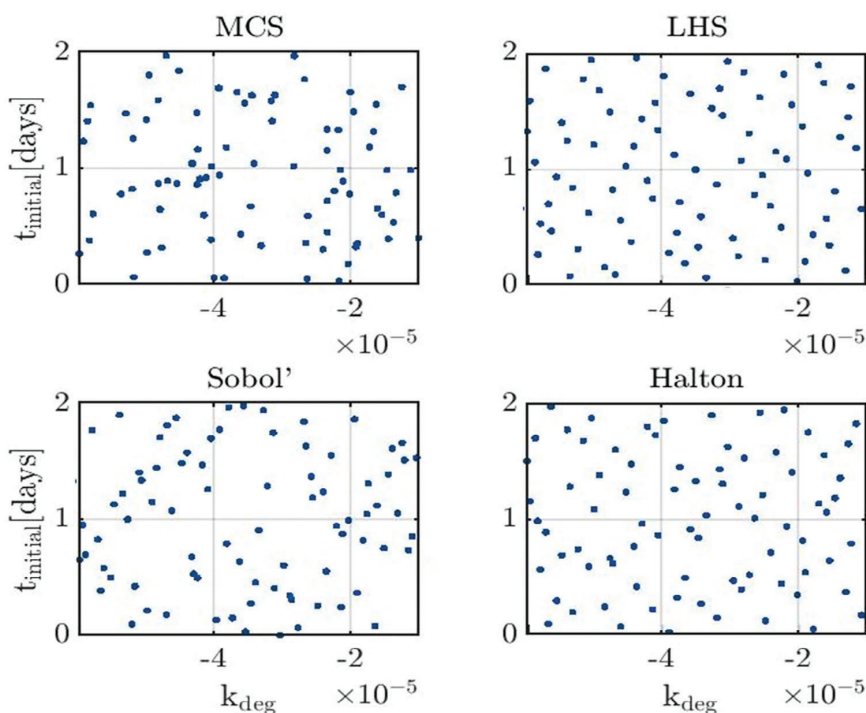


Figure A1. Samples generated by various sampling scheme of the two input parameters; t_{init} and k_{deg} . The parameters are plotted against each other in pairs, using different sampling schemes: Monte Carlo sampling (MCS), Latin hypercube sampling (LHS), sampling based on Sobol' sequences and Halton sampling. Each of the parameters follows independent a uniform distribution within the range [03] for t_{init} and $[-1 \times 10^{-4} - 1 \times 10^{-3}]$ for k_{deg} .

sensitivity analysis not only streamline the modeling process, but also suggest avenues for further research into the mechanisms governing the elemental behaviors in the system.

4. Conclusion

This research paper presents a comprehensive Uncertainty Quantification (UQ) workflow, designed to enhance the development and quantification of mathematical models simulating the biodegradation of magnesium-based implants. Key findings include:

1. Surrogate model selection is crucial: Kriging excels in parameter estimation, while PCE and PCK are superior for uncertainty prediction, particularly in high-dimensional systems.
2. Adaptive sampling significantly reduces required sample sizes without compromising accuracy ($\epsilon_{LOO} < 10^{-4}$), addressing the computational challenges of UQ analysis.
3. The workflow demonstrates high adaptability across various degradation systems and model complexities, providing a robust framework for UQ implementation.
4. Rigorous validation of surrogate models is essential to maintain system accuracy and reliability.

The developed UQ workflow offers a scalable and efficient approach for quantifying uncertainty in Mg-based implant degradation models. While future work may focus on more complex in

vivo corrosion scenarios, this study establishes a solid foundation for surrogate modeling in simpler in vitro models. The methods presented are well-established and flexible, making them applicable to a wide range of corrosion and degradation models, regardless of complexity. This research significantly contributes to the field by providing a best-practice guide for implementing UQ in biodegradation modeling, paving the way for more accurate and computationally feasible analyses in biomedical engineering and related disciplines.

Moreover, future work could focus on applying the proposed UQ workflow to a wider range of stochastic and phenomenological degradation models. Additionally, it would be valuable to investigate the performance of surrogate models in capturing multi-scale interactions in complex degradation processes, as well as exploring the integration of domain-specific knowledge to enhance surrogate model accuracy for specialized degradation phenomena.

Appendix A: Brief Review of the Sampling Strategies

For the scope of the current work, we compared four different sampling strategies Monte Carlo sampling (MC), Latin Hypercube sampling (LHS), Sobol' sequence sampling (Sobol) and Halton sequence sampling (Halton). Statistically, these models are good choices because of their one-shot sampling characteristics, which allows them to determine the sample size at once. The main problem associated with these methods

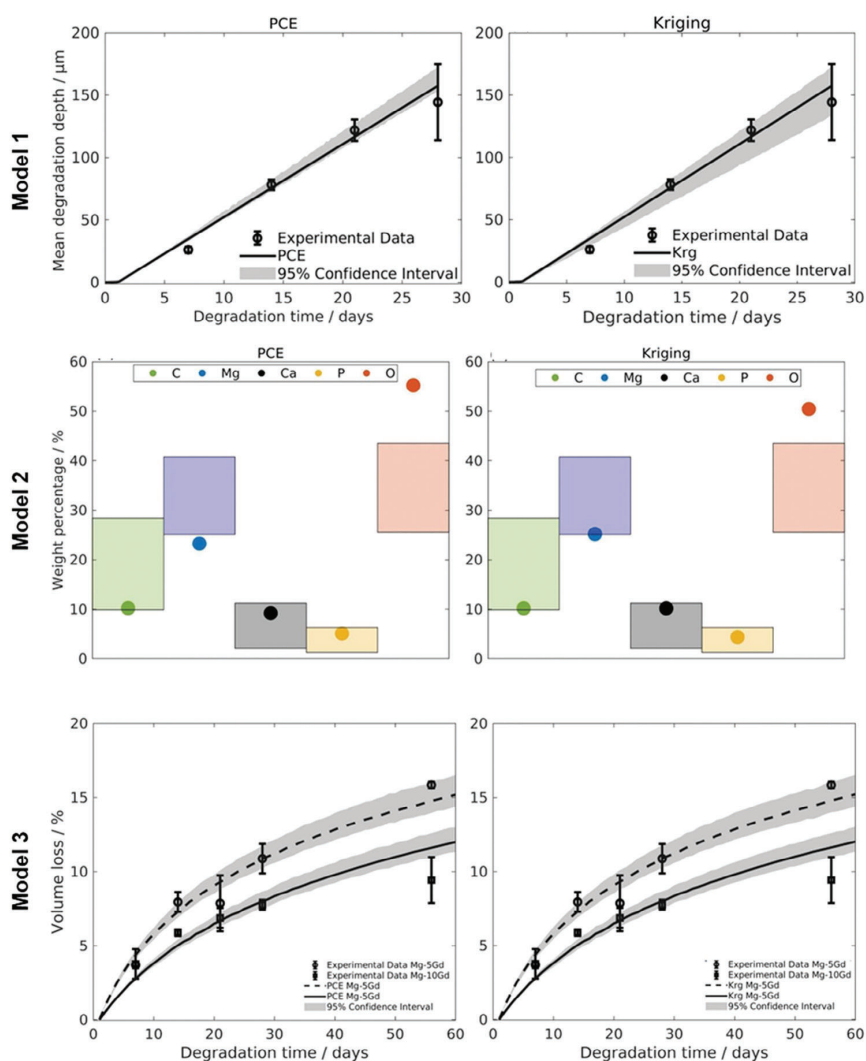


Figure B1. The performance of PCE and Kriging for the three degradation models.

is the possibility of under- or over-sampling.^[25] MC sampling is a non-intrusive method, no changes to the model are required, and it is a straight forward method, where random samples are drawn from the probability distribution of the input and then run it through the test models. Slow conversion is one of the major drawbacks of MC, where the sampling error decreases as $O(1/\sqrt{N})$. For a half-reduction in sampling error, the sample size needs to be quadrupled.^[90] Nonetheless, for UQ tasks with high dimensionality, MC is still a competitive method because it is not affected by the dimensionality of inputs, which does not affect sampling error.^[91] By using Latin Hypercube sampling (LHS), the number of samples is reduced while maintaining inference accuracy with a sampling error $O((i-1)/N, i/N)$. LHS generates random samples by dividing the ranges of the input variables into equally probable intervals, where each interval in each dimension is only sampled for one time, which avoid the random clumping that can occur with pure MC, as seen in Figure A1. Due to this LHS has better space-filling properties compared to other sampling methods.^[65,90,92]

There is no dimensional limitation to LHS, which is an advantage over the Halton sampling $O(\log(N)^d/N)$. Adding to that, Helton sampling is a deterministic method that works for $d > 1$ and tends to generate samples with strong correlations for lower dimensions.^[22] Sobol sampling claimed to be superior to MC and LHS but to reduce the sampling error and ensure convergence a non-realistic number of samples is required (above 1 million).^[22,90] Considering the previous discussion, for the biodegradation system for Mg-based implants we choose to use LHS, which is able to produce more consistent results with fewer number of runs across different dimensions of the models.^[65,90,92] Furthermore, the use of LHS is more advantageous for models with high input, such as the formation of precipitates on a Mg surface model. This is a higher dimensional model with eight input parameters. The increased number of samples can be added to the experiment design through sample enrichment. This is where additional samples are generated based on the analysis of the previous samples via nested LHS, where the enriched samples formed a pseudo LHS.^[93]

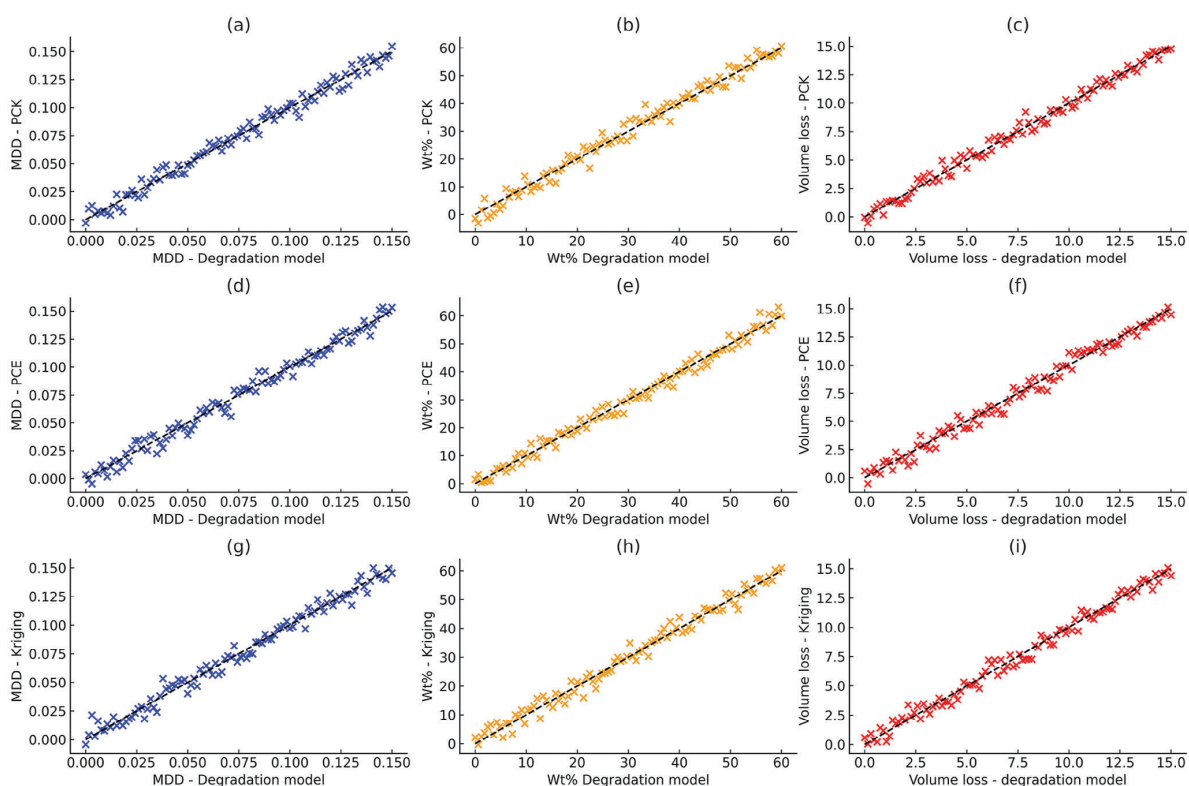


Figure B2. QQ plots for the three degradation models, columns are model 1, model 2 and model 3, row 1 is QQ plot to compare degradation models predictions versus PCK, row 2 is QQ plot to compare degradation models' predictions versus PCE and row 3 row 1 is QQ plot to compare degradation models predictions versus Kriging.

Appendix B: The Performance of Surrogate Models

The **Figure B1** shows the performance of the surrogate models for the three degradation models estimated using PCE and Kriging, while **Figure B2** shows the QQ-plots, which compare the predictions of the degradation models versus the surrogate models.

Acknowledgements

This research was supported in part through the Maxwell computational resources operated at Deutsches Elektronen-Synchrotron, Hamburg, Germany. This work was supported by the Helmholtz-Incubator project Uncertainty Quantification and the German Ministry for Education and Research (16DKWN112C).

Open access funding enabled and organized by Projekt DEAL.

Conflict of Interest

The authors declare no conflict of interest.

Author Contributions

T.A. contributed to various key aspects of the project, including conceptualization, formal analysis, software development, methodology, investigation, and the writing of the original draft. R.W.R. played a supervisory

role while also providing valuable insights through writing review and editing. Meanwhile, B.Z.P. focused on supervision and secured funding for the project, in addition to contributing to conceptualization, editing and writing of the original draft.

Data Availability Statement

The data that support the findings of this study are available from the corresponding authors upon reasonable request.

Keywords

biodegradable Mg-implants, propagation, surrogate model, uncertainty, UQ

Received: April 4, 2024

Revised: September 2, 2024

Published online:

- [1] J. Gonzalez, R. Q. Hou, E. P. S. Nidadavolu, R. Willumeit-Römer, F. Feyerabend, *Bioact. Mater.* **2018**, *3*, 174.
- [2] B. Luthringer, F. Feyerabend, R. Willumeit, *Magnes. Res.* **2014**, *27*, 142.

- [3] A. Myrissa, N. A. Agha, Y. Lu, E. Martinelli, J. Eichler, G. Szakács, C. Kleinhans, R. Willumeit-Römer, U. Schäfer, A.-M. Weinberg, *Mater. Sci. Eng.: C* **2016**, *61*, 865.
- [4] A. Rasheed, O. San, T. Kvamsdal, *IEEE Access* **2020**, vol. 8, pp. 21980–22012.
- [5] M. de Angelis, A. Gray, S. Ferson, E. Patelli, *Mechan. Syst. Signal Process.* **2023**, *186*, 109877.
- [6] Á. Bárkányi, T. Chován, S. Németh, J. Abonyi, *Processes* **2021**, *9*, 476.
- [7] A. Hermann, A. Shojaei, D. Steglich, D. Höche, B. Zeller-Plumhoff, C. J. Cyron, *Int. J. Mech. Sci.* **2022**, *220*, 107143.
- [8] T. Al Baraghteh, A. Hermann, A. Shojaei, R. Willumeit-Römer, C. J. Cyron, B. Zeller-Plumhoff, *Corros. Mater. Degrad.* **2023**, *4*, 274.
- [9] M. Abdallah, A. Joplin, M. Elahinia, H. Ibrahim, *Corros. Mater. Degrad.* **2020**, *1*, 219.
- [10] E. L. Boland, R. Shine, N. Kelly, C. A. Sweeney, P. E. McHugh, *Ann. Biomed. Eng.* **2016**, *44*, 341.
- [11] Z. Zhang, X. Lu, Y. Yan, *J. Magnesium Alloys* **2021**, *10*, 2847.
- [12] E. L. Boland, R. Shine, N. Kelly, C. A. Sweeney, P. E. McHugh, *Ann. Biomed. Eng.* **2016**, *44*, 341.
- [13] T. Albaraghteh, R. Willumeit-Römer, B. Zeller-Plumhoff, *J. Magnesium Alloys* **2022**, *69*, 191.
- [14] Y. Wang, D. L. McDowell, *Uncertainty Quantification in Multiscale Materials Modeling*, Elsevier, Amsterdam, Netherlands **2020**.
- [15] R. Ghanem, D. Higdon, H. Owhadi, *Handbook of Uncertainty Quantification*, vol. 6, Springer, Cham, Switzerland **2017**.
- [16] J. Zhang, J. Yin, R. Wang, *Math. Probl. Eng.* **2020**, *2020*, 6068203.
- [17] M. Baniassadi, M. Baghani, Y. Remond, in *Applied Micromechanics of Complex Microstructures*, Elsevier, Amsterdam, Netherlands **2023**, pp. 253–297.
- [18] O. P. Le Maître, O. M. Knio, H. N. Najm, R. G. Ghanem, *J. Comput. Phys.* **2001**, *173*, 481.
- [19] J. Son, Y. Du, *Comput. Chem. Eng.* **2020**, *134*, 106685.
- [20] O. M. Knio, O. P. Le Maître, *Fluid Dynam. Res.* **2006**, *38*, 616.
- [21] D. Ye, A. Nikishova, L. Veen, P. Zun, A. G. Hoekstra, *Reliab. Eng. Syst. Saf.* **2021**, *214*, 107734.
- [22] R. G. McClarren, *Uncertainty Quantification and Predictive Computational Science*, vol. 1, Springer International Publishing, Cham, **2018**.
- [23] B. Sudret, *ETH Zürich Research Collection* **2018**.
- [24] B. Sudret, S. Marelli, J. Wiart, *2017 11th European Conference on Antennas and Propagation (EUCAP)*, IEEE, Paris, France **2017**.
- [25] K. Cheng, Z. Lu, C. Ling, S. Zhou, *Struct. Multidisc. Optimiz.* **2020**, *61*, 1187.
- [26] M. P. Rumpfkeil, D. Bryson, P. Beran, *Algorithms* **2022**, *15*, 101.
- [27] C. K. J. Hou, K. Behdinan, *Data Sci. Eng.* **2022**, *7*, 402.
- [28] M. Böttcher, F. Leichsenring, A. Fuchs, W. Graf, M. Kaliske, *PAMM* **2021**, *20*, 1.
- [29] A. I. J. Forrester, A. Söbester, A. J. Keane, *Engineering Design via Surrogate Modelling*, Wiley, Chichester, UK **2008**.
- [30] K. McBride, K. Sundmacher, *Chem. Ing. Tech.* **2019**, *91*, 228.
- [31] B. Gaspar, A. Teixeira, C. G. Soares, *Probabil. Eng. Mech.* **2014**, *37*, 24.
- [32] N. T. Kirkland, M. P. Staiger, D. Nisbet, C. H. J. Davies, N. Biribilis, *JOM* **2011**, *63*, 28.
- [33] A. Atrens, G.-L. Song, M. Liu, Z. Shi, F. Cao, M. S. Dargusch, *Adv. Eng. Mater.* **2015**, *17*, 400.
- [34] J. Gonzalez, R. Q. Hou, E. P. S. Nidadavolu, R. Willumeit-Römer, F. Feyerabend, *Bioact. Mater.* **2018**, *3*, 174.
- [35] J. Song, J. She, D. Chen, F. Pan, *J. Magnesium Alloys* **2020**, *8*, 1.
- [36] N. Wint, N. Cooze, J. Searle, J. Sullivan, G. Williams, H. McMurray, G. Luckeneder, C. Riener, *J. Electrochem. Soc.* **2019**, *166*, C3147.
- [37] M. Kieke, F. Feyerabend, J. Lemaître, P. Behrens, R. Willumeit-Römer, *BioNanoMaterials* **2016**, *17*.
- [38] B. Zeller-Plumhoff, M. Gile, M. Priebe, H. Slominska, B. Boll, B. Wiese, T. Würger, R. Willumeit-Römer, R. H. Meißner, *Corros. Sci.* **2021**, *182*, 109272.
- [39] B. Zeller-Plumhoff, T. AlBaraghteh, D. Höche, R. Willumeit-Römer, *J. Magnesium Alloys* **2022**, *10*, 965.
- [40] B. Zeller-Plumhoff, D. Laipple, H. Ćwieka, K. Iskhakova, E. Longo, A. Hermann, S. Flenner, I. Greving, M. Storm, R. Willumeit, *Bioact. Mater.* **2021**, *6*, 4368.
- [41] B. Zeller-Plumhoff, H. Helmholz, F. Feyerabend, T. Dose, F. Wilde, A. Hipp, F. Beckmann, R. Willumeit-Römer, J. U. Hammel, *Mater. Corros.* **2018**, *69*, 298.
- [42] W. Sun, G. Liu, L. Wang, T. Wu, Y. Liu, *J. Solid State Electrochem.* **2013**, *17*, 829.
- [43] J. A. Grogan, B. J. O'Brien, S. B. Leen, P. E. McHugh, *Acta Biomater.* **2011**, *7*, 3523.
- [44] S. Scheiner, C. Hellmich, *Corros. Sci.* **2007**, *49*, 319.
- [45] Z. Shen, M. Zhao, D. Bian, D. Shen, X. Zhou, J. Liu, Y. Liu, H. Guo, Y. Zheng, *J. Mater. Sci. Technol.* **2019**, *35*, 1393.
- [46] J. A. Grogan, S. B. Leen, P. E. McHugh, *Acta Biomater.* **2014**, *10*, 2313.
- [47] J.-C. Zhao, *Annu. Rev. Mater. Res.* **2005**, *35*, 51.
- [48] D. Krüger, S. Galli, B. Zeller-Plumhoff, D. F. Wieland, N. Peruzzi, B. Wiese, P. Heuser, J. Moosmann, A. Wennerberg, R. Willumeit-Römer, *Bioact. Mater.* **2022**, *13*, 37.
- [49] B. Zeller-Plumhoff, M. Gile, M. Priebe, H. Slominska, B. Boll, B. Wiese, T. Würger, R. Willumeit-Römer, R. H. Meißner, *Corros. Sci.* **2021**, *182*, 109272.
- [50] D. Krüger, B. Zeller-Plumhoff, B. Wiese, S. Yi, M. Zuber, D. C. Wieland, J. Moosmann, R. Willumeit-Römer, *J. Magnesium Alloys* **2021**, *9*, 2207.
- [51] S. Zeng, X. Duan, J. Chen, L. Yan, *Adv. Aerodyn.* **2021**, *4*, 3.
- [52] G. Aversano, G. D'Alessio, A. Coussement, F. Contino, A. Parente, *Results. Eng.* **2021**, *10*, 100223.
- [53] B. S. J. W. R. Schöbi, P. Kersaudy, *ETH Zurich, Switzerland; Orange Labs research, HAL Id: hal-01432550* **2014**.
- [54] G. Blatman, B. Sudret, *J. Comput. Phys.* **2011**, *230*, 2345.
- [55] A. Bhosekar, M. Ierapetritou, *Comput. Chem. Eng.* **2018**, *108*, 250.
- [56] J. P. C. Kleijnen, *Europ. J. Operat. Res.* **2009**, *192*, 707.
- [57] J. Tian, C. Sun, J. Zeng, H. Yu, Y. Tan, Y. Jin, in *2017 IEEE Symposium Series on Computational Intelligence (SSCI)*, IEEE, New Jersey **2017**, pp. 1–8.
- [58] X. Shang, Z. Zhang, H. Fang, B. Li, Y. Li, *Adv. Eng. Inform.* **2023**, *58*, 102186.
- [59] X. Wu, C. Wang, T. Kozłowski, in *Int. Conf. Math. Comput. Meth. Appl. Nuclear Sci. Eng., Jeju, Korea* **2017**.
- [60] P. S. Palar, K. Shimoyama, in *AIAA Scitech 2019 Forum*, **2019**, p. 2209.
- [61] P. Benner, S. Griwet-Talocia, A. Quarteroni, G. Rozza, W. Schilders, L. M. Silveira, *System-and Data-driven Methods and Algorithms, De Gruyter, Berlin* **2021**.
- [62] J. C. García-Merino, C. Calvo-Jurado, E. García-Macías, *J. Math. Chem.* **2022**, *60*, 1555.
- [63] G. Aversano, G. D'Alessio, A. Coussement, F. Contino, A. Parente, *Results Eng.* **2021**, *10*, 100223.
- [64] Z. Liu, S. Zhouzhou, P. Zhu, X. Can, *ASME 2020 International Design Engineering Technical Conferences and Computers and Information in Engineering Conference* **2020**, ASME, Virtual, Online.
- [65] A. Bhosekar, M. Ierapetritou, *Comput. Chem. Eng.* **2018**, *108*, 250.
- [66] B. Ankenman, B. L. Nelson, J. Staum, *Oper. Res.* **2010**, *58*, 371.
- [67] L. Geris, D. Gomez-Cabrero, *Studies in Mechanobiology, Tissue Engineering and Biomaterials* **2016**, *10*, 973.
- [68] G. Lee, W. Kim, H. Oh, B. D. Youn, N. Kim, *Struct. Multidisc. Optimiz.* **2019**, *60*.
- [69] L. Zhao, K. Choi, I. Lee, *AIAA J.* **2011**, *49*, 2034.
- [70] S. Marelli, B. Sudret, *Vulnerability, Uncertainty, and Risk*, ASCE, UK, **2014**, pp. 2554–2563.
- [71] J. A. Paulson, M. Martin-Casas, A. Mesbah, *PLoS Comput. Biol.* **2019**, *15*, e1007308.

- [72] B. Sudret, S. Marelli, J. Wiart, *2017 11th European Conference on Antennas and Propagation (EUCAP)*, IEEE, Paris, France, **2017**, pp. 793-797.
- [73] J. N. Fuhg, A. Fau, U. Nackenhorst, *Arch. Comput. Meth. Eng.* **2021**, *28*, 2689.
- [74] E. Camporeale, A. Agnihotri, C. Rutjes, *Int. J. Uncertainty Quantif.* **2017**, *7*, 4.
- [75] R. Jin, W. Chen, A. Sudjitanto, *ASME 2002 International Design Engineering Technical Conferences and Computers and Information in Engineering Conference*, ASME, Montreal, Quebec, Canada **2002**.
- [76] A. Golzari, M. Haghghat Sefat, S. Jamshidi, *J. Petrol. Sci. Eng.* **2015**, *133*, 677.
- [77] D. R. Jones, M. Schonlau, W. J. Welch, *J. Global Optimiz.* **1998**, *13*, 455.
- [78] S. H. Kim, Á. F. Boukouvala, S. H. Kim, F. Boukouvala, *Optimiz. Lett.* **2020**, *14*, 989.
- [79] S. S. Jin, H. J. Jung, *Comput. Struct.* **2016**, *168*, 30.
- [80] R. Alizadeh, J. K. Allen, F. Mistree, *Res. Eng. Design* **2020**, *31*, 275.
- [81] I. Azzini, T. A. Mara, R. Rosati, *Environm. Modell. Softw.* **2021**, *144*, 105167.
- [82] N. Tsokanas, R. Pastorino, B. Stojadinović, *Mach. Learn. Knowl. Extract.* **2021**, *4*, 1.
- [83] H. Forero-Hernandez, M. N. Jones, B. Sarup, A. D. Jensen, J. Abildskov, G. Sin, *Comput. Chem. Eng.* **2020**, *133*, 106631.
- [84] C. Lataniotis, S. Marelli, B. Sudret, *Int. J. Uncert. Quantif.* **2020**, *10*, 55.
- [85] C. van Mierlo, A. Persoons, M. G. Faes, D. Moens, *Computers & Structures* **2023**, *275*, 106910.
- [86] J. P. C. Kleijnen, *Europ. J. Operat. Res.* **2009**, *192*, 707.
- [87] L. Chen, H. Qiu, L. Gao, C. Jiang, Z. Yang, *Computer Meth. Applied Mechan. Eng.* **2020**, *362*, 112861.
- [88] J. Stein, M. Poppel, P. Adamczyk, R. Fabry, Z. Wu, M. Kölle, J. Nüßlein, D. Schuman, P. Altmann, T. Ehmer, V. Narasimhan, C. Linnhoff-Popien, *arXiv preprint arXiv:2306.05042* **2023**.
- [89] W. Gong, Q. Duan, *Environm. Modell. Softw.* **2017**, *95*, 61.
- [90] X. Wang, F. Tsung, W. Li, D. Xiang, C. Cheng, *Appl. Math. Modell.* **2021**, *100*, 303.
- [91] D. E. Ricciardi, O. A. Chkrebti, S. R. Niezgodna, *Integrat. Mater. Manufact. Innov.* **2019**, *8*, 273.
- [92] D. A. Cole, R. B. Christianson, R. B. Gramacy, *Statist. Comput.* **2021**, *31*, 33.
- [93] D. Chen, S. Xiong, *J. Quality Technol.* **2017**, *49*, 337.

Part III

Summary and Outlook

Summary and Outlook

7.1 Summary

Understanding the degradation of biodegradable implants is crucial to adapting the degradation rate to the human body. This challenging process requires extensive *in vitro* and *in vivo* experiments. An alternative to predicting degradation is to utilize *in silico* methods, if sufficiently accurate mathematical models can be established. The mathematical models developed for simulating the degradation of biodegradable implants are complex and multi-scale in nature, which results in complex and expensive to evaluate models. Although computational methods could provide a theoretical understanding of biodegradation and its underlying interactions, the developed mathematical models inherently incorporate uncertainty into the formulated mathematical models. To enhance the reliability and predictability of computational models in predicting the degradation of biodegradable implants, these uncertainties must be addressed and quantified. Therefore, integrating uncertainty quantification into the computational workflow is pivotal. Nevertheless, both the computational load and complexity of UQ methods are correlated with the computational model's complexity, presenting a new challenge for the implementation of UQ methods within the field of biodegradable implants. The current dissertation addressed these challenges by developing and implementing a computational UQ workflow that simulated the degradation of magnesium-based biodegradable implants. It also identified and quantified the uncertainties associated with different computational models of biodegradable implants under various conditions. Moreover, the developed UQ workflow focused on integrating different types of surrogate models as a solution to overcome the complexity, high computational load, time, and data required for UQ analysis.

To fulfill these aims, this dissertation began by conducting an exhaustive analysis of published computational models of biodegradable Mg-based implants up to that point. As a matter of fact, several reviews were conducted over the last decade, examining the existence of degradation models. Within these studies, degradation models were classified into physical, phenomenological, analytical, and machine-learning-based models. However, these reviews lacked a clear connection between the different degradation models and a sense of continuity with experimental studies related to the same aspects of biodegradation (e.g., degradation rate, volume loss, weight loss, mechanical properties). As part of **Chapter 3**, a comprehensive and critical review of published degradation models, both *in vitro* and *in vivo*, was presented. The focus was not solely on addressing the available degradation models but also on establishing a connection between different types of computational models and experimental studies. Additionally, the review aimed to demonstrate how various types of computational models could be utilized to model the different aspects of the biodegradation process.

For the purpose of establishing these connections, new sub-classes were added to the classical classification of degradation models. The introduced sub-classes allowed for addressing the advantages as well as the disadvantages of each computational model. As part of this process, it was necessary to review the different experimental studies used to determine degradation rates and how this information was utilized or could be utilized for the validation of different types of computational models. Moreover, **Chapter 3** examined a variety of approaches for validating, verifying, and quantifying degradation models. Most importantly, the key role of uncertainty quantification was addressed and connected not only to the computational models but also to the availability of experimental data and the complexity of the biodegradation process. Overall, the review effectively conveyed a coherent understanding by integrating theoretical knowledge of the biodegradation process with the different aspects of the *in silico* approach. The review also discussed how to consider the challenges in designing biodegradable implants within computational models.

Motivated by the comprehensive discussion presented in **Chapter 3**, the subsequent chapters utilized various UQ methods to enhance the reliability and predictability of biodegradation models. However, the implementation of UQ methods posed a significant challenge, particularly when employing sampling-based UQ methods. This challenge arose from the necessity to repeatedly evaluate highly accurate approximations of the complex biodegradation models involved in the quantification process. Consequently, surrogate models were explored for the first time as a potential approach to provide easy-to-evaluate models and reduce the high computational load associated with UQ methods.

In **Chapter 4**, the application of surrogate models was explored to enhance and accelerate the performance of the parameter estimation phase. Specifically, Kriging surrogate models were constructed to perform parameter estimation for an in-house developed biodegradation model of pure Mg under physiological conditions. The complexity of parameter estimation for the degradation models stemmed from the lack of reliable information and values for the model parameters, such as reaction rate constants, diffusion coefficients, and porosity. Kriging models proved to be well-suited for addressing parameter estimation challenges due to their ability to capture various types of relationships, interactions, and complex dependencies between input parameters and their associated model responses. Furthermore, robustness was demonstrated by Kriging models in scenarios involving noisy or limited calibration data, making them particularly effective for handling the inherent variability in measurements. This was observed in both *in vitro* and *in vivo* degradation experiments. Additionally, Kriging models served as a basis for conducting global sensitivity analyses. In parameter estimation, sensitivity analysis is useful for understanding and identifying the parameters that have the greatest impact on the model response, providing valuable insights into the relative significance and interactions of different parameters. The application of Kriging models to calibrate the computational model presented in **Chapter 4** resulted in a reduction of computational time for the anodic dissolution-related degradation process of pure Mg in SBF from eight minutes per run to twenty seconds, with an error of 7% for the simulation results. For the first time, the degradation model simulated precipitate formation during degradation in terms of elemental weight percentage. The precipitation reactions involved in the precipitation of five elements were considered in this model, namely carbon, phosphorus, calcium, oxygen, and magnesium. Simulating precipitation required constructing multi-input, multi-output Kriging models to calibrate precipitate reaction constants. Kriging models reduced the computational time from twenty-seven minutes into approximately nine minutes with an NRMSE error between 0.40 (the lowest) for phosphorus vs. 1.03 (the highest) for magnesium. Furthermore, the surrogate-based sensitivity analysis indicated that the precipitate formation model parameters were correlated, and further development of the computational model might be necessary. Overall, the calibration process using

Kriging models enhanced the reliability of the degradation model at a competitive computational cost, time, and CPU usage.

Motivated by the positive results of the calibration process based on Kriging models and derived by the ability of Kriging models to estimate the values of model parameters through interpolation, where the parameter values were predicted within the range of calibration data, as well as extrapolation, where the parameter values were predicted outside the range of calibration data. Rigorous number of studies has verified this favorable property [57, 214–216], especially when estimating parameters in unexplored regions or when a limited number of experimental data points is available, as was reported in [57, 214–216].

Motivated by these properties of Kriging, a novel methodology to bridge the gap between *in vitro* and *in vivo* degradation was developed and presented in **Chapter 5**. The development of this methodology was accomplished by combining Kriging models with a 3D peridynamic degradation model derived by Hermann *et al.*, [64] and experimental observations of Mg-xGd implants (Mg-5 wt.% Gd and Mg-10 wt.% Gd) conducted by Krüger *et al.*, [132, 217] and Willumeit-Römer *et al.*, [26]. The novel methodology enabled the derivation of a time-independent ratio based on the diffusivity of Mg²⁺-ions from the implant surface to the degradation media. Using the derived time-independent ratio, it became possible to infer the *in vivo* biodegradation of implants based on *in vitro* degradation. To the best of our knowledge, this represents the first time that a method has been developed and verified to bridge the gap between *in vitro* and *in vivo* biodegradation.

The analysis of different degradation models in the previous chapters revealed the need for tailoring the UQ analysis to the specific degradation models and problems. To achieve this aim, a UQ workflow was introduced in **Chapter 6**. The introduced UQ workflow was a generic and flexible workflow designed to create numerical experiments (DOE), integrate different types of degradation models, and efficiently perform various UQ analyses, including parameter estimation, sensitivity analysis, and uncertainty propagation, based on different surrogate models. The scientific value of this UQ workflow was exemplified through three different degradation models involving various implants, degradation media, and dimensions. The development process of the UQ workflow presented in **Chapter 6** included a comprehensive investigation into various methods for designing numerical experiments and sampling techniques, as well as integrating three different types of surrogate models. Kriging models served as an example of surrogate models that generated predictions based on the structural correlation of response data. Kriging-like surrogate models captured the local variation and behaviour of the computational model response by approximating it using interpolation and regression techniques. The second type of surrogate model integrated was the non-intrusive polynomial chaos expansion model (PCE). PCE models utilized a series of orthogonal polynomials to capture the global behaviour of the model response. The UQ workflow also integrated hybrid surrogate models. Here, Polynomial Chaos Kriging models (PCK), which were originally developed to identify the most relevant basis functions for model responses [62, 218]. PCK utilized regression-type PCE to capture the computational model's global behaviour and incorporated interpolation-type Kriging to capture local variations, providing a more comprehensive approximation of the model response. In comparison to PCE and PCK, Kriging demonstrated superior fitting for parameter estimation problems in biodegradation systems. This advantage was evident in terms of computational cost, the number of required samples, and the achieved level of accuracy. However, this benefit came with a trade-off; acquiring additional samples was time-consuming and costly, especially when the underlying system was complex or challenging to evaluate, as was the case with biodegradation models. In cases where generating a large number of samples was not computationally expensive, the PCK model outperformed the Kriging and PCE models

in terms of performance and validation. Ranking the uncertain model parameters according to their significant impact on model predictions using surrogate-model-based sensitivity analysis, PCE and PCK demonstrated better alignment with biodegradation physical phenomena than Kriging. Most importantly, the flexibility of the developed UQ workflow made it possible to utilize it to study different degradation models and surrogate models.

It was demonstrated through this dissertation that *in silico* methods had a very high potential for accelerating the development of biodegradable implants. However, the inherent uncertainty within these models must be identified and quantified to enhance the reliability and predictability of degradation models. The use of UQ methods proved to be efficient for quantifying the uncertainty associated with different aspects of biodegradation models. The computational load of these methods, however, posed a new challenge. Surrogate models enabled UQ analysis by reducing computational load, as well as the complexity of degradation models. It was also demonstrated that the integration of UQ analysis into various stages of modeling and simulating the degradation process significantly improved the predictability and reliability of the degradation models. Identifying the most influential factors, providing a comprehensive understanding of the relations within the biodegradation process, and thus, improving degradation models.

7.2 Outlook

As a first step in future work, a study should be designed to examine the impact of uncertainty associated with dynamic degradation behaviour. This entails considering the time dependency of the key parameters and their interactions and correlations within the biodegradation process as uncertain parameter, which will provide a comprehensive understanding of the overall behaviour of the biodegradation process can be captured. This deeper insight into how parameters vary over time and influence degradation is crucial for predictive models development. The study has recently received funding from the Helmholtz Information and Data Science Academy (**HIDA**) and will be carried out in partnership with the scientific computer center at the Karlsruhe Institute of Technology. In general, conducting a systematic study of degradation dynamics will accurately demonstrate how associated uncertainties with these models and parameters impact the propagation of uncertainty within degradation models. To achieve this goal, extending surrogate models across space and time is essential. This expansion is coupled with optimizing numerical experiment design and employing uncertainty quantification methods and algorithms for quantifying uncertainties in time-dependent degradation models. Additionally, the task includes identifying and modelling sources of non-stationary variation in degradation models. This entails developing appropriate methods to account for these variations. A more comprehensive understanding of dynamic degradation processes can be achieved by addressing these challenges.

A second step in future work can be build based on the given the assumption and demonstration that a time-independent ratio can be estimated between *in vitro* and *in vivo* degradation based on the diffusivity of Mg^{2+} -ions, it is worthwhile to explore and assess the potential for generating analogous ratios under diverse physiological conditions and for various types of implants.

The optimization and enhancement of the management of uncertainties associated with various methods and approaches used to study the degradation of biodegradable implants are of great importance. To achieve this, it is necessary to utilize UQ methods to optimize the experimental design of *in vitro*, *in vivo*, and *ex vivo* tests. This will, in turn, enhance the calibration and validation processes of the computational models developed to simulate the degradation pro-

cess. Moreover, the UQ workflow should be expanded to incorporate methods and techniques that can explore, identify, and quantify the uncertainties associated with the experimental data, as well as develop suitable computational models to improve this process. This approach contributes to a better understanding and characterization of the inherent uncertainties in both experimental setups and computational models, ultimately enhancing their reliability.

Part IV

Other publications

Publications, their content and own contribution

This chapter encapsulates my collaborative involvement in published research, which was not incorporated into this dissertation. The content within this section is adapted from original publications. Moreover, I have highlighted my own contribution alongside the team's collective research findings.

1. Isaac Appelquist Løge, Peter Winkel Rasmussen, Henning Osholm Sørensen, Stefan Bruns, *Tamadur AlBaraghteh*, Anders Nymark Christensen, Anders Bjorholm Dahl, and Philip Loldrup Fosbøl. Revealing the complex spatiotemporal nature of crystal growth in a steel pipe: Initiation, expansion, and densification. *Chemical Engineering Journal* 466 (2023): 143157. <https://doi.org/10.1016/j.cej.2023.143157>.

Abstract: Crystallisation fouling is a challenge in numerous applications. To mitigate fouling we need to determine the basic mechanisms involved in the process. While *ex situ* techniques have been widely used in previous studies, they cannot capture complex dynamic effects. We conducted an *in situ* investigation of the dynamic effects of crystallisation fouling in a steel pipe (length 3 cm, diameter 3 mm) using X-ray micro-computed tomography (μ CT) over more than six days. We employed a custom-developed image reconstruction algorithm, which ensured high spatiotemporal resolution from a laboratory instrument. We quantified the evolving fouling using advanced segmentation techniques of 4D images. To understand how the pipe interface structure impacts reactive transport, the experimental geometries of the flow system were used to perform computational fluid dynamic simulations. These new data allowed us to identify three growth phases: initiation, expansion, and densification.

Own contribution: Methodology, CFD-study by deriving, building and implementing the model. Evaluation the simulation results and validate the models outcomes with the experimental study. Moreover, participating in writing – original draft, Writing – review and editing.

2. Sana Riyaz, Yu Sun, Heike Helmholz, Tuula Penate Medina, Oula Penate Medina, Björn Wiese, Olga Will, *Tamadur AlBaraghteh*, Ferhad Haj Mohammad, Jan-Bernd Hövener, Claus Christian Glüer, Regine Willumeit Römer. Inflammatory response towards Mg-based metallic biomaterial implanted in a rat femur fracture model. **Under review**, *acta biomaterialia*

Abstract: The immune system plays an important role in fracture healing, by modulating the

proinflammatory and anti-inflammatory responses occurring instantly upon injury. Imbalance in these responses can result in adverse outcomes such as fracture nonunion. Implants are used to support and stabilize broken bones. Biodegradable metallic implants offer the potential to avoid a second surgery for implant removal, unlike nondegradable implants. However, considering our dynamic immune system it is important to conduct in-depth studies on the immune response to these implants in living systems. In this study, we investigated the immune response of Mg and Mg-10Gd *in vivo* in a rat femur fracture model with external fixation. *In vivo* imaging using liposomal formulations was used to monitor the fluorescence-related inflammation over time. We combine *ex vivo* methods with our *in vivo* study to evaluate and understand the systemic and local effects of the implants on the immune response. We observed nonsignificant effects locally and systemically in the Mg-10Gd implanted group in comparison to the SHAM and Mg implanted group over time. Our findings illustrate that Mg-10Gd is a slightly better implant material than Mg with no adverse effects in the early phase of fracture healing of our 4-week study.

Own contribution: Calculations re-analysis, writing-review and editing.

3. Kamila Iskhakova, D.C. Florian Wieland^{1*}, Romy Marek, Uwe Schwarze, Anton Davydok, Hanna Ówieka, *Tamadur AlBaraghteh*, Jan Reimers, Birte Hindenlang, Sandra Sefa, André Lopes Marinho, Régine Willumeit-Römer and Berit Zeller-Plumhoff. Sheep bone ultrastructure analyses reveal differences in bone maturation around Mg-based and Ti implants. **submitted**, *Journal of Functional Biomaterials*

Abstract: Magnesium alloys are one of the most convenient biodegradable materials for bone fracture treatment due to their tailorable degradation rate, as well as their biocompatibility and mechanical properties resembling those of bone. One such alloy is ZX00 (Mg-0.45Zn-0.45Ca inwt.%), whose alloying elements Zn and Ca naturally occur in the body. While magnesium-based implants generally and ZX00 in particular have been shown to have suitable degradation rates and good osseointegration, knowledge gaps remain in the understanding of the influence of the degrading material on the bone ultrastructure. In this study, we present the first comparative analysis of bone ultrastructure parameters around ZX00 and Ti implants after 6, 12, and 24 weeks of healing depending on the distance from the implant surface. For this purpose, high-resolution scanning small angle X-ray scattering and X-ray diffraction were employed. The mineralization was investigated to reveal a significant decrease in the lattice spacing of the (002) Bragg's peak closer to the ZX00 implant in comparison to Ti, while no significant difference in the crystallite size was observed. The hydroxyapatite platelet thickness and osteon density demonstrated a decrease closer to the ZX00 implant interface. Correlative nano-indentation and X-ray diffraction measurements revealed higher strain values around Ti at the early time points. Thus, the results suggest the incorporation of Mg²⁺ ions into the bone ultrastructure, as well as a lower degree of remodelling and stiffness of the bone in the presence of ZX00 implants than Ti.

Own contribution: Data acquisition (participation in beamtimes), manuscript review.

Lists

List of Figures

1.1	Schematic diagram of traditional deterministic model vs. applying UQ methods to model predictions (inspired by [51]).	5
2.1	Schematic description of the complexity of the biodegradation process. Adapted from [66] under CC BY 4.0 license.	10
2.2	Schematic diagram of epistemic and aleatory uncertainties within the modelling domain.	13
2.3	Forward and backward uncertainty quantification.	15
2.4	Forward intrusive (red lines) and non-intrusive (blue line) quantification analysis.	18
2.5	Schematic diagram of the construction of a surrogate model for a system characterised by two input parameters.	28
2.6	Classification of surrogate models.	29